Aircraft trajectory optimization in North Atlantic oceanic airspace

Olga Rodionova

THÈSE

En vue de l'obtention du

DOCTORAT DE L'UNIVERSITÉ DE TOULOUSE

Délivré par : *l'Université Toulouse 3 Paul Sabatier (UT3 Paul Sabatier)*

Présentée et soutenue le *30/06/2015* **par :**

Olga RODIONOVA

Optimisation des trajectoires avion dans l'Atlantique Nord

Aircraft trajectory optimization in North Atlantic oceanic airspace

---

JURY

Cyril BRIAND	Professeur UT3 Paul Sabatier
Richard CURRAN	Professeur Delft University of Technology
Daniel DELAHAYE	Enseignant-chercheur ENAC
Brigitte JAUMARD	Professeur Concordia University
Marcel MONGEAU	Enseignant-chercheur ENAC
Christian PRINS	Professeur Université de Technologie de Troyes
Mohammed SBIHI	Enseignant-chercheur ENAC
Karim ZEGHAL	Chercheur Eurocontrol

École doctorale et spécialité :

MITT : Domaine Mathématiques : Mathématiques appliquées

Unité de Recherche :

Mathématiques Appliquées, Informatique et Automatique pour l'Aérien (MAIAA)

Ecole Nationale de l'Aviation Civile (ENAC)

Directeur(s) de Thèse :

Marcel MONGEAU et *Mohammed SBIHI*

Rapporteurs :

Brigitte JAUMARD et *Christian PRINS*

Resumé

Cette thèse est consacrée à l'étude du trafic aérien dans *l'espace océanique de l'Atlantique Nord* (NAT) et de pistes visant à son amélioration. NAT est l'espace aérien océanique le plus fréquenté dans le monde. Le contrôle aérien confine les vols sur quelques routes (quasi-parallèles) tracées chaque jour, en fonction de la position des vents dominants (*jet streams*). Le décalage horaire impose quant à lui une *concentration des vols* sur deux fenêtres de temps assez limitées. La prédiction des trajectoires des vols ainsi que leur surveillance sont particulièrement difficiles à cause de *l'absence de couverture radar*, ce qui impose un espacement très conséquent entre les avions. Tous ces facteurs induisent une congestion dans l'espace aérien continental, voisin de l'océan, pendant les heures de pointe. En outre, les avions subissent *d'importants retards* et suivent des trajectoires et des profils d'altitude *non optimaux* vis-à-vis de la consommation carburant et du coût total des vols.

Aujourd'hui, plusieurs projets sont a l'étude pour moderniser le système global du transport aérien et la gestion du trafic aérien. La modernisation se focalise sur le développement des nouvelles technologies liées à l'aviation, telles les *technologies de surveillance et de communication* d'une part, et l'implémentation des nouvelles procédures dans la planification et le contrôle du trafic aérien, telles le *concept de free flight* et la *séparation à bord des avions*, d'autre part. Dans le présent travail, on propose *trois pistes possibles* dans la cadre d'une telle modernisation du système du trafic aérien qui permettent d'améliorer l'efficacité du trafic dans l'espace particulier de NAT.

Tout d'abord, on considère le système du trafic océanique actuel, dans lequel les avions traversant le NAT sont obligés de suivre les rails établis, nommés *Organized Track System* (OTS). L'introduction des nouvelles technologies permettra de réduire l'espacement entre avions. Ainsi, au lieu de retarder les avions, on favorise le *re-routage* entre les rails (changement de rail) dans OTS afin de diminuer la congestion dans l'espace aérien pré-océanique. On utilise des *mèthodes stochastiques d'optimisation* afin de trouver une configuration des vols *sans conflits* en considérant les *normes de séparation réduites*. Les résultats de cette étude révèlent que la réduction des normes de séparation et l'autorisation des re-routages peuvent engendrer d'importants bénéfices.

Ensuite, on simule la *prédiction des trajectoires* au niveau tactique (au moment des vols) en utilisant un échange d'informations entre avions voisins. On appelle cette approche *Wind Networking* (WN). Aujourd'hui, la source principale des erreurs dans la prédiction du temps le long d'une trajectoire est *l'incertitude dans les données météorologiques*, en particulier, les vents. Le WN permet aux avions d'échanger les données de vents mesurés et d'ajuster leur prédictions en utilisant cette information plus récente et plus proche de

la réalité. Nos simulations numeriques montrent que les bénéfices d'une telle approche sont remarquables, surtout lorsque les vents sont forts.

Finalement, on étudie la possibilité d'introduire le *concept de free flight* dans NAT. Cette étude est effectuée en collaboration avec le centre de recherche de la NASA qui nous a fourni des données de *trajectoires vent-optimales* pour plusieurs jours de vols dans NAT. On développe et applique une *mèthode stochastique d'optimisation* visant à *réduire* (voir éliminer) *le nombre de conflits* induits par ces routes au niveau stratégique (quelques heures avant les vols), tout en conservant les trajectoires proches de leurs routes optimales. La réduction des normes courantes de séparation permet de réduire considérablement le nombre de conflits entre les vols dans le champ de vent du jet stream.

Nos résultats montrent qu'il existe plusieurs pistes pour réduire la congestion du trafic océanique dans NAT en considérant les nouvelles technologies de surveillance et de communication et les nouveaux concepts dans la planification des trajectoires.

Abstract

This thesis is devoted to studying the air traffic situation in the *North Atlantic oceanic airspace* (NAT) and the possibilities to improve this situation. Because of the passenger demands, time zone differences, limited economical height band and strong winds, the *jet streams*, the NAT is *highly congested* during peak hours and within the major airline-preferred routes. Flight prediction and flight control is particularly difficult in this vast airspace *not covered by radars*. All these factors cause *large delays* in flight schedules and *additional congestion* in the pre-oceanic continental airspace. It often obliges aircraft to follow *non-optimal trajectories* and altitude profiles, increasing fuel consumption and total flight costs.

Nowadays, several projects are launched, aimed at modernizing the global air transportation system and air traffic management. This modernization supposes developing new aviation-related technologies, such as *surveillance and broadcast technologies*, on one hand, and implementing new air traffic planning and air traffic control procedures, such as the *free-flight concept* and *airborne separation*, on the other hand. In this work, we propose *three possible approaches* in the frame of such a modernized air traffic system, allowing improving the traffic efficiency in the particular NAT airspace.

First of all, we consider the current oceanic traffic conditions, where the aircraft crossing NAT are obliged to follow predefined routes established in NAT, the *Organized Track System* (OTS). We favor *re-routing maneuvers* via OTS in order to decrease congestion in the pre-oceanic airspace. We optimize a set of given trajectories using *stochastic methods for optimization* in order to find a *conflict-free* flight configuration considering *reduced separation standards*. The results of this study reveal that significant potential benefits can be obtained from reducing the separation standards and authorizing re-routings.

After that, we simulate tactical *trajectory prediction* using the information obtained from previous aircraft flying a common route. We call this approach *Wind Networking* (WN). Nowadays, the main source of errors in time prediction along an aircraft trajectory is the *uncertainty in meteorological data*, especially the wind. WN permits aircraft to exchange measured wind data and adjust their trajectory predictions by using more recent and more exact information. The benefits of such an approach are remarkable, especially in strong-wind conditions.

Finally, we address the possibility of introducing the *free flight concept* in NAT. This study is conducted in collaboration with NASA Ames Research Center (CA) that provided us with *wind-optimal trajectories* for several full days of NAT flights. We design

apply a *stochastic method of optimization* aimed at *reducing* (up to eliminating) the *number of conflicts* induced by these flights on the strategic level, while keeping the trajectories close to the optimal routes. The reduction of current NAT separation standards is crucial for efficient free-flight performance in the jet-stream wind fields.

Our results demonstrate that there are several different ways to improve the air traffic situation in the highly congested NAT when considering new surveillance and broadcast technologies and new concepts in trajectory planning.

Acknowledgements

I would like to take some time to sincerely acknowledge people whose assistance and support made it possible for me not only to accomplish this PhD research, but also to evolve significantly in the professional area as well as in the personal life.

First of all, I wish to thank my advisor, Marcel Mongeau, for his patience and comprehension, especially in my moments of weakness when I was quite far from the picture of a "good student"; for the hours he passed while reading, correcting and re-reading my reports, articles and finally, this thesis; for his vast knowledge in the optimization gratefully shared with me during rich discussions; for the possibility to see Quebec, his native region; for being always in a good spirit that inspires and always available for any questions...

I wish equally to thank my co-advisor, Mohammed Sbihi, who was all the time present for me since the very first day of my arrival; who helped me with my integration in the life of laboratory as well as with my integration in the subject of the research work; for the long and productive discussions we had; for the new ideas and new research branches proposed; for his sense of humor and his tolerance in the moments when I showed unreasonable obstinacy...

Many thanks I owes to Daniel Delahaye, my third (the last but not the least) co-advisor; who believed in my capabilities since the first meeting and proposed me to conduct this research at ENAC; for his inspiring ideas; for his personal attitude and comprehension; for the opportunity to fulfill two great projects at the same time, the thesis and the birth of my daughter; for my initiation into jogging along the channel; for discovering his amazing universe of mountains during exhaustive tracking; for several enriching trips to the other end of the world; for opening the doors in the aviation research community and propositions for my future career that followed...

In the second turn I would like to thank the reporters, Professor Brigitte Jaumard and Professor Christian Prins, for their careful reading of this manuscript (I certainly realize at which point that was a great job taking into account its size and my love for the acronyms); for their precise remarks that I have tried to take into account in the final version and that permitted to improve the clearness of the exposition; and for their favorable reports that permitted me to proceed to the thesis defence.

I wish equally to thank Professor Cyril Briand, who accepted being the president of the defence jury, as well as the two other members of the jury, Richard Curran and Karim Zeghal, who performed the displacements in order to participate in this defence; for their attentive listening, meaningful questions (even if I was not able to answer all of them)

and interesting discussions; and for their favorable note having been given to my work, that allowed me to obtain the doctoral degree.

I'm also extremely grateful to people who contributed a lot in my research work by providing me with data and knowledge in this new for me area of civil aviation. Thank you to Philippe Louyot, who kindly supplied me with the real aircraft report messages and the accompanying documentation, which made it possible to perform the simulations for the first track of my research. Thank you to Karim Legrand, for sharing his experience in the ATM and flight planning taking into account the winds, crucial for the second track of my research.

Finally, a great thanks to Banavar Sridhar from NASA Ames, who accommodated me at his place, elaborated a joint paper with us and gave me the chance to continue research experience in the aviation field as a postdoctoral fellow. Thank you to Hok K. Ng from the same research team, who provided me with real aircraft data used in the third track of my research and took his time to answer, attentively and thoughtfully, to all my questions. Thanks to Supatcha Chaimatanan, also a PhD student at ENAC, for providing me the access to her work, her papers and her code, so that the third track of my research could be based on these data, and for her kindness when answering all my questions, not all of which were related to work.

I'm still far from the end, and I would like to thank a lot all the members of MAIAA laboratory and occupants of Z-building, who gave me the place among them and permitted me to feel as being home. I really appreciated this time spent at ENAC during these four years. Even if I'm grateful to all of my colleagues and persons whom I met during my staying at ENAC, I tend to mark out several particular names and to thank them personally.

Thanks to Puechmorel Stéphane, our chef, for his impressive ability to resolve any kind of problems and to answer any kind of questions. Thanks to Pascal Lezaud, for greeting me each morning with his smile and often with philosophical conversations, and in particular for the opportunity to try myself in the role of a professor, and for patient discussions that this role involved. Thanks to Ludovic d'Estampes, for his sense of the humor. Thanks to Florence Nicol, for interesting anecdotes concerning not only the teaching practice, but also the young mother experience. Thanks to Sonia Cafieri, for her flowing enthusiasm and charming Italian accent.

Thanks to Jean-Paul Imbert, for interesting conversations, invitations to jogging and his patience when resolving endless problems with my computer. Thanks to Serge Roux, who shared with Jean-Paul the honor to fix my informatics problems, as well as the problems with organization of any kind, starting from "pots" and finishing with moving

to another house. Thanks to Gwenael Bothorel for his permanent presence when I arrived early in the morning, for interesting discussions and useful explanations of the particularities of flight progress, including provided data. Thanks to Laurant Lapasset, who accepted to drive me each week to the climbing gym and one time even climbing on the rocks.

Thanks to Celine Smith and Sabine Cantayre, for their assistance with all kinds of administrative problems that I have the tendency to attract, including scholarship and travel reimbursements. Thanks to Colette Roy and Catherine Migot, for their kindness and their assistance that made my travels to conferences (including family travels) possible. Thanks to Martine Labruyere, for her efficient assistance not only in thesis defence preparation, but also in the inscription to the postdoctoral program (that I made at the last moment as usual, which did not facilitate her task).

I leave a special word to thank all the PhD students of MAIAA laboratory, for this great time that I have spent being one of them, for the lunches and coffee breaks with endless talking, for the initiation into new table games, for common attendance of the conferences, for the picnics and evenings with a glass of beer.

Thanks to Laureline for her optimism, delicious pan-cakes and staying in contact even after her leaving. Thanks to Brunilde for her passion to sport, great photos and being capable to keep secrets. Thanks to Caroline for her enviable talent of communication and big heart. A particular thanks to the girls for being here to share my most important personal event of the past years. Thanks to Loic for his passion for the chess and the attempt to learn us the mystery of this game. Thanks to Andrija for enriching scientific discussions and sharing the experience of being a father. Thanks to Romaric for his extremely wide erudition and for organizing the coffee-breaks.

Thanks to Clement for sharing with me the experience of being a "professor" and for consolidating our "PhD community" at students seminars as well as during out-of-work events. Thanks to Ning and Jun for sharing their stories, their culture and for extremely tasty dishes for picnics. Thanks to Catya for her endless enthusiasm and participating in all the activities. Thanks to Man, Tambet, Jean-Michel, Vincent, Imen, Nour and others (whom I apologize to do not mention), each of them imported something special to our small community, something that arose the desire to follow his example.

A particular thanks to Marina, my compatriot, office-mate and friend, for the possibility to speak Russian every day at work, for being attentive listener when I was in troubles, for being always here ready to support and to help, for the assistance in the organization of important events in my life, for understanding the real problems of being in couple with a French, for being appreciated by my daughter...

That would be not honest not to thank my family, that stayed in Russia while I left to France. My mother, my father, my sister, my grand parents. Without their permission, their "benediction" and their support, moral and financial, this project of conducting a research work in a foreign country would never become true. They were always here, ready to help in any kind of problems, and ready to share my pride when some important task was accomplished.

And in particular, I would like to thank Fabien, my boyfriend, and since a couple of weeks my husband, who gave me the strongest motivation to succeed in the PhD work in France; who introduced me the French culture and explained me all the complicated administrative procedures; who was here to disprove my doubts of whether I would cope with the task; who encouraged me by mentioning all the time that, from his point of view, I did not work enough and did not spend a lot of time at work; who shared with me the crazy project to have a baby at the same time than a thesis; who spent the days and the nights taking care of our daughter when I had a rush job, a summer school in another city, a conference at the other end of the world or a thesis to submit the next day...

And finally, the last but the most important acknowledgment I wish to address to my little Auriane, my sunray, my life sense, my daughter, who was calm, kind, patient, comprehensive and dutiful enough to permit her mother to sleep well at nights and to work hard during the days in order to fulfill this important step in her professional career and to become a Doctor.

Contents

List of Figures

List of Tables

Abbreviations

ACARS	**A**ircraft **C**ommunication **A**ddressing and **R**eporting **S**ystem
ADS	**A**utomatic **D**ependent **S**urveillance
ADS-B	**A**utomatic **D**ependent **S**urveillance-**B**roadcast
AMDAR	**A**ircraft **M**eteorological **DA**ta **R**elay
ANS	**A**ir **N**avigation **S**ystem
ARB	**A**ircraft **R**eserved **B**lock
ARTCC	**A**ir **R**oute **T**raffic **C**ontrol **C**enter
ASAS	**A**irborne **S**eparation **A**ssurance **S**ystems
ASEP-ITM	**A**irborne **SEP**aration **I**n-**T**rail **M**erge
AT	**A**ircraft **T**rajectory
ATA	**A**ctual **T**ime of **A**rrival
ATC	**A**ir **T**raffic **C**ontrol
ATFM	**A**ir **T**raffic **F**low **M**anagement
ATM	**A**ir **T**raffic **M**anagement
ATOMS	**A**ir **T**raffic **O**perations and **M**anagement **S**imulator
ATS	**A**ir **T**raffic **S**ervices
CARAT	**C**limb **A**dvisory **R**equest **A**ssistance **T**ool
CDR	**C**onflict **D**etection and **R**esolution
CFC	**C**onflict-**F**ree **C**riterion
CLR	**CL**ea**R**ance
CPDLC	**C**ontroller-**P**ilot **D**ata **L**ink **C**ommunications
CSS	**C**urrent **S**eparation **S**tandards
EET	**E**stimated **E**lapsed **T**ime
EQA	**EQ**uipped **A**ircraft
ERAS	**E**n-**R**oute **A**irspace **S**tructure

ETA	**E**stimated **T**ime of **A**rrival
ETAF	**E**lapsed **T**ime **A**nd **F**orecast
FAA	**F**ederal **A**viation **A**dministration
FAP	**F**light **A**ltitude **P**rofile
FFC	**F**ree **F**light **C**oncept
FIR	**F**light Information Region
FL	**F**light **L**evel
FPL	**F**light **PL**an
GA	**G**enetic **A**lgorithm
GADS	**G**lobal **A**ircraft **D**ata **S**et
GAT	**G**lobal **A**ir **T**raffic
GC	**G**reat **C**ircle
GPS	**G**lobal **P**ositioning **S**ystem
GS	**G**round **S**peed
HF	**H**igh **F**requency
ICAO	**I**nternational **C**ivil **A**viation **O**rganization
ILP	**I**nteger **L**inear **P**rogramming
INS	**I**nertial **N**avigation **S**ystem
ITC	**I**n-**T**rail **C**limb
ITP	**I**n-**T**rail **P**rocedure
JS	**J**et **S**tream
LFP	**L**ateral **F**light **P**rofile
LS	**L**ocal **S**earch
MDCRS	**M**eteorological **D**ata **C**ollection and **R**eporting **S**ystem
MF	**M**eteorological **F**orecast
MIP	**M**ixed-**I**nteger **P**rogramming
MNPS	**M**inimum **N**avigation **P**erformance **S**pecifications
MNT	**M**ach **N**umber **T**echnic
MSS	**M**inimum **S**eparation **S**tandards
NAS	**N**ational **A**viation **S**ystem
NASA	**N**ational **A**eronautics and **S**pace **A**dministration
NAT	**N**orth **AT**lantic oceanic airspace
NEQA	**N**on-**EQ**uipped **A**ircraft

NextGen	**Next Gen**eration Air Transportation System
NM	**N**autical **M**ile
NOAA	U.S. **N**ational **O**ceanic and **A**tmospheric **A**dministration
NOPAC	**NO**rth **PAC**ific track system/model
NWP	**N**umerical **W**eather **P**rediction
NWS	U.S. **N**ational **W**eather **S**ervice
OACC	**O**ceanic **A**rea **C**ontrol **C**enter
OCA	**O**ceanic **C**ontrol **A**rea
OCLR	**O**ceanic **CL**ea**R**ance
OSE	**O**bservation **S**ystem **E**xperiment
OTS	**O**rganized **T**rack **S**ystem
POS	**POS**ition report
PTIT	Strategy of modifying one **P**articular **T**rajectory and all **I**nteracting **T**rajectories
RCL	**CL**earance **R**equest message
RH	**R**elative **H**umidity
RLatSM	**R**educed **Lat**eral **S**eparation **M**inimum
RMSE	**R**oot-**M**ean-**S**quare **E**rror
RMSVD	**R**oot-**M**ean-**S**quare **V**ector **D**ifference
RSS	**R**educed **S**eparation **S**tandards
RUC	**R**apid **U**pdate **C**ycle
RVSM	**R**educed **V**ertical **S**eparation **M**inima
SA	**S**imulated **A**nnealing
SAW	**S**ituation **AW**areness
SESAR	**S**ingle **E**uropean **S**ky **A**TM **R**esearch
TAMDAR	**T**ropospheric **A**ircraft **M**eteorological **DA**ta **R**elay
TAS	**T**rue **A**ir **S**peed
URET	**U**ser **R**equest **E**valuation **T**ool
UTC	**C**oordinated **U**niversal **T**ime
WN	**W**ind **N**etworking
WO	**W**ind-**O**ptimal
WP	**W**ay**P**oint
WS	**W**ind **S**peed

Symbols

a	altitude	feet, m, km
a_k	altitude of the FL k in the OTS	feet, m, km
d^f	track entry delay of the flight f	sec
e^f	actual OTS entry track for flight f	
f, g	flight index, or aircraft index	
i	WP index within an OTS track	
j	track index within an OTS	
k	FL index within an OTS track	
$l_{i,s}$	length of link segment between subnodes	
	s and $s+1$ on a link joining WPs i and $i+1$	
l	link in the OTS grid structure	
n	node in the OTS grid structure	
o^f	actual OTS exit track for flight f	
p^f	cruising time within an OTS of the flight f	sec
$p_a(s \to s', T)$	probability of acceptance of the state transition	
	as a function of temperature T in the SA	
q_i^f	i-th 2D point of FFC AT of flight f	
$\bar{q}_i^f$	i-th 2D point of initial WO AT of flight f	
s, s'	states of the system in the SA	
s	subnodes on the link joining WP i and $i+1$	
$slot$	minumal time interval by which a flight	sec
	can be delayed	
t^f	desired OTS track entry time for flight f	sec
t_n^f	time at which a flight f passes a node n	sec
t_i^f	real time at which flight f passes WP i	sec

$\tilde{t}_i^f$	forecast time at which flight f passes WP i	sec
$\hat{t}_i^f$	predicted time at which flight f passes WP i	sec
	adjusted using WN	
$\Delta t_{i,s}^f$	cruising time of aircraft f between subnodes	
	s and $s+1$ on a link joining WPs i and $i+1$	
u	west-east (longitudinal) wind vector component	knots, m/s
v	south-north (lateral) wind vector component	knots, m/s
$\vec{v}$	aircraft True Air Speed	knots, m/s
v_i^f	TAS of aircraft f at WP i	knots, m/s
x_i^f	binary variable equal to 1 if flight f	
	re-routes at a WP i	
x_τ^f	binary variable equal to 1 if route τ	
	is chosen by aircraft f	
y	vector of decision variable over all flights	
y^f	vector of decision variables for flight f	
$y_{\tau,\theta}^{f,g}$	a binary variable equal to 1 if ATs τ and θ	
	are chosen by aircraft f and g	
C_t	total number of conflicts	
$C_{\mathcal{L}}$	number of conflicts on links	
$C_{\mathcal{N}}$	number of conflicts on nodes	
$E(s)$	energy function of the state s in the SA	
F	objective function	sec
F_2	objective function with relaxed	sec
	collision-avoidance constaints	
D	total delay at track entry over all flights	sec
FL_i^f	FL index at WP i for the fligth f	
G	total deviation delay over all flights	sec
L_{OTS}^f	AT length within the OTS for flight f	km
M	number of aircraft neighboring to aircraft f	
N	total number of flights in a set	
N_d	number of discrete delays autorized	
	being attributed to a flight	

N_h	number of system states examined at each step of heating in the SA	
$N_{ijj'}$	number of subdivisions of link $(i,j,k)-(i+1,j',k)$, where $j'=j$, $j'=j-1$, or $j'=j+1$	
N_t	number of transitions performed at the same temperature level in the SA	
N_G	maximal number of generations in the GA	
Nx	number of WPs for each track in the OTS model	
Ny	number of tracks in the OTS model	
Nz	number of FLs for each track in the OTS model	
P	total cruising time within the OTS over all flights	sec
P_c	probability to apply a crossover operator in the GA	
P_m	probability to apply a mutation operator in the GA	
Q_i^f	i-th 4D point of FFC AT of flight f	
$\bar{Q}_i^f$	i-th 4D point of initial WO AT of flight f	
R_τ^f	cost of AT τ of aircraft f	
S_e^f	distance between actual and desired entry tracks	m
S_o^f	distance between actual and desired exit tracks	m
S_P	population size in the GA	
T	temperature parameter in the SA	
T_0	initial temperature in the SA	
T_f	final temperature in the SA (stopping criteria)	
TD_e^f	desired OTS entry track for flight f	
TD_o^f	desired OTS entry track for flight f	
$\vec{V}$	aircraft Ground Speed	knots, m/s
$\vec{\tilde{V}}$	forecast Ground Speed	knots, m/s
V_i^f	GS of aircraft f at WP i	knots, m/s
$\vec{W}$	Wind Speed	knots, m/s
$\vec{\tilde{W}}$	Forecast Wind Speed	knots, m/s
$\vec{\hat{W}}^f$	Wind Speed measured by aircraft f	knots, m/s
$\vec{\hat{W}}_{adj}^f$	Wind Speed adjusted using WN by aircraft f	knots, m/s
$W_{ijj'}$	WS along the link $(i,j,k)-(i+1,j',k)$, where $j'=j$, $j'=j-1$ or $j'=j+1$	knots, m/s

$\mathcal{G}$	OTS grid with nodes and links	
$\mathcal{L}$	set of links in the OTS grid structure	
$\mathcal{N}$	set of nodes in the OTS grid structure	
$\mathcal{T}^f$	set of all feasible 4D ATs for aircraft f	
$\mathcal{T}_{f,g}$	set of pairs of 4D ATs of aircraft f and g where the ATs in each pair are in conflict	
α	weighting coefficient for the part of the objective function not related to conflicts	
α_d	weighting coefficient of the total track entry delay in the objective function	
α_g	weighting coefficient of the total deviation delay in the objective function	
α_p	weighting coefficient of the total cruising time in the objective function	
β	tempreature increasing (heating) coefficient in the SA	
γ	temperature decreasing (cooling) coefficient in the SA	
δ^f	index of the OTS track entry time delay (in the list of autorized delays) attributed to flight f	
$\delta^{f,g}_{\tau,\theta}$	number of conflicts induced by AT τ of flight f and AT θ of flight g	
$\delta^{\nu,f,g}_{\tau,\theta}$	binary coefficient equal to 1 if route τ of flight f is in conflict with route θ of flight g on node or link η	
ϵ	a small parameter used in fitness calculation in the GA	
$\tilde{\epsilon}^f_i$	error in time prediction by MF for flight f at WP i	sec
$\hat{\epsilon}^f_i$	error in time prediction by WN for flight f at WP i	sec
λ	geographical longitude	degrees, $^\circ$
λ^j_i	longitude of a WP i on a track j	degrees, $^\circ$
μ	initial acceptance probability in the SA	
ν	index of a grid element (a node or a link)	
$\vec{\rho}^f$	wind measurement error of aircraft f	knots, m/s

ϕ	geographical latitude	degrees, $^\circ$
ϕ_i^j	latitude of a WP i on a track j	degrees, $^\circ$
τ, θ	feasible 4D ATs for an aircraft	
Δ	longitudinal MSS within OTS	

Introduction

Air transport system nowadays plays an important role in persistent economical progress and social benefits in most of the countries, all over the world. The development and strong growth of the global airline industry originates from several important technological innovations such as the commercial use of jet aircraft (1950s) and the creation of wide-body jumbo jets (1970s). Since that time, the average increase of *Global Air Traffic* (GAT) was being approximately 5% per year during the last 30 years (nevertheless, varying much from one year to another depending on the current economic situation in different regions of the world). Thus, GAT has doubled in size every 15 years since 1977. Even considering rather low economic growth for the next 10-15 years, a continued 4-5% annual increase in GAT is expected to near-double the GAT during this period [1].

According to the data collected by ATAG[1], nowadays the global airline industry includes about 1,500 commercial airlines, operating more than 25,000 aircraft, covering more than 3,800 airports. In 2014, the world airlines flew more than 37 million scheduled commercial flights worldwide, covered more than 5 trillion kilometers, over almost 50,000 routes (see Fig.1) and during 45 million hours. These flights transported almost 3 billion passengers, with average aircraft occupancy of almost 80%, which is much higher than for other forms of transport. Over 50% of international tourists prefer to travel by air. Currently, almost 100,000 flights are carrying over 8 million passengers every day [2].

Evidently, if all pilots operating these 100,000 aircraft flew without regard for others, chaos would occur and efficient transportation would be impossible. In order to prevent such chaos, flight rules and laws are designed for airways and implemented in the world *Air Navigation System* (ANS). The elaboration of such rules, and the control of their

[1] Air Transport Action Group, an association representing all sectors of air traffic industry and working to promote aviation sustainable growth for the benefit of our global society

FIGURE 1: Map of the world air routes today[2]

execution is ensured at the national levels by *National Aviation Authorities* (NAAs[3]) as well as on the international level by the *International Civil Aviation Organization* (ICAO[4]).

The regulations that ICAO has adopted in terms of technical specifications are referred as *Standards And Recommended Practices* (SARPs) and are destinated at achieving the uniformity in standards and procedures in all the fields and organizations related to ANS. These regulations guarantee air navigation safety on one side, and limit the air traffic system development on the other side. A considerable part of the global ANS is currently guided by conceptual approaches that originated from the early 1920's [1]. These legacy air navigation capabilities not only constrain air traffic capacity and growth but are also responsible for unnecessary CO_2 atmosphere emissions. In the circumstances of the predicted GAT growth during the next years, it is expected to outpace the existing regulatory and infrastructure developments needed to support it, which will increase safety risks.

The solution to such a deadlock is a fully-harmonized global ANS built on modern

[2] From [2]

[3] Also known as civil aviation authority, a government statutory authority in each country that oversees the approval and regulation of civil aviation. For example, the Federal Aviation Administration (FAA) is the NAA of the USA. In the European Union, in addition to proper NAAs of each country there exists a cooperative European Aviation Safety Agency (EASA).

[4] A specialized agency of the United Nations which systematizes the techniques and regulations of international air navigation and incites the design and development of air transport system to ensure its safe and constant growth

performance-based technologies and procedures. To ensure continuous safety improvement and air navigation modernization, ICAO has developed a strategic systems approach linking progress in both areas under complementary frameworks, referred to as the *ICAO Global Air Navigation Capacity & Efficiency Plan* (GANCEF), and extended over 15 years in the future (2013-2028). This structured approach will allow states and stakeholders to realize the safe, sustained GAT growth, increased ANS efficiency, and responsible environmental management required by societies and economies [1].

The key element of the ANS is *Air Traffic Management* (ATM). It covers all systems, procedures and tools serving to guide the aircraft all along the flight from the departure airport to the destination airport. Nowadays in the world there are two major projects working on ATM modernization: the FAA *Next Generation Air Transportation System* (NextGen) project in the USA [3–5] and the *Single European Sky ATM Research* (SESAR) program in Europe [6–8]. Both are complex, multilayered, long-term processes, involving Communications, Navigation, Surveillance and ATM services and aimed at developing and implementing new technologies and changing the operating environment in order to handle more traffic with greater safety, at a lower cost, with reduced environmental impact of flying. The projects have already achieved certain benefits from implementing new technologies and have evolved very challenging plans [9, 10].

The current research work assumes that such new generation ANS is already available. We propose new strategies for long-term planning and optimization of robustly safe aircraft trajectories in *North Atlantic Oceanic Airspace* (NAT) where the ATM is particularly complicated, with such strategies being disposable due to new surveillance and broadcast technologies.

Chapter 1 first briefly describes the current ATM system, including flight planning and traffic monitoring, and the challenges of the next generation ATM based on new technological implementations. After that, the specific features of NAT traffic situation and oceanic ATM are described in detail. Finally, the improvements that can be brought by the new technologies in this particular airspace are revealed, and the branches of the current research work are stated. The chapter is accompanied with a great amount of Appendices, that are not necessary for understanding the present study, but contain a wide broad description of the ANS for those who are interested in.

In general, the current work can be divided into three more or less independent parts, each of which is devoted to a particular approach aimed at improving the current air traffic situation in NAT and is presented in a separate chapter. Below, the brief overview of these chapters is given. All the new notions appearing in this overview are fully explained in Chapter 1.

Chapter 2 presents the results of the first part, where the current oceanic traffic conditions are considered, obliging the aircraft to follow predefined quasi-parallel routes established in NAT, referred to as *Organized Track System* (OTS). First, the approaches existing in the literature are discussed, and then, a new approach addressed in the present study is described. We favor the re-routing maneuvers via OTS, in order to decrease congestion in pre-oceanic continental airspace. Then, we optimize the given trajectories using stochastic algorithms in order to find a safe (conflict-free) flight configuration, and we reveal the benefits obtained from using the *Reduced Separation Standards* (RSS). The preliminary results of this work were presented at ICRAT[5] conference in 2012 [11], and the final results were published in IEEE Transactions on Intelligent Transportation Systems [12].

In Chapter 3, related to the second research part, we simulate the aircraft trajectory prediction using *Wind Networking* (WN) approach. Nowadays, the main source of errors in time prediction along a 3D trajectory is the uncertainty in meteorological data, especially the wind. First, we discuss the questions of wind forecast, airborne wind measurements, wind models and their accuracies, relying on the previous studies. After that, we present the WN approach, that permits the aircraft to exchange measured wind data and to adjust their predictions using more recent and more exact information, thus producing more precise 4D trajectories. Finally, the benefits obtained from the application of WN are demonstrated. The results of this work were presented at DASC[6] conference in 2014 [13].

Chapter 4 presents the last part of study, devoted to the introduction of the *Free Flight Concept* (FFC) in NAT. As usual, the chapter starts with the discussion of the previous related works, followed by the presentation of our innovative approach. This part is

[5]ICRAT 2012, 5th International Conference on Research in Air Transportation, University of California, Berkeley (USA)

[6]33d DASC, 33rd Digital Avionics Systems conference, Colorado Springs, Colorado (USA)

done in collaboration with NASA[7] Ames Research Center[8] that provides us with wind-optimal trajectories for several full days of NAT flights. We apply a stochastic algorithm aimed at reducing the number of (up to eliminating) conflicts induced by these flights. These trajectories are then reevaluated to obtain their new cost (e.g. fuel consumption, etc.). The aim of this study is to eliminate as many conflicts as possible on the strategic level, while keeping each trajectory as close as possible to its optimal route. The results of this study are to be presented at the next ATM seminar[9] [14].

The work is crowned with a conclusion, where all the obtained results are summarized, their significance is estimated, and possible research extensions are highlighted.

[7] National Aeronautics and Space Administration, the US government agency responsible for the civilian space program and aerospace research.

[8] One of the 10 NASA field Centers, located in the Silicon Valley (California, USA).

[9] ATM2015, Eleventh USA/Europe Air Traffic Management Research and Development Seminar, that will take place in Lisbon, Portugal in June 2015.

Chapter 1

Problem Context

In this chapter the main Air Navigation System (ANS) notions are introduced and particularities are explained. The chapter starts with the description of the current Air Traffic Management (ATM) system in general, including flight planning, traffic monitoring and aircraft separation. Further, the NextGen and SESAR propositions and solutions for the future ATM modernization are stated. Finally, the general properties being defined, the ANS scope is restricted to the case of North Atlantic Oceanic Airspace (NAT) and the features specific to this particular context, considered in the sequel of this study are highlighted.

1.1 Introduction to Air Traffic Management

The primary purpose of ATM worldwide is to prevent collisions, organize and expedite the flow of traffic, and provide information and other supports for pilots. This section presents an overview of ATM main components, concepts and systems.

1.1.1 Main components of Air Traffic Management

The main task of the ATM is to ensure the *safety* and *efficiency* of air traffic progress. Safety is supported through *separation maintenance*, and efficiency is afforded through *congestion management* (defined in detail in Section 1.1.3). In addition to this, ATM is also responsible for providing *flight information* to aircraft, and alerting corresponding

authorities about aircraft in need of *search and rescue*. Thus, three prior components can be distinguished in the ATM:

- *Air Traffic Control* (ATC) is the process by which aircraft are safely separated in the sky as they fly, and at the airports where they land and take off.
- *Air Traffic Flow Management* (ATFM) is an activity that assures the airspace capacity requirements[1] and is undergone before flights take place.
- *Aeronautical Information Services* (AISs[2]) are aimed at promoting the safety, regularity and efficiency of air navigation.

Thus, shortly speaking, ATC has a *tactical* mission, while ATFM is concerned with the more *strategic* task. Further in this section, the ATC features are presented in more details.

ICAO (International Civil Aviation Organization) has divided the world airspace into Flight Information Regions (FIRs), that define which country controls a particular airspace, stipulate the procedures to be used, and provide the basic level *Air Traffic Services* (ATS[3]) [15]. FIRs are the largest regular division of airspace in use in the world today[4] (Fig. 1.1).

[1]For safety reasons, the number of flights ATC can handle at any one time is limited. Sophisticated computers used by ATFM precalculate aircraft positions at any given time moment, and check whether the responsible controllers can safely cope with the flight. Otherwise, the aircraft is delayed on the ground until it is authorized to take off.

[2]AISs are responsible for the assembly, producing and distribution of all aeronautical information necessary to airspace users, including weather prediction, information on safety and navigation, technical, administrative or legal matters and their updates. The information can be given in the maps displaying air routes, ATC centers and the areas of their responsibility; in the notes or publications; or in form of orders to be fulfilled

[3]Basic ATS include a *flight information service* and an *alerting service*. They provide information necessary for the safe and efficient conduct of flights, and they alert the relevant authorities if an aircraft is in distress.

[4]Every portion of the atmosphere belongs to a specific FIR. In general, the FIR boundaries follow the geopolitical boundary of the underlying country, and this country is responsible to control its own sovereign airspace. It is the ICAO that determines who provides ATC services within international airspace and oceanic airspace.

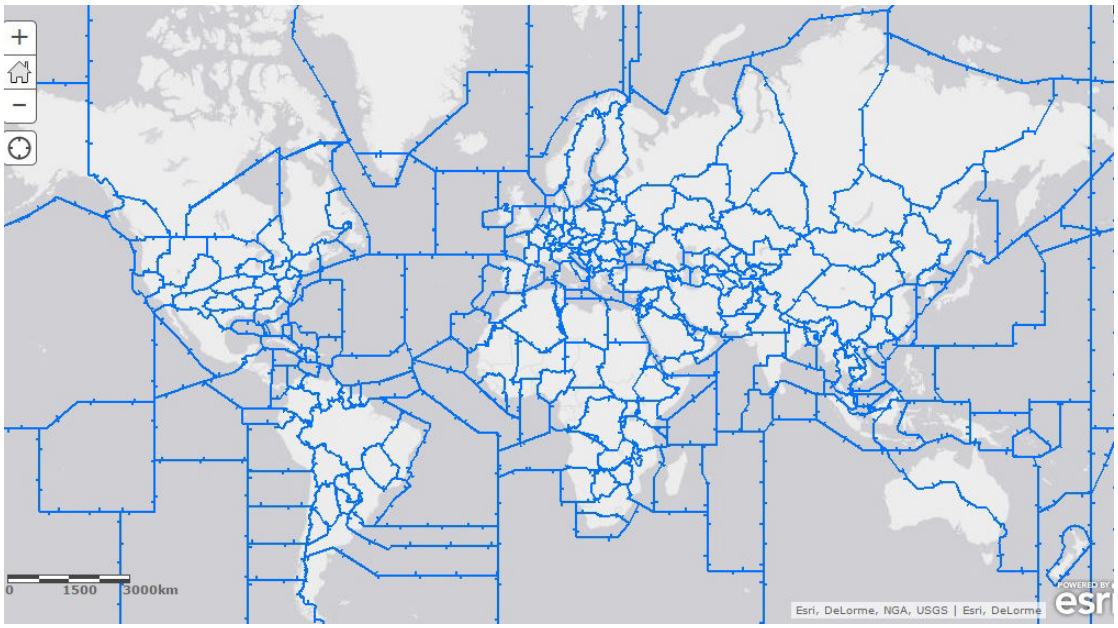

FIGURE 1.1: World Flight Information Regions[5]

Nowadays, the two sets of regulations governing all aspects of civil aircraft operations are known as VFR[6] and IFR[7]. Most commercial aircraft are designed to be operated via IFR. Thus, further in the present study we consider only IFR flights. The airspace where the ATC separates the IFR flights (and where VFR flights provide their own separation, if permitted by weather) is called the *controlled airspace*. Within each FIR, the ATC responsibilities can be globally subdivided between:

- *Local ATC*, destinated at separating the aircraft in the immediate vicinity of *the airport*, and usually performed by:
  - the *Air Traffic Control Tower* (ATCT), or
  - the *Terminal Radar Approach Control* (TRACON);
- and *En-route ATC*, whose main function is to separate aircraft traveling *between* airports.

[5]From:
http://www.arcgis.com/home/webmap/viewer.html?webmap=724dfc8916604483a0ab06b4f3cbe57f

[6]The *Visual Flight Rules* establish the rules, under which a pilot operates an aircraft in *Visual Meteorological Conditions* (VMC), when he is able to guide the aircraft with visual reference to the ground, and by visually avoiding obstructions and other aircraft. In VMC, the weather must be better than basic VFR weather minima, specified in the rules of the relevant aviation authority.

[7]The *Instrument Flight Rules* govern flights in the conditions, when flying by outside visual reference is not safe, where the navigation is based with reference to instruments in the flight deck and to electronic signals.

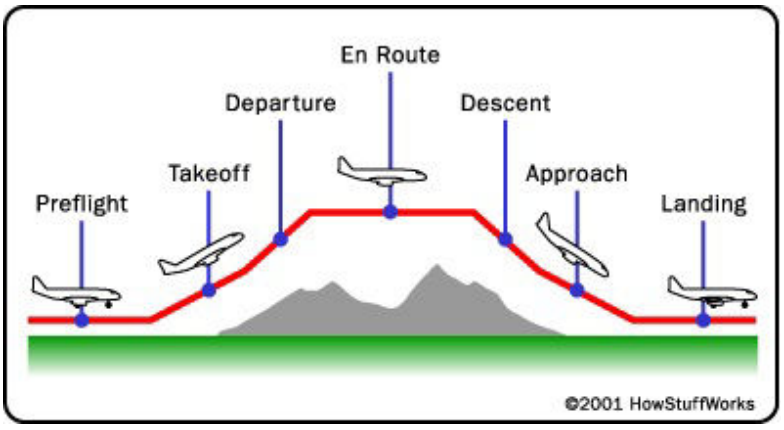

FIGURE 1.2: Typical flight phases[8]

The local ATC will not be considered in detail in the present study. The en-route ATC is performed by *Air Route Traffic Control Centers* (ARTCCs). Depending on the size and the complexity of a particular airspace, a FIR can be divided into several ARTCCs[9]. Furthermore, each ARTCC is subdivided into numerous smaller areas called *sectors*[10].

Typical *flight phases* (or, *flight profile*) are presented in Figure 1.2. All of them, from *Preflight* (starting with taxi-out) to *Landing* (finishing with taxi-in), require to be approved by ATM. For each such phase, particular ATC operations are established and separate controllers are delegated. Some details on such operation can be found in Appendix A.

The ATC functionality is supported by the means of the *ATC generic systems*, that are shown in Figure 1.3 and listed below [16, Chapter 13]:

- Communication Systems, providing the possibility for pilots and controllers to interact with each other;
- Navigation Systems, permitting the aircraft to fly exactly the defined routes, or *Aircraft Trajectories* (ATs);
- Surveillance Systems, allowing the controllers to monitor the traffic situation.

[8] From:
http://science.howstuffworks.com/transport/flight/modern/air-traffic-control1.htm

[9] For example, the national airspace of the USA is controlled by 24 ARTCCs. In Europe, usually only one ARTCC is assigned with each country.

[10] The sectors are designed in a logical manner, in order to take into account prevalent traffic flows and to facilitate the controller task of aircraft separation within a sector. Each ARTCC is partitioned horizontally and vertically; usually, two groups of sectors are identified: low-altitude and high-altitude groups.

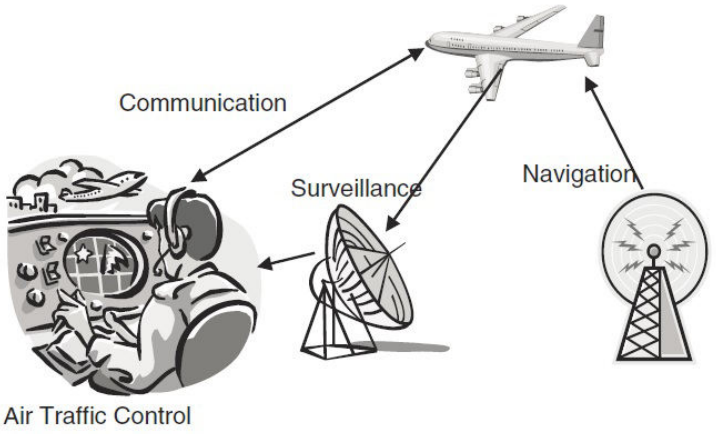

FIGURE 1.3: Generic systems of Air Traffic Control[11]

Different types of existing means of communication, navigation and surveillance are described in Appendix B. The availability and the choice of these types determines in turn the type of *separation norms* that are applied by ATC to separate the ATs with a given rate of safety. Before introducing different existing separation standards (in Section 1.1.3), we need to define precisely what an AT is, and how it is elaborated and established. This process is known as *Flight Planning*, and is discussed in the next section.

1.1.2 Flight Planning

Before any flight can occur, several pre-flight operations should be fulfilled in order to meet the regulatory requirements of airline network and ANS in general. This work is started by the *Airline Planning Process* (APP), performed by the responsible airlines and consisting of identifying the airline fleet, the network of preferred routes, and the appropriate flight schedule [16]. The APP is described in detail in Appendix C. The next important task is the *flight planning*, *i.e.,* selecting the *best path* (in terms of time, fuel burn, ride conditions, etc.) given the available information (destination, desired departure time, etc.).

All aircraft being part of the Global Air Traffic (GAT), from a business aeroplane to an airliner, prior to being operated, must *file* (work out) a *Flight Plan* (FPL) beforehand and send it to a central repository, where these FPLs are analyzed and computed. FPL elaboration is a complicated process that involves a large number of parameters and

[11] From [16]

conditions to be taken into account. It is started by airlines, and finalized by ATM services (see below). The resulting FPL is the mean by which a dispatcher communicates the details of flights to pilots (available one hour before departure time, but is subject to last-minute changes). The FPL can be directly programmed into the aircraft automation. The main contents of an FPL are given in Appendix D.

To summarize, the elaborated FPL provides the detailed *flight path*, or *Aircraft Trajectory* (AT) to be followed in order to realize the desired *flight schedule* from origin to destination. Below, we describe more precisely the three components of an FPL, defining an AT in four dimensions (space and time, further referred to as 4D AT):

- altitude,
- speed and
- waypoints (WPs).

Aircraft *altitude* is expressed in terms of feet for lower altitudes and in terms of *flight levels* (FLs) at higher altitudes. FLs are measured in hundreds of feet (1 FL = 100 feet), but they are defined for each thousand of feet and regularly written under the form FLxx0 (e.g. FL270 = 27,000 feet). The cruise FLs used during *En route* phase of flight typically belong to the range from FL310 to FL410. More information about altitude measurement, FL definition and transition between feet and FLs can be found in Appendix E.

Figure 1.2 can be viewed as a typical *flight altitude profile* (FAP), in a first approximation: from *Takeoff* to *Approach* phases (*Preflight* and *Landing* being ground operations). An optimal FAP can be calculated based on the models of aircraft dynamics by minimizing the fuel consumption subject to certain constraints [17, Section 2.6], [18]. As a result, in an optimal FAP of an aircraft cruising at *constant speed*, the altitude should continuously increase as fuel is burned (and as a distance flown increases). In practice, such continuous FAPs are not applicable due to ATC constraints. They are rather approximated with *step climbs* (changing from the current cruising FL to the following, higher one). The step climbs can be introduced in the FPL in order to keep the resulting FAP as close to the optimal FAP as possible (see Figure 1.4 as an example, and Appendix E for more explanations). For the *Descent* phase, similarly, the optimal fuel-saving FAP is replaced by step descents.

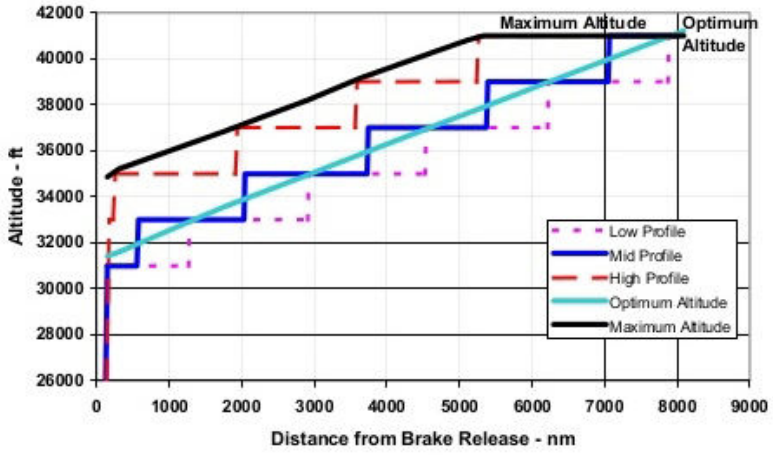

FIGURE 1.4: Continuous optimal flight altitude profile vs. step climbs[12]

The *aircraft speed* is typically described by three values:

- *True Air Speed* (TAS), the aircraft speed relative to the air,
- *Ground Speed* (GS), the horizontal aircraft speed relative to the ground, and
- *Mach number* (Mach), the ratio of the TAS to the speed of sound in the atmosphere.

TAS is traditionally measured in knots[13]. The GS is measured in knots, mph or m/s according to the applications. The GS can be determined by the vector sum of the aircraft TAS with the current *Wind Speed* (WS), as displayed in Figure 1.5. Mach, by definition, is a dimensionless quantity. It is used by the ATC in a special technique of aircraft separation, referred to as *Mach Number Technique* (MNT), whereby consecutive aircraft following the same route are prescribed to maintain appropriate Machs for a relevant portion of this route. Mach is linearly related with TAS.

The optimal flight speed profile depends on aircraft-dynamics parameters (e.g. aircraft weight), similarly to the optimal FAP. The modern aircraft are designed for optimal performance at their cruise speed, typically 475-500 knots. Thus, most common cruise Machs range between 0.75 and 0.85 [16, Section 8.3]. In general, the cruise Mach remains constant during the *En route* phase. Nevertheless, sometimes it can be changed to more desirable Mach, if accepted by ATC. More information about different ways to define

[12] From [19]

[13] Nautical miles per hour. A *Nautical Mile* (NM) is a unit of distance that is approximately one minute of arc measured along any meridian, and is set to be equal to 1.852 meters exactly

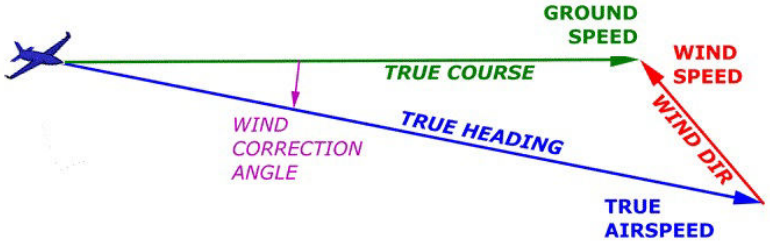

FIGURE 1.5: Aircraft true air speed (TAS), ground speed (GS) and wind speed (WS) triangle

aircraft speed is given in Appendix F. More practical formulas relating Mach, TAS and altitude can be found in Appendix G.

An optimal *Lateral Flight Profile* (LFP) can be calculated from aircraft dynamics (in an analogous manner as for FAP and speed profile) by optimizing the aircraft performance (e.g. fuel consumption) in the current conditions (surrounding traffic, weather, etc.). This involves a complex non-linear optimization problem that has been treated in a number of studies, some of which are discussed in Chapter 4. Unfortunately, the optimal LFPs are not applicable in practice because of strict ATM regulations. Thus, in general, the aircraft are prescribed to follow some predefined routes, referred to as *airways*. The network of available airways is called *En-Route Airspace Structure* (ERAS). It depends on the particular region in which the flight is operating [20, Chapter 1], [21, Chapter 1]. Some more information about different ERASs is given in Appendix H. The particular oceanic airways are described in detail in Section 1.2.2.

An AT within an ERAS can be viewed as a sequence of WPs to be followed, connected with straight segments, called *legs* (see an example in Figure 1.6). The WPs are the fixed references in the space [22, Chapter 15], that can be defined in several different ways (e.g. geographical coordinates, airways intersections, etc., see Appendix H for more details). The legs are actually the arcs of *Great Circle* (GC[14]) joining these WPs.

Once the FPL of a flight is elaborated and filed by an airline, it should be processed by the ATM. As a result, an air traffic *Clearance* (CLR) is generated [15, Chapter 3]. It should be issued prior to the aircraft departure. The CLR finalizes the definition of ATs to be flown by either accepting the proposed FPL, or modifying it, if necessary. In the latter case, however, the ATM controllers attempt to clear the aircraft on a route

[14] Also known as an *orthodrome*, the intersection of the sphere (the Earth, in navigation) and a plane that passes through the center point of the sphere

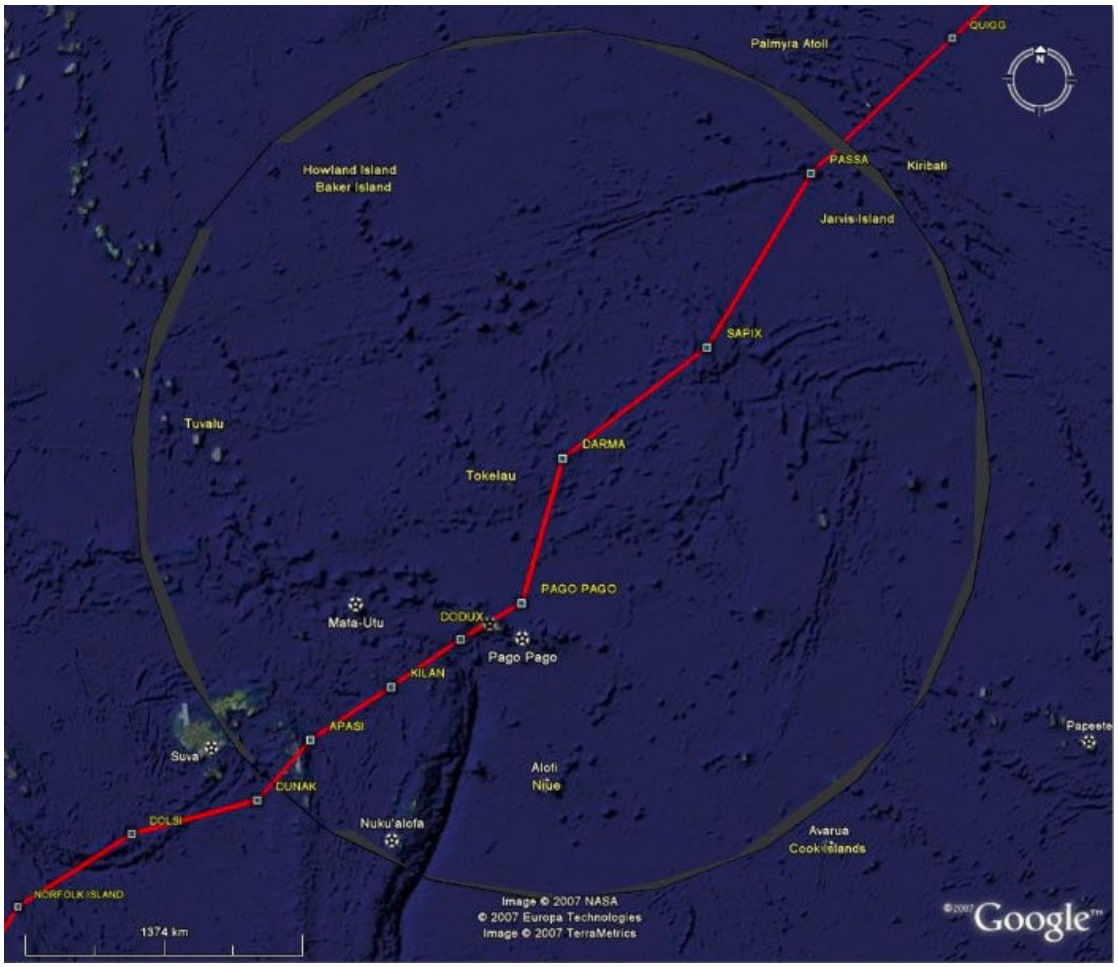

FIGURE 1.6: Waypoints on the flight route from Sydney (Australia) to Los Angeles (USA)[15]

as close as possible to its desired (optimal) FPL. Some more detail on Clearance can be found in Appendix I

The resulting ATs are strongly affected by the weather. Inappropriate meteorological conditions that are often hardly predictable are the main source of hazard occurring during flight. Weather plays an important role in a number of aviation accidents and incidents. In addition, weather is the cause of a significant number of flight delays (about 70%), and AT deviations from a nominal filed FPL (performed on ground by ATFM or en-route by ATC) all around the world (Fig. 1.7). In Appendix J, several of the most important particular meteorological conditions are listed [23].

The main meteorological component the aircraft and ATC must always face is the *wind*. The forecast winds should be taken into account during FPL elaboration, as they effect

[15]From http://lostpedia.wikia.com/wiki/Talk:Flight_path_of_Oceanic_815

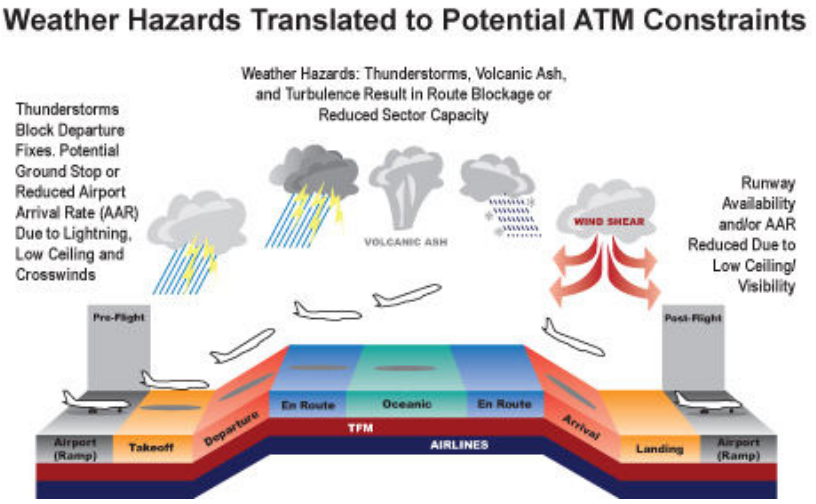

FIGURE 1.7: Weather conditions affecting flights[16]

the estimated times of passing the WPs recorded in FPLs. More details on wind forecast and AT prediction using winds are given in Chapter 3.

1.1.3 Separation and congestion

In this section, two crucial notions of ATC - *separation procedures* and *congestion management* - are explained in detail. As stated above, one of the main tasks of ATC is to maintain the safe *separation* between aircraft en-route and within terminal areas. The precision of ATC is constrained by the performance of ATC generic systems[17] (in particular, surveillance systems).

Thus, the ATC must consider the worthiest scenario and ensure a sufficient margin of safety, covering even the eventuality of the maximal possible errors. As a result, the separation between the aircraft cannot be reduced below certain minima, known as *Minimum Separation Standards* (MSS). ATC accomplishes this condition by reserving a block of airspace for each aircraft, further referred to as *Aircraft Reserved Block* (ARB). It is assumed that an aircraft could be located anywhere withing its ARB. Thus, ATC must separate each ARB from the ARBs of other aircraft, *i.e.,* ensure that the ARB of one aircraft does not overlap any other ARB[18] (see Figure 1.8). The situation in

[16] From http://www.avmet.com/avmet/index.cfm/our-business1/

[17] The ATC generic systems performance depends on many variables, such as ground-based and airborne navigation equipment errors; relatively slow update rate, resulting in uncertainty in aircraft position; communication delays; variability of pilots responses and their mistakes; wind alofts and weather forecast errors, etc.

[18] That is the only way to ensure that the aircraft remain safely separated.

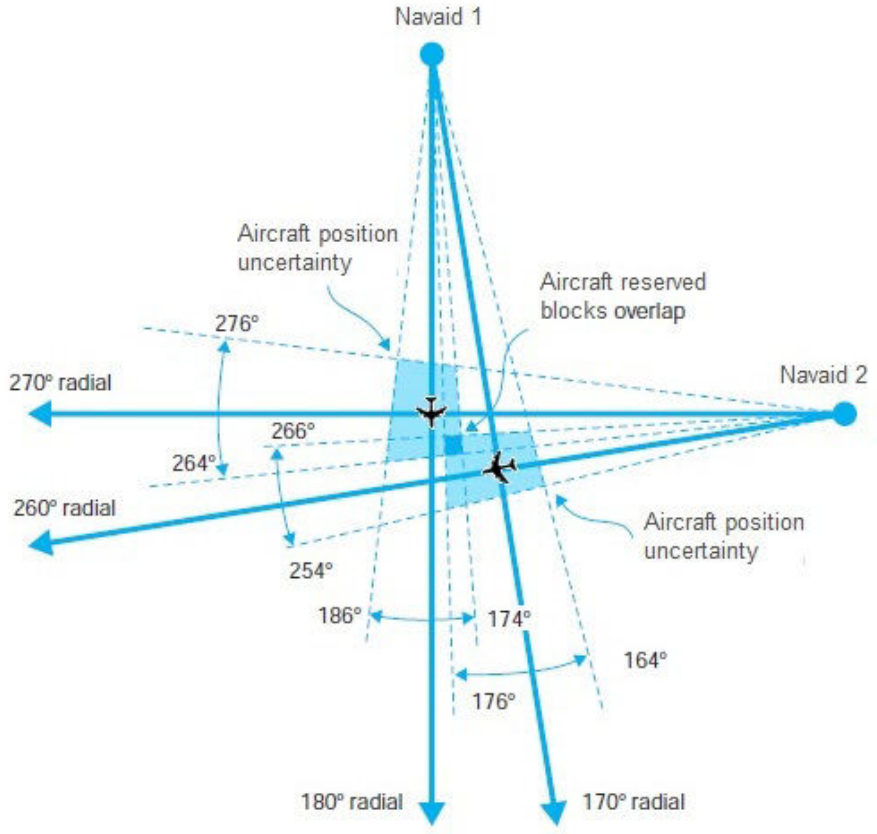

FIGURE 1.8: Separation of aircraft reserved blocks[19]

which such an overlap does occur, is known as *separation error*, or *separation violation*, or *conflict* (from [15, Chapter 7]).

Different separation techniques are applied for different flight phases, among which:

- *En-route separation*, described below, and
- *Terminal separation*, not considered here in detail.

There exist three basic methods used by controllers to separate aircraft:

- Vertical separation,
- Lateral separation, and
- Longitudinal separation.

[19] From [15]

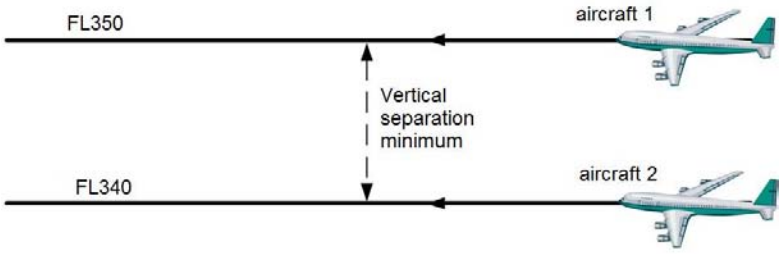

FIGURE 1.9: Vertical separation

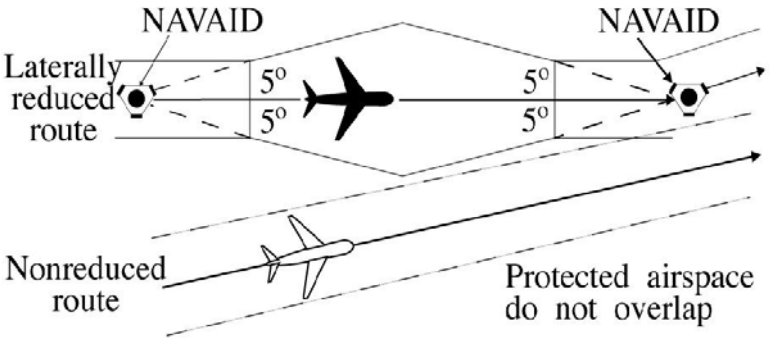

FIGURE 1.10: Lateral separation of aircraft on different routes[20]

Vertical separation is assured by assigning different altitudes/FLs to different aircraft (Fig. 1.9). As long as this altitude difference exceeds the required separation minimum, the aircraft maintaining such altitudes remain vertically separated. The basic vertical separation minimum is 1,000 feet (see below). Thus, the FLs are designed in such a way that two adjacent FLs are automatically separated. ATC assures vertical separation by clearing aircraft at "free" FLs, while pilots are obliged to maintain such cleared FLs. Vertical separation is the easiest way to separate the aircraft, but its exclusive use results in inefficient airspace usage, reduced traffic flows and increase fuel costs.

Lateral separation presumes that the considered aircraft are on different routes and their ARBs does not intersect (Fig. 1.10). Thus, to be laterally separated, two aircraft should operate within different airways, whose central lines are apart by at least the required separation minimum. In addition, lateral separation is also achieved if the two aircraft are established on different radials of the same *navaid*[21] (see Appendix H for definition and Appendix B for more detail) and their ARBs do not overlap when they pass this common naviad.

[20] From http://www.faa.gov/air_traffic/publications/atpubs/atc/atc0804.html

[21] *Navigational Aids*, any device external to an aircraft specifically intended to assist navigators in determining their position and safe course, or to warn them of dangers or obstructions to navigation.

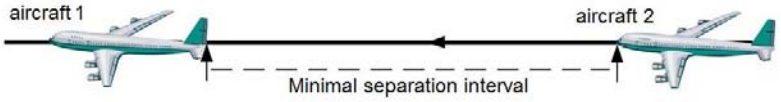

FIGURE 1.11: Longitudinal separation of aircraft on the same route

Longitudinal separation is used to separate the aircraft cruising at the same altitude along the same route, or on airways whose protection airspaces overlap (central lines are closer than the required separation minimum). Basically, longitudinal separation is applied to aircraft flying at the same TAS, or if the leading aircraft is faster than the following one, in order the prevent loss of separation due to aircraft overtaking[22]. The aircraft are prescribed to maintain a predefined *minimal separation interval* between each other (Fig. 1.11). This interval is expressed either in terms of *time* (in minutes), or in terms of *distance* (in NM) and depends on the separation technique being used, as well as on the difference in aircraft speeds and aircraft current maneuvers (climbing, descending, rerouting). Longitudinal separation is usually more efficient than vertical separation for busy airways.

Besides the three basic procedures described above, let us mention two additional separation methods that will not be considered in detail here:

- Initial separation[23], and
- Visual separation[24].

The size of ARBs (width, length and depth) corresponding to different MSS (lateral, longitudinal, vertical) is determined by various factors such as the types of ATC generic systems in use, the aircraft altitude and distance from navaids, the aircraft performance, etc. According the the availability of surveillance systems, two types of separation techniques are distinguished [15]:

- *Non-radar separation*, and

[22]Even if several exceptions to this rule exist (permitting even to separate aircraft flying the same route in opposite directions), they are rarely applied in practice

[23]Used to separate aircraft beginning or ending their flight within an airport, as standard vertical, lateral and longitudinal separations are difficult to apply in this case because of constantly changing aircraft position and altitude. Within an airport area, location of each aircraft can be determined with high precision; thus, separation intervals can be significantly reduced.

[24]Requires that either one of the pilots sees the other aircraft and provides necessary separation, or that a controller can observe both aircraft and safely separate them. It is most often applied in terminal areas.

- *Radar separation*[25].

Vertical MSS are defined to be the same for radar and non-radar separation. The vertical MSS applied to separate two aircraft depend on their cruising altitude and equipment. In the late 1990s, a new separation standard, known as *Reduced Vertical Separation Minima* (RVSM), was implemented; it reduced the basic vertical MSS below FL410[26]. Since 2010, the global airspace respects the RVSM regulation between FL290 and FL410[27] (except for several local areas). Thus, currently the following vertical MSS are established in the world airspace:

- 1,000 feet below FL290;
- 1,000 feet above FL290 and below FL410 for RVSM-equipped aircraft;
- 2,000 feet above FL290 and below FL410 for non-RVSM aircraft;
- 2,000 feet above FL410;
- 4,000 feet above FL450 in oceanic airspace.

Thus, basically the aircraft cruising on different FLs are safely separated by FL definition. Most of the airways are designed to accommodate air traffic in both directions. In order to safely separate the aircraft moving in opposite directions within one airway all along their flight, a separate group of FLs is assigned to each direction. This method is known as the *Semi-Circular Rule* (SCR). By default, SCR is based on the East/West orientation of the flight[28]: *westbound* flights (having track angle between 0° and 179°) are assigned to *even* FLs, while *eastbound* flights (with track angle from 180° to 359°) are assigned to *odd* FLs[29] (Fig. 1.12).

The basic values of *lateral MSS* are defined as follows:

- 3 NM, for terminal airspace;

[25]Radar is used by ATC as a supplemental tool, that does not completely replace non-radar separation procedures, but permits to reduce lateral and longitudinal MSS, thereby, increasing the ATC efficiency.
[26]That was permitted due to the development of improved altimetry.
[27]In general, to benefit from such reduced MSS, the aircraft must be appropriately equipped and specially certified.
[28]In some countries, due to airway structure or other local regulation, the SCR can be based on the North/South orientation.
[29]See Appendix E for formal definition of even and odd FLs

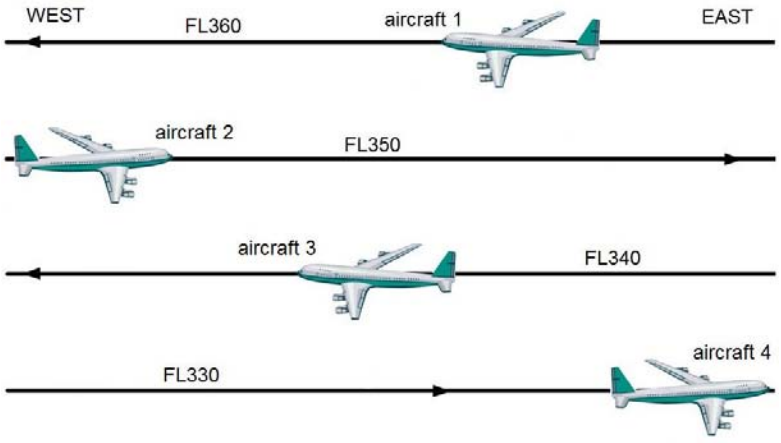

FIGURE 1.12: Vertical separation of aircraft by semi-circular rule

- 5 NM, for en-route airspace within radar surveillance;
- 60 NM, for en-route airspace not covered by radars (e.g. oceanic airspace, see Section 1.2).

Currently, huge lateral MSS are demanded for non-radar airspaces, as the surveillance there is based only on aircraft *position reports* (POSs) and can be constrained with potential communication delays (see Appendix B for more detail). Nevertheless, in some cases it can be reduced, if permitted by good communication and navigation capabilities.

The *longitudinal MSS* for *radar* airspaces have the same values as the corresponding lateral MMS:

- 3 NM, for terminal airspace, extended less than 40 NM from radar antennas;
- 5 NM, for en-route airspace, further than 40 NM from radar.

Thus, for example, an ARB of a RVSM-equipped aircraft during en-route phase is represented by a cylinder with diameter equal to 5 NM and height equal to 1,000 feet (Fig. 1.13).

Longitudinal MSS for *non-radar* airspaces are defined either in terms of time interval, or in terms of distance, and depend on the speed and the current maneuvers of the aircraft to be separated. The following basic cases of longitudinal MSS for aircraft operating along the same route in the same direction can be outlined:

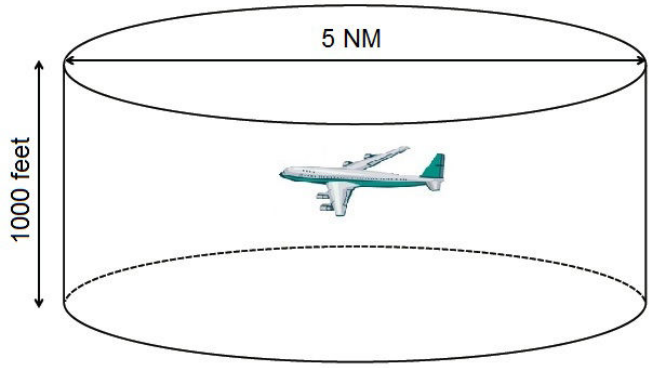

FIGURE 1.13: Aircraft reserved block within en-route radar separation

- 3 minutes, if the leading aircraft TAS is at least 44 knots greater than that of the following one;
- 5 minutes, if the leading aircraft TAS is at least 22 knots greater than that of the following one;
- 5 minutes, if one of the aircraft is climbing/descending through the cruising FL of another one;
- 10 minutes, otherwise.

For aircraft operations along crossing routes, the longitudinal MSS at crossing points can be further increased (up to 15 minutes, see Section 1.2.4 for more detail).

Another crucial notion of the ATM, in addition to the conflicts, is *Congestion*. It is primarily related with *air transportation network capacity*. As GAT grows, the demand starts to exceed the capacity at key points and at critical times. These local overloads create the airspace congestion and result in flight delays. Further, these delays are propagated to other parts of the network, amplifying the congestion there. Nowadays, ATC and airspace capacity constraints have become an air traffic limiting factor in many regions in the world. In the current work, we do not explicitly calculate the airspace capacity, and we study the potential conflicts as the sole measure of congestion. Thus, we leave a detailed discussion on capacity and congestion to Appendix K.

The management of airspace capacity, potential conflicts, congestion and the delays, induced as a result of airspace saturation, is one of the most important ATM functions. We distinguish three levels of management, that are defined in detail in Appendix K:

- *strategic level*, responsible for system capacity evaluation on a time horizon of several hours to several days;
- *pre-tactical level*, responsible for flow planning at timescales from 30 minutes to 2 hours;
- *tactical level*, responsible for traffic planning at the 5- to 20-minute time scale.

All techniques and procedures described above are used to ensure safe aircraft separation and efficient traffic flow. In reality, imposition of such procedural restrictions separate *potential* traffic, not the real aircraft. As a result, aircraft may be denied to enter a desired airspace that is actually free. In most cases, the real factor limiting airspace capacity and leading to restriction imposition is the controller's workload [24], and not airspace saturation. In the conditions of constantly growing GAT, these limitations become crucial. Thus, an ATM modernization is necessary in order to increase airspace capacity, controller's productivity and the whole system efficiency [25, 26]. Different aspects of such modernization projects are described in the next section.

1.1.4 Future of Air Traffic Management

In order to provide the potential for air traffic growth, numerous approaches aimed at improving the capacity, efficiency and performance of the ATM are under consideration. In the regions with the highest airspace congestion, *i.e.,* the USA and Europe, these approaches are joint into long-term planning projects: SESAR and NextGen. These projects generally share many elements, that are discussed below in this section. At the higher level, all modernization concepts can be subdivided into:

- modernization of technologies used in ATC generic systems;
- modernization of ATC procedures.

All the efforts are made to increase the level of ATM automatization that would significantly reduce controllers' workload and increase their productivity.

One of the goals of SESAR and NextGen projects is the development and implementation of *new technologies* that would increase the performance of ATM main functions:

flow management, communication, navigation and surveillance. Several suggestions to address this issue are mentioned below (from [15, Chapter 12]).

For *ATFM*, new sophisticated *traffic flow management programs* are under consideration, among which conflict probe program, departure delay program, and en-route sector loading program. There objective is to increase the overall system efficiency without reducing MSS.

For *ATC*, a new *En Route Automation Modernization* (ERAM) computer system that is intended to replace current ARTCC systems is currently under consideration. ERAM will be integrated with new surveillance and data processing capabilities and will provide enhanced traffic flow sequencing, traffic monitoring and control, conflict alerts, data processing and analysis systems.

The *communication* between aircraft and ground ATC centers in the future is supposed to rely less on radio signals and more on *digital data* transmitted via *data link*[30] technology.

In *navigation*, it is planned that the *Global Positioning System* (GPS) will become the primary source of data in the future. However, to do so, the ATM must elaborate strategies to deal with possible GPS disruptions, especially deliberate and long-term interruptions. GPS is discussed a little bit more in the next section.

The *navigation* would be performed with an increased level of accuracy, known as *Required Navigation Performance* (RNP). The main goal of RNP is to turn down with ground-based fixed navaid system and to use navigation technologies selected by pilots as the most suitable for each flight phase. RNP defines the navigation performance accuracy level that must be achieved by an aircraft to be allowed to operate within a defined airspace. Thus, the pilots become responsible of correctly estimating their aircraft capabilities and of advising the controllers in case such capabilities do not achieve the RNP.

In *surveillance systems* of the future, the leading role will be given to *Automatic Dependent Surveillance* (ADS) technologies, in particular, to ADS-B (*Automatic Dependent Surveillance-Broadcast*). *ADS-B* is an advanced surveillance technology that combines

[30]The overall system for entering, processing, transmitting and displaying information; designed to transmit and receive air-ground voice, alphanumeric and graphic information.

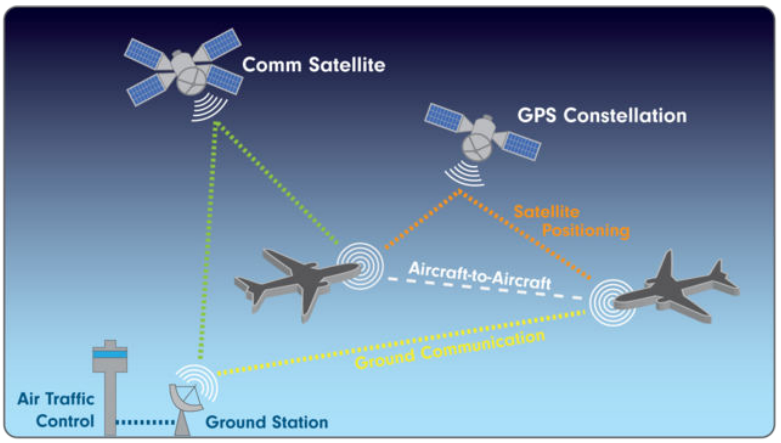

FIGURE 1.14: Automatic Dependent Surveillance-Broadcast technology[31]

aircraft positioning sources, aircraft avionics, and a ground infrastructure to create an accurate surveillance interface between aircraft and ATC (Fig. 1.14). It uses the GPS satellite signals for navigation, and data link technologies for communication and broadcasting the aircraft information to ground ATM facilities and to other neighboring aircraft. ADS-B is discussed in detail in Appendix L.

Several suggestions were also made to transform current *ATC procedures* in order to make ATC more flexible, automatic and efficient. Once implemented, these new procedures will permit increasing the number of aircraft to cruise closer to each other on more direct and optimal routes and reducing the delays. The most important of these suggestions are listed below.

Free Flight Concept (FFC) will allow flight operators to select freely their ATs, altitudes and speeds in real time. Thus, performance will be optimized in terms of distance traveled or fuel consumption. ATC controllers will intervene only in case of separation loss.

4D Aircraft Trajectories (4D ATs) will be used to define a dynamic flight route in four dimensions (space and time). A full 4D AT will include time constraints obliging an aircraft to be at a specified geographical point at a specified time (also known as *Controlled Time of Arrival*, CTA), as well as altitude and speed limitations, crossing requirements and typical navigation requirements, when necessary. If a pilot is not able to maintain the given 4D AT, it should coordinate with a controller for a new one.

[31] From http://airfactsjournal.com/2013/01/ads-b-101-what-it-is-and-why-you-should-care/

Trajectory Based Operations (TBO) is a new concept destinated to move ATC from clearance-based methods of control to more flexible methods of management. Controllers will manage ATs by evaluating traffic flows and adjusting individual trajectories that present a risk of separation violation. Automated conflict probes will be developed to constantly monitor ATs, to recognize potential conflicts, and to provide possible resolutions to controllers and pilots.

Flexible airspace management will make the ATC flexible enough so that sector boundaries and other elements of airspace structure can be adjusted in real time if necessary to accommodate changing traffic flows. This concept will help to avoid the artificial areas of congestion that are created by rigid systems of airways and sectors.

Collaborative Air Traffic Management (CATM) is an attempt to accommodate the maximum of aircraft operator preferences by imposing restrictions only when actually needed. Thus, CATM will satisfy the real-time aircraft demand rather than constraining demand to match the system capabilities. Pilots will also be allowed to advise possible resolutions of imposed restrictions in accordance to their operational efficiency.

Airborne separation, or *aircraft delegated separation* is a regime where the pilots are totally responsible to keep their aircraft safely separated from the surrounding traffic. It becomes envisage thanks to the increased confidence of generic systems. This concept also supports the implementation of the FFC and results in reduction of MSS.

To sum up, new generation ATM will have a decentralized and distributed structure, with separation and management tasks shared between ground controllers and flight crews. This will significantly increase the ANS performance in many aspects. The current study aims at elaborating several new approaches in the framework of new generation ATM in order to improve the air traffic situation in NAT. In the next section, the particularities of NAT are highlighted.

1.2 Air Traffic Control in North Atlantic oceanic airspace

In the previous section, the global ATM system is described via its general components and typical procedures. In this study, however, we do not consider the *global* ANS as this are of investigation is too broad, but we restrict the scope to the air traffic situation

in the *North Atlantic oceanic airspace* (NAT). Below, we present a list of notions that will be taken into account in the present research.

- We consider the flight within a *limited airspace region* referred to as *NAT*, and which is carefully defined in Section 1.2.1.
- As a consequence, we restrict our study to the sole *En-route phase* of the flights.
- As NAT traffic is composed mostly of commercial subsonic jet aircraft [27, Section 4.1], we only consider such types of aircraft in our study.
- Flights can *change their Mach and FL* as defined in the regulations that are stated in Section 1.2.3.
- Among all possible meteorological conditions, we only take into account the *winds*.
- We consider that flights operate within a modernized ATM, supplied with *new generation surveillance and broadcast technologies*, in particular *ADS-B*. Thus, aircraft en-route position can be precisely determined on one hand, and aircraft can broadcast all the demanded information to ATM and to surrounding traffic. Aircraft can also receive the necessary information from neighboring aircraft in real time.
- We suppose that *all the aircraft* in the study case are *appropriately equipped* so that new generation ATM concepts, *i.e.,* FFC and airborne separation, can be applied.
- This motivates the fact that the *reduction of the current MSS* explained in Section 1.2.4 is assumed.
- We are mainly interested in *conflict resolution*, taking the number of potential conflicts as the only measure of congestion.
- For a great part of the work, we are placed on the *strategic level* of ATM, attempting to find a conflict-free flight configuration for a given set of flights within one day before these flights take off (Chapters 2 and 4).
- Another part of our work addresses the *pre-tactical level* of ATM, predicting flight progress within one hour, and taking into account updated information about the real winds (Chapter 3).

In this section, the current air traffic situation in NAT is described and the imposed ATC regulations typical for this area are stated. After that, several ideas towards the improvement of the system are discussed and the current PhD research objectives are formulated.

1.2.1 North Atlantic oceanic airspace characteristics

NAT accommodates air traffic between two densely populated continents - North America and Europe. This airspace is divided into five *Oceanic Control Areas* (OCAs), namely: Reyjavik, Shanwick, Gander, Santa Maria Oceanic and New York Oceanic (Fig. 1.15), each of which is controlled by an independent *Oceanic Area Control Center* (OACC).

Currently, the ATC in NAT has to deal with several difficulties particular for this airspace, among which:

- high traffic density and airspace congestion: NAT is the busiest oceanic airspace in the world; there are more than 1,000 flights crossing it in each direction daily;
- the lack of possibility to perform direct controller-pilot communications for most part of NAT;
- the inability to perform standard radar-based surveillance;
- the presence of strong winds perturbing flight prediction.

The main mean of surveillance in NAT is HF[32] voice POSs (see Appendix B for detail), communicated by each aircraft to the corresponding OACC for position, progress and intent data. Pilot mistakes, communication equipment failures and poor propagation conditions can compromise the integrity of this information. In order to overcome these difficulties, ATC usually applies strategic traffic planning, and issues *oceanic CLRs* that are pre-coordinated with the appropriate OACCs. Aircraft that follow such pre-coordinated strategic oceanic CLRs are thereby guaranteed conflict-free progress to an oceanic exit, even if no ATS communications are possible with any one (or even with all) of these aircraft. Every effort is made by the initial NAT OACC to clear aircraft

[32]High Frequency

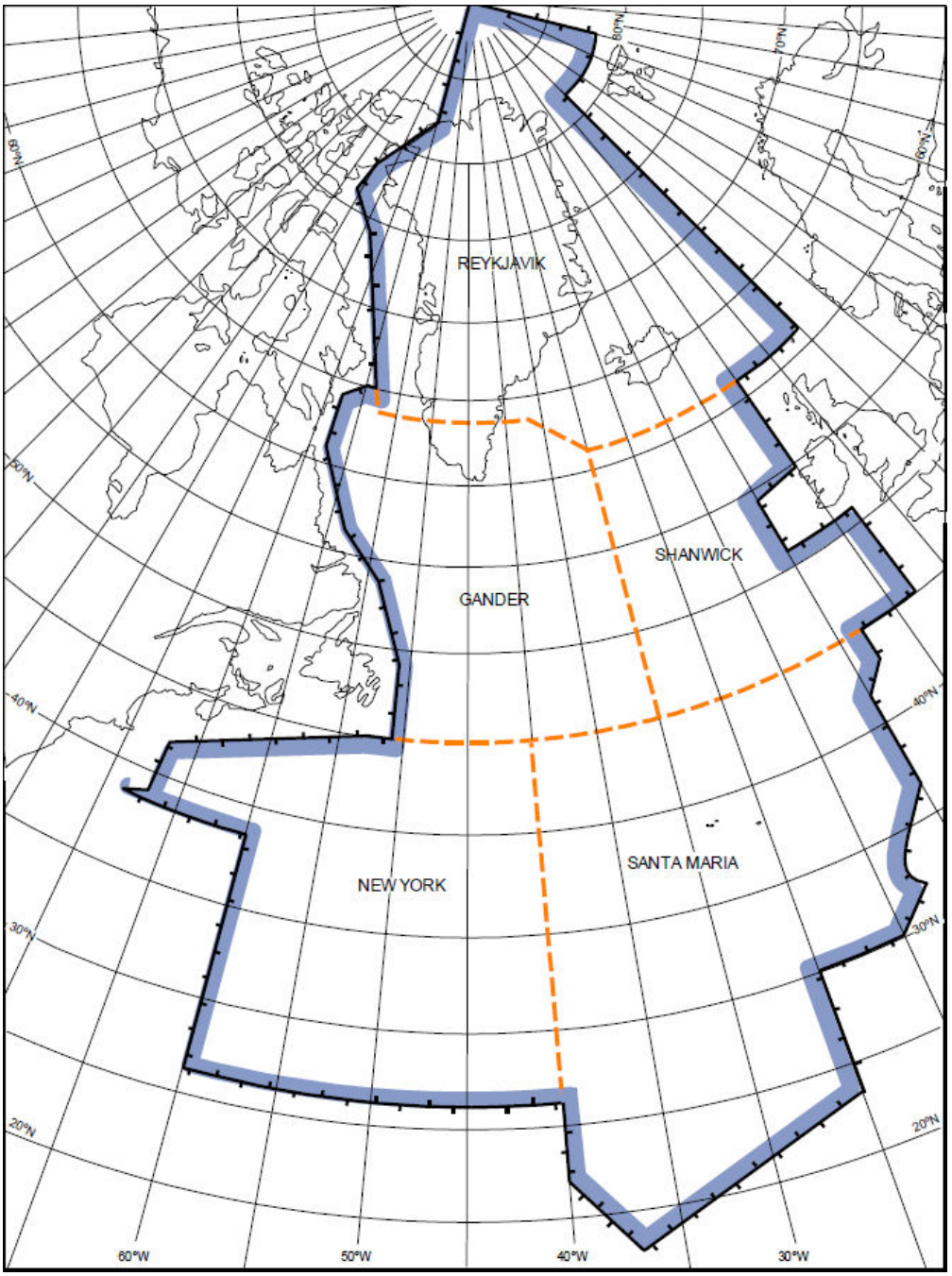

FIGURE 1.15: Oceanic Control Areas in North Atlantic MNPS airspace[33]

as per their FPL. However, this is not always possible, particularly during peak traffic flow periods [28, Section 6.6]. More details about FPLs and CLRs in NAT are given in Section 1.2.3.

In addition to this, aircraft crossing NAT are subject to very strong winds caused by the presence of *Jet Streams* (JSs). JSs are fast, narrow, predominantly west-east air

[33] From [28]

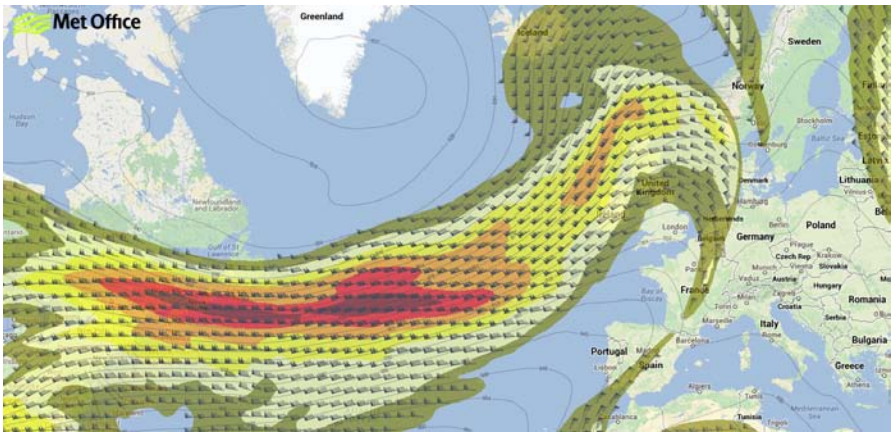

FIGURE 1.16: Jet Streams in North Atlantic oceanic airspace[34]

currents, mainly located in the upper troposphere that are caused by a combination of the Earth rotation and atmospheric heating (Fig. 1.16). The speed of the JS is typically 100 kts but can reach 200 kts. More detail on the JSs can be found in Appendix M.

In order to ensure nevertheless the aircraft separation and flight safety, the highest standards of navigation performance/accuracy and of operating discipline are demanded. These standards are referred as *Minimum Navigation Performance Specifications* (MNPS), and the part of NAT for which these standards are mandatory is referred to as *NAT MNPS airspace* correspondingly. The flights must not be planned across the NAT MNPS airspace unless they are in possession of the appropriate approval certifying that the aircraft possesses the minimal demanded equipment, and that appropriate crew procedures and trainings have been adopted [28, ii].

The vertical dimension of NAT MNPS airspace is between FL285 and FL420 (*i.e.,* in terms of normally used cruising levels, from FL290 to FL410 inclusive). Laterally, NAT MNPS airspace extends between the North Pole and the 27th parallel (27°N) under the coverage of the first four OCAs, and the portion of New York Oceanic excluding the area that is west of 60°W and south of 38°30'N (see Figure 1.15).

1.2.2 Organized Track System

Air traffic in NAT mainly contributes to two alternating flows: a westbound flow departing from Europe in the morning, and an eastbound flow departing from North America

[34]From https://metofficenews.wordpress.com/tag/jet-stream/

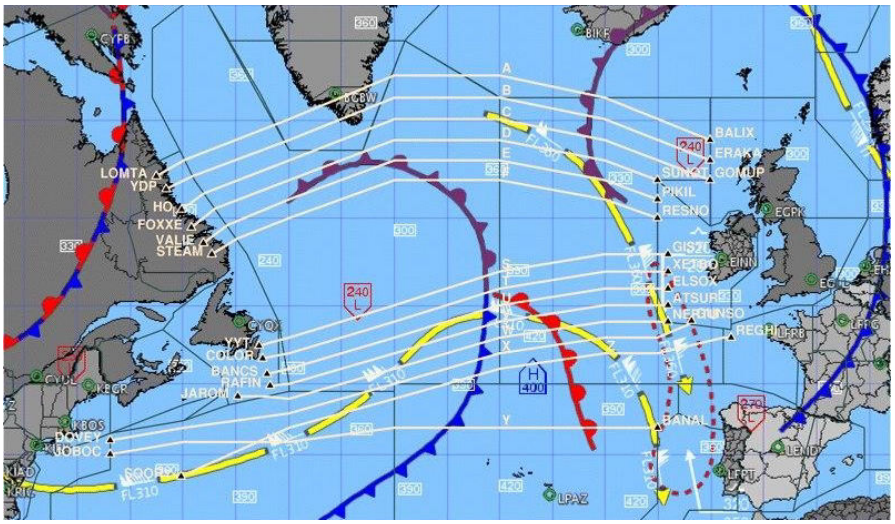

FIGURE 1.17: Organized Track Systems: westbound and eastbound[35]

in the evening. These flows originate from specific passengers demand, time zone differences and airport noise restrictions. As a result, most of the traffic is concentrated unidirectionally, with peak westbound traffic crossing the 30°W longitude between 1130 UTC[36] and 1900 UTC, and peak eastbound traffic crossing 30°W between 0100 UTC and 0800 UTC. Moreover, each of these unidirectional flows tends to be spatially concentrated around the wind optimal routes guided by the west-east JSs. To be exact, the westbound traffic attempts to avoid the inhibitory headwind from JSs, while the eastbound flow prefers to exploit the tailwind from JSs. Due to this temporal and spacial concentration, to the limited economical height band, and to large separation standards (detailed in Section 1.1.3), the NAT is highly congested at peak hours [28, Chapter 2].

In order to guarantee the safe flight progress in such conditions of high congestion and low surveillance ability, a system of organized airways is constructed to accommodate as many flights as possible within the major flows on or close to their minimum-time wind-optimal routes and optimal altitude profiles. Due to the energetic nature of the NAT weather patterns, JSs in particular, consecutive eastbound and westbound minimum-time routes are seldom identical. Thus, an independent airways system needs to be established for each of the major flows. These airways structures are referred to as the *Organized Track System* (OTS) (Fig. 1.17).

[35] From http://www.turbulenceforecast.com/atlantic_westbound_tracks.php

[36] *Coordinated Universal Time*, where the first two digits stand for hour and the last two - for minutes of the Greenwich Mean Time (GMT)

An OTS consists of several (usually, from 5 to 8) quasi-parallel tracks, laterally separated by at least 1° of latitude. Each track in the horizontal dimension is represented by a sequence of GC segments (legs) joining successive significant WPs. The OTS WPs include predefined *named* WPs and *latitude crossings* of all oceanic ten-degree meridians, that are commonly planned so that the specified ten degrees of longitudes: 10°W, 20°W, etc. are crossed at *integer* degrees of latitude [28, Section 4.1]. In the vertical dimension, several FLs in the range from FL290 to FL410 are defined to be available for each track independently.

Separate OTSs are published each day for eastbound and westbound flows. Usually, they are developed 24 hours before their actual use. The appropriate OACC constructs the OTS so as to propose minimum-time tracks. This OTS construction depends on:

- the position of cyclones and anticyclones;
- dominating winds;
- airlines preferred routes;
- the availability of airline preferred FLs;
- airspace restrictions (danger or military areas);
- opposite-direction traffic requirements;
- the impact on domestic route structure.

In general, the east-west tracks are situated more northerly than the west-east tracks. The system moves slightly to the north or to the south according to the meteorological situation. The night-time OTS is produced by Gander OAC and the day-time OTS by Shanwick OACC (Prestwick). After determining the minimum-time tracks, OACC planners coordinate with adjacent OACCs, and domestic ATC agencies to ensure that the proposed system is available.

The agreed OTS is published via the *NAT Track Message* (see an example and explanation in Appendix N) and can be accessed by the interested users. In such messages, the most northern track of westbound (day-time) system is designated Track A; and the next most northern track is designated Track B, etc. In the eastbound (night-time)

system, the tracks are labeled with letters in the inverse alphabetic order, starting from Z for the most southern track (Fig. 1.17).

A typical time of publication of the day-time OTS is 2200 UTC, and its period of validity corresponds to the peak hours of the westbound traffic, from 1130 UTC to 1900 UTC. Night-time OTS is published at 1400 UTC for the period from 0100 UTC to 0800 UTC (its period of validity). To ensure a safe transition from night-time to day-time OTSs and vice-versa, a period of several hours is interposed between the termination of one system and the commencement of the next. These periods are from 0801 UTC to 1129 UTC and from 1901 UTC to 0059 UTC. During the changeover periods, some restrictions to flight ATs and FLs can be imposed.

The OTS is the most significant airways structure within NAT MNPS. In addition to this, there exist other route systems within and adjacent to NAT MNPS. We do not consider these structures in the current study because of their relatively low traffic frequency.

1.2.3 Flight progress in NAT

Currently, about half of all flights flying over NAT from North America to Europe and backwards, utilize the OTS [28, Section 2.1]. Generally speaking, the use of OTS is not mandatory for NAT flights. Aircraft may fly on random routes which remain separated from the OTS, or may fly on any route that joins or leaves an external track of the OTS. Moreover, a flight route may be planned to cross the OTS. However, in these cases, operators must take into account that OACCs will make every effort to clear random traffic across the OTS, thus, re-routes or significant changes in planned FLs are very likely to occur for such traffic.

In the remaining of this section, we consider only flights that plan to utilize the OTS, *i.e.,* that intend to operate within the OTS tracks, from their oceanic entry point to their oceanic exit point. Such flights should plan to operate on GC legs joining OTS track WPs at any of the FLs published for this track on the current daily NAT Track Message at a constant predefined Mach. The initial planned Mach and FL for the OTS track should be specified at either the last domestic reporting point prior to NAT entry, or at the OTS track entry point. The assigned oceanic FL must be achieved prior to

entering NAT and normally while the aircraft is within radar coverage. The desired FPL is communicated to the OACC via FPL messages, whose specific format for NAT is discussed in Appendix O. An FPL is normally filed after the corresponding OTS has been published and before the aircraft departure.

Step climbs and Mach changes can be included in the FPL, although each FL/Mach modification must be requested by the pilot and approved by the ATC, depending on potential traffic conflicts. FL/Mach changes are only authorized at WPs. Each such WP must be specified by geographical coordinates in latitude/longitude or as a named WP either in the FPL, or within an additional *Clearance Request Message* (RCL) issued directly by the pilots while en-route. According to flight data analysis, approximately 50% of the OTS flights perform step-climbs [27, Section 4.2]. Remark that within NAT, the aircraft are usually allowed only to climb, not to descend, in accordance to the optimal en-route fuel consumption flight profile. Current practice shows that 2-FL climbs are very rare. Moreover, speed difference between two consecutive WPs does not usually exceed 0.02 Mach.

Pilots may also request to change track within OTS, *i.e.,* to re-route from the current WP of the current track to the next WP of an adjacent track (northern or southern). Most of time, such maneuvers, if needed, are specified directly in the FPL (see Appendix O). When demanded via RCLs, in the majority of the cases the re-routing is rejected by the ATC because of the traffic density, and because of much larger MSSs that must then be imposed to re-routing aircraft (explained in detail in the next section). Thus, current practice shows that pilots do not even (or very rarely) ask for such a maneuver while en-route.

Oceanic Clearances (OCLRs) are required for all flights within NAT controlled airspace. Pilots are recommended to request the initial OCLR, that authorizes the aircraft to enter the NAT, at least 40 minutes prior arrival to the desired oceanic entry time. Such OCLRs are normally issued through domestic ground communication facilities. An OCLR contains three main elements: route (track, WPs), Mach and FL. When requesting an OTS track, the CLR request should include the next preferred alternative track. OCLR assignment is based on comparison of the aircraft requested route and FL with projected positions of surrounding traffic, and on respecting the established MSS (see the next section).

The ATC usually tries to preserve the requested or planned FLs and Machs, but this is not always possible in high-density traffic conditions. In such a case, an alternative assignment is developed; it may involve aircraft delays, lateral and/or vertical flight deviation, and/or speed modifications. If any of the route, FL, or Mach in the OCLR differs from those that were initially planned, requested or previously cleared, particular attention must be paid to such changes when the OCLR is delivered. However, the cleared FLs/Machs should rarely differ much from the demanded ones. For example, the ATC almost never assigns a Mach more than 0.01 faster or 0.02 slower than the requested one.

After obtaining and reading back[37] the CLR to enter the NAT, the pilot should monitor the forward estimated time for oceanic entry, and if it changes by 3 minutes or more, the pilot must communicate a revised estimated time to ATC. Once in NAT, and all along its OTS route, the pilots must communicate POSs to the corresponding OACC. Unless otherwise requested, POSs are to be issued when crossing the WPs defined for a track, or explicitly listed in the FPL. Thus, depending on the WP locations, POSs are issued at 45 to 60 minute intervals. A POS includes the aircraft position, expressed in terms of latitude (in degrees and minutes) and longitude (in degrees only), except when flying over named WPs. All times should be expressed in four-digit format giving the hour and the minutes UTC.

In addition to the POSs, pilots may transmit other messages to ATC:

- RCL message, already mentioned above, that contains FL/Mach change request made in order to achieve better fuel efficiency or to avoid some areas (e.g. turbulence);
- WAH (*When Able Higher*) report, that is used as a prior advice to ATC of the time or position, when a flight will be able to accept the next higher FL, in order to ensure the optimal usage of available altitudes (*i.e.,* a more effective airspace utilization while providing more fuel-efficient flight profiles)[38].

[37] The readback procedure is mandatory for HF voice communications

[38] Information provided by WAH indicates simply an aircraft future *ability* and not an advance *request* for a step climb. Furthermore, ATC acknowledgment of a WAH *is not* a CLR to change altitude.

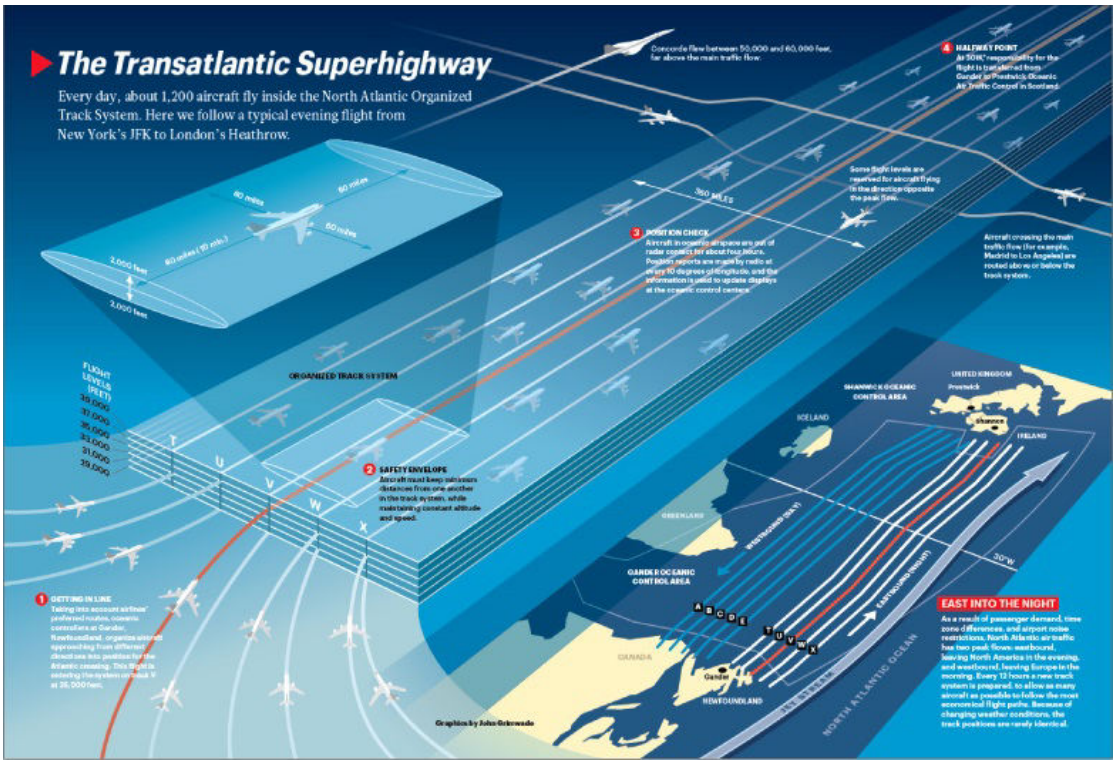

FIGURE 1.18: NAT traffic model with separation standards[39]

1.2.4 Separation Standards in NAT

Currently, the aircraft operating over the NAT are separated using non-radar techniques, as explained in Section 1.1.3. In this section, the separation within the OTS is described in more detail. The particularities of strategic flight planning (see Section 1.2.1) require that the separation between two aircraft intended to use the OTS must be established over their oceanic entry points in a way so that separation remain guaranteed throughout the oceanic crossing. As a consequence, the ATC intervention is only necessary if one of the aircraft demands a Mach/FL change.

To be exact, the *vertical* separation minimum in NAT is 1,000 feet. It is ensured through the use of different predefined FLs. The *lateral* separation minimum is set to be 60 NM, that is equal to approximately 111.11 km, or 1° of latitude. It is automatically maintained for aircraft on adjacent tracks thanks to the OTS construction[40]. Thus, the OTS tracks can be seen as corridors, for which the ARBs of aircraft flying inside these corridors surely do not intersect at least in two dimensions (see Figure 1.18).

[39] From http://www.johngrimwade.com/D1.html

[40] Actually, the OTS is constructed in this way: with tracks outlying by 1°, in order to maintain this prescribed lateral separation minimum

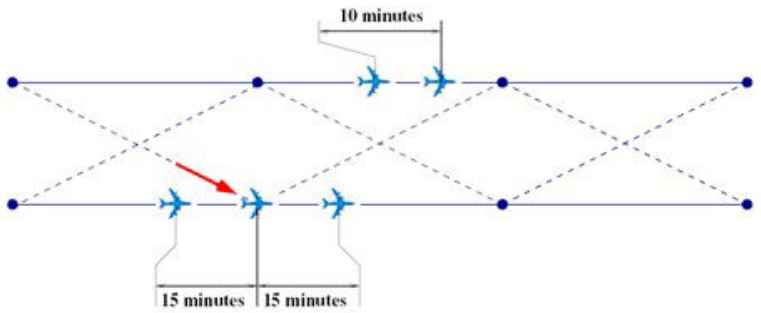

FIGURE 1.19: Current longitudinal separation standards in NAT (CSS)

Thus, the only separation that can eventually be violated within OTS, and that requires ATC surveillance, is the *longitudinal* separation. Longitudinal separation between subsequent aircraft following the same track, also referred to as *in-trail* separations, in the NAT MNPS airspace is assessed in terms of differences between ATAs (*Actual Times of Arrival*) and ETAs (*Estimated Times of Arrival*) at common WPs (from [28, Section 1.3], and are expressed in clock minutes. The maintenance of longitudinal separation is aided by the application of the MNT (see Appendix F for more detail).

Currently, the following separation minima are established in NAT for the aircraft that have reported over a same common WP, and that follow the same track [29, Section 5.4.2]:

- 10 minutes, if the preceding aircraft maintains its Mach equal or greater than that of the following one;
- 9 minutes, if the preceding aircraft is 0.02 Mach faster than the following one;
- 8 minutes, if the preceding aircraft is 0.03 Mach faster;
- 7 minutes, if the preceding aircraft is 0.04 Mach faster;
- 6 minutes, if the preceding aircraft is 0.05 Mach faster;
- 5 minutes, if the preceding aircraft is 0.06 Mach faster.

Specification that the aircraft should have reported over the same WP is important here, as their longitudinal relationship is established by their POSs and thus, in this case, any error in forward position estimates can be assumed to cancel out since they both experience the same weather. But this assumption can not be applied in the case where the antecedent flight route differs, e.g. when a particular aircraft re-routes onto an

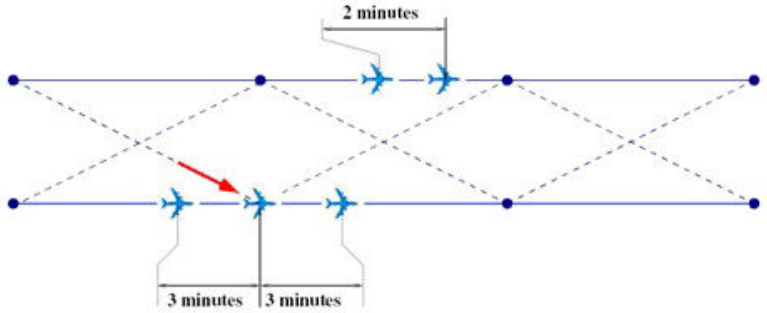

FIGURE 1.20: Reduced longitudinal separation standards in NAT (RSS)

adjacent track (Fig. 1.19), as on different routes they have experienced different weather. As a consequence, current regulations impose an increased longitudinal separation of 15 minutes in this case. In a sequel, the set of MSS defined above will be for simplicity referred to as *Current Separation Standards* (CSS).

Implementation of new-generation surveillance and broadcast technologies (e.g. ADS-B) improves the ATS performance on one hand, and controller monitoring and intervention capabilities on the other hand. Thus, such technologies provide the basis for significant reduction in the CSS [27, Section 3.2]. To be exact, it is admitted that the following separation norms could be applied for aircraft under the new generation ATM control:

- 1,000 feet for the *vertical* separation (not changed);
- 30 NM for the *lateral* separation;
- 2 minutes for the *longitudinal* separation of aircraft on a *same track*;
- 3 minutes for the *longitudinal* separation of *re-routing* aircraft (see Fig. 1.20).

In the remaining of this work, these norms are referred to as *Reduced Separation Standards* (RSS). The application of RSS reveals several remarkable benefits that are stated in the next section, and deeply examined and quantified in the present study.

1.3 Potential ways of NAT ANS improvement

Prior to discuss the potential ways aimed at improving of air traffic situation, we need to explain how *improvement* can be *quantified*, and how the *benefits* obtained from

implementing new technologies and concepts can be *measured*. To this end, *performance metrics* are developed. These metrics stand for a measure of quality of the provided air navigation services, *i.e.,* how predictable and flexible the services are, and how the user priority requests are handled. A very good summary of existing performance metrics, in particular for oceanic flights, that are the subject of the present study, is provided in [30]. The detail on these ideas is given in Appendix P.

Below, we summarize the particularities of the current ATM concepts and procedures applied to NAT traffic that were described in this chapter. The difficulties that the ATC in NAT is confronted to include:

- high traffic density and airspace congestion due to traffic temporal and space concentration into two major flows,
- the inability to perform direct controller-pilot communications and standard radar-based surveillance for the most part of NAT,
- strong JS winds perturbing flight prediction.

These difficulties yielded the following very rigid rules, standards and procedures to be maintained by the aircraft intended to cross the NAT:

- an OTS structure with predefined tracks attributed to aircraft,
- constant Mach/FLs maintained until any desired change is approved by the ATC,
- inability (or very rare possibility) to perform re-routing within NAT,
- very large CSS,

These rules decrease the potential efficiency of NAT airspace utilization as well as the efficiency of each single flight as they:

- limit the number of flights authorized to cross the NAT at the same time;
- provoke flight delays;
- result in flight deviations (horizontal and vertical) from desired ATs;

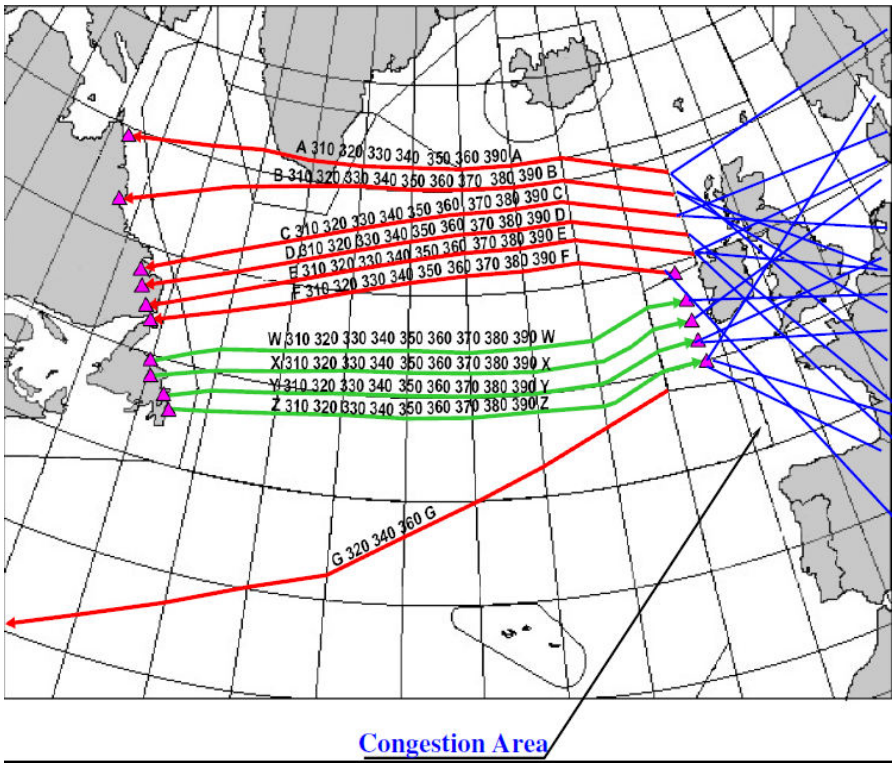

FIGURE 1.21: Congestion in the pre-oceanic continental airspace due to flight rerouting

- induce artificial speed regulations for aircraft on a common track[41];
- provoke additional congestion in the pre-oceanic continental airspaces[42] (see Fig. 1.21).

Reducing the CSS to RSS, which is available with the implementation of new surveillance and broadcast technologies, implies several significant ameliorations in NAT air traffic situation, some of which are discussed below.

To start with, we can consider to preserve the current OTS structure (construction of a structure of predefined tracks that aircraft are prescribed to follow), but while applying the RSS to separate the aircraft within this structure. In this case, the following quite evident NAT ANS improvements can be revealed:

- the number of aircraft that can be cleared on the same track increases;

[41] According to the current in-trail separation definition, the leading aircraft cannot be slower than the following one.

[42] For example, an aircraft flying from the north of the USA to the south of Europe can be attributed a northern track and is then prescribed to follow this track until the oceanic exit point. Once entering the radar-covered continental airspace, this aircraft must be re-routed to the south towards its destination airport. At the same time, there may be another aircraft, exiting a southern track and destinated at the north of Europe. The aircraft routes therefore intersect, causing thereby additional congestion.

- the number of aircraft that can be cleared on the demanded optimal FL increases;
- the expected waiting time for entering the prescribed track and FL decreases;
- the probability that an aircraft deviates from its desired track or FL, or assigned to a Mach different from that demanded, decreases;
- the number of potential routes available for a unit of airspace increases, opening thereby the possibility to create additional tracks within the OTS;
- as the track spacing thereby decreases, aircraft are more likely to be assigned to their optimal tracks;
- the aircraft ability to perform re-routing *within* the OTS, by moving from the prescribed track to an adjacent one increases;
- this in turns allows aircraft to follow more optimal routes from origin to destination, by performing the necessary re-routing within OTS;
- finally, the congestion in pre-oceanic continental airspace decreases.

Several studies aimed at identifying and quantifying the benefits coming from CSS reduction within OTS are described and discussed in Chapter 2. Continuing to investigate this track of research it appears that no previous work was conducted in the direction of allowing aircraft to perform re-routing *within* the OTS. Thus, we concentrate our interest to study the benefits that such an approach could bring to the NAT ANS.

Another possible way to improve the NAT air traffic situation, is to ameliorate the approaches designed to exploit the changing wind fields when predicting the flight progress. Previous works have revealed that inaccuracy in wind forecast is the main source of errors in flight prediction. These studies are presented and discussed in Chapter 3, where wind forecast errors are characterized and quantified.

At the same time, all aircraft are capable of performing instant meteorological data (temperature, pressure, wind amplitude and direction) measurements. These measurements can be used to update, refine and calibrate the models developed in meteorology for wind prediction. On the other hand, such measurements are made with some inaccuracy that should be taken into account. Approaches proposing to use wind measurements in wind prediction, and their application to improving real air traffic are also presented

in Chapter 3. While for the majority of such studies, the airborne measurements are incorporated into the weather forecast models, we propose an innovative approach, Wind Networking (WN), that permits an aircraft to use wind measurements obtained from preceding aircraft directly in the tactical prediction of its trajectory.

Finally, having the possibility to reduce the CSS and to predict the wind with high precision, we can think of introducing the FFC in the NAT. Here, two challenging tasks can be distinguished. The first task is wind-optimal (or climate-optimal) trajectory design, being given aircraft performance characteristics, wind fields and probably other meteorological constraints. A great amount of works is devoted to address this problem, some of which are stated in Chapter 4.

The second task to be accomplished in order to render FCC possible, is deconflicting a given set of individually-optimal trajectories. First, the conflicts are to be identified, which is more complicated in FCC as there is no longer the structure of airways and WPs. After that, identified conflicts are to be resolved. Several methodologies developed in this area are also presented in Chapter 4. Both tasks can be solved consecutively or simultaneously. In the current study, we propose to aggregate the existing methods of wind-optimal trajectory construction and conflict resolution, and then to adapt the resulting methodology to the particularities of NAT traffic. The final objective is to estimate and quantify the potential benefits offered by the FCC in this region.

Thus, as it will be seen in the following chapters, even if a great amount of approaches and methods already exists in this domain, their application to the particular NAT airspace has not been much considered and opens a vast area for further research.

Chapter 2

Optimization of aircraft trajectories within the OTS

In this chapter, the current air traffic situation in North Atlantic oceanic airspace (NAT) is considered and the benefits coming from Current Separation Standards (CSS) reduction within the Organized Track System (OTS) are investigated. The chapter starts with the discussion of existing works related to this topic. After that, we define in detail our particular research interest in this domain. We propose a mathematical formulation of the defined problem as an optimization problem and we develop two stochastic optimization algorithms to solve it. Furthermore, we perform simulations of air traffic progress in NAT, using first, the artificially-generated flight sets, and second, the real flight sets for two days of flights over NAT. Finally, we propose a possible track for further research: a new mathematical formulation of our problem as an integer linear program.

2.1 Problem statement and literature review

This section reviews research works related to reduction of the separation standards in oceanic airspace, and the induced benefits. The section is concluded by identifying a research area poorly explored in previous studies, where we concentrate our research effort.

2.1.1 Previous studies on separation standards reduction in oceanic airspaces

In this section we mention several works aimed at investigating the benefits from possible reduction of the CSS, including vertical, lateral and longitudinal separation norms, in the oceanic airspaces within the established track systems. The common point of these studies is that they perform *simulation* of air traffic (replay computationally the traffic scenarios) with different Minimal Separation Standards (MSS) (and not optimization, no decision variables involved). Moreover, only aircraft using the established track systems are considered. Finally, such aircraft are prescribed to follow *one predefined* track from its entry point to the exit point (no re-routing between tracks).

An early study of 1993 [31] analyses the advantages of reducing the vertical, lateral and longitudinal separation standards in North Pacific oceanic airspace. In this airspace, a system of tracks, similar to OTS, referred as *NOPAC*, is the primary air transportation link between North America and Far East. In the end of 20th century, the MSS within NOPAC were even greater than CSS. With new separation norms, the NOPAC could be upgraded, and seven tracks could be created at the place of the five nominal tracks. In addition to this, step climbs would more likely to be accepted, in comparison to the common situation of the early 90's, when about 40% of Pacific traffic was performed at constant Flight Levels (FLs).

In [31], simulations are performed for the real air traffic of year 1993 and for the grown traffic predicted for year 2000. The results of these simulations reveal that:

- reduction of longitudinal separation increases the capacity of the preferred routes, with a significant positive impact on the system efficiency;
- lateral separation reduction seems to affect much less the system performance;
- vertical separation reduction, together with step-climbs acceptance, decreases significantly fuel consumption.

The authors mention also, that winds have an important impact on flight operation performance, and thus, methods to improve wind prediction accuracy are to be investigated (this will be discussed in Chapter 3).

A detailed report of year 2000 [32] presents a comprehensive study on the fuel saving benefits coming from several scenarios of MSS reduction in NAT. Five scenarios with different values of vertical, lateral and longitudinal separation norms are considered in this study. In order to perform numerical simulation of air traffic, a sophisticated traffic model is needed. In [32], first an overview of models of oceanic traffic (existing by year 2000) is given. Nevertheless, Gerhardt-Falk *et al.* consider these models insufficient. Thus, they introduce a new NAT traffic model: the *Integrated North Atlantic Air Traffic Simulation Model* (INATSIM).

The results of the simulations confirm that considerable benefits could be expected from separation standard reduction for several ATC criteria, *i.e.,*:

- fuel savings (up to 0.8%),
- communication volume (increased by not more than 1.5%),
- step climbs, requested and granted (up to 65%),
- detected conflicts (decreased almost by twice).

Moreover, these results show that the simultaneous reduction of vertical, lateral and longitudinal separation tends to increase these benefits.

In [33] Williams *et al.* investigate the benefits obtained from implementing the *Airborne Separation Assurance Systems* (ASAS) *In-Trail Climb* (ITC) procedure in the *South Pacific oceanic airspace* (SOPAC). The main particularity of the SOPAC is that the interactions between flights:

- are infrequent, on one hand, due to the user preferred routings and to the small number of daily flights;
- result in increased *contingency fuel*[1] requirements across all the flights, on the other hand, because of the long stage length.

The ASAS ITC allows an *appropriately equipped aircraft* (further referred as EQA; as opposed to *non-equipped aircraft*, denoted as NEQA) to climb through an FL and bypass

[1]The amount of fuel carried in addition to the fuel requirement specified by the ATM and company policies, in order to create the reserve for unexpected situations, e.g. inefficient FAP due to traffic interactions or WSs different from the forecast.

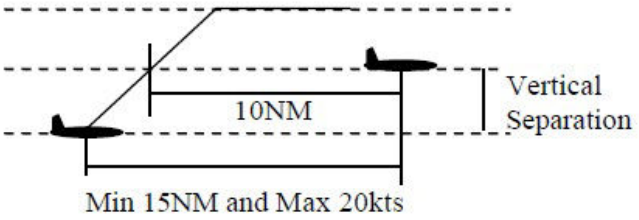

FIGURE 2.1: Longitudinal separation using ASAS ITC procedure[2]

an aircraft (also EQA) cruising at this FL with reduced longitudinal separation of 10 NM (note that the nominal longitudinal separation is 10 minutes, which is set to be equivalent to 80 NM in this study). This requirement translates into an initial longitudinal separation between two aircraft of at least 15NM for the *speed closure rate*[3] of up to 20 kts (Fig. 2.1). This procedure can be authorized due to the availability of advanced ADS-B (Automatic Dependent Surveillance-Broadcast) information. In [33], all the flights are supposed to be appropriately equipped[4], and six scenarios with different MSS are investigated in the simulations.

The results of the simulations demonstrate evident benefits from reduction of the separation standards and from applying the ASAS ITC. These benefits translate into:

- reducing the average fuel consumption (up to 1.3% per affected flight);
- reducing the variance in fuel consumption per flight (up to 1.2%), and thus,
- increasing the accuracy in fuel estimation per flight, and
- reducing the amount of fuel carried;
- reducing the aircraft operational cost (by almost 300M$ per month);
- additional cargo revenue potential (about 12M$ per year).

A similar study was performed by Williams *et al.* in [34] for NAT air traffic. The main differences with the study described in [33] are listed below.

[2]From [33]

[3]Or, *closing speed*, the rate of decreasing distance between two objects moving towards each other (not necessarily in opposite directions).

[4]Actually, the aircraft in NOPAC tend to be the first to be equipped in the frame of ATM modernization projects.

- The ASAS ITC procedure (permitting a climbing aircraft to pass a cruising aircraft at longitudinal separation of 10 NM) is applied to the flights within the OTS in NAT.
- In addition to the ASAS ITC, the introduction of the *Climb Advisory Request Assistance Tool* (CARAT) was investigated. CARAT is a tool that provides the pilots with increased awareness of the surrounding traffic. It has an advisory function and does not contribute in decreasing the MSS, but it favors more frequent climb requests thanks to more information available, which results in more frequent step climbs.
- Different aircraft equipage levels (of ADS-B, CARAT and ASAS ITC) are considered.
- The EQA are authorized to perform step climbs in order to follow their optimal Flight Altitude Profiles (FAPs), while NEQA are restricted to a single FL.

The main results obtained in [34] are as follows:

- the percentage of flights with benefits (60-65%) is much higher than the percentage of penalized flights[5] (35-40%), and the average benefits per flight (4-5%) are also higher than the average penalties per flight (about 3%);
- on average, flights benefit from separation standards reduction, regardless of the equipage; thus, even NEQA do realize fuel and time savings;
- however, these benefits are higher among the CARAT/ASAS EQA (up to 10 times) and they increase with equipage; thus, it tends to motivate the airlines to equip their aircraft.

A similar approach is further discussed in [35]. Here, the special procedure for separating a climbing aircraft, analogue to ASAS ITC, is referred to as *ADS-B In-Trail Procedure* (ITP). It allows the aircraft equipped with ADS-B In to perform step climbs through a cruising level of another aircraft (also EQA) on the same track with reduced separation, resulting in initial separation of 15 NM between the aircraft concerned. In addition

[5] Some flights may experience penalties from being constrained by others having obtained their desired FL earlier.

to the ITP, the standard *Situation Awareness* (SAW) is also considered in this study. SAW is the analogue of CARAT in [34]; it does not impact the MSS, but it favors climb requests by pilots, awared of the current traffic situation and of FLs availability. Even if the basic ideas in [35] are similar to those discussed in [34], the methodology and the investigated scenarios are different.

Only the eastbound OTS is considered in [35], as it has been shown that westbound traffic flow gives similar results. Various values of the following parameters are considered and the corresponding scenarios are simulated in the study:

- the percentage of aircraft equipped with ADS-B (Out/In);
- the density of aircraft in the NAT OTS;
- the ITP capability, *i.e.* whether an aircraft equipped with ADS-B In is capable to perform the ITP.

Comparing the climb-request approvals over the scenarios, Chartrand *et al.* note that, on the one hand, the percentage of approved requests increases (up to 70%) as ADS-B In equipage increases, but on the other hand, the majority of these requests are non-ITP requests. This means that the possibility for aircraft to change their altitudes exists in the OTS already nowadays, but aircraft are not aware of this possibility. The authors conclude that if all aircraft that desire a FL change did make a request, then about half of these requests could be approved in the current system. However, it would almost certainly lead to an overload of Air Traffic Control (ATC). Thus, a solution is to provide the mean by which an aircraft could make more informed requests, which is the objective of ADS-B ITP.

Comparing the fuel savings, the authors noted that:

- combination of SAW and ITP is more efficient than SAW alone, but the contribution of SAW to the savings is greater than of that of ITP;
- the probability of ADS-B In EQA saving fuel is increased compared to NEQA; however, the savings of NEQA are evenly distributed around 0, thus, the NEQA are not penalized by the increased number of EQA.

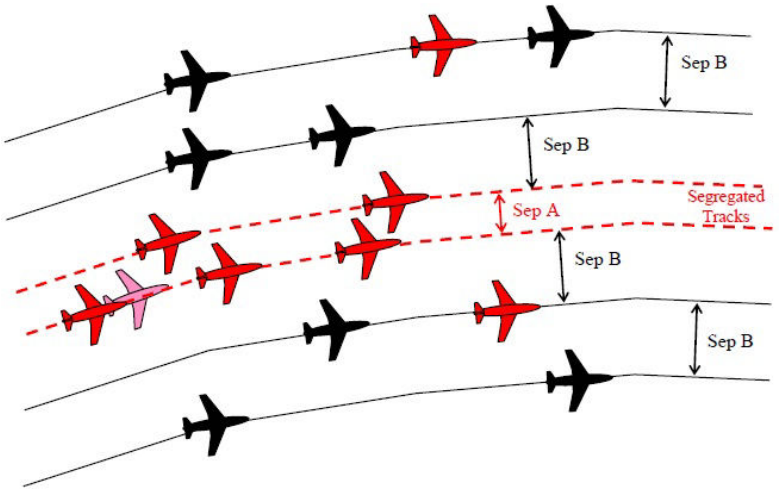

FIGURE 2.2: Creating of segregated tracks within the OTS with reduced lateral separation[6]

In [36], Williams and Greenfeld also consider the NAT OTS, but in order to improve the step-climb procedures, they focus on improving the horizontal flight procedures by reducing longitudinal and lateral separation standards. In this study, the reduced MSS of 30 NM (for both longitudinal and lateral separation minima) are applied to the flights that are appropriately equipped (EQA). Longitudinal separation reduction is introduced by simple reduction of the minimal authorized spacing between two consecutive EQA. The reduction of lateral separation is supported within OTS by creating intermediate additional tracks, referred to as *segregated tracks*. These tracks are reserved for EQA only. They are separated from each other by reduced separation minimum, and from nominal OTS tracks by standard separation minimum of 1° (see Fig. 2.2). The simulations are performed separately for the two cases:

- the OTS consisting of the regular nominal tracks only, and thus, the flights benefit only from longitudinal separation reduction;
- the OTS adapted to include the segregated tracks in addition to regular tracks, where the traffic flows for EQA/NEQA are separated by segregated/regular tracks respectively.

Obviously, the amount of benefit depends on the frequency and distribution of EQA. Thus, different levels of equipage are considered in the study. Moreover, simulation with

[6] From [36]

predicted NAT traffic are performed for several years in the future. These simulations rely on the following assumptions:

- flights do not switch tracks once entered the OTS; thus, the traffic on one track can be considered independently of the traffic on the adjacent tracks;
- EQA are authorized to follow their optimal step-climb FAP and speed profile, while NEQA are limited to a single FL within OTS;
- EQA maintain the reduced MSS with other EQA, and can be assigned a segregated track; NEQA maintain the current MSS with other aircraft (either EQA or NEQA) and are not authorized to enter segregated tracks.

The main benefits are:

- average total cost savings per flight increase with equipage level and with demand level (up to 0.45%, equal to 182$ per flight);
- for a same demand level, the percentage of flights that benefit from reduced MSS increases with equipage, as well as the percentage of flights with penalties; however, the average penalty per flight remains lower (from 3 to 7 times) than the average benefit;
- the benefits from additional cargo revenue are on average 20% higher for EQA than for NEQA, while the penalties are from 2 to 5 times lower;
- the total annual benefits increase with both equipage and demand level (estimated up to 500M$ for fully equipped fleet);
- the portion of a flight duration flown at an optimal FL is increased with increased equipage, and is decreased with demand, as well as the percentage of step-climb requests granted.

These results clearly motivate the airlines to equip their aircraft: as equipage increases, the cumulative benefits increase as well. In addition to this, Williams and Greenfeld note that the benefits depend on spacial and temporal flight distribution, *i.e.* whether all the aircraft in such clusters are equipped.

On the other hand, for the segregated tracks, it was found out that it was slightly more expensive on average to use the operations segregated according to the equipage instead of the regular mixed operation within the OTS. However, the authors explain this phenomenon by a particularity of the construction of the segregated tracks[7] and the redistribution of the flights based on this construction. They claim that for different sets of segregated tracks, flights would select different routes that would be likely to have positive outcomes. More detail on this study can be found in [37].

At the same time, the final goal of the Air Navigation System (ANS) is to equip all the aircraft with new surveillance and broadcast technologies. In this case, the segregated tracks could be created between all the regular tracks, and no aircraft would be restricted to a particular track type. Thus, the drawback mentioned above would disappear. That is what ICAO (International Civil Aviation Organization) is planning to do in the future. The European and North Atlantic (EUR/NAT) Office of ICAO has developed an implementation plan of lateral separation reduction in NAT, referred to as *Reduced Lateral Separation Minimum* (RLatSM) [38].

According to this plan, RLatSM will provide the reduced MSS between adjacent tracks (Fig. 2.3): 0.5° (as measured between segments anchored every 10° meridians), or 25 NM (as measured perpendicularly between tracks). In Figure 2.3, the result of RLatSM introduction through the entire OTS is presented. It is established, that in order to use the RLatSM, the aircraft are to be supplied with on-board equipment providing the CPDLC (Controller-Pilot Data Link Communications), ADS-C (Automatic Dependent Surveillance-Contract) and GPS (Global Positioning System) capabilities or equivalent (e.g. ADS-B). In [38], some more detail on the equipment required are given, and also several more topics on the RLatSM implementation process are addressed.

To summarize, all the previous studies discussed in this section, reveal significant benefits (frequency of optimal FL assignments, cruising time savings, fuel savings, additional cargo potential, etc.) from reducing the current MSS, especially for high level of aircraft equipage with new generation services. The most commonly proposed values of MSS reduction are:

[7] The segregated tracks were selected based on the preferences of the majority of the EQA. Thus, only the optimal choice of each EQA was considered and not the interactions. The drawback of the method is that the NEQA are not considered at all.

[8] From [38]

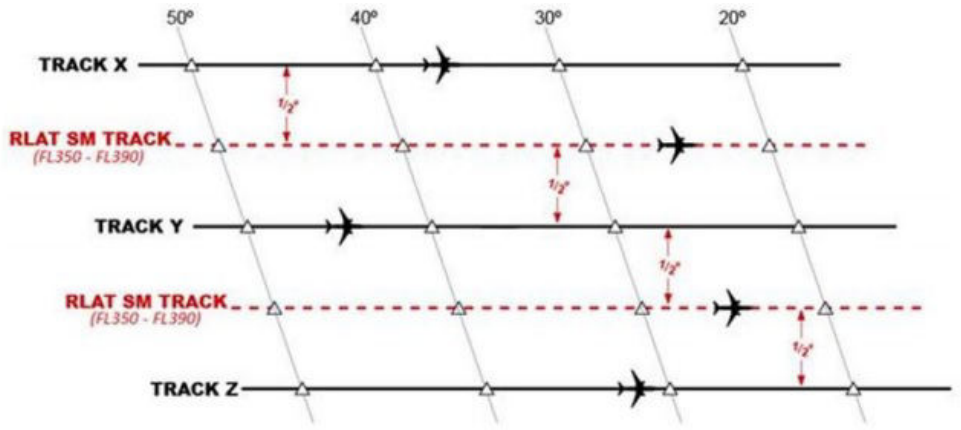

FIGURE 2.3: Creating of additional tracks within the OTS according to RLatSM[8]

- 1,000 feet for vertical separation (which is already applied almost everywhere);
- 30 NM (0.5° degree) for lateral separation;
- 30 NM, or 5 minutes, for longitudinal separation.

However, for all of the mentioned studies, the flights were constrained to follow a single track. A different approach, allowing re-routing between tracks, is presented in the next section.

2.1.2 Re-routing within OTS with reduced longitudinal separation

In the air traffic simulation performed in the previously discussed studies, the aircraft were restricted to follow one predefined track, from its entry point to the exit point, and major savings induced by separation reduction were found to be a consequence of more optimal FAP. In Louyot *et al.* [39], in the framework of ASSTAR[9] project, the interest of separation standards reduction is investigated in the context of re-routings between tracks. As the reduced separation can be applied to the appropriately equipped aircraft only, in this study, the ADS-B In/Out equipment is considered. The objective of this study is:

- to quantify the need of flight re-routing within the OTS,
- to estimate the frequency of such re-routing ability with different separation norms (current and reduced),

[9]Advanced Safe Separation Technologies and Algorithms, funded by European 6th RTD Framework Program

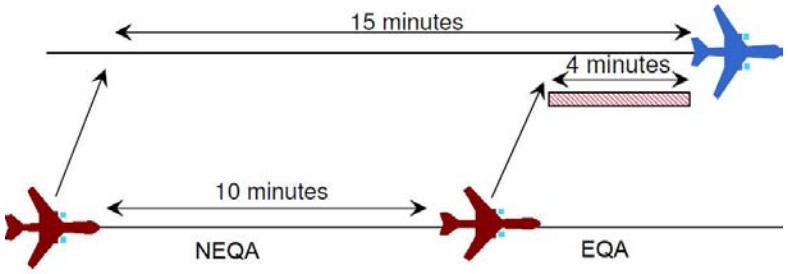

FIGURE 2.4: Separation standards for re-routing aircraft depending on their equipment[11]

- to investigate the influence of the ADS-B In/Out equipage on this frequency.

The simulations in [39] rely on the following assumptions:

- only eastbound OTS traffic is considered,
- re-routings are performed between longitude 20°W and 15°W[10],
- flights can be re-routed to adjacent tracks only,
- all flights keep their last cleared Mach and FL,
- several days of NAT traffic[12] are simulated,
- the wind is modeled[13] and taken into account,
- several ADS-B equipage rates are investigated[14];
- FIFO[15] principle is applied to the flights desired to re-route[16]

The following separation scenarios are simulated:

- procedural separation, with CSS, *i.e.* 15 minutes, as defined in Section 1.2.4 (Fig. 1.19);

[10]This zone is situated in the end of eastbound OTS. Thus, it is the last oceanic zone before exiting the NAT. The re-routing is investigated within this limited zone only, while the flight data was available for the entire flight.
[11]From [39]
[12]Two days in December 2005; five days in August 2006.
[13]The wind tab is computed from all flights with POSs using their Machs, FLs and computed GSs.
[14]They were simulated using the Monte-Carlo method.
[15]First In First Out
[16]Evidently, a re-routing performed by a flight affects directly the feasibility of the re-routings of the following traffic.

- *Airborne Separation In-Trail Merge* (ASEP-ITM), is investigated with different reduced MSS ranging from 2 to 6 minutes.

Figure 2.5 presents an example of traffic performing re-routing. In this figure, the aircraft are colored:

- in white, if the current track is appropriate for their destination,
- in light blue, if north re-routing is desired but not authorized,
- in blue, if north re-routing is performed using procedural separation,
- in dark blue, if north re-routing is performed using ASEP-ITM,
- in light red, if south re-routing is desired but not authorized,
- in red, if south re-routing is performed using procedural separation,
- in dark red, if south re-routing is performed using ASEP-ITM.

As mentioned in Section 1.2.3, the procedural re-routing is rarely authorized, and thus, even more rarely demanded. For example, for the data used in [39], only 0 to 1 flight per day were actually re-routed between 20°W and 15°W, and only 2 to 5 flights per day were re-routed between 30°W and 20°W. Obviously, applying the ASEP-ITM increases the number of possible re-routings. This is proved by the results obtained from the discussed simulations, the most important of which are listed below:

- a third of the aircraft desiring to re-route actually could be re-routed using the current procedural separation;
- another third could be re-routed using ASEP-ITM with 4 minutes[18];
- the ASEP-ITM feasibility increases almost linearly with the reduction of the separation value;
- the number of feasible ASEP-ITM re-routings increases with increased ADS-B equipage level; thus, ASEP-ITM seems to require a rather high level of ADS-B equipage.

[17] From [39]

[18] Note that all the flights re-routable using the procedural separation are re-routable using ASEP-ITM by default.

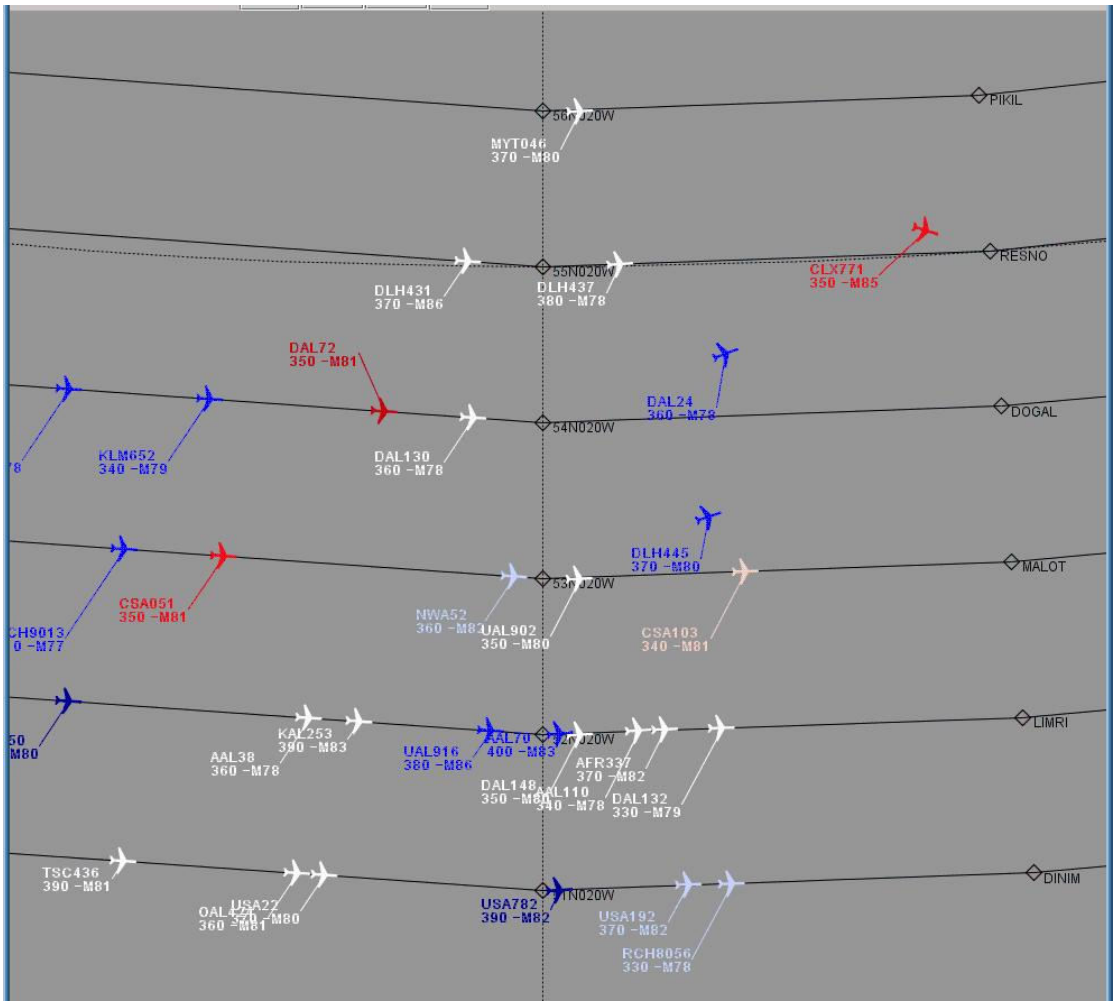

FIGURE 2.5: Traffic re-routing within OTS between 20°W and 15°W[17]

The main conclusion that can be drawn from this study is that the separation standard reduction due to ADS-B aircraft equipage increases significantly the aircraft possibility to re-route to more convenient track within OTS, and that, in turns, improves a single Aircraft Trajectory (AT) and the overall NAT traffic situation.

2.1.3 Separation standards reduction perspectives examined in the present thesis framework

As concluded from [39], permitting the aircraft to re-route directly within the OTS, which is especially efficient with Reduced Separation Standards (RSS), can improve not only a single AT, but the whole air traffic situation in NAT by reducing the congestion in pre-oceanic airspace. There is a significant number of studies investigating longitudinal

separation reduction within a single track, but to our knowledge, none addresses traffic re-routing along the whole ATs within NAT.

Thus, in the current thesis, we propose to extend the idea of re-routing maneuvers described in [39], from a single OTS exit zone to the whole NAT OTS. We intend to simulate the flight progress over the OTS for a whole day, while allowing re-routing maneuvers. In order to obtain the highest benefits from such maneuvers, we consider that the desired entry and exit tracks for an aircraft are the tracks closest to its departure and arrival airports respectively. In our simulations, we keep the current OTS structure (thus, no change in the lateral separation) and we perform simulations with two different values for the longitudinal separation: the CSS and the RSS, as defined in Section 1.2.4.

The objective of this study is to reveal the benefits obtained from re-routing on one hand, and from separation reduction on the other hand. The proposed methodology and the obtained results are described below.

2.2 Mathematical model of the NAT ANS

The current NAT ANS is fully described in Section 1.2. Below, we briefly highlight its particularities that will be used in our computational tests, with some assumptions made in order to simplify the problem. After that, we formalize these particularities mathematically, so that they could be expressed as input data and decision variables of an optimization problem. Finally, we formulate this optimization problem that consists in searching for the optimal Flight Plans (FPLs) for a set of flights within OTS.

2.2.1 OTS model

Further in this study, we will perform our simulations using the following assumptions that sometimes simplify the real NAT ANS.

- Only the eastbound traffic (cruising from North America to Europe) is taken into consideration, and thus, only the eastbound OTS is constructed. This can be made without loss of generality, as the eastbound and westbound traffic are mainly separated in time (due to the specific demands) and in space (correspondingly with

the OTS structure), and thus, they can be considered independently. Note that in practice, there may be westbound flights crossing the NAT during the eastbound OTS period of validity, but their number is negligibly small.

- We consider the eastbound OTS system established in NAT to be a regular grid, having an equal number of waypoints (WPs) and equal number of FLs for each track. That is not always the case in reality: some FLs may be restricted to a limited number of tracks; moreover, some tracks may have additional WPs in the continental airspace. In such a case, either these extra WPs and FLs were extracted from the OTS, or a complete track "standing out" from the rest was taken out of consideration in our simulations. The aim is to simplify the OTS modeling, and the presentation, but this assumption does not change the base principle of the mathematical model presented below.

Taking into account these assumptions, the OTS can be represented by a $Nx \times Ny \times Nz$ grid of WPs, where:

- Ny is the number of OTS tracks,
- Nx is the number of WPs on each track, and
- Nz is the number of FLs for each track.

The tracks are labeled with j ranging from 1 to Ny, starting from the most northern. The WPs on each track are labeled with i ranging from 1 to Nx, starting from the most western. The FLs are labeled with k ranging from 1 to Nz, starting from the lowest. Thus, the 3D position of an eastbound aircraft located on track j at WP i at FL k is completely specified by the vector (i, j, k). The geographical coordinates of this point are given by the vector $(\lambda_i^j, \phi_i^j, a_k)$, where λ_i^j is the point longitude, ϕ_i^j is the point latitude, and a_k is the point altitude.

Every pair of consecutive WPs, (i, j, k) and $(i + 1, j, k)$, on the same track j and the same FL k are joined with straight lines called *links*. Similarly, every pair of consecutive WPs on adjacent tracks (and the same FL) are joined with links: northern, from (i, j, k) to $(i + 1, j - 1, k)$; southern, from (i, j, k) to $(i + 1, j + 1, k)$. Thus, each WP (except for those on the outer tracks) has three outgoing links. We denote $\mathcal{L}$ the set of all links of the OTS.

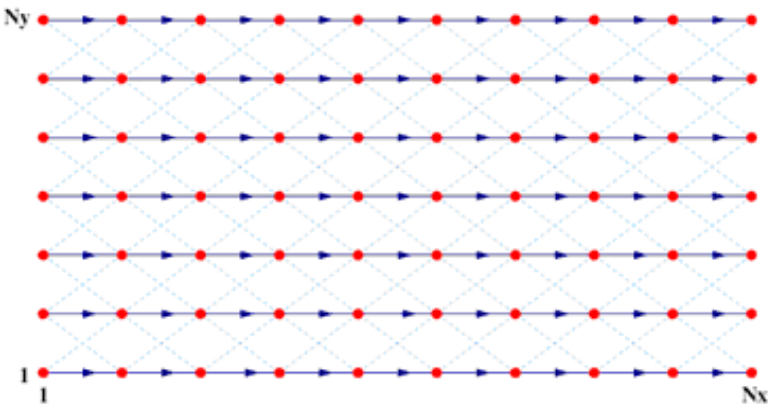

FIGURE 2.6: Horizontal section of the OTS grid model with nodes and links

We call the link intersection points as *nodes*. Figure 2.6 displays the horizontal section (one FL) of our OTS model represented by a grid of nodes joined with links. In addition to WPs that are located on tracks and that belong to the OTS grid structure (red nodes in Figure 2.6), the node set also contains the points of intersection of the links joining adjacent tracks (blue nodes in Figure 2.6). We denote $\mathcal{N}$ the set of all nodes of the OTS.

This node-link structure is also used in the sequel in order to define ATs and conflicts. Where it is appropriate, we will denote the OTS grid as $\mathcal{G}$, where $\mathcal{G} = (\mathcal{N}, \mathcal{L})$. In this case, we suppose that we enumerate the nodes first and the links after.

2.2.2 Flight model

In this section we define how flights are modeled in our study. First of all, note that we perform our simulations using two types of data sets: artificially-generated and real flight sets. They are described in detail in Sections 2.4.1 and 2.4.2 respectively. Here we bring the attention simply to the fact that the artificial flights were randomly generated in order to satisfy the assumptions and restrictions, presented below; concerning the real data, note that sometimes we had to exclude some flights from the simulations, if these last do not match with these NAT ANS restrictions. These assumptions and restrictions are as follows.

- As stated in the previous section, only eastbound traffic is considered.
- In our simulations, we take into account only the part of each flight trajectory that belongs to the OTS, from its oceanic entry point to the exit point, as the subject

of our study is the NAT. Thus, the optimization is made only for NAT phase of the flights.

- Only the flights crossing the NAT during the eastbound (night-time) OTS period of validity are considered (the flight should exit the OTS in the range of this period). Note that in real data, there exist a number (which is not negligible in this case) of eastbound flights that exit the OTS after its official period of validity is finished (due to accumulated delays on one hand, and the particular schedules on the other hand). Thus, for the real data, we decided to enlarge artificially the standard period of validity, in order to take into account as many flights as possible (see more detail in section 2.4.2).

- The user-preferred entry and exit OTS tracks for flight f are further referred to as the *desired entry and exit tracks* and are denoted as TD_e^f ("e" stands for "entry") and TD_o^f ("o" stands for "out") respectively. These are *given input data* for our optimization problem. They are assumed to be chosen as optimally with respect to some particular criterion, that can be defined according to the airline and/or ATC preferences. In our simulations, for the real data, we choose as desired entry and exit WPs: the WP closest to the departure and arrival airport respectively, in order to reduce congestion in the pre-oceanic continental airspace.

- We authorize the *assigned entry and exit tracks*, denoted as e^f and o^f respectively, to differ from the desired TD_e^f and TD_o^f, otherwise quite often the state space becomes too restricted due to high traffic density. As a result, the desired tracks cannot always be attributed to all aircraft without provoking conflicts. In the present study, we allow an aircraft entering/exiting the OTS to deviate just by one track to the north or to the south from its desired entry/exit track (more precisely, for e^f: $|TD_e^f - e^f| \leq 1$), otherwise its AT is supposed to be to far from the optimum. The assigned entry and exit tracks will be decision variables for our optimization problem.

- An aircraft entering an assigned track at a predefined FL is assumed to follow this track at the same FL as long as no changes of its AT are made. According to the imposed regulations, such changes are only allowed at the WPs. Thus, from a given WP (i, j, k), an aircraft has several possibilities to pursue its route:

  - to follow the same track at the same FL,

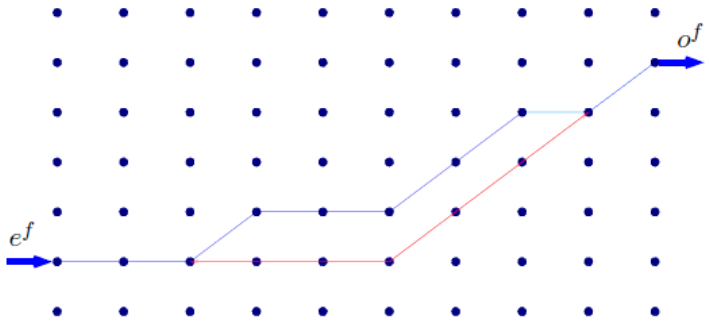

FIGURE 2.7: Two possible aircraft trajectories for a given flight in the horizontal section

  - to re-route to an adjacent track at the same FL or
  - to change the FL.

- We authorize aircraft to perform *re-routings* between the tracks. Thus, we allow the assigned entry and exit tracks not to be identical, in contrast to the actual situation in NAT. However, we only allow re-routings in one direction (either northern, or southern), from the entry track towards the exit tracks, as zigzagging unnecessarily prolongates the aircraft route and creates additional congestion. Thus, the number of required re-routing maneuvers for an aircraft directly depends on the difference ($|o^f - e^f|$) between the assigned entry and exit track labels. If these tracks are identical, then the aircraft has no opportunity to vary its trajectory in space.

- Re-routings are only authorized between WPs. More precisely, an aircraft, leaving its current track at WP (i, j, k) should reach the adjacent track at WP $(i+1, j-1, k)$ in case of northern re-routing, or at WP $(i + 1, j + 1, k)$ in case of southern re-routing. Thus, an AT within an OTS actually represents, in horizontal section, a sequence of links joining successive WPs on a same track or on adjacent tracks. Each flight crosses Nx WPs, and therefore its AT consists of $Nx - 1$ links. For example, in Figure 2.7, two possible trajectories for a flight with given entry and exit tracks are represented. The choice of the WPs, where aircraft perform re-routings will form another group of *decision variables* for our optimization problem.

- We also authorize aircraft to perform *step climbs* (but no descends), which can only occur at WPs. Step climbs are fixed beforehand, during the initial FPL elaborations, in such a way, that the aircraft could follow its optimal altitude profile in terms of fuel consumption. This is in contrast with re-routings, that are flexible

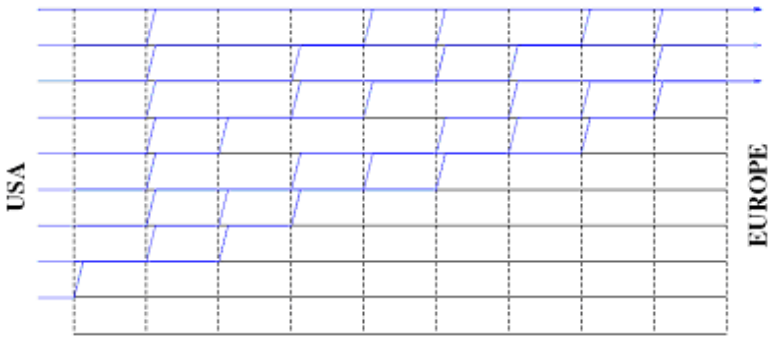

FIGURE 2.8: Model of the instantaneous aircraft step climbs in the vertical section

and that are defined in the optimization process during the strategic planning, which is the subject of the present study, taking into account flight interactions. Thus, we assume that for an aircraft f its FL_i^f at WPs $i = 1, ..., Nx$ are considered as *given input data* and are not to be changed during our simulations.

- In our model, we neglect the time required by an aircraft to reach the new flight level during climb. This *instantaneous-climbing hypothesis* is reasonable, as the distance between the WPs (10° of longitude, which is about 500 km) is much longer than the distance between FLs (1,000 feet, equal to 0.3048 km). Correspondingly, we neglect also the distance between the real horizontal position of the aircraft at the new FL and at the previous WP (see Figure 2.8), as it is even smaller than the distance between FLs. Thus, we suppose that an aircraft climbs vertically, and "jumps" immediately from its current WP (i, j, k) to the next WP $(i, j, k+1)$ on the upper FL. In some rare cases in the real flight sets, aircraft may climb directly two FLs. This is also modeled as an instantaneous vertical "jump" from WP (i, j, k) to WP $(i, j, k+2)$, going through WP $(i, j, k+1)$.

- We also allow the aircraft to *change their Machs*, but, as for FLs, such changes are defined beforehand in correspondence with the optimal aircraft performance, and we consider them as given input data. Machs can also only be changed at WPs. Thus, the True Air Speed (TAS) of flight f is supposed to be constant all along the link outcoming a given WP i, and is denoted as v_i^f. These are also *given input data* for our optimization problem.

- In a preliminary study, we do not take the wind into account. For the case of the real flight data, we perform simulations considering the winds, but we use a very *simplified wind model*. The wind field is supposed to be constant in time. The

wind is defined at the links only, and is described only by the wind component parallel to each of such links, which is also supposed to be constant along this link. The process of wind extraction from the real data is described in Section 2.4.2.

- The *desired aircraft track entry time*, denoted t_{in}^f, is *given input data* defined according to airline preferences and constraints. It must fit into the period of the OTS validity, as stated below. However, strictly fixing the OTS entry time render the search space too limited to accommodate the whole traffic (as it was empirically observed during our study). Thus, some relaxation of the prescribed entry time is needed. We allow some delays for a flight f to enter the NAT, that we refer to as d^f. As large delays are clearly not desired by airlines and passengers, we limit the maximum delay attributed to an aircraft to 30 minutes. Furthermore, as the simplest and cheapest way to delay an aircraft is via ground delay, we must also satisfy the airport operation practice, *i.e.* departure times must be scheduled as multiple of 5 minutes. Correspondingly, we attribute random delays to the NAT flights, multiple of 5 minutes, this value being called *slot*. Thus, each flight f can be delayed by $d^f = 0, 5, 10, 15, 20, 25$ or 30 minutes, and its delay can be represented as:

$$d^f = \delta^f \cdot slot, \tag{2.1}$$

where $\delta^f \in \{0, 1, ..., 6\}$. Then, its *assigned track entry time* is defined as: $t_{in}^f + \delta^f \cdot slot$, and δ^f form another group of *decision variables*.

Thus, to summarize, the assigned entry and exit tracks, together with the selected WPs at which the re-routings are performed, fully define the AT 2D horizontal profile (see Figure 2.7). The 3D AT is determined if one moreover specifies the FLs at each WP. Finally, one obtains the full 4D AT by incorporating times, calculated using the aircraft assigned track entry times, and the TAS together with the Wind Speed (WS) on each AT link. These 4D ATs are used in the sequel in the simulations in order to determine potential conflicts (Section 2.2.3) and flight efficiency (Section 2.2.4). The optimization formulation we are proposing, based on the input data and decision variables given above, is given in Section 2.2.5.

2.2.3 Conflicts model

Based on the route network structure, conflicts may happen only at nodes and on links. Thus, we introduce the two following different variables:

- $C_{\mathcal{N}}$ - the number of conflicts on nodes;
- $C_{\mathcal{L}}$ - the number of conflicts on links.

As stated in the previous section, the 4D ATs can be computed on the OTS grid, based on the provided data and chosen values for the above-defined decision variables. This means that we can calculate the time at which the aircraft will be at any point of its AT, that is used, in its turn, to calculate the number of conflicts on nodes and links. Thus, before calculating the number of conflicts, we perform some preprocessing which idea is described by Algorithm 2.1.

The complexity of the presented algorithm is $O(N)$ (on considering the number of WPs in the OTS to be fixed). Note that Algorithm 2.1 only gives a general idea, and omits implementation detail that render it more efficient. First, evidently, the exit time for link l is the entry time for the next link, $l+1$: $\tilde{t}_l^f = t_{l+1}^f$. Second, the entry time, t_l^f, for the link l, is also the arrival time, t_n^f, for the node n from which link l outgoes. Thus, the two inner loops (starting at lines 7 and 10 respectively) can be combined in a single one, if one treats appropriately the case of middle link nodes, created at the points of intersections of crossing links.

Two aircraft, f and g, passing a same node n are considered in conflict at this node (this conflict is shown with a red circle in Figure 2.9) if the longitudinal separation constraint, Δ, is violated for these aircraft at this node, *i.e.* if $|t_n^f - t_n^g| < \Delta$, where Δ depends on the previous flights maneuvers (straight, re-routing, climbing) and the MSS in use (CSS, RSS). To calculate the number of conflicts on nodes for all flights, we apply the procedure described by Algorithm 2.2.

The complexity of the presented algorithm in the worst case is $O(N \log N)$ (it is actually the complexity of the sorting algorithm in the case when all the aircraft pass through the same WPs). Note that the number of conflicts detected by Algorithm 2.2 can underestimate the actual number of conflicts on nodes between all possible pairs of

Algorithm 2.1 Flight preprocessing for computing the number of conflicts

Input: $\mathcal{G} = (\mathcal{N}, \mathcal{L})$ - OTS grid of nodes and links;
$\{AT^f\}_{f=1}^{N}$ - a set of aircraft trajectories, where N is number of flights and
AT^f contains the sequence of nodes $n \in \mathcal{N}$ and links $l \in \mathcal{L}$ passed by flight f.

Output: $\{A_n\}_{n\in\mathcal{N}}$, where A_n contains the records of flights
passing through n with their times of arrival;
$\{E_l\}_{l\in\mathcal{L}}$, where E_l contains the records of flights
passing over l with their times of entry of l;
$\{O_l\}_{l\in\mathcal{L}}$, where O_l contains the records of flights
passing over l with their times of exit (out) of l.

1: **for** each $n \in \mathcal{N}$ **do** // for each node n of the grid
2: $A_n := \emptyset$
3: **for** each $l \in \mathcal{L}$ **do** // for each link l of the grid
4: $E_l := \emptyset$
5: $O_l := \emptyset$

6: **for** $f := 1$ to N **do** // for each flight f in set
7: **for** each $n \in AT^f$ **do** // for each node n encountered by AT^f
8: $t_n^f :=$ ARRIVE_TIME(n) // compute the arrival time of f at n
9: $A_n := A_n \cup (f, t_n^f)$ // record flight f at node n
10: **for** each $l \in AT^f$ **do** // for each link l in a sequence of AT^f
11: $t_l^f :=$ ENTRY_TIME(l) // compute the time when f enters l
12: $\tilde{t}_l^f :=$ EXIT_TIME(l) // compute the time when f exits l
13: $E_l := E_l \cup (f, t_l^f)$ // record flight f entering link l
14: $O_l := O_l \cup (f, \tilde{t}_l^f)$ // record flight f exiting link l

Algorithm 2.2 Computing the number of conflicts occurring on nodes of OTS grid

Input: $\mathcal{N}$ - a set of nodes of the OTS grid;
$\{A_n\}_{n\in\mathcal{N}}$, where A_n contains the records of flights
passing through n with their times of arrival.

Output: $C_{\mathcal{N}}$ - total number of conflicts on nodes

1: $C_{\mathcal{N}} := 0$
2: **for** each $n \in \mathcal{N}$ **do** // for each node n of the grid
3: $m := |A_n|$ // number of flights encountered for n
4: $[(f_1, t_n^{f_1}), ..., (f_m, t_n^{f_m})] :=$ SORT$_t(A_n)$ // sort the flights encountered for n
// according to their arrival times t_n^f
5: **for** $i := 1$ to $m - 1$ **do** // for each pair of consecutive
// flights in the sorted sequence
6: $\Delta :=$ SEP_NORM$(n,\ f_i,\ f_{i+1})$ // determine the longitudinal separation Δ
7: **if** $t_n^{f_{i+1}} - t_n^{f_i} < \Delta$ **then** // if longitudinal separation is violated
8: $C_{\mathcal{N}} := C_{\mathcal{N}} + 1$ // number of conflicts is increased

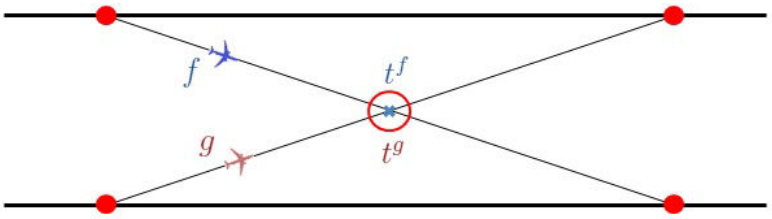

FIGURE 2.9: Conflict between two aircraft at a common node

aircraft. For example, if we are given a sequence $[f_1,\ f_2,\ f_3]$ of flights passing a node n ordered according to their times of arrival, *i.e.* $t_n^{f_1} < t_n^{f_2} < t_n^{f_3}$, and if $t_n^{f_2} - t_n^{f_1} < \Delta$ and $t_n^{f_3} - t_n^{f_2} < \Delta$, then Algorithm 2.2 counts two conflicts: between flights f_1 and f_2, and between flights f_2 and f_3. However, if we also have $t_n^{f_3} - t_n^{f_1} < \Delta$, then flights f_1 and f_3 are also in conflict, and thus, the actual number of conflicts at node n is equal to three. Computing the number of conflicts between all possible pairs of aircraft demands more computational time ($N_n(N_n - 1)/2$, where N_n is the number of aircraft passing node n) and is not necessary from the implementation point of view, as our aim is to eliminate conflicts, and once Algorithm 2.2 returns zero conflicts, the number of conflicts occurring on nodes is necessary zero for all pairs of aircraft as well.

A conflict occurring on a link is referred to as an *overtaking*. It happens when an aircraft is slower than the one following it on the same track, *e.g.* when aircraft f enters link l before aircraft g: $t_l^f < t_l^g$, but exits this link after aircraft g: $\tilde{t}_l^f > \tilde{t}_l^g$. To compute the number of conflicts on links for all aircraft, we apply a procedure described by Algorithm 2.3.

The complexity of this algorithm is also $O(N \log N)$. Similarly to the number of conflicts on nodes, the number of conflicts on links detected by Algorithm 2.3 may be different from the actual number of overtakings between all possible pairs of aircraft. For example, if flights $f_1,\ f_2,\ f_3$ enter link l in the order $[f_1,\ f_2,\ f_3]$ and exit this link in the order $[f_2,\ f_1,\ f_3]$, then Algorithm 2.3 counts two conflicts, although only one overtaking takes place. Furthermore, if the exit order is rather $[f_3,\ f_2,\ f_1]$, then only two conflicts are detected, while actually there are three overtakings. However, as for the number of conflicts on links, we do not need to know the exact total number of conflicts on nodes, as in any case the output, $C_{\mathcal{L}}$, of Algorithm 2.3 is zero if and only if the actual number of conflicts occurring on links is zero. Our procedure permits to calculate $C_{\mathcal{L}}$ without considering each possible pair of aircraft.

Algorithm 2.3 Computing the number of conflicts occurring on links of OTS grid

Input: $\mathcal{L}$ - a set of links of the OTS grid;
$\{E_l\}_{l\in\mathcal{L}}$, where E_l contains the records of flights passing over l with their times of entry of l;
$\{O_l\}_{l\in\mathcal{L}}$, where O_l contains the records of flights passing over l with their times of exit (out) of l.

Output: $C_{\mathcal{L}}$ - total number of conflicts on links

1: $C_{\mathcal{L}} := 0$
2: **for** each $l \in \mathcal{L}$ **do** // for each link l of the grid
3: $m := |E_l|$ // number of flights encountered for l
4: $[(f_1, t_l^{f_1}), ..., (f_m, t_l^{f_m})] := \mathrm{SORT}_t(E_l\ )$ // sort the flights encountered for l // according to their entry times t_l^f
5: $[(g_1, \tilde{t}_l^{g_1}), ..., (g_m, \tilde{t}_l^{g_m})] := \mathrm{SORT}_t(O_l\ )$ // sort the flights encountered for l // according to their exit times $\tilde{t}_l^f$
6: **for** $i := 1$ to m **do** // for each corresponding pair of // flights from E_l and O_l
7: **if** $f_i \neq g_i$ **then** // if flight enter/exit orders differ
8: $C_{\mathcal{L}} := C_{\mathcal{L}} + 1$ // number of conflicts is increased

In the sequel in general we will speak about the *total number of conflicts*, denoted by C_t, where:

$$C_t = C_{\mathcal{N}} + C_{\mathcal{L}}. \tag{2.2}$$

The main objective of the present study is to find a conflict-free flight configuration:

$$C_t = 0. \tag{2.3}$$

Condition (2.3) will be referred to as the *Conflict-Free Criterion* (CFC). It represents a strong requirement for the proposed optimization problem, which it is not easy to satisfy.

2.2.4 Flight efficiency model

As the objective of the present study is to find optimal FPLs for a set of flights within OTS, we need to define the criteria of optimality. In this section, we present several criteria that we have chosen for our optimization problem:

- D - the total delay at track entry, summed over all flights,
- P - total cruising time within the OTS, and
- G - total deviation delay (the sum of the estimated delays caused by aircraft deviations from their desired entry/exit tracks).

The *total entry delay* is expressed in terms of time and is evidently obtained by summing up delays over all flights f:

$$D = \sum_{f=1}^{N} d^f, \tag{2.4}$$

where N is the total number of flights.

The *cruising time for a single aircraft* f, denoted as p^f, is the time elapsed from entering to exiting OTS tracks. It is calculated directly in simulations, from 4D AT. The *total cruising time* is the sum of cruising times for all aircraft:

$$P = \sum_{f=1}^{N} p^f \tag{2.5}$$

The *total number of deviations*, which is the sum, over all the flights, of the deviations of each single flight from its desired entry/exit tracks (*i.e.* when a flight is assigned an adjacent track instead of its desired track), could be taken as a criterion of optimality. However, this number is not expressed in terms of time. We would like to have the same units for all the criteria under consideration, in order to simplify the procedure of finding the balance between these criteria (the weighting coefficients, see the next section). Thus, we choose to use a rough estimation of the total number of deviations in terms of time, namely, the *total deviation delay*.

To do so, we sum up, over all aircraft, the times necessary for each aircraft to reach its desired entry/exit track from its assigned entry/exit track, and we denote this sum by G. This criterion can be calculated as follows:

$$G = \sum_{f=1}^{N} [\frac{S_e^f}{v_1^f} + \frac{S_o^f}{v_{Nx-1}^f}], \tag{2.6}$$

where, for each flight f,

- S_e^f is the distance between TD_e^f and e^f (the distance between the corresponding entry WPs),
- S_o^f is the distance between TD_o^f and o^f (the distance between the corresponding exit WPs),
- v_1^f is the aircraft entry speed (aircraft speed at the first WP and along the first link), and
- v_{Nx-1}^f is the aircraft exit speed (aircraft speed at the WP $Nx-1$ and along the last link, the speed at which aircraft f arrives to the track exit).

We bring the attention once more to the fact, that G is an artificial measure, introduced to penalize flight configurations involving flight deviations from their desired entry/exit tracks. As a result, G involves units of measurements, coherent with those of the two other criteria (D and P).

Note that these three criteria are chosen in order to address the particularities of the presented problem. More precisely, each of these criteria is important:

- D: once we allow to delay aircraft, we would like to control these delays, as they are not desirable;
- G: similarly, once we allow aircraft to deviate from their desired entry/exit tracks, we should penalize such deviations;
- P: we should allow aircraft re-routings, while minimizing the time aircraft spend in NAT in the presence of wind field.

One may consider any other criteria of optimality, such as AT length, total cruising time from departure to arrival, total fuel consumption, etc. To do so, it suffices to define a procedure to compute the criterion value from the input data and chosen decision variables. Then, these alternative criteria can be simply incorporated into the optimization problem formulation that is presented in the next section.

2.2.5 Optimization problem formulation

In this section, we propose an optimization formulation of our problem expressed in terms of the notations, decision variables and input data presented in the previous section.

For each flight f, the following **input data** are given:

- $TD_e^f \in \{1, 2, ..., Ny\}$ - the desired entry track;
- $TD_o^f \in \{1, 2, ..., Ny\}$ - the desired exit track;
- $t_{in}^f \in I\!R^+$ - the desired entry time;
- $v_i^f \in I\!R^+$ - aircraft speeds at WP i, $i = 1, 2, ..., Nx$, (assumed to be constant throughout the outgoing link and to satisfy the aircraft operational conditions);
- $FL_i^f \in \{1, 2, ..., Nz\}$ - flight level at WP i, $i = 1, 2, ..., Nx$, defining the flight altitude profile (assumed to satisfy the following conditions:
  $FL_{i+1}^f \geq FL_i^f$, $i = 1, 2, ..., Nx - 1$).

In addition to this, in the computational experiments where we do take the wind into account, we also consider a given wind field as input data.

For each flight f, the **natural decision variables** are defined as follows:

- x_i^f - binary variables defining the flight re-routing maneuver at WP i, $i = 1, 2, ..., Nx - 1$:
  $$x_i^f = \begin{cases} 1 & \text{if flight } f \text{ changes track at WP } i, \\ 0 & \text{otherwise.} \end{cases}$$
  In other words, when $x_i^f = 1$, aircraft f leaves its current track at WP i, and re-routes towards the appropriate adjacent track (the next track towards the exit track).
- To simplify the notations, we define the vector $x^f = (x_1^f, ..., x_{Nx-1}^f)$. Thus, for a given flight f, x^f forms a binary vector of size $Nx - 1$, where the number of ones is equal to the distance between the entry and exit tracks (that will be given as a constraint).

- Where it is appropriate, we will also refer simply to vector x, where $x = (x^1, ..., x^N)$.

As mentioned above, preliminary experiments have shown that for many practical cases, a search space definition involving only these re-routing binary variables is not rich enough to guarantee existence of a set of conflict-free trajectories (no feasible solution exists). In order to avoid this situation, we moreover allow aircraft to enter (or to exit) an adjacent track. Furthermore, this can be done with some entry delay that is to be chosen among a number, N_d, of discrete values, multiple of a fixed time duration denoted as *slot*. More precisely, the **new associated decision variables** for flight f are:

- $e^f \in \{1, 2, ..., Ny\}$ - the assigned entry track;
- $o^f \in \{1, 2, ..., Ny\}$ - the assigned exit track;
- $\delta^f \in \{1, 2, ..., N_d\}$ - the index among the discrete values, that defines the time delay at track entry through equation (2.1).

Similarly, we can accumulate these decision variables into corresponding vectors:

- $e = (e^1, ..., e^N)$;
- $o = (e^1, ..., e^N)$;
- $\delta = (\delta^1, ..., \delta^N)$.

On the other hand, sometimes it is useful to group together all the variables corresponding to one flight. Thus, we denote:

- $y^f = (\delta^f, e^f, x^f, o^f)$.

All the decision variables for all the flights can be accumulated in a single vector y, where y can be viewed into two different ways, according to the convenience of the presentation:

- $y = (y^1, ..., y^N)$; or

- $y = (\delta, e, x, o)$.

The decision variables must satisfy the following **constraints** for each flight f:

$$\left| e^f - TD_e^f \right| \leq 1, \tag{2.7}$$

$$\left| o^f - TD_o^f \right| \leq 1, \tag{2.8}$$

$$\sum_{i=1}^{Nx-1} x_i^f = \left| o^f - e^f \right|. \tag{2.9}$$

Constraints (2.7) and (2.8) define the tolerance with regards to the desired entry and exit tracks respectively. Constraints (2.9) define the total number of re-routing maneuvers for each aircraft f. Furthermore, the decision variables should provide a conflict-free solution, thus, the CFC constraint (2.3) must be satisfied.

The **objective function** should take into account all the desired criterion of optimality. As all such criteria presented above are expressed in terms of time, they can be accumulated in a single objective function using appropriate *weighting coefficients* set by the user according to his priorities. For the described optimization problem the following objective function $F(y)$ is to be minimized:

$$F(y) = \alpha_d D(y) + \alpha_p P(y) + \alpha_g G(y), \tag{2.10}$$

where α_d, α_g, α_p are non-negative user-defined weighting coefficients that enable to include/exclude different criteria in the objective function as well as to consider various trade-offs. Thus, our optimization problem is stated as follows:

$$\min_{y=(\delta,e,x,o)} \alpha_d D(y) + \alpha_p P(y) + \alpha_g G(y), \tag{2.11}$$

$$\text{s.t. } C_t(y) = 0;$$

$$\left|e^f - TD_e^f\right| \leq 1, \ f = 1, ..., N;$$

$$\left|o^f - TD_o^f\right| \leq 1, \ f = 1, ..., N;$$

$$\sum_{i=1}^{Nx-1} x_i^f = \left|o^f - e^f\right|, \ f = 1, ..., N;$$

$$\delta^f \in \{0, ..., N_d\}, \ f = 1, ..., N;$$

$$e^f, o^f \in \{1, ..., Ny\}, \ f = 1, ..., N;$$

$$x_i^f \in \{0, 1\}, \ f = 1, ..., N, \ i = 1, ..., Nx - 1.$$

Results from a preliminary study shows that a conflict-free solution may not exist in some practical cases, that is to say the CFC constraint (2.3) cannot be satisfied. Furthermore, even in cases where a conflict-free set of trajectories does exist, finding such an acceptable configuration for a given set of flights is not an easy task. In other words, it is not evident to generate feasible solutions for the presented optimization problem. In order to overcome this difficulty, we propose to address the problem with a first stage, where violation of the CFC condition (2.3) is allowed. To that aim, we include a CFC constraint violation measure, the total number of conflicts C_t, as an additional criterion in the objective function, using the additional non-negative weighting coefficient α:

$$F_2(y) = C_t(y) + \alpha(\alpha_d D(y) + \alpha_p P(y) + \alpha_g G(y)). \tag{2.12}$$

Minimizing such an objective function enables to eliminate the conflicts and to reduce the en-route delays at the same time. The choice of a small value of the weighting coefficient α gives a high priority to the CFC. Thus, when solving the problem, we expect that the optimization algorithm will attempt at eliminating all the conflicts primarily. Once this is done (if it is possible), as we will observe in our tests, the en-route delays will then be reduced in a second stage of the optimization process, while ensuring that the considered solutions remain conflict-free. The corresponding optimization problem is then formulated as follows:

$$\min_{y=(\delta,e,x,o)} C_t(y) + \alpha(\alpha_d D(y) + \alpha_p P(y) + \alpha_g G(y)), \tag{2.13}$$
$$\left|e^f - TD_e^f\right| \leq 1,\ f = 1, ..., N,$$
$$\left|o^f - TD_o^f\right| \leq 1,\ f = 1, ..., N,$$
$$\sum_{i=1}^{Nx-1} x_i^f = \left|o^f - e^f\right|,\ f = 1, ..., N,$$
$$\delta^f \in \{0, ..., N_d\},\ f = 1, ..., N;$$
$$e^f, o^f \in \{1, ..., Ny\},\ f = 1, ..., N;$$
$$x_i^f \in \{0, 1\},\ f = 1, ..., N,\ i = 1, ..., Nx - 1.$$

When considering $\alpha = 0$, only the conflict-free criterion is taken into account and the objective function is then defined by:

$$F_2^0(y) = C_t(y). \tag{2.14}$$

This particular objective function can be useful for verifying whether a conflict-free solution does exist or not, for a given set of flights. We will use this objective function in our preliminary simulations on the artificial flight sets.

The formulated optimization problem to be solved is an integer non-linear problem. Moreover, the objective functions, (2.10), (2.12), (2.14), cannot be written in an explicit way as a function of the decision-variable vector y. These functions are to be computed directly through the calls of corresponding algorithms (*e.g.* Algorithms 2.2, 2.2 for CFC constraints). This limits much the types of optimization methods that can be used to solve our problem in the proposed formulation.

Furthermore, the problem involves $N \times (Nx + 2)$ decision variables, among which:

- $N \times (Nx - 1)$ binary variables x_i^f;
- N integer variables e^f and N integer variables o^f, each of which can in fact take 3 possible values for inner tracks, and 2 possible values for extreme tracks (taking into account constraints (2.7) and (2.8 respectively);

- N integer variables δ^f, that can take N_d possible values.

For instance, if we consider $N = 500$ flights on the OTS with $Nx = 8$ WPs (a realistic case, as it will be described in Section 2.4), then the total number of decision variables would be equal to 5,000. If we consider further that the number of discrete delays is $N_d = 6$, and if we suppose that an average number of track changes required among $Nx - 1$ transition segments is $N_c = 3$ (again, a realistic case), then the total number of possible combinations of decision variable values would be of the order of:

$$\left((N_d + 1) \times \begin{pmatrix} Nx - 1 \\ N_c \end{pmatrix} \right)^N = 245^{500},$$

which represents a significantly large search space.

Unfortunately, we could not provide a proof of the complexity status of the defined problem. We can simply show that our problem (or its confinements) can be reduced to an instantiation of known NP-hard combinatorial optimization problems, such as the maximum clique problem, the Boolean satisfiability problem (SAT, or 3-SAT), or the job shop scheduling problem [40]. However, we did not manage to construct an instantiation of our problem from any of the known NP-hard problems, as it represents a very particular case of optimization problems. This particularity arises, prior, from the particular route network established in the NAT: aircraft are not free to change their ATs in order to avoid potential conflicts, but should follow the OTS structure and can only re-route at WPs. This simplifies the problem on one hand, as it is always more convenient to work with a well-defined particularly simple route structure, but complicates it on the other hand, as the space of feasible solutions renders often very difficult to provide conflict-free solution.

Nevertheless, formulation (2.13) is highly combinatorial, non-linear, with a non-explicit objective function (we cannot express it in terms of decision variables), thus, rather complicated. As a consequence, we propose to solve the problem using a *stochastic method*. When using this term we mean stochastic (non-deterministic) methods for addressing global/discrete optimization problem (do not confuse with stochastic optimization). In the next section, we describe the metaheuristic algorithms we are proposing to address problem (2.13).

2.3 Stochastic algorithms

In this section we describe the two stochastic algorithms that were used to solve the considered optimization problem:

- Genetic Algorithm (GA), and
- Simulated Annealing (SA).

2.3.1 Genetic Algorithm

The *Genetic Algorithm* (GA) is a stochastic method of optimization, based on the evolutionary theory and implementing such concepts as *mutation*, *crossover* and *selection* [41, 42]. Each possible solution of the problem is encoded as a *chromosome* via a specific encoding. The algorithm creates randomly the first *population* of chromosomes. The ability of each chromosome to solve the problem, referred to as *fitness*, is then evaluated. The best individuals, according to their fitness, are selected, and then crossovers and mutations are applied, with user-defined probabilities Pc and Pm respectively, to obtain a new population of chromosome, called the next *generation* (see Figure 2.10). The size of the population S_P and the number of generations N_G are also parameters to be adjusted by the user for the algorithm, as well as the types of evolutionary operation used in order to reach the best convergence (trade-off between the quality of the solution obtained and the CPU time required to reach it). The choice of the user-defined parameter values is usually made empirically.

To specify the correspondence between the described mathematical model and the GA, we first need to define the chromosome encoding. For our problem, a chromosome represents the ATs of the set of N flights, using a vector y, consisting of N vectors y^f, each of which refers to a particular flight f. A vector y^f contains an instantiation of decision variables: δ^f, e^f, o^f, x_i^f, $i = 1, 2, ..., Nx - 1$ (Fig. 2.11). An AT is completely defined by these variables together with the flight input parameters, *i.e.* TD_e^f, TD_o^f, FL_i^f, v_i^f, $i = 1, 2, ..., Nx - 1$.

Further, we need to adapt the genetic operators to the model being studied. These operators should allow the algorithm to search throughout the whole set of feasible

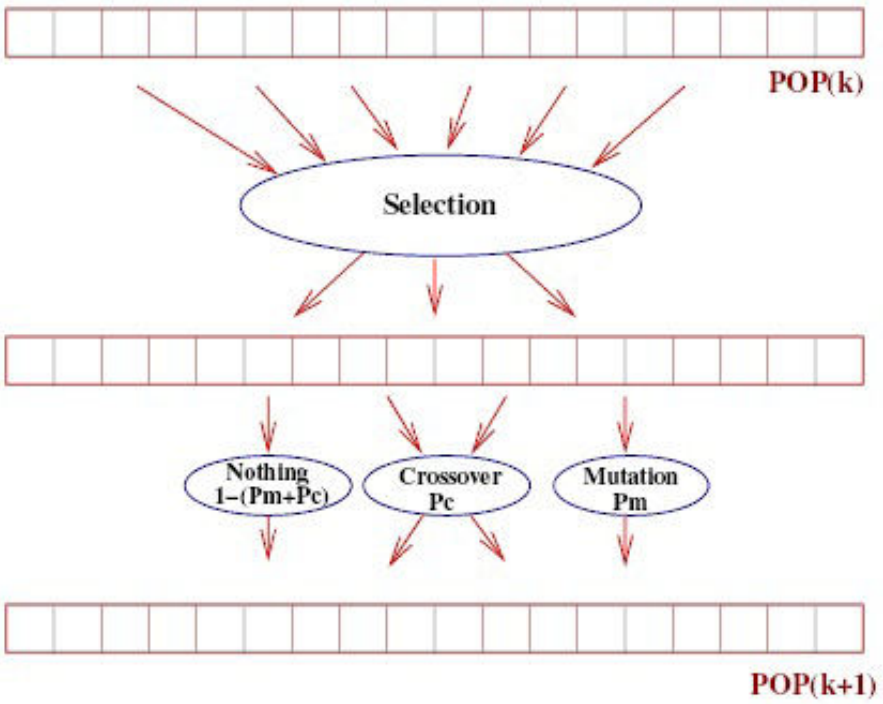

FIGURE 2.10: Genetic Algorithm scheme

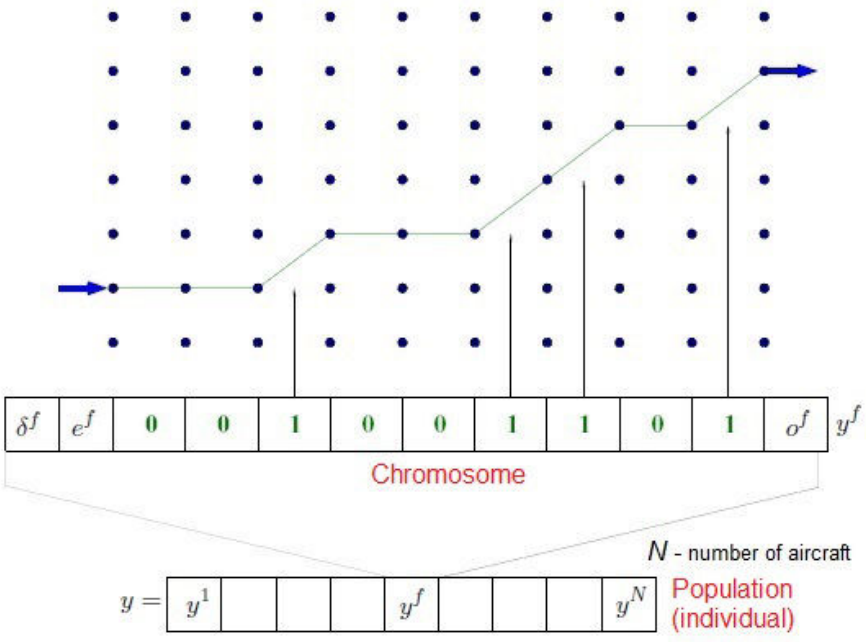

FIGURE 2.11: Chromosome representing a set of flights

solutions. The *crossover* operator aims at finding better solutions by combining features of two good individuals of the previous generation. The chosen crossover operator, when applied to the chromosomes representing the set of ATs, inverts the *complete ATs* only, meaning that a particular AT cannot be cut in the middle in order to be concatenated

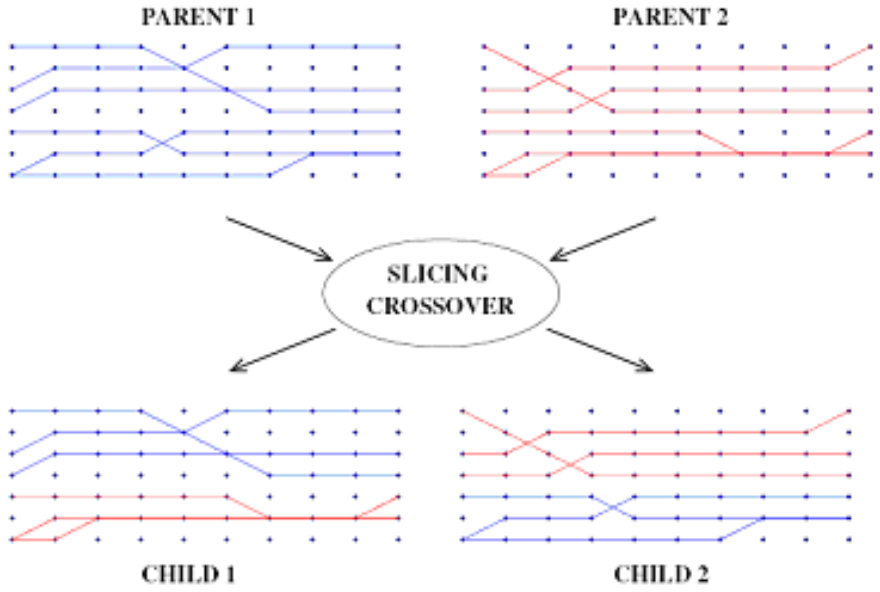

FIGURE 2.12: Crossover operator applied to two flight sets

with the corresponding part of another AT (Fig. 2.12). In other words, the usual crossover principle is here applied to a *set of flights*.

In contrast to the crossover, the mutation operator that we have implemented, is applied to a *single trajectory* (not to the whole set). A *mutation* operator aims at diversifying the search, *i.e.* diversifying the genes in the population in order to explore as much as possible the problem state space. The mutation we propose for our model consists in choosing randomly one flight f, and changing randomly some of its variables. For example, the mutation of re-routing variables involves choosing randomly two variable x_i^f and x_j^f having different values (0 and 1), and permuting their values (Fig. 2.13).

In our study, we implemented a version of GA that solves a maximization problem. Thus, the fitness function should be inverse of the objective function, $F_2(y)$, introduced in the equation (2.12) (Section 2.2.5). We have chosen to define it as follows:

$$fitness(y) = \frac{1}{\epsilon + F_2(y)}, \tag{2.15}$$

where ϵ is a user-defined small coefficient.

Different operators of selection, crossover and mutation were tested empirically on typical problem sets (that will be defined later) to achieve the best computational results.

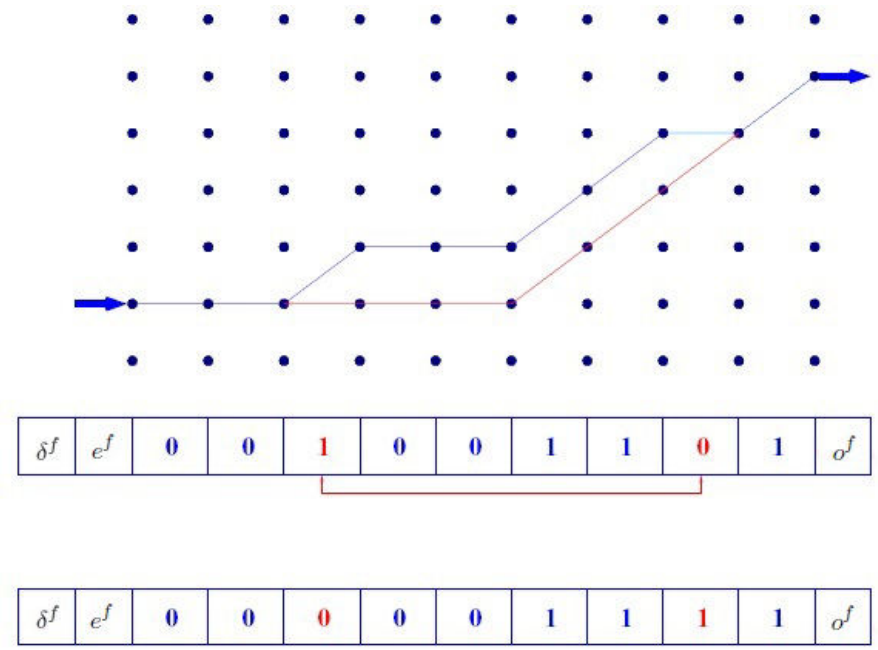

FIGURE 2.13: Mutation operator applied to a flight trajectory

These tested operators are described more precisely in Appendix Q, where we also identify those, giving the best performance of the GA and that are chosen for further simulations. Finally, we give here the values of several GA parameters that were empirically determined after several tests:

- $Pc = 0.5$;
- $Pm = 0.4$;
- $S_P = 200$;
- $N_G = 1,000, 3,000$ and $5,000$ (we will report results for these three values);
- $\epsilon = 0.01$.

The results of the GA application are presented in Sections (2.4).

2.3.2 Simulated Annealing

Simulated Annealing (SA) is a metaheuristic based on the thermodynamics theory [43, 44]. It imitates the annealing of the metal, involving *heating* and controlled *cooling*. Each point s of the search space is considered to be analogous to a *state* of some physical

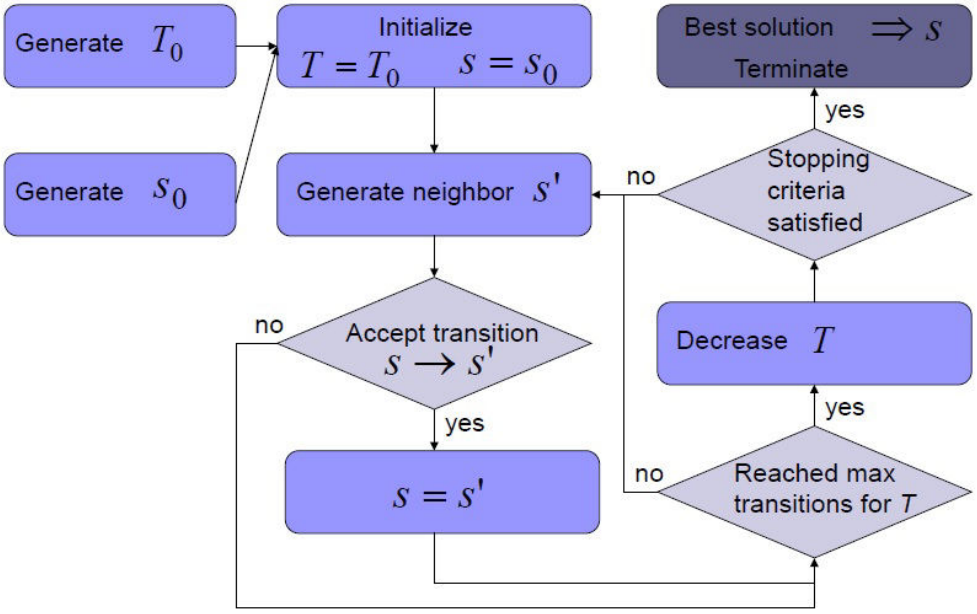

FIGURE 2.14: Simulated Annealing scheme (cooling process)

system, and the objective function to be minimized is analogous to the *internal energy*, $E(s)$, of the system in that state. The goal is to bring the system, from an arbitrary initial state, to a state with minimal energy (an optimal solution of the minimization problem).

At each step, the SA heuristic considers some neighboring state (solution) s' of the current state (solution) s, and probabilistically decides between moving the system to state s' or staying in state s. This probability depends both on the difference between the corresponding function values $E(s)$ and $E(s')$, and also on a global parameter T (called the *temperature*), that is gradually decreased during the process (more precisely, at each iteration). The dependency is such that the choice between the previous and the current solutions is almost random when T is large (during the first iterations), but the better solutions are increasingly selected as T decreases towards zero (as the number of iterations grows). The process of temperature decreasing is referred to as *cooling*. Typically, this step is repeated until the system reaches a state that is considered good enough, or until a given computation budget has been exhausted.

A basic scheme of SA (cooling process) is presented in Figure 2.14. Several notions and parameters are to be defined and adjusted in order to establish the correspondence between the stated optimization problem and the SA notations:

- the representation of a state of the system (a solution), s, from the search space;
- the energy function (the objective function of the minimization problem), $E(s)$;
- the method to generate the neighboring state (or solution), s' from the current state, s;
- the probability of acceptance of the state transition from s to s' as a function of the temperature, denoted $p_a(s \to s', T)$;
- the initial temperature T_0;
- the law of temperature decreasing, defining the temperature schedule;
- the number of transitions N_t performed at a same temperature level;
- the stopping criterion for the algorithm.

The state of the system for the SA can be defined in the same way as the chromosome for the GA. Thus, here the state s will represent the trajectories of the set of N flights using a vector y (Fig. 2.11).

Since the studied optimization problem is a minimization problem, and since SA minimizes the energy $E(s)$, we define the energy function to be exactly the objective function defined in the equation (2.12): $E(s) = F_2(y)$.

To generate a neighboring state s' from the current state s, we implement mutation methods analogues to those used in GA (Fig. 2.13). The goal is to explore widely the search space at high temperatures (diversification at the beginning) and to reduce the search area as the temperature decreases in order to concentrate the search near the optimum to favor convergence (intensification at a later stage). Several mutation methods and their combinations were tested, and those giving the best convergence were chosen (see Appendix R).

The probability of acceptance of the state transition in the classical SA is defined by the following formula:

$$p_a(s \to s', T) = \begin{cases} 1 & \text{if } E(s') < E(s) \\ e^{\frac{E(s)-E(s')}{T}} & \text{if } E(s') \geq E(s) \end{cases} \tag{2.16}$$

The initial temperature T_0 is to be adjusted for a particular class of problems, so as to provide an acceptance of most of the proposed transitions. The process of the initial temperature adjusting is analogue to the process of *heating the metal*. It starts with some small temperature value, denoted T_0^0, that can be obtained from examining some number, N_h, of different system states, $\{s_i\}_{i=1}^{N_h}$, that we choose randomly:

$$T_0^0 = \frac{0.01}{N_h} \cdot \sum_{i=1}^{N_h} E(s_i). \tag{2.17}$$

Then at each step the current temperature is increased by multiplying it with some user-defined value $\beta > 1$:

$$T_0^i = \beta \cdot T_0^{i-1}. \tag{2.18}$$

These steps are repeated until the acceptance probability at the current temperature becomes sufficiently large, *i.e.* when: $p_a(s \to s', T_0^i) \geq \mu$, where μ is a user-defined initial acceptance probability, usually relatively large. The last obtained temperature is then chosen as the initial temperature T_0.

The process of temperature decreasing is the analogue of the system cooling in the metallurgy paradigm. The cooling should be sufficiently slow so as to allow the system to reach the thermodynamic equilibrium, or, in terms of our optimization problem, so as to avoid premature convergence towards a non-interesting local minimum. We choose the usual exponential cooling scheme:

$$T_i = \gamma \cdot T_{i-1}, \tag{2.19}$$

where γ is a user-defined parameter whose value is close to but smaller than 1. Again, different values of γ were tested for the algorithm.

In our adaptation of SA, we choose the number of transitions, N_t, tested at each particular temperature level, to be constant. The algorithm stops either when an optimal solution, $s*$, is found, or when the temperature goes below a predefined (user-defined) critical value, denoted T_f.

After several tests on typical instances of our problem (that will be described later) we choose the following parameter values:

- $N_h = 1,000$;
- $\beta = 0.2$;
- $\mu = 0.8$;
- $\gamma = 0.9, 0.95, 0.99$;
- $N_t = 1,000, 2,000$;
- $T_f = 0.0001 \cdot T_0$.

2.3.3 Computational environment

The GA and SA algorithms are implemented in Java. For most of the tests, they are run under Windows-32 operational system, on Intel Core$^T M$ 2 CPU with 1.73 GHz. The results of these implementations are presented in the next section, where we give the CPU times for some tests. These times may seem to be quite large; that is due to the limited performance of the computer used. The CPU times can be significantly decreased for more efficient operational systems. For example, launching the same tests under Windows-64 operational system, on Intel Core i7-3610QM CPU with 2.30 GHz yields the results up to 3 times faster.

2.4 Results of simulations

In this section, we summarize the results of the application of the developed algorithms to real air traffic crossing the NAT. Prior to address the real data, we first present results of the algorithms on to artificially generated data. This data is used first, to prove the algorithms applicability to solve the postulated problem, and next, to adjust the algorithm parameters to achieve the best convergence. After that, we describe the real oceanic data. Finally, we demonstrate how applying the implemented stochastic algorithms ameliorates the air traffic situation in NAT.

2.4.1 Random flight data

This section presents the results obtained with GA and SA applied to artificially generated data. Using such sets permits to adjust several important algorithm parameters

and to test algorithm efficiency for various input data. On this preliminary step, we are interested in conflict resolution only. The corresponding objective function to be minimized, thus, includes the total number of conflicts induced by the flights. It is defined by equation (2.14).

To test the proposed algorithms, five flight sets are generated randomly. An aircraft flight set consists of $N = 500$ flights randomly generated on a 4-hour time period with realistic altitude profiles and speed. Each flight f is defined by the values TD_e^f, TD_o^f, t_{in}^f, v_i^f, FL_i^f, for $f = 1, 2, ..., 500$. The aircraft TAS is set constant through the whole flight over NAT. It is randomly uniformly selected in the range from 450 knot to 500 knot. For this preliminary study, we do not take the wind in account, considering the flights to cruise without winds. The aircraft are allowed to select an entry time delay in the range {0, 5, 10, 15, 20, 25, 30} minutes, *i.e.* $N_d = 6$ and $slot = 5$ min.

The OTS is modeled with a regular grid consisting of $Ny = 7$ tracks having $Nx = 10$ WPs and involving $Nz = 10$ FLs each. The distance between the tracks is set to be 1°, which corresponds to 60 NM (111.11 km). The distance between WPs is 10°, *i.e.* 30 NM (558 km) at the latitude of 60° (taken as an example). The distance between the FLs was 1,000 feet (304.8 m). In our simulations, we neglect the climbing time and climbed distance. In order to compensate the error caused by this simplification, we multiply the longitudinal separation value between two consecutive aircraft, Δ, by 1.1 at a WP, if one of these aircraft changed its FL at this WP.

For each algorithm, two types of tests are conducted involving the same generated flight sets.

- In the first case, the CSS is applied to all aircraft in the set. We recall, that longitudinal separation value for the CSS is 10 minutes for consecutive aircraft and 15 minutes for re-routing aircraft.
- In the second case, we suppose all aircraft to be equipped with new generation surveillance and broadcast technologies (e.g. ADS-B). Thus, we could apply the RSS, where the longitudinal separation is set to be 2 minutes for consecutive aircraft and 3 minutes for re-routing aircraft.

For the flights under CSS, non of the algorithms can find a conflict-free solution. This confirms that aircraft are obliged to fly the routes that are not optimal. However, both

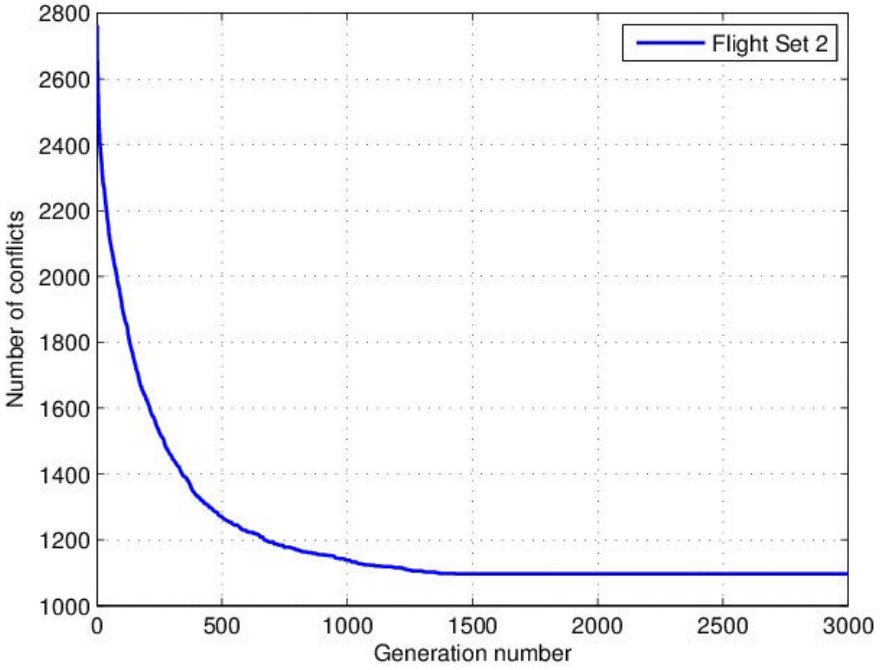

FIGURE 2.15: Genetic Algorithm progress for a flight set with CSS

algorithms can decrease the total number of conflicts by about a factor of 3 in comparison to the initial number of conflicts.

For the GA, different values for the number of generations, N_G, are tested in order to seek better solutions. Figure 2.15 represents the GA progress for one of the test flight sets with $N_G = 3,000$. The initial number of conflicts in this case is 2,764; final number of conflicts is 1,096; and the time of algorithm execution is 58 minutes.

For the SA, different values of the temperature decrease parameter, γ, are tested. The results of simulations for the same flight set are represented in Figure 2.16. The initial number of conflicts in this case was 2,885. The best solution involves 791 conflicts.

Comparison of the GA and the SA algorithms is made over two criteria: the quality of the best solution found and the CPU time of execution. Table 2.1 represents the results of this comparison for the same flight set. From these results, it can be concluded that for this test with RSS, SA finds better solutions than GA and it does so in much less time.

For the flight sets, where all aircraft are considered to be equipped with modern technologies, and where the RSS are thereby applied, both algorithms find an optimal (*i.e.* conflict-free) solution for all the studied tests.

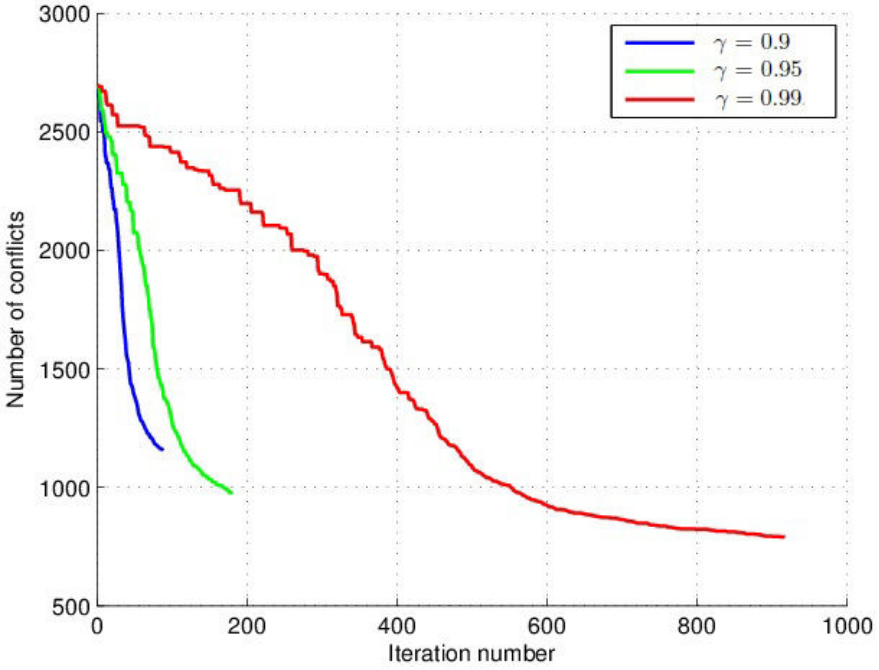

FIGURE 2.16: Simulated Annealing progress for a flight set with CSS

Algorithm (initial number of conflicts)	- GA: N_G - SA: γ / number of iterations cooling / total	- GA: S_P - SA: N_t	Number of objective function evaluations	CPU time (min.)	Best solution, final number of conflicts
GA (2,764)	1,000	200	200,000	21.5	1,374
	3,000	200	600,000	57.5	1,096
	5,000	200	1,000,000	102.5	10,24
SA (2,775)	0.9/88/101	1,000	101,000	8.5	1,156
	0.95/180/193	1,000	193,000	15.0	972
	0.95/180/193	2,000	386,000	30.5	911
	0.99/917/930	1,000	930,000	66.0	791

TABLE 2.1: Computational results comparison of GA and SA for a flight set with CSS

GA produced an optimal solution in less than 1,000 generations for all the tests. For each particular test, the time of execution depends on the number of generations, thus it differs between the tests. The average number of generations sufficient for solving the problem for the 5 tested flight sets is 683, and the average time of execution is 14.5 minutes. The average time of algorithm execution for 1,000 generations is 23 minutes. Figure 2.17 represents the GA progress.

SA generates an optimal solution with both values of the temperature decrease parameter: $\gamma = 0.9$ and $\gamma = 0.95$, for all the studied tests. As the temperature decrease

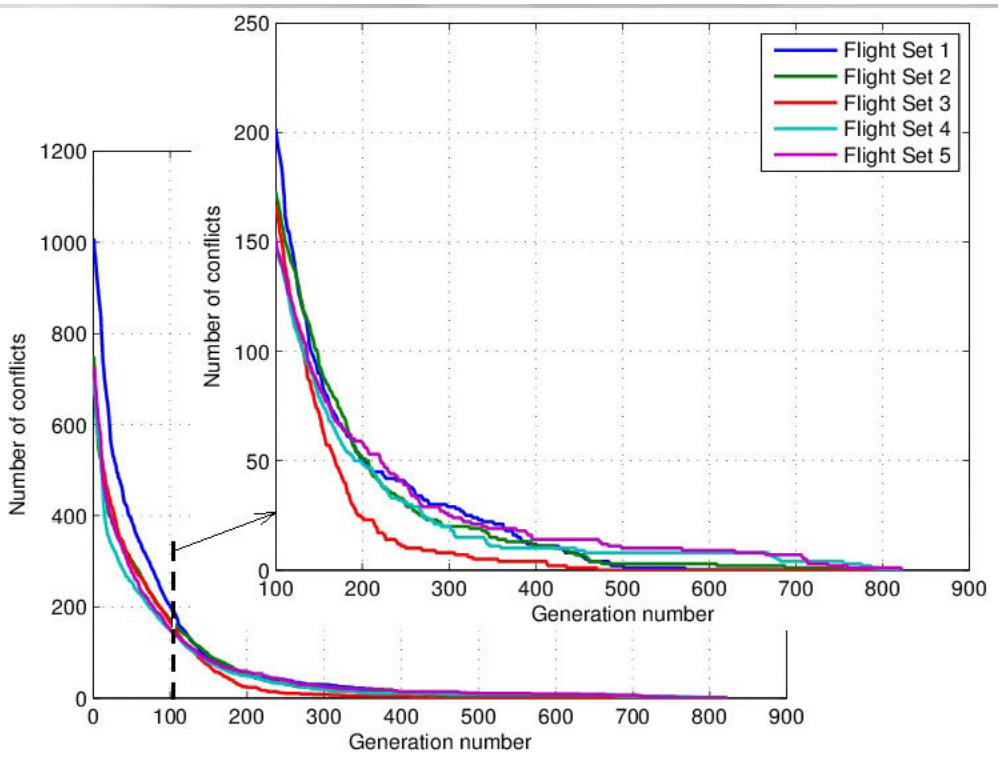

FIGURE 2.17: Genetic Algorithm progress for flight sets with RSS

parameter $\gamma = 0.9$ yields better convergence results, it is chosen be used for the following experiments. The average number of iterations during the heating process for the 5 test is 13. The average number of iterations for cooling with $\gamma = 0.9$ is 40. The average time of algorithm execution is 8 minutes. Figure 2.18 presents the SA progress (cooling process, the number of conflicts as a function of the number of iterations, for the 5 flight sets, and as a function of the number of transition for one of the flight sets).

Table 2.2 displays the results of comparison of GA and SA for tests with RSS. From these results, we conclude that, for these tests with RSS, SA finds optimal solutions faster than GA.

The main conclusions that we draw from these simulations, for the studied artificial flight sets, are:

- no conflict-free flight configuration seems to exist when CSS applied;
- a conflict-free solution always exists when RSS is applied;
- SA is more efficient than GA (in terms of computational time).

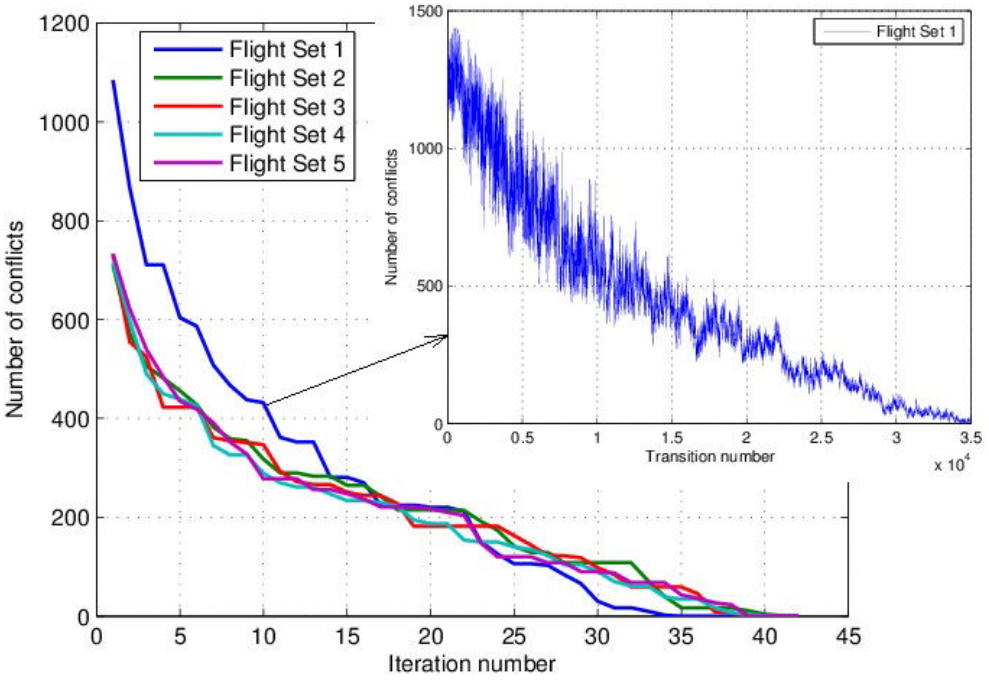

FIGURE 2.18: Simulated Annealing progress for flight sets with RSS

Algorithm	Flight Set	Initial number of conflicts	Final number of - generations (GA) - heating/cooling iterations (SA)	Number of objective function evaluations	CPU time (min)
GA ($N_G = 1,000$ $S_P = 200$)	1	1,009	573	114,600	13.5
	2	750	755	151,000	15.5
	3	730	471	94,200	10.0
	4	699	795	159,000	16.0
	5	727	822	164,400	17.5
SA ($\gamma = 0.9$ $N_t = 1,000$)	1	1,263	14 / 36	65,000	8.0
	2	890	13 / 43	70,000	8.0
	3	874	13 / 41	68,000	8.0
	4	790	13 / 42	69,000	8.0
	5	880	13 / 40	67,000	8.0

TABLE 2.2: The GA and the SA computational results comparison for flight sets with RSS

2.4.2 Real flight data

In order to build test sets based on real data, we select two days: **August 3, 2006** and **August 4, 2006**. The oceanic traffic data was obtained from the report files from Shanwick OACC (Oceanic Area Control Center). Each such file contains the report messages received by Shanwick OACC from different sources, including NAT messages, FPL messages, OCLR (Oceanic Clearance) messages, flight POSs (Position Reports) etc.

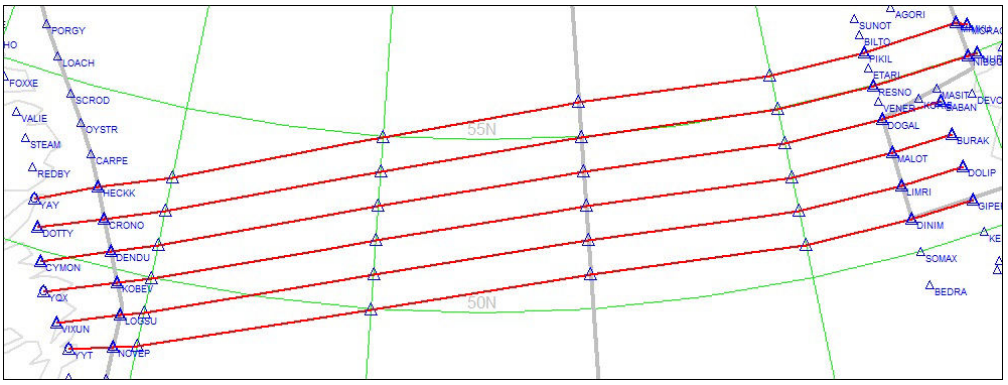

FIGURE 2.19: Eastbound OTS tracks for August 3rd 2006

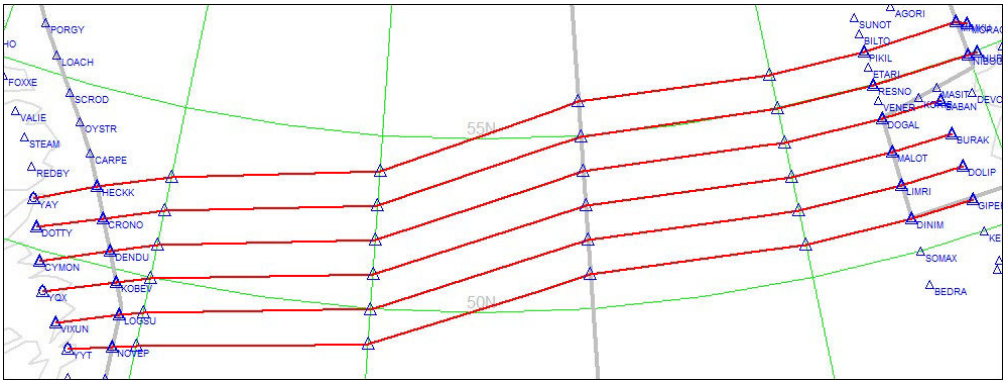

FIGURE 2.20: Eastbound OTS tracks for August 4th 2006

The process of extracting the information necessary for our simulations, is described in Appendix S.

The OTS is modeled with a grid of WPs extracted from NAT messages (see Appendix N for more detail). For the two selected days, the OTS consisted of $Ny = 6$ tracks (*U, V, W, X, Y* and *Z*) involving $Nx = 8$ WPs each, and $Nz = 9$ FLs (from FL320 to FL400). The WPs are defined by their geographic coordinates. The distances between them is measured according to these coordinates along the Great Circles (GCs) connecting these WPs (the corresponding formula is given Appendix Y). Figures 2.19 and 2.20 present the eastbound oceanic tracks for the dates August 3rd and August 4th 2006 respectively.

The set of flights for each of the studied days is extracted from FPL messages (see Appendix O for more detail). We select only the eastbound flights that planned to utilize the night-time OTS during its period of validity, and which FPL messages provided all the information necessary for our simulations, *i.e.* the Machs/FLs at WPs, and the track entry times (see Appendix S). The track entry time, t^f_{in}, if not defined directly, is calculated using the *Estimated Elapsed Times* (EETs) declared for the following track

WPs and the estimated times of cruising between the WPs (see Appendix T). Aircraft speeds, v_i^f, (obtained from Machs, see Appendix G) and FLs, FL_i^f, if not defined directly at some WPs, are extrapolated from previous WPs. The resulting files with extracted data used in our simulations are available online [45]. To sum up, for the studied days, we obtain flight sets consisting of:

- $N = 331$ flights, for August 3rd, 2006;
- $N = 378$ flights, for August 4th, 2006.

Furthermore, for the real flight sets, we do take into account the wind during the simulations. As the Jet Streams (JSs) have predominantly the eastern direction, they contribute mainly to the tails winds for eastbound flights. The average tail WSs between the OTS WPs are calculated on the basis of the EETs of cruising between these WPs, obtained from ETAF (Elapsed Time And Forecast) messages (see Appendix T). They are then denotes as W_{ijj} for the link $(i, j, k) - (i + 1, j, k)$. For the crossing links, *i.e.* the links $(i, j, k) - (i + 1, j', k)$, where $j' = j - 1$ or $j' = j + 1$, the corresponding WSs along these links are denoted $W_{ijj'}$. They are obtained via a linear interpolation of the closest determined values: W_{ijj} and $W_{ij'j'}$. Thus, when performing the flight progress, the magnitude of the aircraft Ground Speed (GS) along a link $(i, j, k) - (i + 1, j', k)$, where $j' = j$, $j' = j - 1$ or $j' = j + 1$, is computed by adding the corresponding WS, $W_{ijj'}$, to the aircraft TAS, v_i, obtained from the Mach defined in the FPL.

We note that the WS depends strongly on the FL. Figure 2.21 presents the distribution of the use of the track FLs among the N flights of each data set. It reveals that the most occupied level is FL370.

Figures 2.22 and 2.23 represent the distribution of the wind between the OTS tracks for FL370. Each column of the diagrams represents the average tail WS between the corresponding WPs (in m/s). One can observe that the wind significantly differs from one track to another. For August 3rd (Fig. 2.22), at the west part of the OTS it is more preferable to use southern tracks, while for the east part, the northern tracks feature stronger winds (this corresponds to the way OTS is constructed). For August 4th (Fig. 2.23), the wind distribution is more variable, with a slight preference for northern tracks in the east part of OTS as well.

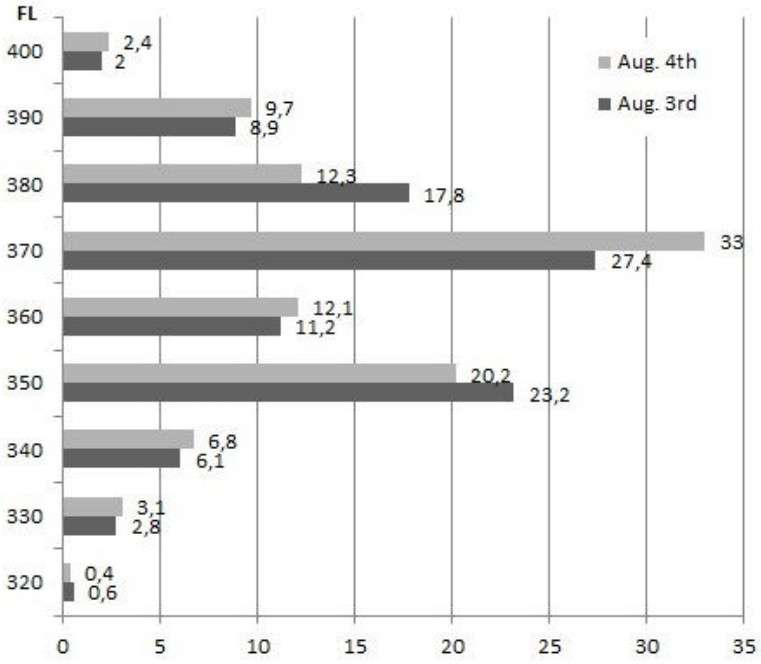

FIGURE 2.21: Percentage of track flight level usage for the two flight sets

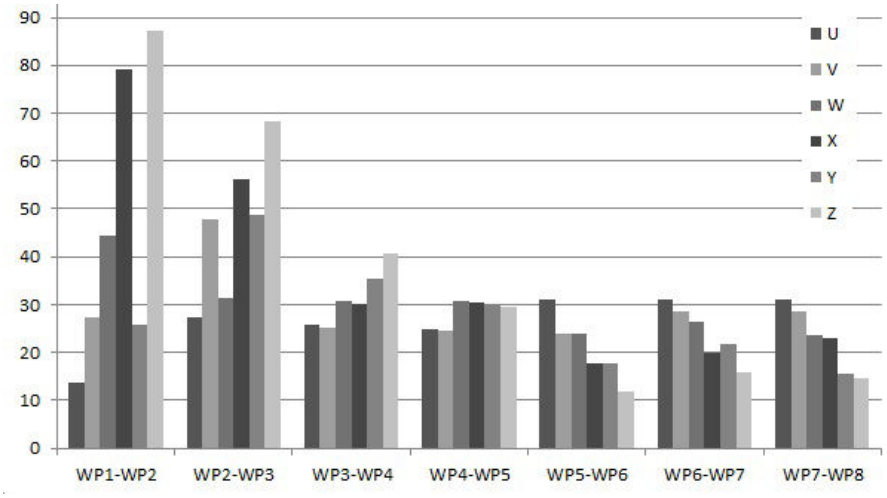

FIGURE 2.22: Wind speeds (m/s) between track waypoints on FL370 for August 3rd, 2006

2.4.3 Definition of desired entry and exit tracks

As mentioned before, in this study we consider that the *desired entry and exit tracks* of flight f (TD_e^f and TD_o^f) are those *closest* to the departure and arrival airports of this flight (*i.e.* the desired entry track of flight f is the track which entry point is the closest to the departure airport of this flight). Such a desired track definition makes sense as it permits to reduce the continental route crossings and, therefore, to reduce airspace congestion.

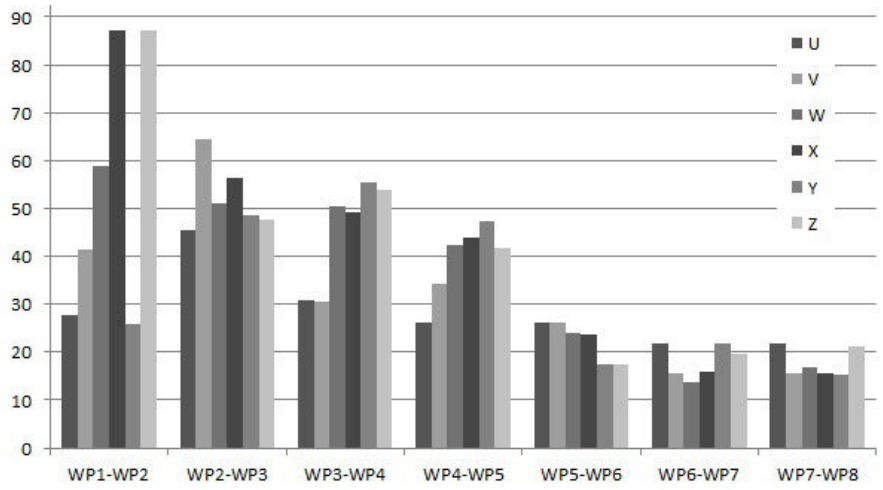

FIGURE 2.23: Wind speeds (m/s) between track waypoints on FL370 for August 4rd, 2006

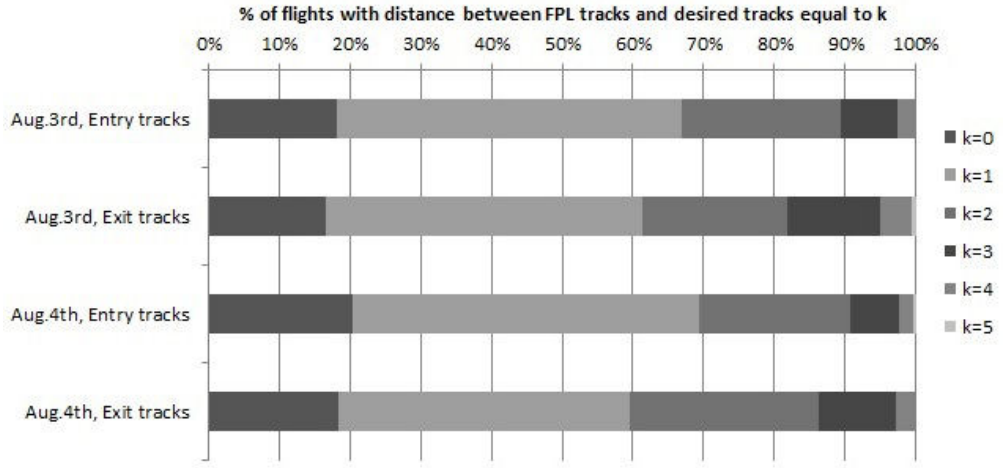

FIGURE 2.24: Comparison of FPL declared entry and exit tracks with corresponding computed desired tracks

Figure 2.24 compares the entry and exit tracks defined in FPLs with the desired entry and exit tracks. As can be seen from this diagram, according to FPLs, aircraft should generally follow tracks that are not optimal in terms of entry and exit points. Only about 20% of all flights enter the computed desired track, and only about 17% of flights exit the computed desired track. The number of flights that both enter and exit their desired tracks (according the FPLs) is only about 12 per set (about 3%). Figure 2.24 also reveals that the entry tracks are in general closer to desired tracks than the exit tracks are. This can be explained by the fact that the entry track to be put in the FPL, is chosen to be rather close to the departure airport, while the exit track in the FPL in most cases simply coincides with the entry track (as the re-routings are avoided in practice).

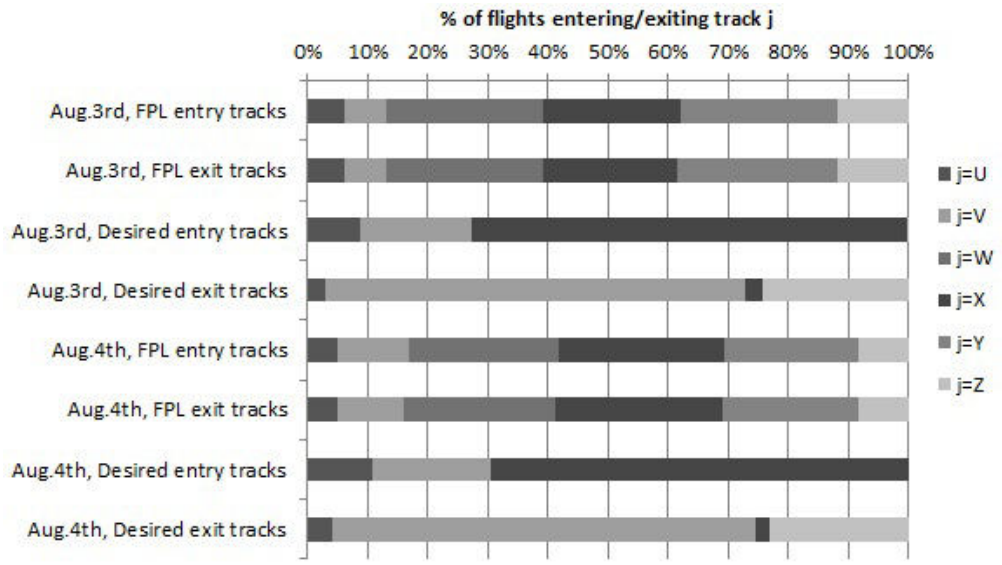

FIGURE 2.25: Repartition of flights over OTS tracks according to initial FPLs and to the computed desired entry/exit tracks

Figure 2.25 presents the repartition of flights over the OTS tracks. Tracks are ordered starting from the north. From this diagram it can be concluded that in the initial FPL, the repartition of the OTS tracks is more or less uniform, with a slight preference for using the middle tracks (those that benefit more from tail winds in the JSs). On the other hand, for the computed desired entry/exit tracks there is an evident tendency to attribute almost always the same tracks to aircraft (track X for entering; track V for exiting).

To show the advantages of using desired entry/exit tracks (based on the airport coordinates) rather than FPL-declared entry/exit tracks, we have calculated the number of flight route crossings in the continental airspace before entering and after exiting NAT. To do so, in each of the continental airspaces, we consider the flight route as an arc of the GC going from the departure airport to the track entry point, and from the track exit point to the arrival airport, respectively. A route crossing in the continental airspace is considered to be equivalent to a crossing of these arcs, not taking into account departure times. The airspace congestion is evidently related to the number of such route crossings. On the other hand, the flights utilizing the same routes in continental airspaces, as well as the flights entering/exiting the same tracks also contribute to congestion. However, these situations are considered more easily manageable than crossings. The corresponding quantities are presented in Table 2.3.

	FPL	Desired	FPL	Desired
Date	August 3rd		August 4th	
Total NbF (N)	331		378	
For American continental airspace before entering NAT				
Nb departure airports	33		38	
Total NbR	88	33	101	38
Max NbF for track	86	240	104	263
NbR in common	47	20	62	22
NbF with common routes	290	318	339	362
Max NbF for route	23	67	26	74
NbR crossings	961	0	1,447	0
NbF crossings	12,736	0	17,316	0
For European continental airspace after exiting NAT				
Nb arrival airports	44		51	
Total NbR	92	44	97	51
Max NbF for track	88	231	105	267
NbR in common	49	29	53	29
NbF with common routes	288	316	334	356
Max NbF for route	27	57	31	60
NbR crossings	677	0	497	0
NbF crossings	5,308	0	4,872	0

TABLE 2.3: Flight route crossings in continental airspace

In Table 2.3, the columns "FP" correspond to flight sets with entry/exit tracks extracted from FPLs, while the columns "Desired" give the values for flights with entry/exit tracks closest to departure/arrival airports. The abbreviation "Nb" stands for "Number"; "NbR" means "Number of routes" (here the routes in continental airspaces are concerned); and "NbF" means "Number of flights". We note that even if the number of common routes ("NbR in common") is almost twice as low for the "Desired" track attribution, the number of flights utilizing these routes ("NbF with common routes") is greater in this case. Moreover, there are more aircraft on a single route, as well as much more aircraft entering/exiting a single track for the "Desired" track attribution. This can augment the continental congestion. On the other hand, Table 2.3 presents two quantities related to crossings: the *number of route crossings* ("NbR crossings") which does not take into account the number of aircraft using these routes, and the *number of flight crossings* ("NbF crossings"), which depends on the number of aircraft using crossing routes. For the track attribution based on the initial FPL, crossings are quite numerous. However, for the "Desired" track attribution, there are no route crossings in the continental airspace. This choice would therefore decrease the congestion level, as expected.

Date	August 3rd	August 4th
Total number of flights (N)	331	378
Number of conflicts, C_t, CSS	811	876
Number of conflicts, C_t, RSS	245	259

TABLE 2.4: Conflicts produced by sets of flights declared in FPL messages

% of flights with different:	August 3rd	August 4th
Routes (Tracks/WPs)	2.4%	3.4%
Flight levels	40.8%	45.5%
Speeds	23.3%	26.5%
Track entry time	96.7%	97.1%
Track entry time $>$ 30 minutes	65.6%	67.5%
Track entry time $>$ 2 hours	8.8%	19.3%

TABLE 2.5: Percentage of aircraft having en-route flight parameters different from those defined in initial FPLs

To conclude the explanation of the particularities of the real oceanic data used in our simulations, we present some remarks concerning initial FPLs extracted from the record files. Each flight trajectory is defined in the FPL via the sequence of WPs followed in some cases with particular FLs and/or Mach numbers. We express this trajectory data in terms of the mathematical model input data: TD_e^f, TD_o^f, t_{in}^f, v_i^f, FL_i^f and the decision variables x_i^f. Furthermore, we consider: $e^f = TD_e^f$, $o^f = TD_o^f$, and $\delta^f = 0$, for each flight f. We obtain thereby one instantiation of the optimization problem (one particular solution). Further, this set of trajectories is evaluated over the corresponding OTS grid and the number of conflicts, C_t, induced by these flights is computed. As one can see from the results of this simulation presented in Table 2.4, even with RSS, there still remain aircraft in conflict according to their initial flight plans. Thus, the published FPLs for the two sets of flights could not be fulfilled as such in reality (there has been changes imposed by ATC).

Table 2.5 reveals how the flights in the reality are deviated from their initial FPLs. The table displays for each day, the percentage of flights having route parameters (tracks, FPLs, speeds, entry times) different from those defined in the FPL. Note that almost all flights are affected by deviations.

The goal of the next section is to produce new FPLs for the sets of flights with respect to the desired departure and arrival points and track entry time that would guarantee no conflicts, at least with RSS.

MSS	Test (N)	Algo	Algorithm parameters	N_d	Total num.: GA generat. SA iterat.	CPU time (min)	Init. num.of confl.	Best num of. confl.
CSS	Aug 3 (331)	GA	$N_G = 3,000$	6	3,000	34	1,055	129
		SA	$\gamma = 0.99$	6	917	36.5	1,133	51
	Aug 4 (378)	GA	$N_G = 3,000$	6	3,000	38	1,316	219
		SA	$\gamma = 0.99$	6	917	39	1,415	96
RSS	Aug 3 (331)	GA	$N_G = 1,000$	6	112	1	255	0
				1	784	8	285	0
		GAm		1	1,000 (635)	9.5	285	0
		SA	$\gamma = 0.9$	6	8	1	329	0
				1	13	1	376	0
	Aug 4 (378)	GA	$N_G = 1,000$	6	167	2	330	0
				1	700	8	386	0
		GAm		1	1,000 (762)	11	386	0
		SA	$\gamma = 0.9$	6	10	1	453	0
				1	12	1	474	0

TABLE 2.6: Results of conflict reduction by GA and SA applied to real oceanic traffic data

2.4.4 Computational results: comparing the GA and SA algorithms

In this section we present the results of the GA and SA algorithms when applied to the real oceanic data. We first present preliminary results aiming at eliminating conflicts essentially. Further, we include other criteria in the objective function. The comparison of the presented stochastic methods is made at the same time.

First, let us compare the number of conflicts in the obtained solutions and the algorithm computational time. The obtained results of algorithm application qualitatively are analogous to the results obtained on the simulated artificial data, presented in Section 2.4.1:

- when subject to CSS, no conflict-free ATs can be generated for the real flight sets;
- on the other hand, in presence of RSS, the algorithms produce conflict-free FPLs;
- SA converges to an optimal solution much faster than GA.

Quantitative results are presented in Table 2.6. The lines of Table 2.6 corresponding to GA and GAm demand some additional explanations. For GA, the objective function involves only the number of conflicts, as defined by equation (2.14). Thus, once a solution with no conflicts is found, GA stops. The variant GAm, considers several criteria in the

Date (N) of flights)	Algo	N_d	Percentage of flights					Total delay (hours)
			with desired tracks			not delayed	delayed by 5 min.	
			entry	exit	entry &exit			
August 3rd (331)	GA	6	93.4%	93.4%	87.0%	13.9%	12.4%	84.2
		1	83.1%	84.0%	69.5%	53.2%	46.8%	12.9
	GAm	1	95.8%	94.9%	90.6%	71.9%	28.1%	7.8
	SA	6	49.2%	54.7%	27.5%	13.0%	14.2%	84.8
		1	49.2%	48.9%	23.6%	51.1%	48.9%	13.5
August 4th (378)	GA	6	91.5%	91.3%	83.6%	13.2%	11.9%	100.5
		1	85.7%	84.4%	74.3%	52.6%	47.4%	14.9
	GAm	1	91.3%	94.0%	85.2%	73.5%	26.5%	8.3
	SA	6	49.7%	49.2%	25.1%	17.5%	11.6%	97.4
		1	47.4%	50.3%	23.0%	49.2%	50.8%	16.0

TABLE 2.7: Comparison of GA and SA solutions in terms of the optimality of entry and exit tracks and track entry delays

objective function ("m" stands for "multi"): the number of conflicts, C_t, the total track entry delay, D, and the total deviation delay, G, as defined via equation (2.12) by setting: $\alpha = 1/36,000$; $\alpha_d = 1$; $\alpha_g = 1$; and $\alpha_p = 0$:

$$F_2^1(y) = C_t(y) + \alpha(D(y) + G(y)). \tag{2.20}$$

Thus, GAm aims at eliminating conflicts while reduces en-route delays. The choice of a small value of α gives the highest priority to the conflict-free criterion. As a result, the algorithm tends to eliminate first all the conflicts. Once it is done, GAm does not stop (contrary to GA) but it continues to reduce the en-route delays, while ensuring the solution to remain conflict-free. The lines of column 6 ("Total num.: GA generat. SA iterat.") of Table 2.6 corresponding to GAm contain two numbers. The first one (1,000) gives the total number of generations performed (that determines the CPU time). The second number (mentioned in parentheses) represents the generation number at which all conflicts were eliminated.

Table 2.7 presents some more results of GA and SA applications for flight sets with RSS. From Table 2.6, we observe that both algorithms find optimal conflict-free solutions for all studied flight sets, and that SA is much more efficient in terms of execution time than the GA. In Table 2.7 the comparison of the obtained solutions is made over two other criteria: the number of flights entering/exiting their desired tracks, and the track entry delays.

The first conclusion that can be drawn from Table 2.7 is that GA satisfies the aircraft desired entry/exit track demands much better than SA:

- Indeed, more than 80% of aircraft from GA solution enter/exit their desired entry/exit track, while for SA this value is only about 50%.
- Concerning the total number of aircraft that are not delayed, and the total value of delays, both algorithms give approximately the same results: about 13% of aircraft are not delayed, and the total delay is between 80 and 100 hours.

Thus, although SA converges much faster than GA, it gives much worse results in assigning desired tracks to aircraft. This observation can be explained by the fact that the SA performs much more mutation operations than GA does (for the same number of objective function evaluations), and this permits to find a conflict-free solution faster. However, the high number of mutations leads to an approximately equal distribution between the aircraft that enter/exit the desired track and those that are deviated. From the presented results we conclude that, if the aim is to obtain ATs that are not only conflict-free but also feature minimal values of delays and track deviations, it is more favorable to use GA .

The next observations concern the total number of time slots, N_d, used to deliver the track entry delay, d^f, to an aircraft f.

- Evidently, the fewer the number of slots could be delivered, the smaller would the total entry delay, D, be. This statement is confirmed by the results of both algorithms (GA and SA): decreasing N_d from 6 to 1 leads to a significant increase in the number of not-delayed flights from around 13% to around 50% and to a great decrease of the total entry delay from 84 to 13 hours, and from 100 to 15 hours, for August 3rd and 4th respectively.
- At the same time, for GA, decreasing the number of slots results in an increase of the number of aircraft deviated from their desired entry/exit tracks (approximately from 10% to 20%). This fact is rather intuitive too: having lost the degrees of freedom for one optimization parameter ($\delta \in \{1, ..., N_d\}$) the algorithm applies the mutation operation more often to the other optimization parameters (e^f, o^f).

- For SA, this operation does not produce an important effect, as in any case the distribution between deviated and non-deviated flights is almost identical.

Finally, we conclude that the two criteria: the number of deviations and the value of delays, are opposite: decreasing one of them leads to an increase of the other. Thus, interesting solutions are compromises. GAm aims at producing this kind of solutions: it minimizes simultaneously the number of deviations and the delays. Table 2.7 presents the results of the GAm application with $N_d = 1$. As it can be seen, the resulting solutions are better than those produced by GA (they dominate the solutions yielded by GA):

- the number of flights entering/exiting desired tracks is increased by 2% in comparison with the solution of GA with $N_d = 6$, and achieves 95%;
- the number of non-delayed flights is increased by 20% in comparison with the solution of GA with $N_d = 1$, and exceeds 70%;
- the total entry delay is decreased by 5-7 hours in comparison with the solution of GA with $N_d = 1$; it is only 8 hours (which is not much, for more than 300 flights).

To summarize, we conclude that the best solution in terms of number of conflicts, number of desired track deviations, and value of delay is given by the GAm algorithm with a minimal number of possible time slots, although GAm demands more CPU time. In the next section, we discuss some more results, that involving the GAm application.

2.4.5 Computational results: different criteria in the objective function

As it can be concluded from the previous section, including criteria other than the number of conflicts in the objective function can improve the resulting solution from the point of view of Air Traffic Management (ATM). In this section, some more criteria of optimality are investigated and the corresponding solutions are compared. Several test problems with different objective functions (defined by equation (2.12) using different weighting coefficients) are constructed based on the real flight sets for each day (August 3rd and 4th). Four of them are described in Table 2.8, in the first five lines (note,

Test		1	2	3	4
Criteria		D, G	P	D, P	D, G, P
Weighting coefficient values	α_d	1	0	1	1
	α_g	1	0	0	1
	α_p	0	1	1	1
August 3rd 2006					
% of flights with desired entry track		**95.8%**	28.7%	31.1%	94.0%
% of flights with desired exit track		94.9%	12.1%	16.3%	**95.2%**
% with desired entry & exit tracks		**90.6%**	3.0%	4.5%	90.3%
% of not delayed flights		71.9%	49.8%	**84.6%**	72.5%
Total entry delay D (hours)		7.75	13.83	**4.25**	7.58
Total cruising time P (hours)		1,055.81	**1,024.31**	1,025.66	1,049.71
Average cruising time (hours)		3.19	**3.09**	3.10	3.17
August 4th 2006					
% of flights with desired entry track		91.3%	49.2%	46.6%	**92.1%**
% of flights with desired exit track		**93.9%**	28.3%	27.0%	92.9%
% with desired entry & exit tracks		85.2%	15.9%	11.9%	**86.0%**
% of not-delayed flights		73.5%	53.9%	**80.7%**	74.9%
Total entry delay D (hours)		8.33	14.50	**6.08**	7.92
Total cruising time P (hours)		1,178.24	**1,148.38**	1,148.82	1,169.36
Average cruising time (hours)		3.12	**3.04**	**3.04**	3.09

TABLE 2.8: Comparison of different criteria implemented in the GAm objective function

that Test 1 corresponds to GAm algorithm from Section 2.4.4). For all the tests, the computational experiments are performed with the same parameter values: $N_G = 1,000$ and $N_d = 1$. The results are compared in Table 2.8 via different criteria. The best values are highlighted in **bold**. The presented results are not surprising:

- The tests that include the track-deviation criterion, G, in the objective function (Tests 1 and 4) give excellent (and equivalent) results in attributing desired tracks to aircraft (more than 90%), while for the remaining tests (Tests 2 and 3) these results are rather poor (less than 50%).

- Similarly, the tests including the track entry delay criterion, D, in the objective function (Tests 1, 3, 4) provide the greatest number of non-delayed aircraft (more than 70% and about 80% for Test 3), while for Test 2 this number is much lower (about 50%).

- Furthermore, in Test 2 the algorithm, obviously, provides the aircraft with the minimal cruising times, P.

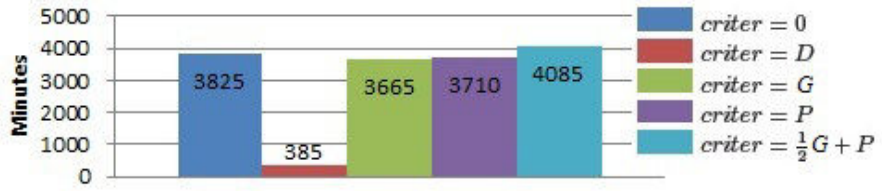

FIGURE 2.26: Total track entry delay (in minutes) for different criteria included in the objective function

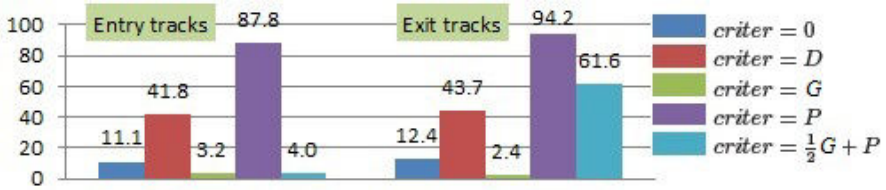

FIGURE 2.27: Percent of flights deviated from their desired tracks for different criteria included in the objective function

FIGURE 2.28: Total cruising time (in hours) for different criteria included in the objective function

Some more results of simulations with other objective functions (other values of weighting coefficients) are presented in Figures 2.26, 2.27 and 2.28. For these tests, the objective function is defined by:

$$F_2^2(y) = C_t(y) + \alpha(criter(y)), \tag{2.21}$$

where *criter* is some combination of D, P, G and their combinations, as it is listed in the legend of the figures. The results of these tests tend to confirm the conclusion stated above. All the three chosen criteria of optimization are opposite one to another. Once any single optimization criterion is included into the objective function, the resulting solution is quite good regarding this criterion, which is obtained by penalizing other criteria. Thus, we consider that the best solution would be a desirable trade-off between the examined criteria. One of such trade-off solutions is given by the last test presented in Figures 2.26-2.28 (light blue columns). The results of this test are very good in terms

of cruising time (Fig. 2.28), and not bad also in terms of desired tracks attribution (Fig. 2.27).

Note that the decrease in total cruising time yielded by the presented algorithm realization, GAm, comes from two sources:

- first, from the increase of time that the aircraft spend on OTS tracks with more preferable winds;
- and secondly, from attributing to the aircraft not the desired entry/exit tracks but the neighboring tracks that are closer one to another than the desired tracks are.

From the second point it is apparent that minimizing the total cruising time and maximizing the number of attributed desired tracks are opposite. Earlier, it was mentioned that minimizing the track entry delay and maximizing the number of desired tracks attributed are also opposite. Thus, the user can decide an appropriate trade-off through the choice of the weighting coefficients.

Further in this section, we concentrate on minimizing the total cruising time, P, as the cruising time is directly related with fuel consumption, a major criterion for airlines. We also take into account the number of desired tracks attributed (to be maximized), as it has a strong influence on air-traffic congestion. Several computational experiments with different parameter values are performed. The weighting coefficients are set to: $\alpha_d = 0$, $\alpha_p = 1$, $\alpha_g = 1, 0.5, 0.2$ (for problem tests 1, 2 and 3 respectively) in the following objective function:

$$F_2^3(y) = C_t(y) + \alpha(\alpha_g G(y) + P(y)). \tag{2.22}$$

Some results are presented in Table 2.9, where the best values are emphasized in **bold**. The number of delay slots, N_d, for these tests is set to 4, since greater freedom in choosing the track-entry time imposes less constraints on the choice of the flight route, which permits, in turn, more flights to follow their optimal routes. Furthermore, the tests are performed with the number of generations, N_G, equal to 3,000. Empirical tests show that increasing N_G from 1,000 to 3,000 significantly improves the quality of final solutions, while further increasing N_G from 3,000 to 5,000 only has a marginal effect.

Test	1	2	3
Weighting coefficient β	1	0.5	0.2
August 3rd			
% of flights with desired entry tracks	**96.4%**	95.5%	63.1%
% of flights with desired exit tracks	**96.7%**	42.6%	19.9%
Total cruising time P (hours)	1,050.30	1,027.69	**1,019.92**
Average cruising time (hours)	3.17	3.10	**3.08**
August 4th			
% of flights with desired entry tracks	**96.3%**	96.0%	59.5%
% of flights with desired exit tracks	**95.2%**	38.4%	27.8%
Total cruising time P (hours)	1,176.40	1,146.73	**1,139.27**
Average cruising time (hours)	3.11	3.03	**3.01**

TABLE 2.9: Comparison of cruising times and number of attributed desired tracks

The average CPU time of one GA execution for 3,000 generations is between 30 and 40 minutes. Table 2.9 shows that:

- Test 1 ($\alpha_g = 1$) gives the best results in terms of number of desired entry/exit tracks attributed,
- Test 3 ($\alpha_g = 0.2$) yields the best results in terms of cruising time,
- and Test 2 ($\alpha_g = 0.5$) yields compromise solutions.

Thus, any of these solutions could be satisfying, depending on the priorities of the user. Note that the results from Table 2.9 are better than those presented earlier in Table 2.8. This is simply because here a greater number of generation, $N_G = 3,000$, issued (instead of $N_G = 1,000$), which allows to achieve additional amelioration.

The presented results show that the choice of entry/exit tracks has a significant impact on the total cruising time. Indeed, when an aircraft is assigned a neighboring track, instead of its desired exit (entry) track, this neighboring track is closer to the entry (exit) track, and the aircraft is to perform fewer re-routings within the OTS. Consequently, its route in the OTS is shorter, and the cruising time thereby decreases.

Another factor that can lead to smaller cruising times the choice of wind-optimal tracks. The wind speed differs from one track to another (see Figures 2.22, 2.23) and from one FL to another. As in our simulations the FLs are imposed to flights, the gain in cruising time may only be obtained by choosing better WPs to perform the re-routing.

Test (Weighting coef. α_g)		Test 2 ($\alpha_g = 0.5$)		Test 3 ($\alpha_g = 0.2$)	
Value (V)		L^f, (km)	p^f, (hours)	L^f, (km)	p^f, (hours)
August 3rd					
Flights with V	decreased	26.0%	48.3%	44.4%	61.0%
	not increased	29.0%	51.1%	47.7%	64.0%
Average val. of V	decrease	34.68	0.04	39.86	0.04
	increase	62.40	0.06	47.18	0.04
Result val. of V decrease		-11,680	-3.90	-2,303	3.86
August 4th					
Flights with V	decreased	29.9%	41.8%	41.8%	51.6%
	not increased	31.5%	43.4%	45.0%	54.8%
Average val. of V	decrease	43.42	0.05	46.26	0.05
	increase	55.12	0.06	34.16	0.04
Result val. of V decrease		-9,371	-3.24	205	4.22

TABLE 2.10: Comparison of aircraft trajectory length and cruising time for initial FPLs with optimized solutions

Let us further concentrate on the comparison of the obtained cruising times with those provided by the initial FPLs.

The cruising time clearly depends on the AT. Let L^f denote the length of the AT of flight f along the OTS. It is computed by summing the lengths of the links (the route segments between the OTS WPs) followed by the aircraft. A decrease of AT length means that the AT obtained by the optimization is shorter than that of the initial FPL trajectory. The value of the length decrease is the difference between the initial (FPL) AT length and the resulting (optimized) AT length. The cruising-time, p^f, decrease is defined in an analogous manner, as well as the AT-length and cruising-time increases. Table 2.10 presents some results of comparison, corresponding to Tests 2 and 3 from Table 2.9 (note that a negative decrease represents in fact an increase).

Test 2 yields solutions for which both the total value of AT lengths and the total value of cruising time increase, although there is a significant number of flights for which these values decrease. The increase of AT length for most flights is not surprising: the ATs from the FPLs follow in most cases one predefined track, while the ATs resulting from optimization include re-routings to satisfy the desired entry and exit demands. The cruising time increase is directly related to the AT length increase. However, the number of flights for which p^f decreases is greater than the number of flights for which L^f decreases. Thus, there are necessarily some flights that cross the ocean faster, even

	August 3rd, 2006		August 4th, 2006	
	Test 2	Test 3	Test 2	Test 3
% of flights for which:				
p^f is decreased	48.3%	61.0%	41.8%	51.6%
L^f is decreased	25.0%	44.4%	29.9%	41.8%
p^f and L^f are decreased	24.2%	39.3%	23.3%	32.8%
only p^f is decreased	24.2%	21.8%	18.5%	18.8%
only L^f is decreased	1.8%	5.1%	6.6%	9.0%

TABLE 2.11: Relationship between cruising-time decrease and trajectory-length decrease

though they follow longer trajectories. This is certainly due to the use of route segments involving preferable winds.

This observation is also confirmed by the results of Test 3, where the cruising time is decreases for more than 50% of all flights. For August 3rd, it is even more evident, as the total value of cruising times decreases by several hours, while the total value of AT lengths increases. Another confirmation of this conclusion can be seen from Table 2.11 that displays the relationship between cruising-time decrease and AT-length decrease. One observes that for about 20% of flights, the decrease of cruising time is clearly obtained due to the selection of wind-optimal routes.

The numerous computational results reported in this study, permit us to conclude, that implementing new technologies can yield a strong positive effect on the traffic in NAT. The reduction of the CSSs makes it possible for aircraft to perform re-routings within the OTS, and therefore to follow more optimal ATs towards their destination. As a consequence, the total flight duration and the congestion level in the pre-oceanic airspace can significantly decrease.

2.5 Perspectives for solving the problem with deterministic methods

The objective function and the CFC constraints of our optimization problem (2.11) as it is stated in Section 2.2.5 are not expressed as explicit functions of the decision variables. Thus, each instantiation (proposition of values for the decision variables) of this problem requires running the computing procedures (*e.g.* Algorithms 2.2 and 2.3 for CFC constraints). In this section, we propose a new formulation of the AT optimization

problem within OTS as a quadratic (Section 2.5.1) and linear (Section 2.5.2) integer program, so that classical deterministic algorithms for these classes of combinatorial optimization problems can be applied.

2.5.1 Problem formulation as a quadratic integer program

Below, we recall the previous notations and we introduce the required parameters, variables, and some new notations:

- Nx - number of WPs;
- Ny - number of tracks;
- Nz - number of FLs;
- $\mathcal{G} = (\mathcal{N}, \mathcal{L})$ - the OTS grid;
- $\mathcal{N}$ contains $Nx \times Ny \times Nz$ regular nodes (WPs) and $(Nx-1) \times (Ny-1) \times Nz$ extra nodes (link crossings);
- $\mathcal{L}$ contains $(Nx-1) \times Ny \times Nz$ straight (in-track) links, $(Nx-1) \times (Ny-1) \times Nz$ northern links (joining a current WP with the next WP on the northern track) and $(Nx-1) \times (Ny-1) \times Nz$ southern links;
- $n \in \mathcal{N}$ - a node index in the OTS grid (regular or extra);
- $l \in \mathcal{L}$ - a link index in the OTS grid;
- N - number of aircraft;
- $f, g \in 1, ..., N$ - aircraft (or flight) indices;
- $\mathcal{T}^f$ - the set of all feasible 4D trajectories (ATs) for aircraft f; this set is fully defined by the desired entry (TD_e^f) and exit (TD_o^f) tracks and consists of all possible ATs, joining all possible combinations of assigned entry (e^f) and exit (o^f) tracks, with all possible track entry delays (d^f);
- The number of feasible 4D ATs for aircraft f, $|\mathcal{T}^f|$, is given by the formula:

$$|\mathcal{T}^f| = (N_d + 1) \times \left(\sum_{e^f = \max(TD_e^f - 1, 1)}^{\min(TD_e^f + 1, Ny)} \; \sum_{o^f = \max(TD_o^f - 1, 1)}^{\min(TD_o^f + 1, Ny)} \begin{pmatrix} Nx - 1 \\ |o^f - e^f| \end{pmatrix} \right);$$

- $\tau, \theta \in \mathcal{T}^f$ -the indices of particular feasible 4D ATs for aircraft f;
- $x_\tau^f \in \{0,1\}$ - binary variable; $x_\tau^f = 1$ if AT τ is actually flown by aircraft f; there is one such variable for each $\tau \in \mathcal{T}^f$ and for each $f = 1, ..., N$;
- R_τ^f - cost of AT τ flown by aircraft f (*e.g.* it may equal to the cruising time, p^f; the delay, d^f; may be related to deviations from desired entry/exit track, etc.), $\tau \in \mathcal{T}^f$, $f = 1, ..., N$.

Then, our objective function, to be minimized, can be written as:

$$f(x) = \sum_{f=1}^{N} \sum_{\tau \in \mathcal{T}^f} R_\tau^f x_\tau^f, \tag{2.23}$$

where $x = (x^1, ..., x^N)$ and x^f is the $|\mathcal{T}^f|$-dimensional vector which τ-th component is x_τ^f ($\tau \in \mathcal{T}^f$, $f = 1, ..., N$).

By definition of the decision variables, the following constraints must be satisfied: one and only one AT can be flown by each aircraft f:

$$\sum_{\tau \in \mathcal{T}^f} x_\tau^f = 1, \ f = 1, ..., N. \tag{2.24}$$

In addition to these natural constraints, we still need to guarantee the CFC to be satisfied. We would like to treat the conflicts on nodes and links simultaneously, thus, we introduce a common index:

- $\nu \in \mathcal{G}$ - index of a particular OTS *grid element*, *i.e.* a node or a link from the OTS structure.

Further, we introduce the following binary parameters (given data of the problem):

$$\delta_{\tau,\theta}^{\nu,f,g} = \begin{cases} 1 & \text{if ATs } \tau \text{ of flight } f \text{ and } \theta \text{ of flight } g \text{ pass} \\ & \text{through node or link } \nu \text{ and are in conflict at } \nu \\ 0 & \text{otherwise} \end{cases}, \tag{2.25}$$

where $\nu \in \mathcal{G}$, $\tau \in \mathcal{T}^f$, $\theta \in \mathcal{T}^g$, $1 \leq f < g \leq N$. The definition of a conflict on a grid element is given in Section 2.2.3. Detection of a node conflict depends on the MSS applied as well as on the maneuvers performed by both aircraft f and g at the corresponding node when following the given ATs τ and θ respectively. Thus $\delta^{\nu,f,g}_{\tau,\theta}$ is defined in a unique way for each pair of aircraft routes and can be computed a priori in a pre-processing step. Further, we denote:

$$\delta^{f,g}_{\tau,\theta} = \sum_{\nu \in \mathcal{G}} \delta^{\nu,f,g}_{\tau,\theta}. \tag{2.26}$$

The number $\delta^{f,g}_{\tau,\theta}$ represents the number of conflicts induced on the whole OTS grid by the pair of aircraft f and g following the ATs τ and θ respectively. Now, the CFC constraint (2.3) for our problem can be written in the following way:

$$\delta^{f,g}_{\tau,\theta} x^f_\tau x^g_\theta = 0, \ \tau \in \mathcal{T}^f, \ \theta \in \mathcal{T}^g, \ 1 \leq f < g \leq N. \tag{2.27}$$

Indeed,

- if aircraft f does not use AT τ, then $x^f_\tau = 0$, and thus, (2.27) is automatically satisfied; the same is true if aircraft g does not use AT θ;
- otherwise, if both ATs, τ and θ, are used, then $x^f_\tau x^g_\theta = 1$ and thus, $\delta^{f,g}_{\tau,\theta}$ should be equal to 0, in order to satisfy (2.27).

In such a formulation of our problem, there is a very large number of constraints of this type, as it is of the order of $\frac{N(N-1)}{2} \times \overline{|\mathcal{T}^f|}^2$ (for each pair of aircraft, and for each pair of routes, where $\overline{|\mathcal{T}^f|}$ denotes the average number of possible 4D ATs over all flights, $\overline{|\mathcal{T}^f|} = \frac{1}{N} \sum_{f=1}^{N} |\mathcal{T}^f|$). This number can be reduced by aggregating constraints. More precisely, taking (2.24) into account, the constraints (2.27) can be summed into:

$$\sum_{\tau \in \mathcal{T}^f} \sum_{\theta \in \mathcal{T}^g} \delta^{f,g}_{\tau,\theta} x^f_\tau x^g_\theta = 0, \ 1 \leq f < g \leq N; \tag{2.28}$$

The sum in (2.28) represents the number of conflicts on the whole OTS induced by the pair of aircraft f and g (according to the routes that are assigned to these aircraft).

Finally, (2.28) can be further summed up over all possible pairs of aircraft f and g, $1 \leq f < g \leq N$:

$$\sum_{f=1}^{N-1} \sum_{g=f+1}^{N} \sum_{\tau \in \mathcal{T}^f} \sum_{\theta \in \mathcal{T}^g} \delta_{\tau,\theta}^{f,g} x_\tau^f x_\theta^g = 0. \tag{2.29}$$

The left-hand side of (2.29) represents the number of conflicts on the whole OTS induced by the total set of aircraft. Thus, instead of a large number of constraints, we have only one, equivalent constraint, (2.29). The resulting optimization problem is then stated in the following way:

$$\begin{aligned} &\min_x \sum_{f=1}^{N} \sum_{\tau \in \mathcal{T}^f} R_\tau^f x_\tau^f \\ &\text{s.t.} \sum_{\tau \in \mathcal{T}^f} x_\tau^f = 1, \ f = 1, ..., N; \\ &\sum_{f=1}^{N-1} \sum_{g=f+1}^{N} \sum_{\tau \in \mathcal{T}^f} \sum_{\theta \in \mathcal{T}^g} \delta_{\tau,\theta}^{f,g} x_\tau^f x_\theta^g = 0; \\ &x_\tau^f \in \{0,1\}, \ \tau \in \mathcal{T}^f, \ f = 1, ..., N. \end{aligned} \tag{2.30}$$

Note that it is possible that the mathematically equivalent formulations of this problem that would replace the unique constraint (2.29) back with its disaggregated counter parts (2.28) or (2.27) may well be more useful in practice, as they may lead to better continuous relaxation (when the problem is addressed via a Branch & Bound scheme for example).

The discrete optimization problem (2.30) involves a linear objective function, $N \times \overline{|\mathcal{T}^f|} = \sum_{f=1}^{N} |\mathcal{T}^f|$ variables and $N + 1$ constraints, among which one constraint (2.29) is quadratic, while the other are linear constraints. Moreover, as we did from formulation (2.11) to (2.13), we can here again propose a new penalized formulation (2.30) into (2.31) as presented below. It suffices just to add the right part of the CFC constraint (2.29) into the objective function.

$$\min_x \alpha \sum_{f=1}^{N} \sum_{\tau \in \mathcal{T}^f} R_\tau^f x_\tau^f + \sum_{f=1}^{N-1} \sum_{g=f+1}^{N} \sum_{\tau \in \mathcal{T}^f} \sum_{\theta \in \mathcal{T}^g} \delta_{\tau,\theta}^{f,g} x_\tau^f x_\theta^g \tag{2.31}$$

$$\text{s.t.} \sum_{\tau \in \mathcal{T}^f} x_\tau^f = 1, \ f = 1, ..., N;$$

$$x_\tau^f \in \{0, 1\}, \ \tau \in \mathcal{T}^f, \ f = 1, ..., N,$$

where α is a user-defined penalty parameter that allows one to put more or less emphasize on minimizing costs with respect to avoiding conflicts. Now in this reformulation all constraints are linear, but the objective function is quadratic. Problems (2.30) and (2.31) can be addressed by specialized existing integer programming methods. The quadratic (in fact bilinear) terms of the problem could either be tackled via McCormick-like linear reformulation, or using methods relying on semi-definite programming relavations. This could be one of the perspectives for future tracks of research following the current study.

2.5.2 Problem formulation as an integer linear program

In this section we propose one of the ways to reformulate our optimization problem as an *Integer Linear Program* (ILP). In order to render problem (2.30) linear, we apply the standard linearization technique, described below. We introduce new variables:

- $y_{\tau,\theta}^{f,g} = x_\tau^f x_\theta^g$, $\tau \in \mathcal{T}^f$, $\theta \in \mathcal{T}^g$, $1 \leq f < g \leq N$.

This equality is equivalent to the following set of constraints for each $\tau \in \mathcal{T}^f$, $\theta \in \mathcal{T}^g$, $1 \leq f < g \leq N$:

$$y_{\tau,\theta}^{f,g} \leq x_\tau^f; \tag{2.32}$$

$$y_{\tau,\theta}^{f,g} \leq x_\theta^g; \tag{2.33}$$

$$x_\tau^f + x_\theta^g - y_{\tau,\theta}^{f,g} \leq 1; \tag{2.34}$$

$$y_{\tau,\theta}^{f,g} \geq 0. \tag{2.35}$$

Indeed,

- if $y^{f,g}_{\tau,\theta} = 1$ then $x^f_\tau = 1$ (from (2.32)) and $x^g_\theta = 1$ (from (2.33));
- if $y^{f,g}_{\tau,\theta} = 0$ then $x^f_\tau = 0$ or $x^g_\theta = 0$ (from (2.34));
- if $x^f_\tau = 1$ and $x^g_\theta = 1$ then $y^{f,g}_{\tau,\theta} = 1$ (from (2.34), and (2.32) or (2.33));
- if $x^f_\tau = 0$ or $x^g_\theta = 0$ then $y^{f,g}_{\tau,\theta} = 0$ (from (2.32) or (2.33), and (2.35));

Thus, the problem is reformulated by replacing simply each bilinear term with the corresponding product variables and by adding all above new constraints (2.32)-(2.35). Note that in such a formulation the variables $y^{f,g}_{\tau,\theta}$ are not required to be defined as binary variables; they will automatically be binary, thanks to the constraints (2.32)-(2.35). Now (2.31) is transformed into:

$$
\begin{aligned}
&\min_x \sum_{f=1}^{N} \sum_{\tau \in \mathcal{T}^f} R^f_\tau x^f_\tau && (2.36)\\
&\text{s.t.} \sum_{\tau \in \mathcal{T}^f} x^f_\tau = 1,\ f = 1, ..., N;\\
&\sum_{f=1}^{N-1} \sum_{g=f+1}^{N} \sum_{\tau \in \mathcal{T}^f} \sum_{\theta \in \mathcal{T}^g} \delta^{f,g}_{\tau,\theta} y^{f,g}_{\tau,\theta} = 0;\\
&y^{f,g}_{\tau,\theta} \le x^f_\tau;\ \tau \in \mathcal{T}^f,\ \theta \in \mathcal{T}^g,\ 1 \le f < g \le N;\\
&y^{f,g}_{\tau,\theta} \le x^g_\theta;\ \tau \in \mathcal{T}^f,\ \theta \in \mathcal{T}^g,\ 1 \le f < g \le N;\\
&x^f_\tau + x^g_\theta - y^{f,g}_{\tau,\theta} \le 1,\ \tau \in \mathcal{T}^f,\ \theta \in \mathcal{T}^g,\ 1 \le f < g \le N;\\
&y^{f,g}_{\tau,\theta} \ge 0,\ \tau \in \mathcal{T}^f,\ \theta \in \mathcal{T}^g,\ 1 \le f < g \le N;\\
&x^f_\tau \in \{0, 1\},\ \tau \in \mathcal{T}^f,\ f = 1, ..., N.
\end{aligned}
$$

Further, we note that actually the inequalities (2.32) and (2.33) can be omitted from the formulation. Thus, instead of four inequalities, we will keep only two: one linear inequality (2.34) and the band constraints (2.35), and we obtain the following formulation:

$$
\begin{aligned}
&\min_{x} \sum_{f=1}^{N} \sum_{\tau \in \mathcal{T}^f} R_\tau^f x_\tau^f && (2.37)\\
&\text{s.t.} \sum_{\tau \in \mathcal{T}^f} x_\tau^f = 1,\ f = 1, ..., N;\\
&\sum_{f=1}^{N-1} \sum_{g=f+1}^{N} \sum_{\tau \in \mathcal{T}^f} \sum_{\theta \in \mathcal{T}^g} \delta_{\tau,\theta}^{f,g} y_{\tau,\theta}^{f,g} = 0;\\
&x_\tau^f + x_\theta^g - y_{\tau,\theta}^{f,g} \leq 1,\ \tau \in \mathcal{T}^f,\ \theta \in \mathcal{T}^g,\ 1 \leq f < g \leq N;\\
&y_{\tau,\theta}^{f,g} \geq 0,\ \tau \in \mathcal{T}^f,\ \theta \in \mathcal{T}^g,\ 1 \leq f < g \leq N;\\
&x_\tau^f \in \{0, 1\},\ \tau \in \mathcal{T}^f,\ f = 1, ..., N.
\end{aligned}
$$

The next proposition demonstrates that formulations (2.36) and (2.37) are equivalent.

Proposition 2.1. *Problems (2.36) and (2.37) are equivalent formulations of the OTS AT-optimization problem. More precisely, from any feasible solution of one problem, one can straightforwardly construct a feasible solution of the other with the same objective-function value. This is obviously true for the cases of optimal solutions.*

Proof. First note that problem (2.37) is a relaxation of problem (2.36), *i.e.* the feasible domain of (2.36) is a subset of the feasible domain of (2.37). Therefore it suffices to show that given feasible solution, $(\hat{x}, \hat{y})$, of (2.37) one can straightforwardly construct a feasible solution, $(\tilde{x}, \tilde{y})$, of (2.36).

Let $(\hat{x}, \hat{y})$ be a feasible solution of (2.37). Then, it must satisfy the CFC constraint. Here, two cases are possible for any $\tau \in \mathcal{T}^f$, $\theta \in \mathcal{T}^g$, $1 \leq f < g \leq N$.

1. If $\delta_{\tau,\theta}^{f,g} = 0$ (conflict) $\Rightarrow \hat{y}_{\tau,\theta}^{f,g} = 0 \Rightarrow \hat{y}_{\tau,\theta}^{f,g} \leq \hat{x}_\tau^f$ and $\hat{y}_{\tau,\theta}^{f,g} \leq \hat{x}_\theta^g$.

Then, we set $\tilde{x}_\tau^f = \hat{x}_\tau^f$, $\tilde{x}_\theta^g = \hat{x}_\theta^g$ and $\tilde{y}_{\tau,\theta}^{f,g} = \hat{y}_{\tau,\theta}^{f,g}$, which implies that

conditions (2.32), (2.33) and (2.34) are satisfied.

2. If $\delta_{\tau,\theta}^{f,g} = 0$ (no conflict),

then we set $\tilde{x}_\tau^f = \hat{x}_\tau^f$, $\tilde{x}_\theta^g = \hat{x}_\theta^g$ and $\tilde{y}_{\tau,\theta}^{f,g} = \min(\hat{x}_\tau^f, \hat{x}_\theta^g)$, which implies that

conditions (2.32), (2.33) and (2.34) are satisfied.

As a consequence, by construction we have: $\tilde{x} = \hat{x}$, the objective-function values of $\tilde{x}$ and $\hat{x}$ are equal, and all the constraints, including the CFC constraint, are satisfied.

□

Further, we can note, that constraints (2.24), that stipulates "one and only one 4D AT is chosen by an aircraft" can be rewritten under the form of inequalities, as "at least one 4D AT is chosen by an aircraft". Moreover, we can also replace the equality CFC-constraint (2.27) by an inequality constraint, taking into account that $\delta^{f,g}_{\tau,\theta} \geq 0$ and $y^{f,g}_{\tau,\theta} \geq 0$. Thus, we obtain a mathematically equivalent formulation of our optimization problem, that can be more convenient to exploit by certain optimization algorithms. Indeed, this relaxation is an equivalent formulation since one can easily show that its optimal solution will necessary be feasible for (2.37) (it is suboptimal to assign several 4D ATs to an aircraft).

Furthermore, in the same way as (2.30) was transformed into (2.31), we can transform (2.37) into its penalized version. The advantage of including the CFC constraints into the objective function is that it is very easy to find an initial feasible solution. Indeed, it suffices to choose an arbitrary AT $\tilde{\tau}$ for each aircraft f, to set $x_{\tilde{\tau}} = 1$ for this AT and $x^f_\tau = 0$ for all other ATs, and to set further $y^{f,g}_{\tau,\theta} = x^f_\tau x^g_\theta$ for all $\tau \in \mathcal{T}^f$, $\theta \in \mathcal{T}^g$ for all $0 \leq f < g \leq N$. The possibility to find quickly a feasible solution can be useful for some optimization methods.

Finally, below we present another mathematically equivalent formulation for problem (2.30). Let us denote, for each pair of aircraft f and g ($1 \leq f < g \leq N$), the set $\mathcal{T}_{f,g}$ of all possible pairs of ATs of these aircraft that are in conflict:

$$\mathcal{T}_{f,g} = \{(\tau, \theta) \in \mathcal{T}^f \times \mathcal{T}^g | \delta^{f,g}_{\tau,\theta} = 1\}. \tag{2.38}$$

Then, for each pair of route $(\tau, \theta) \in \mathcal{T}_{f,g}$ ($1 \leq f < g \leq N$) the CFC constraint can be written as:

$$x^f_\tau + x^g_\theta \leq 1, \tag{2.39}$$

and thus, problem (2.30) can be formulated as follows:

$$
\begin{aligned}
&\min_{x} \sum_{f=1}^{N} \sum_{\tau \in \mathcal{T}^f} R_\tau^f x_\tau^f \\
&\text{s.t.} \sum_{\tau \in \mathcal{T}^f} x_\tau^f = 1, \ f = 1, ..., N; \\
&x_\tau^f + x_\theta^g \leq 1, \ (\tau, \theta) \in \mathcal{T}_{f,g}, \\
&x_\tau^f \in \{0, 1\}, \ \tau \in \mathcal{T}^f, \ f = 1, ..., N.
\end{aligned}
\tag{2.40}
$$

Formulation (2.40) is also an integer linear problem involving a number of constraints that is quadratic from the number of variables.

Linear problems (2.37) and (2.40) could be solved with classical methods of integer linear programming. Nevertheless, at some time the problem size could become limited by the solver capacities. More sophisticated algorithms could then be envisaged to take advantage of the particular structure of these problems, such as Column Generation (CG) method [46] and its extension: simultaneous Column and Raw Generation (CRG) [47]. These methods are applied with success for a wide range of ILP problems, including the aviation-related problems, such as airline operations or crew scheduling [48–54]. This is another perspective for the future work development.

Chapter 3

Trajectory prediction by Wind Networking

In this chapter, we still consider current air traffic regulations in North Atlantic oceanic airspace (NAT) obliging aircraft to follow predefined tracks within Organized Track System (OTS), but we concentrate our research on a particular way to improve the flight prediction, including cruising time prediction and conflict prediction, that we refer to as *Wind Networking* (WN). WN permits aircraft to exchange measured wind data directly during flight and to adjust their trajectory predictions using more recent and more accurate information. In contrast to the study from the previous chapter, here we do not perform any optimization and do not try to resolve the conflicts. Instead, in this study we simply *simulate* flight progress and flight prediction, and *detect* potential conflicts. The main particularity of this study is that we take into account the *uncertainty in wind forecast*.

The chapter is organized as follows. First, we give some detail on the flight prediction accuracy, possible errors and their reasons, wind forecast uncertainty, and wind measurements, and we mention several existing works studying the possibilities to improve the prediction using aircraft measurement and reports. After that, we evoke the idea of a new prediction approach for Aircraft Trajectories (ATs), the WN. We further develop the mathematical model, used for our simulation of flight progress and AT prediction, and discuss the criteria of evaluation of the prediction methods. Finally, we present the

results of our simulations for real and artificial flight sets, and we highlight the benefits yielded by the WN approach.

3.1 Problem statement and literature review

In this section, the research works related to ameliorating aircraft trajectory prediction by incorporating aircraft meteorological measurements are discussed. First, the most common air navigation errors are mentioned, with the attention brought to the weather-related errors. Then, some notions related to weather forecast are given, and the aircraft possibilities to perform on-board meteorological measurements are mentioned. Furthermore, we discuss how these measurements can be used in wind forecast models to improve their accuracy. Finally, we discuss the accuracy of these measurements themselves. The section is concluded by identifying a new approach that have not yet been treated in the existing research works, and that we are going to present in the remaining of this chapter.

3.1.1 Weather-related air navigation errors

Flight safety is the leading priority for air carriers and the ATM (Air Traffic Management), and all the efforts are made to assure safe flight progress. Nevertheless, navigation errors do occur, having different levels of gravity: from simple arriving delays to air crashes with fatal outcomes. There are numerous factors that contribute to such erroneous events in navigation [55]. One of them is the environmental factor, whose most essential component is the changing weather conditions (see Appendix U for more detail). In the majority of cases of erroneous events, it is more reasonable to speak not of a single cause, but of a *chain of errors*, that lead to such an event [55]. The erroneous *Meteorological Forecast* (MF) often plays the role of an initial link of such a chain (see an example in Appendix U).

Leaving apart such important erroneous events, that induce the risks for aircraft safety and result in collisions and even accidents, we will further have a look at *flight delays*, which is a flight performance criterion that is crucially important for airlines. Flight delays are calculated as the difference between the ATAs (Actual Times of Arrival) and ETAs (Estimated Times of Arrival). They have the same origins as the *violation of*

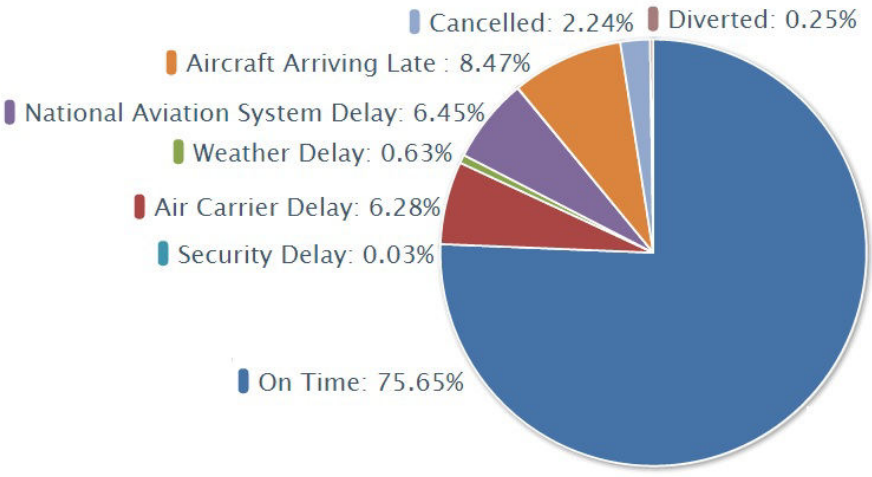

FIGURE 3.1: Aircraft on-time arrival performance in U.S. National airspace from December 2013 to December 2014[1]

longitudinal separation (see Appendix U), for which changing meteorological conditions are considered to be the most frequent cause.

Figure 3.1 shows a diagram reflecting the aircraft on-time arrival performance. It displays the percentage of flights arrived on time, canceled, diverted and delayed due to one of the given reasons (explained in detail in Appendix U), for the year 2014, based on data from [56]. It might be thought, that the weather impact on flight delays is minor: indeed, only about 4% of all delays (*i.e.* the green sector, *Weather Delay*, makes 4% of the top left quarter of Figure 3.1) are caused by *Extreme Weather*. However, one should note that this category consists of flights that were *prevented* by the weather conditions. There is another category: the *National Aviation System* (NAS) Delay category, for which the weather impacts the flights by *slowing* the operations of the system but does not prevent flying.

Nowadays, about a half of the NAS delays (half of the purple sector in Figure 3.1) are due to weather (see the distribution of the NAS delays causes in Figure 3.2). At the same time, the NAS delays constitute 20%-30% of total delays [57]. In addition to this, the largest delay category, *i.e. Late Arriving Aircraft*, takes its origines in many respects from the weather conditions (extreme or non-extreme) as well. Thus, to obtain a true picture of total weather-related delays, one needs to combine the Extreme Weather delays with the NAS weather category and the weather-related delays included in the Late-Arriving Aircraft category. Even if it is not evident to quantify weather impact on

[1]From http://www.transtats.bts.gov/OT_Delay/ot_delaycause1.asp?type=1&pn=1

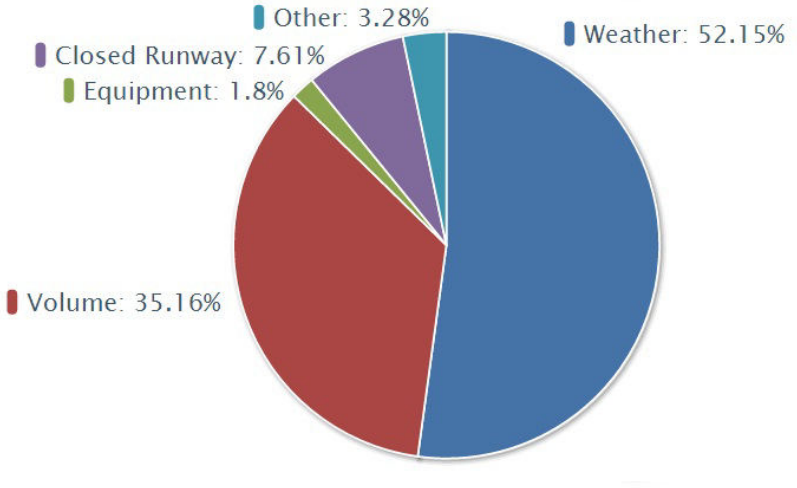

FIGURE 3.2: Distribution of causes of the U.S. National Aviation System Delays from December 2013 to December 2014[2]

the flight performance, it is estimated to be around 30%, which is a rather significant value.

The main reason why the Extreme Weather delays and weather-related NAS delays are calculated separately is that the latter belongs to the category that could be reduced with corrective actions of airlines and airports and with the modernization of ATM. The Extreme Weather case will not be considered in this study. In the non-extreme weather conditions, the main source of differences between ETAs and ATAs, that may result in aircraft delays, longitudinal separation violations and even risky collisions, is the differences in the forecast and the actual wind fields. Thus, the first idea, lying on the surface, is that improvement in the *wind forecast* will bring the improvement into the general ANS (Air Navigation System) performance.

3.1.2 Wind forecast

Wind forecasting is a complicated problem, which requires a large amount of precise meteorological information. Nowadays, wind forecast is performed by the means of *Numerical Weather Prediction* (NWP) models [58], that rely on the combination of all available data sets (see Appendix V for more detail), coming from:

- radiosondes[3],

[2]From http://www.transtats.bts.gov/OT_Delay/OT_DelayCause1.asp?pn=1
[3]The balloon-borne instruments launched around the world at set time intervals.

- satellite systems,
- automated aircraft reports.

In this study, we only focus on one way of wind forecast improvement, which main idea relies on using *automated aircraft reports* that provide the *meteorological data measured by aircraft* en-route. Indeed, each modern commercial aircraft is capable of performing instant measurements of meteorological conditions, such as temperature, air pressure, wind magnitude and direction, directly during the flight using special on-board equipment (see Appendix W). The overview of such capabilities can be found, for example, in [59, Chapter 2], where the basic techniques and corresponding mathematical formulations are briefly discussed. More detailed mathematical models for TAS (True Air Speed) and WS (Wind Speed) measurements and sophisticated formulas used can be found in [60].

Furthermore, more modern methods were proposed and implemented in order to provide more accurate on-board wind measurements. For example, in [61], wind measurements provided by commercial aircraft are improved based on the difference between GPS (Global Positioning System) and INS (Inertial Navigation System) data. Another example of a possibility to improve wind measurements is described in [62], where it is shown how wind information can be extracted from radar observations. These studies develop different methodologies of rough data processing based on *filtering*, that permit to obtain more accurate results. In addition to this, in [62], Delahaye *et al.* propose a method of reconstruction of the continuous wind field from the point wind measurements (see Appendix W). We will not go deeper in detail of the physical processes at the basis of airborne wind measurements. However, in the sequel, we will concentrate on the practical applications of such aircraft capabilities.

Routine meteorological observations are recorded from aircraft since the early beginning of the 20th century. In 1979, the *automated aircraft reports* became available, which increased greatly in the 90's [63]. Automated meteorological reports from aircraft are generally called *Aircraft Meteorological Data Relay* (AMDAR) reports. In the USA however, this data is referred to as *Aircraft Communication Addressing and Reporting System* (ACARS) data, or sometimes as *Meteorological Data Collection and Reporting*

System (MDCRS[4]). These reports usually include temperature and horizontal winds, and sometimes provide measurements of dewpoint and turbulence. The reports are non-evenly distributed all around the world (depending on the AMDAR participating countries, aircraft preferred routes and airlines policy), vertically (most data is gathered at cruising Flight Levels (FLs)) and temporally (peak hours vs. night time). In the next section we discuss how these reports are used in practice to improve wind (weather) forecast, whose accuracy is crucial for the ANS.

3.1.3 Improvement of wind forecast by aircraft observations

In this section, we have a look in the studies devoted to the estimation of the impact that the automated aircraft reports have on the NWP forecast.

In [63] a project, developed in the National Oceanic and Atmospheric Administration (NOAA) Forecast System Laboratory (FSL), is presented. Its objective is to collect the ACARS data and to provide direct access to these data via a website. The observations performed in the frame of this project show that the data from automated aircraft reports coincide well with each other as well as with radiosondes, and with model background fields. The discovered inaccuracies in wind and temperature measurements are discussed in the next section. The AMDAR (and ACARS) are discovered to have a positive impact on the NWP, and are often considered even more important data source than the radiosonde data.

In [58] several supplementary tests are described. They were conducted over the USA for several time periods, covering different seasons of 2002 and 2003. The results obtained from these tests reveal that including the aircraft data in the NWP system leads to improvement forecasts for all areas of the globe, especially for the short-range forecasts (where this improvement reaches 20%), and in particular in the regions of the greatest data density. On average, the forecast for the Northern Hemishere is shown to be improved by 0.5 knots at FL300-FL390 (while in some cases, these improvements can even exceed 10 knots). The authors claim that implementing the ADS (Automatic Dependent Surveillance) systems and establishing new flight routes with more dense global

[4]Actually, the MDCRS contains the ACARS data and the distribution system to match these data to the needs of the NWP centers.

coverage would further increase the importance of aircraft reports and the improvements on meteorological forecast.

Several other works devoted to study the improvement of the MF, were conducted by the USA authorities. Here, the MF is performed by the National Weather Service (NWS), which uses two NWP systems:

- Global Forecast System (GFS), which produces the forecast four times per day as part of WAFS[5], and
- Rapid Update Cycle (RUC[6]), which produces hourly the short-range (3-12 hours) wind forecasts.

The RUC is the system mostly considered in the research works, where two RUC models are distinguished:

- RUC-1, the initial version, that has the following characteristics:
  - horizontal resolution of 60 km,
  - 3-hour assimilation cycle (run every 3 hours),
  - 81 $\times$ 62 horizontal grid,
  - polar stereographic projection,
  - vertical resolution of 50 hPa;
- and RUC-2, the updated version (end of 20th century), characterized by:
  - horizontal resolution of 40 km,
  - 1-hour assimilation cycle,
  - 151 $\times$ 113 horizontal grid,
  - Lambert conformal projection,
  - including in addition velocity azimuth display wind profiles[7].

[5] World Area Forecast Center, providing real-time meteorological information

[6] A mesoscale numerical model developed by the NOAA FSL and run operationally by the NWS

[7] Calculated from radial winds at different elevation angles from NWS weather surveillance radar; available hourly at over 100 sites over the USA; found to be significant for the collected data.

Several research works are devoted to study the improvement of the RUC wind forecast using the ACARS data, among which [64–66].

The study of [65] mainly concerns the RUC-1 forecast and uses the data collected during 343 days from August 1st, 1996 to August 1st, 1997 over Denver. It contains over 1.2 million aircraft reports. The ACARS data were collected in real time and thus, the ACARS reports taken after the RUC forecasts produced, were used to refine these forecasts in order to achieve better agreement with the observations in the minimum-error variance sense. The result of this refinement is referred to as A-RUC-1. Forecast wind field accuracy was determined in comparison with a dataset of independent ACARS wind measurements, that are taken as a baseline. The forecast winds at aircraft locations were computed using linear interpolation over the grid in three dimensions. The main objectives of the study were to determine:

- the error characteristics in the RUC-1 wind forecast;
- the improvements in the error statistics when using near-real-time aircraft reports;
- the factors influencing the error fields (weather regime, observation density).

Below we summarize the main results obtained from the performed tests.

- Addition of the near-real-time ACARS reports reduces the RMSVD[8] (by almost 1.8 m/s, or by almost 30%), as well as the 90th percentile vector error, the high speed bias, the standard deviation in wind direction and error correlation lengths (horizontal, vertical, temporal). This impovement increases as the number of available ACARS reports increases.
- The errors in RUC-1 forecast increase strongly (faster than linear) with the wind magnitude. Addition of ACARS data reduced this influence (by roughly 3-5 m/s). Thus, the errors decrease with decreasing altitude (as the wind speed also decreases).
- The more recently the reports are taken, the more accurate the results are. This motivates to add the ACARS observations more frequently.

[8] Root-Mean-Square Vector Difference

In [66], both RUC-1 and RUC-2 are investigated. The study is performed using the same ACARS data set as in [65], and using similar principles. The wind forecasts for RUC-1 and RUC-2 grids are matched with the aircraft observations using linear interpolation in each of the directions, and matrices of corresponding values are produced. These matrices are used to calculate the statistics in which the authors were interested. Their objectives are to establish:

- the conditions with large wind forecast errors;
- the benefits obtained from RUC-2 in comparison to those of RUC-1;
- the magnitude of trajectory prediction errors during different flight phases.

The main results are as follows:

- Using RUC-2 instead of RUC-1, first, improves the forecast accuracy, and second, improves the forecast availability (the forecast is updated each hour). All together, this improves the average RMSVD by 1.2 m/s, which constitutes about 22% reduction in wind forecast error at short-time scale. Moreover, the percentage of peak errors[9] decreases from 8% to 3% using the 1-hour forecast from RUC-2.
- RUC-2 particularly outperforms RUC-1 when the wind magnitude increases (e.g. for winds over 50 m/s, the improvement in the RMSVD for RUC-2 is over 1.3 m/s).
- Forecast errors has clear seasonal variations, with RMSVDs lower in summer and greater in winter. Moreover, the errors slightly decrease during daytime (when more ACARS observations are available).

More detail on the described studies can be found in [64], where the observed values and calculated statistics, supplying the conclusions made, are given explicitly. Some close studies performed recently are described in [67–69].

[9]The percentage of total forecast-observations differences greater than a defined threshold, being set here to 10 m/s.

In [67], the impact of the aircraft observations on the accuracy of short-range (3-12 hours) MF via RUC[10] in comparison to other weather data sources is discussed. The experiments providing the basis of this study, are referred to as *Observation System Experiments* (OSEs). They are conducted for two 10-day periods in cold and warm seasons[11] over the national region[12] as well as for the Midwest region[13]. The main difference of OSEs with the previous experiments is that OSEs rely on a regional model/assimilation system instead of on global systems. Moreover, this study is broader, as a larger number of observation types are considered (including radiosondes and satellites), as well as a larger number of meteorological features (including temperature and Relative Humidity (RH), in addition to the wind).

The main results that the OSEs gave for the national region concerning the *wind*, reveal that the aircraft observations have the most important impact on the wind vector differences over the full vertical domain of the study (0.3-0.6 m/s in summer, 0.15-0.20 m/s in winter[14]) among all the observation types. In addition, [67] contains some results identifying the impact of different observation types separately by layers, as well as this impact in the particular Midwest region, but we will not go deeper in detail here.

While [67] addresses the importance of aircraft observations in general, in [68] those performed by a special sensor called *Tropospheric AMDAR* (TAMDAR), are investigated. The TAMDAR observations are performed by aircraft cruising on low altitudes (so called, turboprops) serving regional airports. Their main goal is to compensate the absence of AMDAR observations below 20,000 feet between the major airports. TAMDAR reports contain wind and temperature, as AMDAR do, but also RH, turbulence and icing in addition. In [68], the observations are performed over the Great Lake region (upper midwestern U.S. region), for two 10-day periods (in summer and in winter), and for daylight hours (1200-0300 UTC, when TAMDAR is mostly available). To evaluate

[10]The RUC version of 2007 was used in this study. Several modifications were made since RUC-2 was implemented. The 2007 version supported more data sources, used upgraded mathematical models (e.g. in moisture analysis) and algorithms (e.g. digital filter extension). It still had 1-hour assimilation cycle, but 13-km resolution and 50 vertical levels. However, for the present study, the same system, except for a 20-km resolution, was implemented.

[11]One in November-December 2006, another one in August 2007

[12]Covering 48 states of the contiguous USA and significant part of Canada and Mexico

[13]The U.S. domain having exceptionally rich upper-air observational coverage

[14]The stronger impact for summer in comparison to winter, which is not typical, is explained by the particular synoptic-scale regimes of those separate 10-day periods

the impact of TAMDAR data, the RUC model[15] was also used, as in the previous studies. The forecast ability of RUC here was evaluated by comparing with radiosondes observations, taken as a baseline.

The most important results concerning the TAMDAR wind observations show that TAMDAR impacts in average are positive but small. Not surprisingly, TAMDAR seems to be responsible for most of the AMDAR wind impacts on the RUC forecast below 550 hPa; while above 550 hPa, it is AMDAR jets that provide most of the impacts. Some more results concerning the RH are given in [68], but they are out of the scope of the present study.

Further, [69] presents an extension of the studies from [67, 68]. Here, the impact of MDCRS, TAMDAR and AMDAR (a combination of the first two) on RUC forecasts of temperature, RH and wind, is studied. The experiments are performed using the same data sets as in [68]. From the results of the experiments, the authors concluded that TAMDAR observations bring an important positive impact into the RH forecast. However, they do not provide any evident improvement for wind forecast. This last conclusion is most likely explained by the presence of the large wind errors arising from inaccurate heading information provided by the TAMDAR-equipped aircraft. Other sources of meteorological data (i.e. surface observations, vapor-sensing observations, satellite (GPS) observations, etc.) are also considered in this study, but their impact is found to be smaller than those from aircraft observations. The authors noted that there conclusions are only valid for a small region of the Great Lakes where the experiments were hold, and that, therefore they should be used with caution for other regions and longer periods.

In [70], in contrast, a large region, Canada and the contiguous part of the USA, is considered. This study is of particular interest for our research, as it analyses the accuracy of Jet Stream (JS) prediction and the benefits that the aircraft observations could bring to this prediction. The main question addressed is the profitability of these observations, i.e. whether their benefits exceed their cost. The analyses are performed using the aircraft observations from the Global Aircraft Data Set (GADS) experiment[16].

[15] The same 2007-year model, with 13-km and 20-km resolutions, as described in [67]

[16] The GADS experiment uses the wind and temperature measurements recorded by British Airways at 4-second interval and sampled them from every flight since 1996. The GADS observations are used in the simulations as they are independent of the transmission used by the operational centers and they arrive in real-time data stream.

In the study [70], the long-distance flights are selected from GADS, in order to depict the aircraft that are affected by the JSs defining their routes, including transatlantic and transpacific flights. In this study, interpolation is performed in time (between 0000 and 1200 UTC) and in horizontal section, using a high-dimensional grid; while in vertical sections only aircraft flying at (or close to) altitude 250hPa are taken into account. Moreover, to compensate possible errors due to the sharp gradients close to JSs cores, the authors implement so called *Lagrangian approach* and use the coordinate system moving with the JS. The key component of the study is the comparison of the strength of the analyzed JS Wind Speed (WS) with the observed JS strength. As a result of the experiment, the following observations can be highlighted.

- The wind errors increase with wind speed (approximately, from 2% to 9%), and are particularly high for the wintertime period (which contains the strongest portion of the annual cycle of winds).
- The GADS observation provide a unique way to determine the meteorological parameters of shears and vortices with routine global spatial resolution down to 8 km (and 1 km is technically possible).
- The GADS observations have limited impact on the wind error improvement in data-dense regions. In contrast, these observations have a visible impact in data-sparse regions (such as Canada). They produce the most significant improvement to the short- and medium-range JS forecast.

From all the studies described in this section, it becomes clear that using aircraft wind (and other meteorological) measurements and implementing these data in the wind forecast models can significantly improve the accuracy of such forecasts. This, in turn, increases the accuracy of AT predictions and the overall flight efficiency (fuel consumption reduction, additional fuel reduction, flight-delay reduction, etc.). However, it is improper to speak about the improvement of the forecast accuracy by aircraft measurements, without speaking about the accuracy of these measurements themselves. The majority of the studies discussed above addressed this question as well. Nevertheless, we prefer to separate these two notions. Thus, the aircraft measurement errors are discussed in the next section.

3.1.4 Accuracy of the wind measurements

Aircraft perform meteorological measurements using special on-board equipment (as explained briefly in Appendix W). These measurements are evidently accompanied by some inaccuracy. The measurement inaccuracy arises from the proper instrumental uncertainty, defined by the instrument type, realization and quality, but it also depends on the aircraft maneuvers and environmental conditions (e.g. weather changing abruptly). Thus, it is hard to estimate the inaccuracy precisely. In this section, we discuss only the results concerning the uncertainties in wind measurements, although the majority of the work presented below investigates such uncertainties for other meteorological features (*i.e.* pressure, temperature) as well.

In [63], discussed in the previous section, the instrumental uncertainty is given as the result of previously realized studies and is supposed to be 2-3 m/s on average for horizontal winds. The authors mention, however, that uncertainty arises more during maneuvers, on one hand, and also may be as small as 1.1 m/s, on the other hand. They also remark that the accuracy of aircraft observations tends to be comparable with that of radiosondes, and sometimes even better.

In [65], which details were also given in the previous section, the methodology of determining the wind measurement errors from the set of wind measurements is described. The difficulty is that each comparison of the measured wind vector with the modeled wind vector contains both the measurement error and the model error, which are enmeshed. In order to separate these errors and to extract that of the measurements, aircraft reports from different aircraft are paired and their differences are computed. Then, these differences are grouped by the horizontal (2 km), vertical (less than 1 hPa) and temporal (less than 2 minutes) separation between the aircraft in the considered pair. For each group, the wind RMSVD was computed, that further was taken as "true" reference to calculate individual aircraft measurement error. Using this method, Cole *et al.* obtained the wind RMSVD equal to 1.7 m/s. They also observed, that this RMSVD increase by about 0.6 m/s when the altitude decreases.

In [64] some more detail on wind measurement errors obtained using the method described above are provided, including computational formulas. The authors consider the meteorological reports from different aircraft to be independent from each other, and their distribution to be the same as the aircraft distribution. In addition to this, they

consider that these reports are reasonable measurements with errors distributed around zero (or at least about some offset). The measurements that do not coincide with this hypothesis are considered to be the erroneous ones.

A study presented in [71] is fully devoted to meteorological (wind and temperature) measurement errors from aircraft relayed through the ACARS. It is based on the same approach of determining the individual aircraft error statistics as presented above, referred here as *collocation*. The u- (west-east, or longitudinal) and v- (south-north, or lateral) wind-component errors are calculated from the RMSVD by assuming these components to contribute equally to this error. Knowing u- and v-wind-component errors is important as usually these variables are used in data assimilation schemes and wind modeling. The performed experiments show that the ACARS errors seem to increase as the altitude decreases, and are less accurate near the ground (100-200 hPa), most likely due to higher turbulence and wind variation on one hand, and to the increased number of aircraft maneuvers on the other hand. For the altitude 300-400 hPa, the value for the u- and v-wind-component errors is discovered to be 1.1 m/s (it is the smallest recorded value).

Another study reported in [72] has objectives similar to [71], but concerns evaluation of the TAMDAR reports, and it takes place 10 years later. The simulations are hold for the same data set as in [68]. In contrast to [71], here the quality of TAMDAR data is defined in comparison with the RUC cycle, assimilating TAMDAR and AMDAR data. Evidently, the RUC forecast is not considered as the "truth", but rather as a common benchmark[17]. The results of the experiments show that the RMSVDs of TAMDAR measurements are considerably larger than those of AMDAR measurements, which is likely due to less accurate heading information. Furthermore, the largest error in TAMDAR measurements is accounted during the descent phase, which is more likely explained by the aircraft maneuvers.

In several studies discussed above (e.g. [64]), it is mentioned that the measurement errors coming from the same aircraft are in general correlated. Moreover, a suggestion that these errors might depend on the aircraft type is made. In [73], a comprehensive study aimed at discovering aircraft-type-specific errors, is described. The simulations are

[17]The discovered differences of TAMDAR measurements from RUC forecast include both TAMDAR data uncertainties and forecast errors.

based on AMDAR measurements from aircraft of eight different types[18] for more than 300 descents at Frankfurt Rhein/Main airport, reported by Lufthansa flights[19] with a high frequency ($\approx$ 3 flights per minute). The wind speed and direction contained in the AMDAR reports are converted to wind vector components, assuming that the aircraft is in the horizontal plane (no pitch), and that the correction angle (between heading and direction) is very small.

To investigate type-specific differences, all values are compared to a reference value. The authors note that the choice of such a value is arbitrary as long as it remains independent of the measurements. Nevertheless, [73] uses the hourly mean of all measured profiles as the reference value, as no external references were available for this study. In addition to the mean of all wind measurements, being the average of the given value of wind components, Drue *et al.* also calculated the mean of measurements of this value for the aircraft only of a given type (so-called the type average). The RMSE[20] and the systematic deviation[21], computed from these two mean values, defines the measurement quality of this given aircraft type.

This approach gave the following results.

- Systematic deviations of wind magnitude are not significantly different from zero. The systematic deviations for u- and v-wind-vector components strongly depend on altitude for most of the aircraft types.
- For altitudes below 1 km, both u- and v-wind-vector components account for the RMSE of about 0.6 m/s for almost all aircraft types; while above 1 km, the RMSE of both constantly increases with altitude up to 1-2 m/s at 4000 km.
- Errors in the u-component come mainly from TAS measurements, that in turns are related to errors in temperature and pressure measurements, while a great part of errors in the v-component comes from a simplification by considering the pitch and roll equal to zero (as these errors in general depend on the roll).

[18] A300, A319, A320, A321, A330, A340, B737, B747
[19] Reported on 22 days between August 2004 and January 2005
[20] Root-Mean-Square Error
[21] The mean difference between individual measurements of aircraft of the given type and the hourly mean of all types

From all the presented studies, we conclude that wind-measurement errors (being in average 1-3 m/s for more frequent cruising altitudes) should be taken into account if one wishes to use aircraft wind measurements to improve wind forecast.

3.1.5 Perspectives of wind forecast improvement examined in the present thesis framework

As concluded from the numerous studies presented in the previous section, utilizing the aircraft measurements of wind (and other meteorological data) in wind forecast that is further used in AT forecast can improve significantly the accuracy of such forecast. As we have noted, all the previous works are devoted to study improvements obtained from incorporating aircraft measurements into the NWP models (such as RUC cycle). At the same time, the new broadcast technologies being implemented will permit the aircraft to exchange any data available on board with the surrounding traffic directly, in real-time.

Based on this opportunity, we propose, in the frame of the current thesis, a new approach aimed at improving AT prediction, that we have called *Wind Networking* (WN). This concept will allow an aircraft en-route that obtains measured wind data from the neighboring aircraft, to use this data, that is supposed to be more recent and thus, more accurate, directly in order to adjust its wind prediction, and consecutively, its AT prediction.

The objective of this study is to reveal the benefits obtained from implementing the WN approach compared to standard forecast methods based on NWP models.

3.2 Mathematical model of the WN approach

In this section, we present the mathematical models used in our simulations of air traffic progress. First, we explain how we simulate the flight progress in the wind field in real conditions and the flight prediction based on the forecast winds. After that, we introduce the WN approach and define how it can be used to improve the flight prediction. Finally, we present the method to obtain the forecast winds and we discuss the possibilities to simulate the real wind, which is actually unknown. Several existing approaches are mentioned and the one used in our computations is explained.

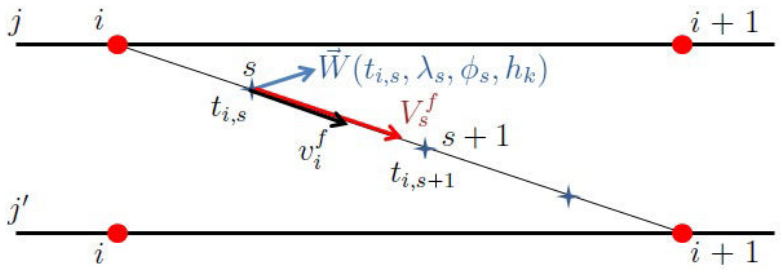

FIGURE 3.3: Simulation of flight between two waypoints

3.2.1 Model of flight simulation and forecast

To simulate the flight progress within NAT, we need to compute for each aircraft the times of passing the route points. These times are computed based on the aircraft Ground Speed (GS). While the aircraft TAS is a given parameter for a segment of flight, the GS varies according to the wind that the aircraft is subjected to.

Let us consider an OTS grid on nodes and links, as it is defined in Section 2.2.1. Let us consider further an aircraft f moving at FL k from waypoint (WP) i on track j towards the next WP $i+1$ on track j' (where $j' \in \{j-1, j, j+1\}$) along the corresponding link (Fig. 3.3). Let us assume that at time t^f this aircraft is located at the point with coordinates (λ, ϕ, a_k). Its TAS is equal to v_i^f at this point (black arrow in Figure 3.3). The real WS[22] at this point is equal to $\vec{W}(t^f, \lambda, \phi, a_k)$ (blue arrow in Figure 3.3). Then, its real GS (red arrow in Figure 3.3) is defined by the formula:

$$V^f(t^f, \lambda, \phi, a_k) = v_i^f + W_{ijj'}(t^f, \lambda, \phi, a_k), \tag{3.1}$$

where $W_{ijj'}(\lambda, \phi, a_k)$ is the projection of the wind vector on the line containing link $(i, j, k) - (i+1, j', k)$.

Given the time t_i^f at which aircraft f was at the WP (i, j, k), we are interested in computing the time t_{i+1}^f at which this aircraft arrives at the WP $(i+1, j', k)$. To compute this time, we divide the corresponding link $(i, j, k) - (i+1, j', k)$ into $N_{ijj'}$ sublinks and obtain $N_{ijj'}+1$ subnodes (marked with stars in the example of Figure 3.3, where $N_{ijj'} = 4$). The GS $V_{i,s}^f$ at each subnode $s = 1, ..., N_{ijj'}+1$ can be calculated via formula (3.1). To simplify the simulation, we suppose that this speed remains constant

[22]Here and after, when speaking about wind speed and wind vector, we mean *horizontal WS*. We neglect the vertical component of the WS. Similarly, we are always speaking about horizontal GS and horizontal TAS.

and equal to $V^f_{i,s}$ along the sublink between subnodes s and $s+1$. Let us denote the length of this sublink as $l_{i,s}$. Then, the time $\Delta t^f_{i,s}$ necessary for aircraft f to move from subnode s to subnode $s+1$ is simply:

$$\Delta t^f_{i,s} = \frac{l_{i,s}}{V^f_{i,s}}. \tag{3.2}$$

Using these time periods $\Delta t^f_{i,s}$ and given the link entry time t^f_i (which is the time of passing the first subnode, $t^f_i = t^f_{i,1}$), the times $t^f_{i,s}$ at which aircraft f passes subnodes s can be successively calculated for $s = 2, ..., N_{ijj'} + 1$:

$$t^f_{i,s} = t^f_{i-1,s} + \Delta t^f_{i,s}. \tag{3.3}$$

We thereby obtain all the necessary information to perform the simulation of aircraft flight along any link (and for the whole OTS). Note that $t^f_{i,s}$ is the *real (actual) time* of arrival of aircraft f at subnode s.

In addition, we define the *forecast times*, noted as $\tilde{t}^f_{i,s}$, i.e. the times at which the aircraft *estimates* to be at subnode s using the available MF information. This time is usually different from the actual time, as the exact values of real oceanic winds are not known. The forecast times $\tilde{t}^f_{i,s}$ can be calculated based on the *forecast wind function* $\vec{\tilde{W}}(t^f, \lambda, \phi, a_k)$ using formulas analogous to (3.1)-(3.3). As it can be concluded from Section 3.1, the forecast wind always differs from the real wind, and sometimes the difference is significant, especially in NAT.

Figure 3.4 displays an example of the differences that can occur between real and forecast flight values. The aircraft TAS, v^f_i, is represented with a black arrow, the real WS, $\vec{W}$, with a blue arrow, while the forecast WS, $\vec{\tilde{W}}$, slightly different, with a green arrow. Thus, the *forecast GS*, $\vec{\tilde{V}}$ (violet arrow) also differs from the real GS, $\vec{V}$ (red arrow).

3.2.2 Wind Networking model

This section describes the main idea of the WN approach. Let us suppose that aircraft f, en-route, passing the point (λ, ϕ, a_k) at time t^f, can measure the wind $\vec{W}(t^f, \lambda, \phi, a_k)$ at this point (dark blue arrow in Figure 3.5, top). Measurements are assumed to be

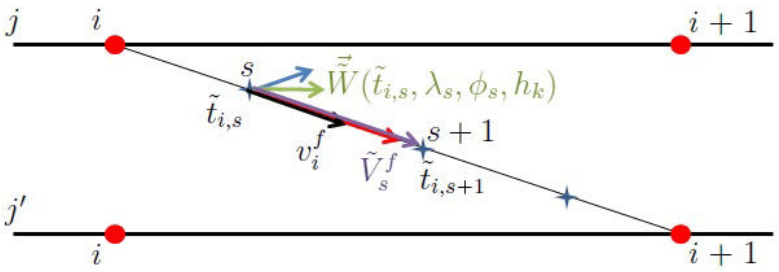

FIGURE 3.4: Estimation of flight between two waypoints

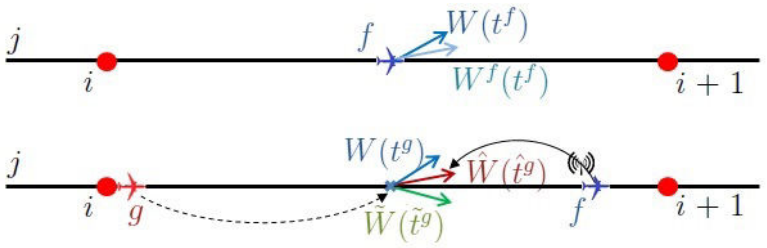

FIGURE 3.5: Adjusting wind predictions by Wind Networking

performed with some error $\vec{\rho}^f$. Thus, instead of the real wind function, the aircraft obtains an approximation (light blue arrow in Figure 3.5, top):

$$\vec{\hat{W}}^f(t^f, \lambda, \phi, a_k) = \vec{W}(t^f, \lambda, \phi, a_k) + \vec{\rho}^f. \tag{3.4}$$

Further, we suppose that aircraft can communicate the results of these measurements to other aircraft (see Figure 3.5, bottom). Based on the information about the winds received from preceding aircraft, the following aircraft (g, shown in red in Figure 3.5) can *adjust* its predictions (dashed arrow in Figure 3.5). This information ($\vec{\tilde{W}}$, red arrow in Figure 3.5) is expected to be more accurate than MF winds ($\vec{\hat{W}}$, green arrow in Figure 3.5), as it is more recent. Thus, the *adjusted predictions* should be closer to the real situation than the initial forecast. That is the main idea of WN.

Let us consider that aircraft f moves at FL k, from WP i on track j towards the next WP $i+1$ on track j' along the corresponding link. Being at the WP i at time t_i^f the aircraft needs to predict its flight until WP $i+1$. To simulate this process, we divide again the link $(i, j, k) - (i+1, j', k)$ into $N_{ijj'}$ sublinks. Using the forecast wind field $\vec{\hat{W}}$, we obtain the forecast times of passing the subnodes: $\tilde{t}_{i,s}^f$, $s = 1, ..., N_{ijj'} + 1$. Here is how we propose to improve these predictions using the WN approach.

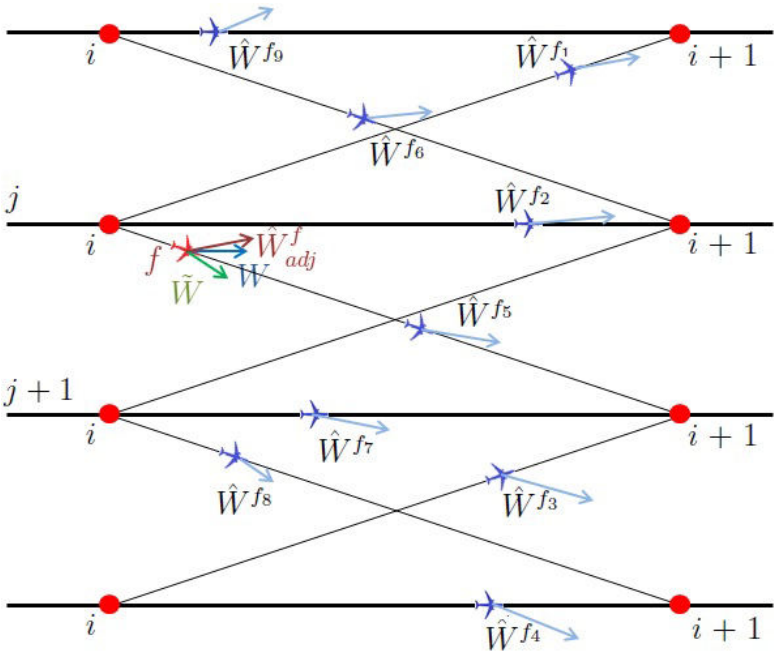

FIGURE 3.6: Adjusting wind predictions by WN using data from several neighboring aircraft

Let us consider M aircraft $f_1, f_2, ..., f_M$ on the OTS on the links *neighboring* to the link $(i, j, k) - (i + 1, j', k)$ that passed the corresponding links before aircraft f does (before t_i^f). The choice of the links that are considered to be *neighboring* to the current link can vary according to user preferences. The set of neighbor links may, for instance, include the current link itself, several upper/lower links and/or several northern/southern links. The way we define these neighbor links for most of our simulations is described in Section 3.2.6. Figure 3.6 displays one example of how one can determine all neighbor aircraft (blue) of a given aircraft f (red) in the horizontal section of the OTS.

Aircraft f then can use the wind measurements from preceding aircraft f_m, $m = 1, ..., f_M$ (all of them, or only some of them) in the prediction of its flight. Considering that each such aircraft f_m measured $N^m_{ijj'} + 1$ winds on the corresponding link, we obtain the following wind data available for aircraft f:

$$\vec{\hat{W}}^{f_m}(t^{f_m}_{i,s_m}, \lambda_{i,s_m}, \phi_{i,s_m}, a_{k_m}), \tag{3.5}$$

$$\text{for } m = 1, ..., M, \;\; s_m = 1, ..., N^m_{ijj'} + 1,$$

$(\lambda_{i,s_m}, \phi_{i,s_m}, a_{k_m})$ are coordinates and $t_{i,s_m}^{f_m}$ is the time of passing of subnode s_m by aircraft f^m, and $\hat{\vec{W}}^{f_m}$ is the wind, measured by this aircraft at this moment (blue arrows in Figure 3.6). Further, we can apply any appropriate extrapolation method to the desired measurements (3.5) in order to obtain the *adjusted wind* at each subnode $s = 1, ..., N_{ijj'}^f + 1$ on the route link of aircraft f:

$$\hat{\vec{W}}_{adj}^f(\hat{t}_{i,s}^f, \lambda_{i,s}, \phi_{i,s}, a_k) = \underset{s_m=1,...,N_{ijj'}^m+1;\ m=1,...,M}{\text{extrapolation}}\{\hat{\vec{W}}^{f_m}(t_{i,s_m}^{f_m}, \lambda_{i,s_m}, \phi_{i,s_m}, a_{k_m})\}, \tag{3.6}$$

Here, $\hat{t}_{i,s}^f$ is the aircraft predicted *adjusted time* of passing subnode s, that can be calculated using formulas similar to (3.1)-(3.3). The adjusted wind $\hat{\vec{W}}_{adj}^f$ is shown with a red arrow in Figure 3.6 and it is supposed to be closer to the real wind (blue arrow) than the forecast wind (green arrow) at the same point.

The idea of the current study is to simulate AT prediction for a set of aircraft using winds obtained from the MF and by the WN approach, and to compare these predictions with the real aircraft progress, which is also to be simulated, in order to determine the accuracy of each of the prediction methods. Thus, to perform such simulations, as explained above, we need in addition to model the wind fields: the real wind, $\vec{W}$, the forecast wind, $\vec{\tilde{W}}$, the measured wind, $\hat{\vec{W}}^f$, and the adjusted wind $\hat{\vec{W}}_{adj}^f$. These models are presented in the next sections.

3.2.3 Model of forecast winds

The forecast wind can be obtained from meteorological databases. In our simulations, we rely on the GRIB data files created by the meteorological centers (NOAA, Meteoblue, FNMOC), which are available online [74]. A GRIB file consists of several grids coded in a special format [75]. Each such grid represents a regular grid of geographical points with maximal resolution of 0.5°, where various MF data is defined for each point. Each grid is defined for a specific time for which the MF is valid (with 3-hour time step) and for a specific altitude.

We decode the GRIB files with the open-source Java library JGrib [76]. For our simulations, we extract the following data:

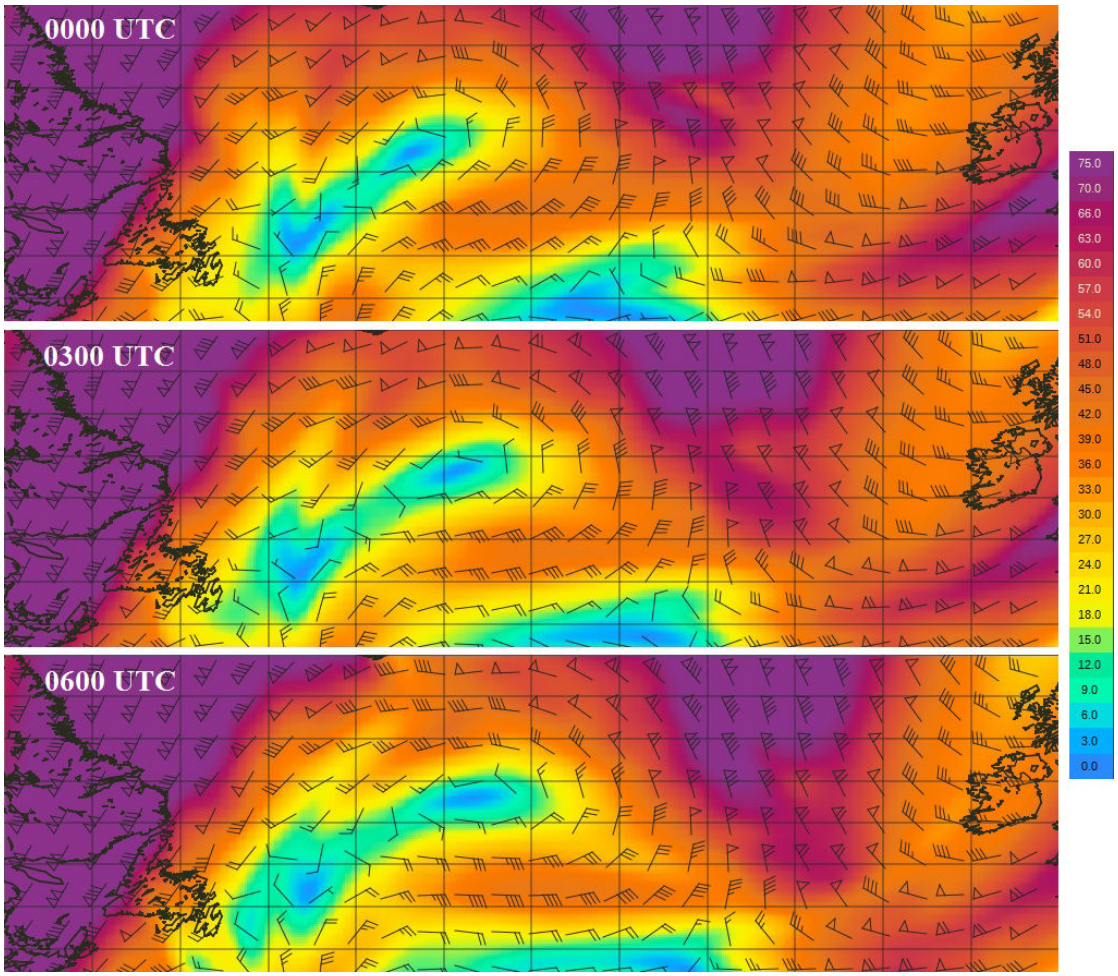

FIGURE 3.7: Model of the forecast wind and its evolution with time for 26 April 2013

- the area from 35°N to 70°N of latitude and from 0°W to 75°W of longitude, which covers the NAT;
- the time period from 0000 UTC to 0900 UTC that includes the eastbound OTS validity period;
- the altitudes 300hPa and 200hPa that bound the published OTS FLs;
- only the u (west-east, longitudinal) and v (north-south, lateral) wind components for each point.

Figure 3.7 displays the wind fields obtained from a GRIB file available for 26 April 2013 at the altitude 200 hPa. Three time moments: 0000 UTC, 0300 UTC and 0600 UTC are considered in this example to illustrate the wind evolution.

GRIB files only provide information about the winds at discrete grid points. We obtain the continuous wind field of forecast winds by linear interpolation over grids in

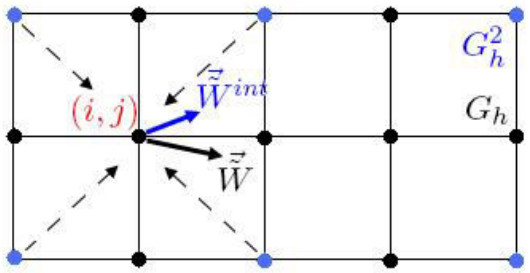

FIGURE 3.8: Interpolation of wind within a reduced grid with power of reduction $p = 2$

4-dimensional space (time, altitude, latitude and longitude). Most of the wind models used in other studies also rely on such an approach (e.g. [65, 70]). However, we would like to check the validity of the linear interpolation hypothesis, especially in the space. To do so, we apply the following method.

We choose a parameter p, that in the sequel we will call the *power of reduction*, and for each horizontal section, G_h, of the wind grid G, of size $N_x \times N_y$, we construct the reduced grid section G_h^p of size $\frac{N_x}{p} \times \frac{N_y}{p}$ by choosing each p-th point from the grid section G_h (further, instead of writing "a section of the grid", we will refer to G_h and G_h^p simply as "grid"). Now G_h can be considered as the refined grid of the grid G_h^p. Figure 3.8 shows an example of such a grid, G_h^2, constructed by reducing grid G_h by power of reduction $p = 2$. The nodes of grid G_h^2 are displayed in blue.

Further, we select the points (i, j) from the grid G_h that do not belong to the grid G_h^p (see Figure 3.8), we get the value of the forecast wind $\vec{\tilde{W}}^{int}(i, j)$ at these points (blue vector in Figure 3.8) using a bilinear interpolation over the grid G_h^p (linear interpolation for longitude and latitude) and we compare this value to the given wind value $\vec{\tilde{W}}(i, j)$ from the grid G_h (black vector in Figure 3.8):

$$\Delta W_x(i, j) = \tilde{W}_x(i, j) - \tilde{W}_x^{int}(i, j), \tag{3.7}$$

$$\Delta W_y(i, j) = \tilde{W}_y(i, j) - \tilde{W}_y^{int}(i, j). \tag{3.8}$$

Here, $\tilde{W}_x(i, j)$ is the longitudinal wind component (u-component), and $\tilde{W}_y(i, j)$ is the latitudinal wind-component (v-component). We illustrate the proposed method using the data from a GRIB file for 26 April 2013 (Fig. 3.7). Table 3.1 displays the parameters of the distribution of the wind differences $\Delta W_x(i, j)$ and $\Delta W_y(i, j)$ with $p = 2$ for these

Values (in m/s)	ΔW_x	ΔW_y
Max value	2.225	2.275
Mean value	-2.875	-2.95
Mean (μ)	0.002	-0.005
Variance (σ)	0.354	0.339

TABLE 3.1: Wind difference statistic parameters for interpolated winds with power of reduction equal to 2 (April 26, 2013)

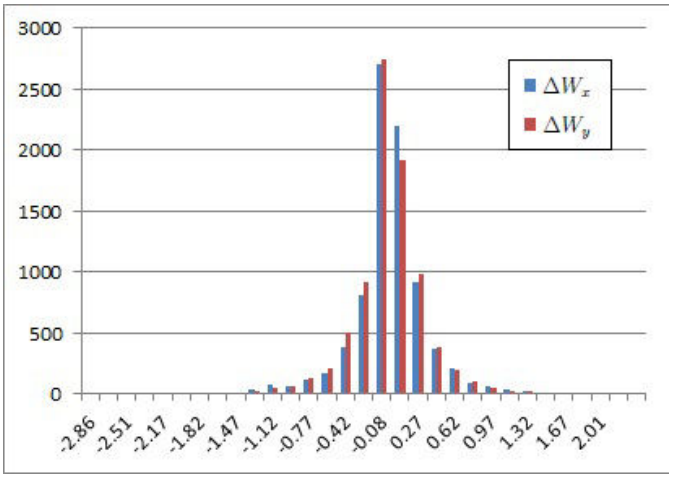

FIGURE 3.9: Wind differences distributions for interpolated wind with power of reduction equal to 2 (April 26, 2013)

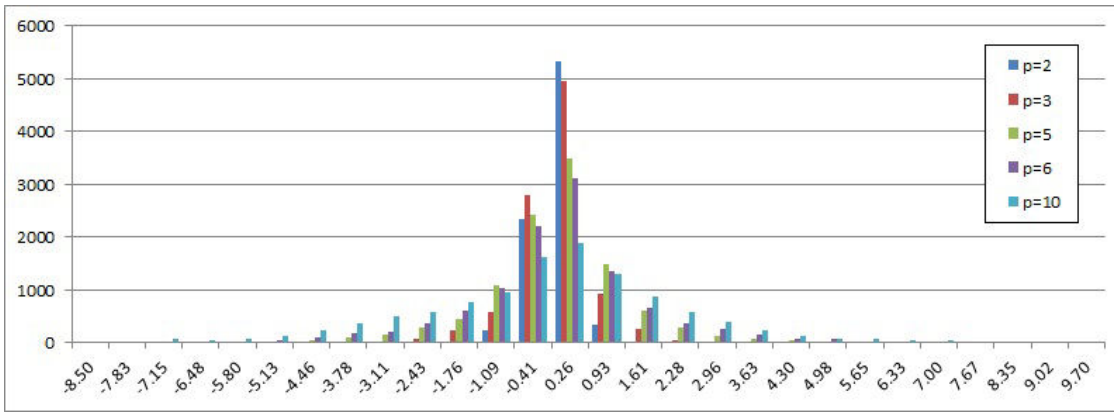

FIGURE 3.10: x wind component differences distribution for interpolated wind depending on the power of reduction. April 26, 2013. Altitude 200hPa

wind grids. Figure 3.9 demonstrates the distribution of the x and y wind components for $p = 2$, and Figure 3.10 shows the distribution of x component $\Delta W_x(i, j)$ for different powers of reductions for forecast winds.

It is quite evident that the rougher the grid G_h^p is, the rougher the results of interpolation are. For the most refined grid, G_h^2 ($p = 2$), the results of interpolation are very good: for all points the absolute values of wind differences do not exceed 3 m/s, and for 97%

of points these values do not exceed 1 m/s, while remaining mostly concentrated around zero. Thus, we conclude, that with current grid resolution (grid points every 0.5° the linear interpolation approximates satisfactorily the reality.

3.2.4 Models of real winds based on statistical deviations in literature

To evaluate the accuracy of the forecast, we need to compare the forecast wind values with the real ones. The difficulty is that the real wind is actually unknown. As the forecast wind can be obtained from meteorological databases, a large number of works devoted to modeling wind for aviation, focus on modeling the deviations of the predicted wind from the real one, $\Delta\vec{W}$ (that we also call the *errors of wind prediction*):

$$\Delta\vec{W} = \vec{W} - \vec{\tilde{W}}. \tag{3.9}$$

Then, once $\vec{\tilde{W}}$ and $\Delta\vec{W}$ are known, the real wind $\vec{W}$ can simply be obtained from equation (3.9). The deviations, $\Delta\vec{W}$, are generally given under statistical form. The most common idea of various studies is to model the correlations in time and space for wind components.

Paper [77, Section 5.4.] analyses the statistical structure of the mid-latitude errors of the short-range wind forecasts by comparing these forecasts with radiosonde data over North America. It provides a comprehensive 3-dimensional and spectral description of the covariance structure of the wind forecast and observation data, under the assumption that errors are locally homogeneous. A truncation distance of 3,000 km is applied to the wind correlation, thereby assuming that wind error is constant over this domain. It is referred to as *large-scale* component of the error. The results are expressed in terms of longitudinal and transverse speed correlations. For the AT prediction, the longitudinal correlations are the most important component of the error for flights not subject to large turns.

In [78], Mondoloni develops further the ideas from [77] and proposes the model of *along-track wind uncertainty*, affecting the AT prediction, as a sum of three stochastic terms, presented below.

- The *error of representativeness effect* (associated with not modeling the smaller, higher frequency scales) is modeled as a random process with zero mean, a known RMS and a correlation function with a given length). The distance-based correlation function is transformed into time-based one, which is further approximated using the power spectral density.

- The *prediction error* (describing the error in prediction occurring at the modeled scales) is represented through a correlation function, which is also expressed by its power spectral density.

- The *large-scale error* (assumed to be constant bias over a range of 3,000 km) is represented by a constant sampled from a normal distribution.

These models of wind-error components require adjusting several parameters and coefficients, that is made empirically in [78]. Further, spectral decomposition, using power spectral density functions, is applied to obtain a second-order continuous shaping filter. The described model is consistent with the results from [77] for the RMS values of each contributor to uncertainty, the cumulative distribution function, the N^{th} percentile errors, the number of hours for which the N^{th} percentile exceeds the threshold. Moreover, the proposed model also accounts for the correlation of errors between altitudes. As stated in [78], uncertainty in wind prediction yields a time-varying wind field, which in turns, affects the AT prediction. Thus, the study of the errors of aircraft GS and along-track position is also performed in this work.

In [79] the real wind is modeled by two components:

- *nominal wind*, modeled as a look-up table, similar in temporal and spatial resolution to meteorological data from NWP available for ATC (Air Traffic Control);

- and *stochastic component* (which can be considered as the prediction error), modeled as jointly Gaussian random variables with a correlation structure in both time and space.

The model of stochastic wind component [79, Section 6.1.] supposes that the random wind field is isotropic in horizontal plane, *i.e.* the correlation structure is presented under rotation in the horizontal plane. Moreover, the three wind components are assumed to

be independent of one another at any time and at any point of the space, and thus, they can be computed separately. Glover *et al.* develop a step-by-step algorithm, that permits to simulate the flight progress in the wind field by computing the WSs for each aircraft at the same time, using recursively calculated matrices guaranteeing the desired correlation structure for the wind components.

The properties of the function that governs the wind correlations, are defined based on the study of the RUC data [79, Section 7.1.]. Glover *et al.* assume that the vertical component of this function is zero, and the horizontal component has a time-space separable structure, that can, thereby be represented as a multiplication of three functions: the function of time, the function of distance, and the function of altitude. The mean and variance of WS, as a function of altitude, are found by using all the available from RUC grid points. To determine the covariance as a function of distance, the discrete bins of fixed size are used. Furthermore, the authors claim, that for a short-range scale (around 1,000 km), the correlation can be closely approximated by the exponential function, with some parameters adjusted according to the available data.

The stochastic wind model from [79] is further used in [80] to compute the wind forecast error field. The airspace is discretized into a 3D-grid of points, for each of which the two wind components (south-north and east-west) are generated. This process is made consecutively, by discretizing the time, and ensuring the desired covariance structure for the wind components. The procedure of each next state calculation is simplified by decomposing the covariance matrix into orthogonal matrices. Further, these generated winds are used in a novel filtering algorithm, referred to as Sequential Conditional Particle Filter, aimed at improving the conflict detection in ATC. More detail on this approach can be found in [81].

In [82] the main drawback of the algorithm described in [79] is pointed out, which is related to its performance. Indeed, the model from [79] is computationally intensive, both in time and in memory, as the computations of covariance performed at each step have to be stored in order to be reused in the recursive computation of the next step. Oliveira *et al.* propose an approximation method based on the original algorithm from [79] and aimed at reducing its complexity. Its idea is to discard part of the past evaluations in order to decrease the size of the covariance matrix. Algorithm implementation choices such as the size of data structure are set according to the requirements of each particular

problem. The results of comparison of the developed algorithm with the original one reveal a significant benefit in CPU time, as well as in memory usage when applying the new algorithm, while the quality of the yielded solution remains very close to that of the original algorithm. Thus, the authors claim that the proposed algorithm is an efficient way to generate wind-prediction error fields.

In [83] a different technique for estimating forecast wind uncertainty is proposed. It is used to determine the uncertainty in the RUC forecast. Lee *et al.* use a time-lagged ensemble of RUC-model upper-level wind forecasts and calculate the statistical measure of forecast spread amongst the ensemble members. The key advantages of the technique are:

- great savings in computational time and resources, in comparison to classical methods based on the perturbation of the model initial fields, as the data is readily available;
- identifying regional variations of wind uncertainty field, related to actual weather phenomena.

The main disadvantage is that:

- the ensembles may exhibit a large degree of correlation with each other.

Nevertheless, the proposed concept, evaluated in [83], gives coinciding results. Furthermore, the impact of the wind forecast uncertainty on trajectory prediction uncertainty is also examined in this study.

While such statistical methods yield satisfactory results, they require adjusting some parameters. This is done based on available data of wind forecast and/or aircraft observations, such as the wind data field over the USA obtained via RUC forecast including MDCRS, given in [64]. As to our knowledge there is no precise study similar to [64] determining the statistical parameters for NAT, we propose another approach to model real winds. It is described in the next section.

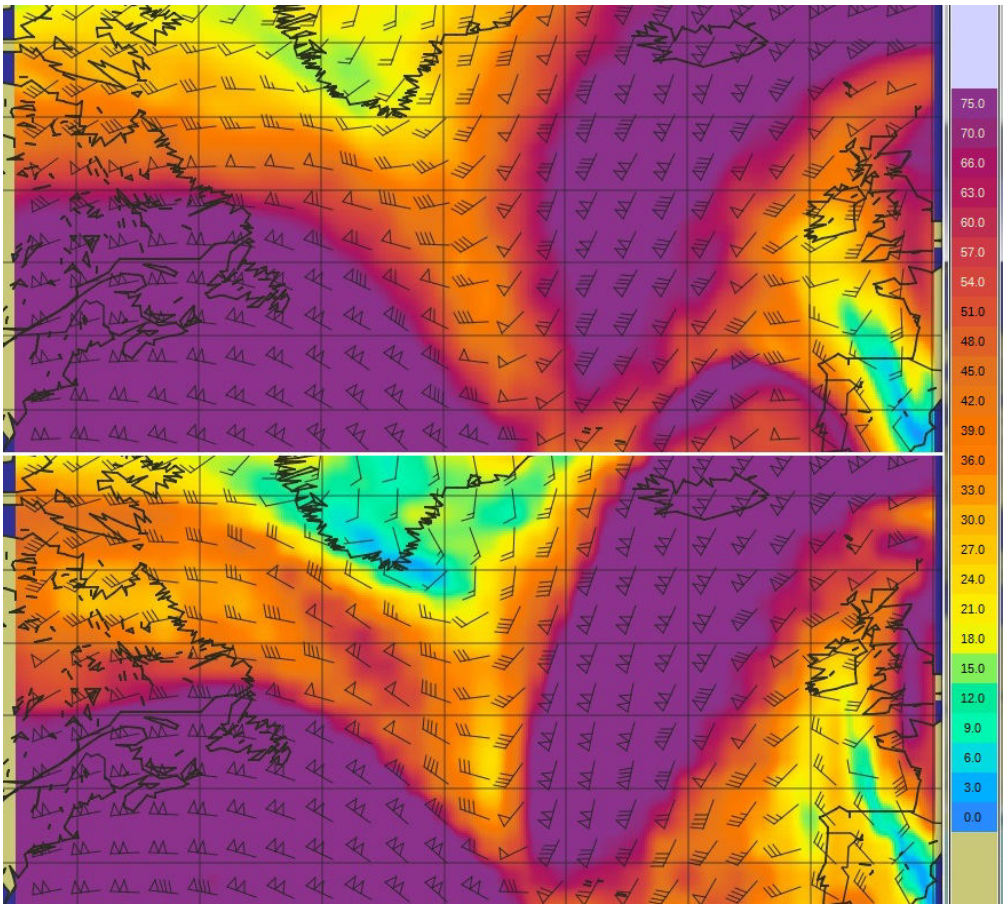

FIGURE 3.11: Forecast winds vs. "real" winds for December 10, 2013

3.2.5 Model of real winds based on forecast used in flight progress simulations

Our approach is in some kind close to the method described in [83], as we also use the previous forecasts. However, we do so not to define the stochastic structure of wind uncertainty, but rather to represent the real wind field directly. More precisely, in order to simulate the real wind field in addition to the forecast wind field, for a particular day, we rely on two GRIB files downloaded with time difference of several (from 18 to 24) hours. We use the data from the first (the oldest) file as forecast winds. The second (the latest) file is used to model the real winds, as its data is more recent and therefore tends to represent better the reality. The obtained discrete wind field is further linearly interpolated, in the same manner as for forecast winds. Figure 3.11 displays the wind fields obtained from the two GRIB files available for 10 December 2013 at 0000 UTC and the altitude 200 hPa; the top field corresponds to the forecast wind; the bottom field simulates the assumed real wind.

	ΔW_x	ΔW_y
Max value	10.4	8.3
Mean value	-9.6	-11.1
Mean (μ)	0.223	0.076
Variance (σ)	2.358	2.345

TABLE 3.2: "Real" vs. forecast wind differences statistic parameters for April 26, 2013

The main advantage of our method is its simplicity, while the main drawback is similar to that pointed out in [83]: the resulting wind fields (forecast and real) might have stronger correlation than in reality, as these two fields are produced by the same NWP model. As it can be seen from Figure 3.11, the forecast and "real" wind fields differ. Let us denote the differences of wind components of real and forecast winds, when defined as explained above, for each grid defined for a time t at altitude a at each grid point (i, j) as:

$$\Delta W_x(t, i, j, a) = W_x(t, \lambda_i^j, \phi_i^j, a) - \tilde{W}_x(t, \lambda_i^j, \phi_i^j, a), \tag{3.10}$$

$$\Delta W_y(t, i, j, a) = W_y(t, \lambda_i^j, \phi_i^j, a) - \tilde{W}_y(t, \lambda_i^j, \phi_i^j, a). \tag{3.11}$$

Then, we can calculate the statistic parameters of distributions of such differences: mean values (μ_x, μ_y) and variances (σ_x, σ_y). The numerical values of these parameters for the three pairs of wind grids[23] for April 26, 2013 are given in Table 3.2 and the graphical representation of the distributions is given in Figure 3.12. Figure 3.13 compares the obtained distributions for ΔW_x and ΔW_y with the normal distributions $N(\mu_x, \sigma_x^2)$ and $N(\mu_y, \sigma_y^2)$ respectively. As it can be seen, the distributions are almost coinciding. Moreover, the distribution parameters for the x- and y-wind-components are very close (with the mean value near zero and the variance about 2.3 m/s). Thus, they can be considered as the random samples from a normal distribution.

3.2.6 Model of adjusted winds

As described in Section 3.2.2, when the WN is applied, the forecast wind is adjusted using the wind measurements from preceding aircraft. The wind, measured by aircraft

[23] for altitude 200 hPa and for times 0000 UTC, 0300 UTC and 0600 UTC

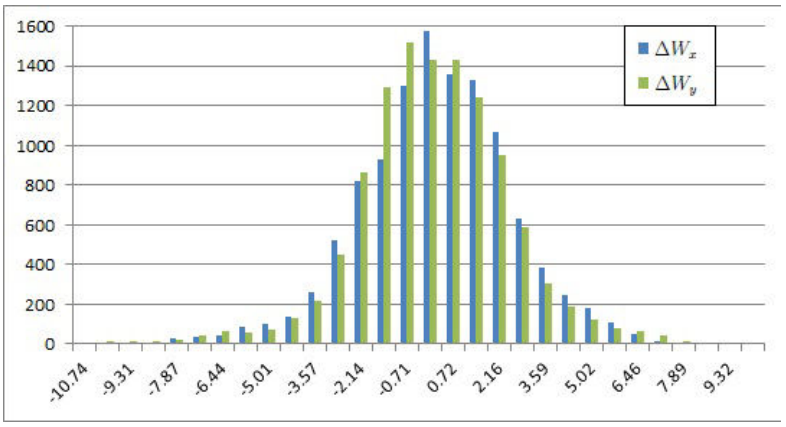

FIGURE 3.12: "Real" vs. forecast wind differences distributions for April 26, 2013

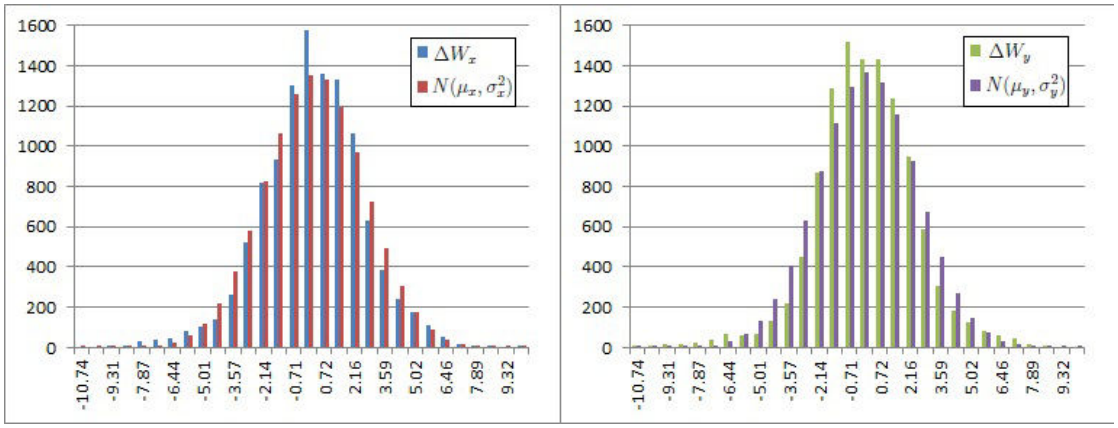

FIGURE 3.13: Wind differences distributions vs. Normal distributions. April 26, 2013

f, $\hat{W}^f$, is defined via equation (3.4), where $\vec{\rho}^f$ is the measurement uncertainty of aircraft f. In our simulations, we consider $\vec{\rho}^f$ to be normally distributed, $\vec{\rho}^f \in N(0,\sigma) \times N(0,\sigma)$, with mean equal to 0 and standard deviation $\sigma = 1.1$ m/s. The value of $\sigma = 1.1$ is set according to the statistics obtained from the previous available studies [64, 71].

Further, we have tested several extrapolation approaches of how an aircraft f following aircraft $f_1, ..., f_M$ on *the same track* j at the same FL k can obtain the adjusted value of wind $\vec{\hat{W}}^f_{adj}(\hat{t}^f_{i,s}, \lambda_{i,s}, \phi_{i,s}, a_k)$ from the wind values measured by these M preceding aircraft $\vec{\hat{W}}^{f_m}(t^{f_m}_{i,s}, \lambda_{i,s}, \phi_{i,s}, a_k)$, $m = 1, ..., M$ (equation (3.6)). The detail on such tests can be found in Appendix X. Note that for these tests, as all aircraft follow the same track, we consider them to report over common points $s = 1, ..., N^f_{ijj} + 1$. With such an assumption, it was found out that using data from the latest available aircraft for the adjusted wind yields results that are as good as (and in some cases, even much better than) when applying any extrapolation method to wind values obtained from several aircraft. Thus, we conclude, that the more recent the measurements are, the

more accurate they are, and we focus only on these last-aircraft results in this paper, *i.e.*

$$\vec{\hat{W}}^{f}_{adj}(\hat{t}^{f}_{i,s}, \lambda_{i,s}, \phi_{i,s}, a_k) = \vec{\hat{W}}^{f_m}(t^{f_m}_{i,s}, \lambda_{i,s}, \phi_{i,s}, a_k),$$

where f_m is the last aircraft passing subnode s prior to f.

Finally, we have tested several approaches to extrapolate the measurements performed by the aircraft neighbor to aircraft f. For each link l of the AT of aircraft f, we consider that the *neighbor aircraft* are those cruising along the links neighbor to l. Here is how we define the *neighbor links* for a link $(i,j,k)-(i+1,j',k)$ in most of our simulations. Let us denote $j_{min} = \min(j,j')$ and $j_{max} = \max(j,j')$. Then, the neighbors of the link $(i,j,k)-(i+1,j',k)$ in horizontal plane (on FL k) are all the possible links between WP i and WP $i+1$ on the tracks $j_{min}-1$, j_{min}, j_{max}, $j_{max}+1$. An example of such neighbor links is displayed in Figure 3.6. In the vertical direction, for inner FLs, we consider the two links on the adjacent FLs: upper and lower, *i.e.* the links $(i,j,k+1)-(i+1,j',k+1)$ and $(i,j,k-1)-(i+1,j',k-1)$. For extreme FLs there is only one such link (upper or lower).

Given numerous wind measurements from different points of such neighbor links and at different times, we choose further which value we use in our extrapolation. Empirical experiments show that in the case of measurements from neighbor aircraft, it is still more favorable to use the *most recent* measurements, even if they come from more distant (from aircraft f) points. Finally, on keeping the most recent measurements, we perform the linear interpolation between them in time and 3D-space in order to obtain the adjusted wind at a current point s of the AT of aircraft f. Some more detail on different interpolation approaches over neighbor aircraft measurements are discussed in Section 3.3.2.

3.2.7 Wind Networking evaluation criteria

The main objective of this study is to compare the quality of the two prediction approaches: using MF and WN. The first criterion of comparison is the error made in the

time prediction. To measure this error, we compute for each flight f and for each WP i of its AT, the difference between the real and the predicted times of arrival at this WP:

- $\tilde{\epsilon}_i^f = \tilde{t}_i^f - t_i^f$ for forecast times;
- $\hat{\epsilon}_i^f = \hat{t}_i^f - t_i^f$ for adjusted times;

and we analyze and compare the prediction error ($\tilde{\epsilon}_i^f$ and $\hat{\epsilon}_i^f$) distributions.

Another criterion of comparison is the number of conflicts detected for the set of flights using each of the prediction approaches:

- the number of conflicts that are predicted (by each of the methods) but do not happen in the reality (*false alarms*);
- the number of conflicts that would happen but have not been predicted (*critical errors*);
- the errors in the conflict duration predictions (related to the time prediction errors).

The process of conflict detection is the same as described in Section 2.2.3. The results of these comparisons are presented in the next section.

3.3 Results of simulations

In this section, we present the results of our computational experiments aimed at simulating the flight progress in the wind field, and performing the flight prediction process using two approaches: MF and WN. First, we consider a simple case, when all aircraft follow each other on a single OTS track. Then, we consider a real OTS system and real flight sets. Finally, we artificially increase the number of aircraft in the flight sets in order to reveal the particular benefits of the WN approach in especially dense traffic environment.

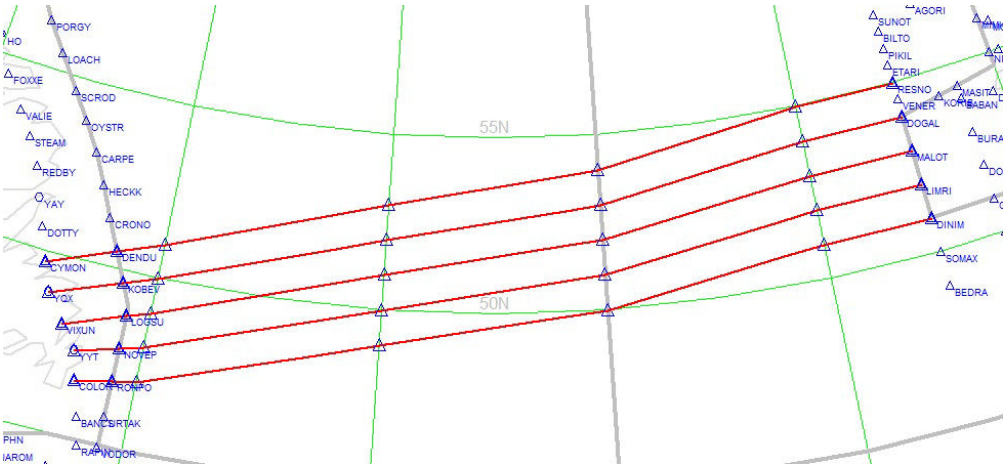

FIGURE 3.14: Eastbound OTS tracks for December 10 2006

3.3.1 Results for one track

Our first preliminary study considers a simple model consisting of several consecutive flights following one track on the same FL. For this model, at each link there are potentially several aircraft entering this link before the first one exits this link, *i.e.* before the wind measurements along the whole link are available. Therefore, these aircraft cannot benefit fully from the WN approach. On the other hand, the remaining aircraft obtain complete information about the winds from all preceding aircraft for each AT point. This case demonstrates the benefits of the WN approach under ideal conditions.

In the example below, we consider the date December 10, 2013. The forecast and real wind fields for this day are obtained from [74] (such fields, at 0000 UTC, are presented in Figure 3.11). The OTS structure for this day (see Figure 3.14) is obtained from the NAT messages (see Appendix N for detail on the format). These messages are available online at [84] for the current OTS of the day and at [85] for archived OTS (historical data). Furthermore, we consider a flight set consisting of 77 aircraft cruising on the middle OTS track (between WPs VIXUN and MALOT, Fig. 3.14) at the altitude 200hPa. The flight track entry times are randomly chosen between 0000 UTC and 0500 UTC so that all aircraft exit the OTS before 0900 UTC and are separated by at least 3 minutes (according to Reduced Separation Standards, RSS) throughout the track.

First, we perform the flight simulations using the real wind field, next using the forecast (MF) wind, and finally using the wind obtained (by WN) from the latest preceding aircraft. We assume that an aircraft, f, that is at WP i at time t_i^f can apply the WN

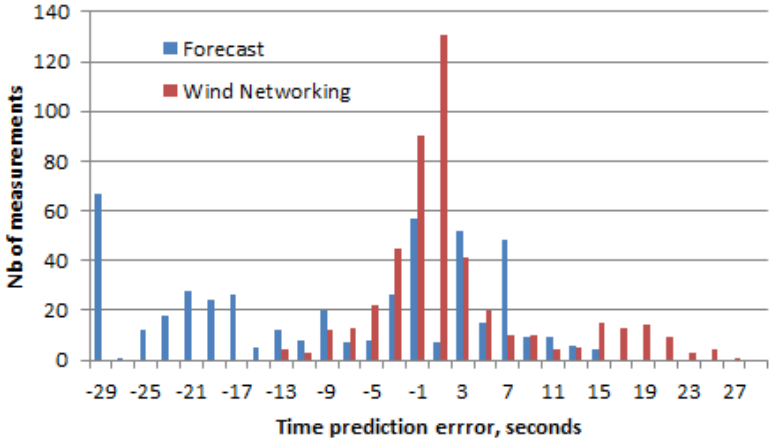

FIGURE 3.15: MF and WN prediction error distribution for 77 consecutive flights on a single track

to predict its time of passing the WP $i+1$, and, obviously, all the times of passing the subnodes, s, on the link between WP i and $i+1$, only in the case, if for each such subnode s at least one wind measurement has been reported before t_i^f. For the presented example, the first 10 aircraft are too close to one another to provide sufficient information, for all subnodes on links, to the following aircraft. Thus, the WN approach is only applied to the remaining 67 aircraft. For each simulation, we record the times of passing the WPs: t_i^f, $\tilde{t}_i^f$ and $\hat{t}_i^f$. Then, for the two prediction approaches, we calculate the prediction errors, $\tilde{\epsilon}_i^f$ and $\hat{\epsilon}_i^f$, at each WP.

Figure 3.15 shows the two prediction-error distributions obtained. The time scale in this diagram is truncated to 30 seconds in order to focus on the mean error values (the extreme left-hand side bar simply cumulates all the errors smaller than -30 seconds). Table 3.3 presents some statistics of the distributions of prediction-error absolute values. As it can be seen from this table and from Figure 3.15, the WN approach improves significantly the prediction of the time of passing the WPs. The average prediction error, from almost half a minute (an important value for RSS), is reduced to less than 5 seconds. These encouraging results of WN application obtained for this artificial flight model give the stimulus to apply the approach to real air traffic in NAT.

3.3.2 Results for real flight sets on OTS

On the next step of our research, we apply the WN approach to real air traffic data. Several data sets are tested. Since the results obtained with different flight sets are

Approach	MF	WN
Error, s	$\lvert\tilde{\epsilon}_i^f\rvert$	$\lvert\hat{\epsilon}_i^f\rvert$
Max	215.61	26.97
Mean	29,67	4.86
Variance	50.83	6.04

TABLE 3.3: MF and WN prediction error statistics for 77 consecutive flights on a single track

similar (that is due to our model of real and forecast winds), we are content here with presenting results on one instance. In the example below we consider the same date: December 10, 2013, and corresponding wind field and OTS models, as in the example from the previous section. The OTS is modeled as described in Section 2.2.1. Furthermore, we consider one of the flight sets described in Section 2.4.2: a set of 378 aircraft cruising from 38 airports in North America to 51 airports in Eurasia (mostly in Europe) for August 4th 2006.

We remind (from Section 2.4.3) that in order to reduce the congestion in the continental airspace, the desired entry track is assumed to be the track that is the closest to the departure airport, and similarly for the desired exit track (closest to the arrival airport). Moreover, for this study, the desired track entry time is first set to be the same as that defined in the FPL (Flight Plan), and then it is adjusted in order to fit into the valid time range of the OTS (starting from 0000 UTC). Finally, to simplify the simulations and the presentation, the flights are reorganized in order to avoid conflicts on links (when faster aircraft overcome slower ones), so that all remaining conflicts are conflicts on nodes. The exhaustive definition of conflicts on links and nodes, as well as the procedures to calculate the number of such conflicts, are given in Section 2.2.3. The flight reorganization mentioned can be performed by any conflict-resolution algorithm (Genetic Algorithm, Simulated Annealing) described in Section 2.3. It suffices to apply the chosen algorithm to an optimization problem (2.13), where the objective is the number of conflicts on links only, *i.e.* $C_{\mathcal{L}}(y)$.

The constructed flight set is evaluated using three different winds (real, forecast, adjusted) and the errors of time prediction of passing the WPs are compared. The adjusted wind is computed by several extrapolation approaches from neighbor preceding aircraft, that are compared in our study. Figure 3.16 displays the prediction error distributions for some of these approaches, *i.e.* when:

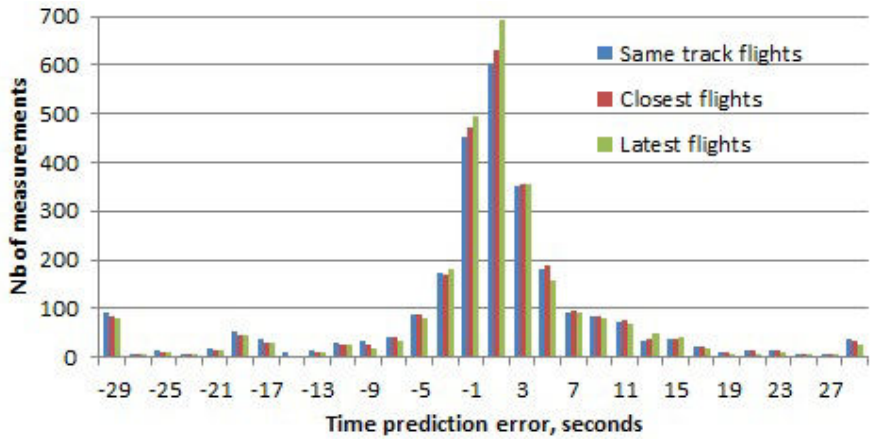

FIGURE 3.16: Comparison of extrapolation method distributions for wind adjustment using measurements from neighboring aircraft

Approach	MF	WN		
		same track	closest	latest
Mean	16.36	7.48	6.87	6.40
Variance	22.05	13.51	12.53	12.21

TABLE 3.4: Comparison of extrapolation method statistics for wind adjustment using measurements from neighboring aircraft (in seconds)

- only the measurements received from the latest aircraft on the *same link* are taken into account (as in the previous section) (blue in Figure 3.16);
- the wind values obtained from the *closest* (in terms of distance) aircraft on the neighbor links are linearly interpolated to adjust the wind at the current aircraft position (red in Figure 3.16);
- the wind values obtained from the *latest* (in terms of time) aircraft on the neighbor links are linearly interpolated (green in Figure 3.16).

The statistics of the distributions of the absolute values of the corresponding prediction errors are presented in Table 3.4. This latter table and Figure 3.16 first show that using the measurements from aircraft on neighbor links improves the results. We also observe that the more recent the measurements are, the smaller the prediction errors are, and the closer to the reality the results are. Thus, in the sequel of this Chapter, the WN approach will always refer to the method based on the measurements from the most recent (latest in time) neighbor aircraft.

Figure 3.17 presents the comparison of the distributions of the prediction errors using the MF approach (its statistics can be found in Table 3.4 as well) and using the WN

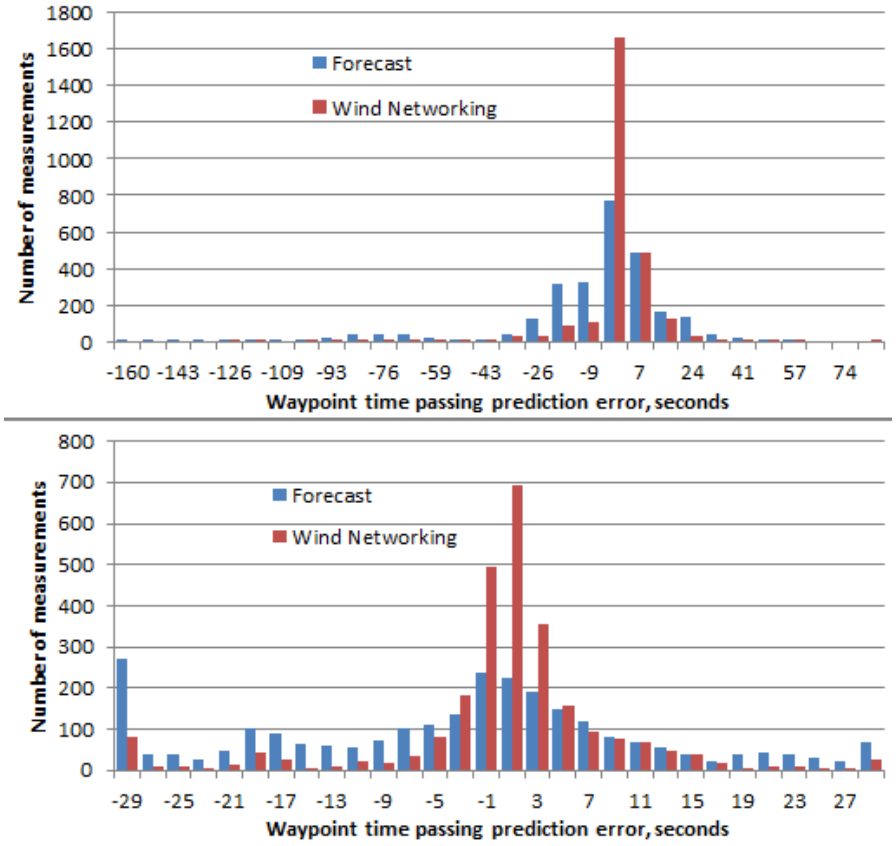

FIGURE 3.17: MF and WN prediction error distribution for 378 flights on the OTS on December 10, 2013

approach (based on the best extrapolation method, "latest flights"); the bottom diagram displays a truncated time scale in order to better demonstrate the distribution behavior near zero.

Comparison of the results from this section (Fig. 3.17) with the previous results (Fig. 3.15) shows that the WN approach seems to be less efficient in the case of several tracks and real aircraft sets: the prediction error, from less than 5 seconds for the one-track artificial flight set, grows up to 7 seconds in the real case. Here are some explanations of this phenomenon:

- the difference in the wind evaluation for different tracks (WN is more efficient if the wind does not change much with time);
- the time period between the consecutive flights (WN is more efficient if this period is short, which was the case for the artificial flight set, but not always the case for the real flight set);

Approach	MF	WN
Correctly predicted, nb.	460	462
False alarms, nb.	11	7
Critical errors, nb.	12	10
Total conflict duration error, min.	46.29	21.63

TABLE 3.5: Comparison of conflict prediction using MF and WN for 378 flights on the OTS on December 10, 2013

- the existence of preceding flights (for the artificial flight set, all flights followed one another; in the real case, some flights on some links may have no preceding flights; this obliges such flights to rely on MF instead of WN, and thus, the predictions are not improved at all).

On the next stage of our prediction method comparison, we concentrate on evaluating the error in conflict prediction. As mentioned above, in the considered model, conflicts can only happen on nodes. First, we perform the flight simulation based on the three wind functions and we record all the pairs of aircraft in conflict (violating longitudinal separation minimum) at each OTS node. This can be done using Algorithm 2.2 with slight modifications, permitting to register the aircraft in conflict. Then, we compare the real situation with each of the prediction methods to determine the number of conflicts that were correctly predicted, the number of false alarms, and the number of critical errors. The first three lines of Table 3.5 display these figures.

The last line of Table 3.5 contains the absolute value of the total conflict duration time error (the difference between the predicted conflict duration time and the real one, considering that if a conflict is not detected its duration is 0). Figure 3.18 represents the distributions of conflict duration errors for both prediction approaches. Again, the scale is truncated at 30 seconds in order to visualize better the distribution near its mean value.

Table 3.5 and Figure 3.18 reveal the improvement in conflict prediction when using the WN approach. Obviously, this improvement is directly related to the accuracy of the approach in time prediction. The results presented above for December 10, 2014 show the typical tendency of prediction improvement by WN, while the numerical quantities of such improvements may slightly differ. This difference mainly comes from the differences in real and forecast wind fields.

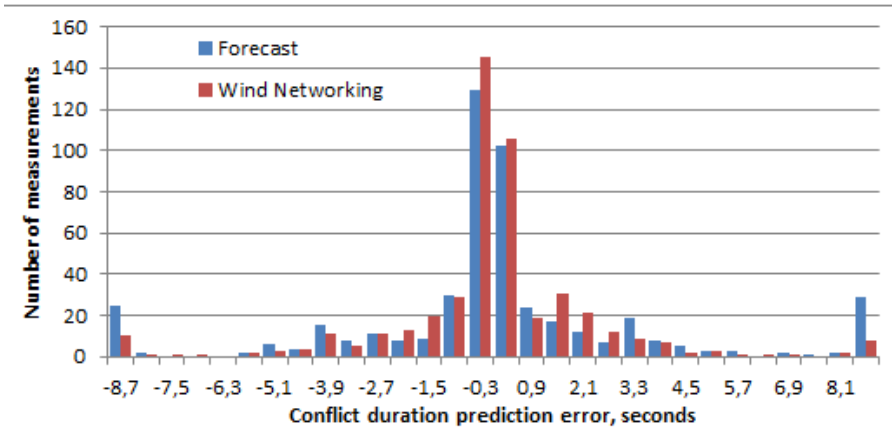

FIGURE 3.18: Distribution of the total conflict duration errors using MF and WN for 378 flights on the OTS on December 10, 2013

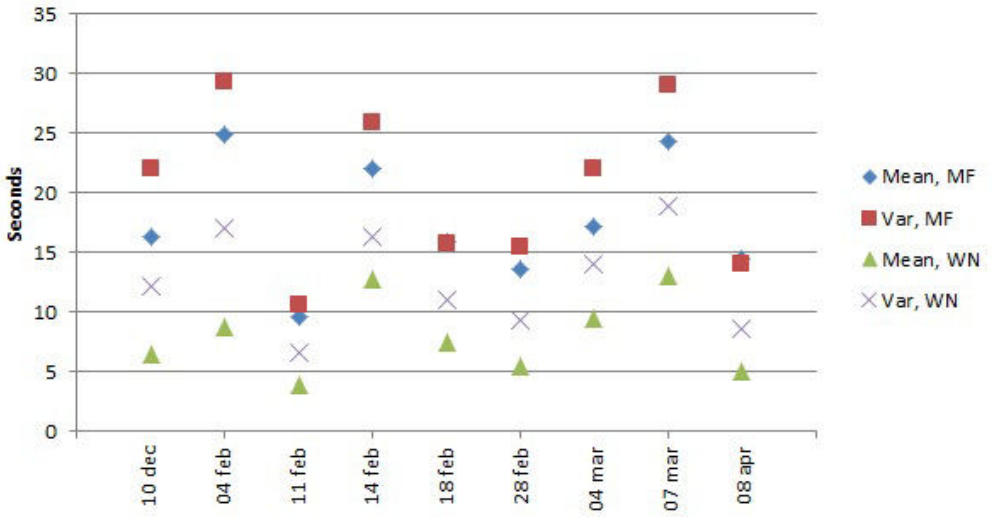

FIGURE 3.19: Statistics for time-prediction errors over 9 days

Figure 3.19 displays the statistical parameters (mean and variance) of the time-prediction error distributions for the two approaches (MF and WN) for several more days of oceanic traffic[24]. Figure 3.20 displays the number of errors (false alarms and critical errors) in conflict prediction for the same days. Both figures reveal the advantages coming from WN implementation, except for the number of false alarms on February 11, 2014, which is slightly larger for WN than for MF. This could be due to the fact that the forecast for this day is relatively accurate, and thus, the WN does not improve much this forecast, taking into account that the simulated wind measurements include slight perturbations.

It seems quite reasonable that the more aircraft there are the greater improvement

[24]Nine days from December 2013 to April 2014, as displayed in Figure 3.19

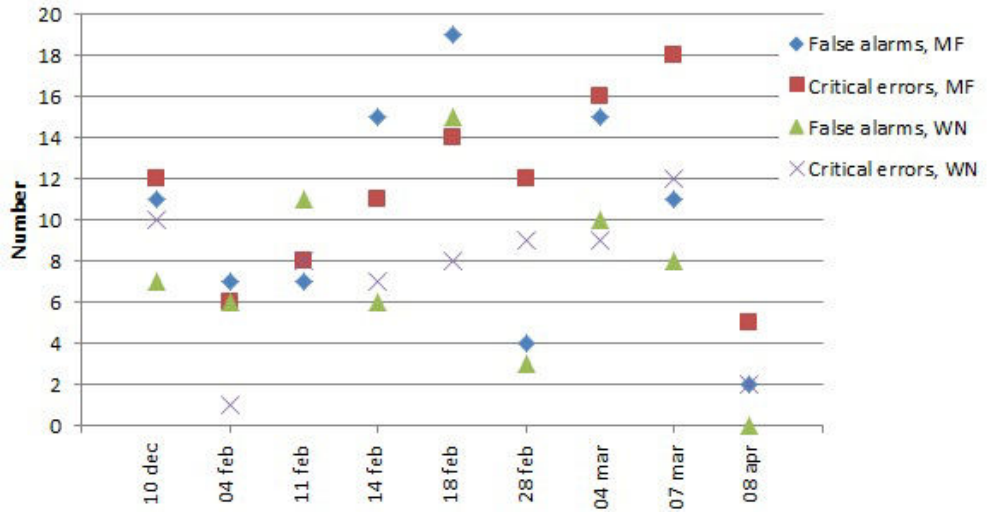

FIGURE 3.20: Number of errors in conflict prediction over 9 days

could be achieved using WN, as more aircraft would benefit from the measurements of preceding aircraft. This hypothesis becomes even more important if one recalls that the number of flights in the airspace is constantly increasing. This fact encourages performing the simulations for artificially increased flight sets.

3.3.3 Results for increased flight set on OTS

In this section, we present the results similar to those discussed in the previous section but for an increased flight set. In the example below we consider 1,000 flights cruising within OTS on December 10, 2013. As such a flight set is artificial, we choose the desired entry and exit track as well as the desired track entry time randomly. Further, these parameters are adjusted in order to eliminate the conflicts on links (similar to the discussion from the previous section). We perform the simulations in the same manner as described in the previous section, *i.e.* we compute:

- the prediction errors of time of passing the WPs for both approaches,
- the number of correctly and incorrectly predicted conflicts,
- and the errors in conflict duration prediction.

Figure 3.21 presents the distribution of time prediction errors (the time scale is truncated at 1 minute). The mean absolute value of MF error in this case is 22.35 seconds; and the mean absolute value of WN error is 5.83 seconds. One can again note the improvement

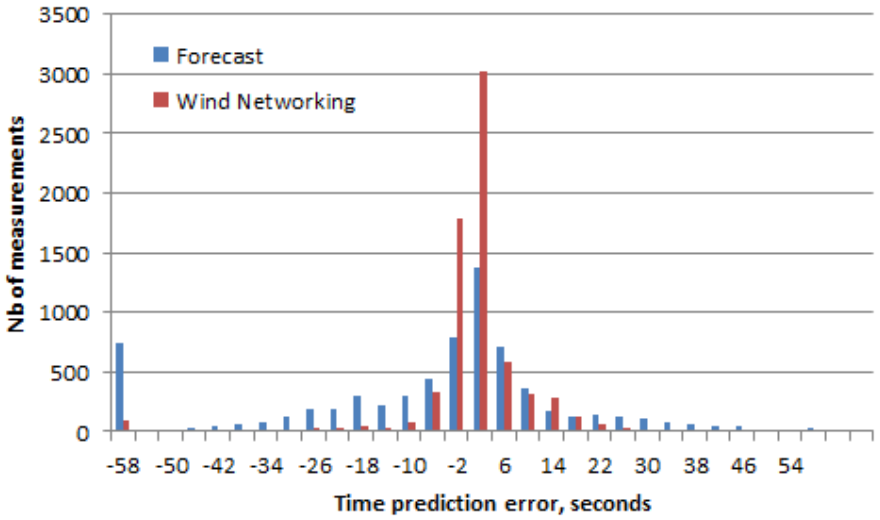

FIGURE 3.21: MF and WN prediction error distribution for 1,000 flights on the OTS

Approach	MF	WN
Correctly predicted, nb.	1175	1229
False alarms, nb.	48	13
Critical errors, nb.	70	16
Total conflict duration error, min.	242.7	63.4

TABLE 3.6: Comparison of conflict prediction using MF and WN for 1,000 flights on the OTS

in WP passing times predictions using the WN, which is even greater for this case of 1,000 flights in comparison to the real 378 flights.

Table 3.6 displays the number of correctly predicted conflicts, the number of false alarms and the number of critical errors, as well as the total absolute value of conflict duration prediction errors. What is remarkable is that in this case, the numbers of incorrect conflict predictions as well as the conflict duration errors on average are reduced by a factor near 4 when applying the WN.

When observing the conflict duration prediction errors distribution (see Figure 3.22) one can also easily note much greater improvement due to WN here in comparison to the real flight set (Fig. 3.18). This fact reveals the absolute benefits of WN approach especially for dense traffic conditions.

Similarly to the previous section, we present also some data on time-prediction error statistics (Fig. 3.23) and conflict-prediction errors (Fig. 3.24) for the 9 days for random flight sets with 1,000 flights. For all the studied days, the benefits obtained from implementing the WN exceed those obtained for the real flight set of 378 aircraft. Moreover,

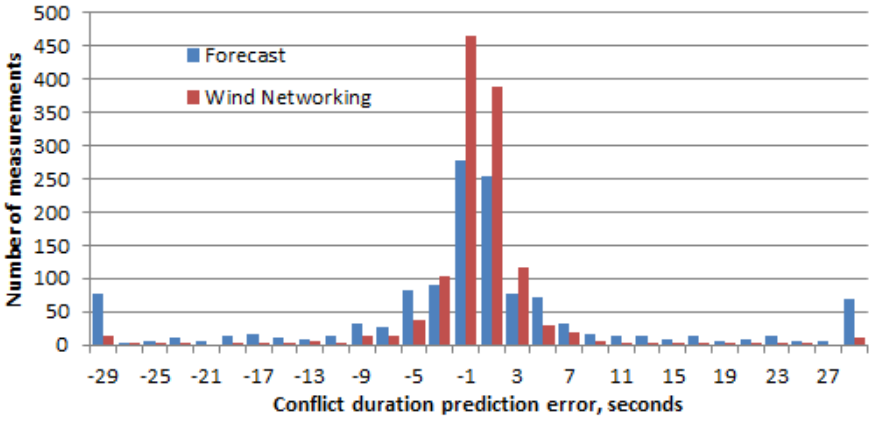

FIGURE 3.22: Distribution of the total conflict duration errors using MF and WN for 1,000 flights on the OTS

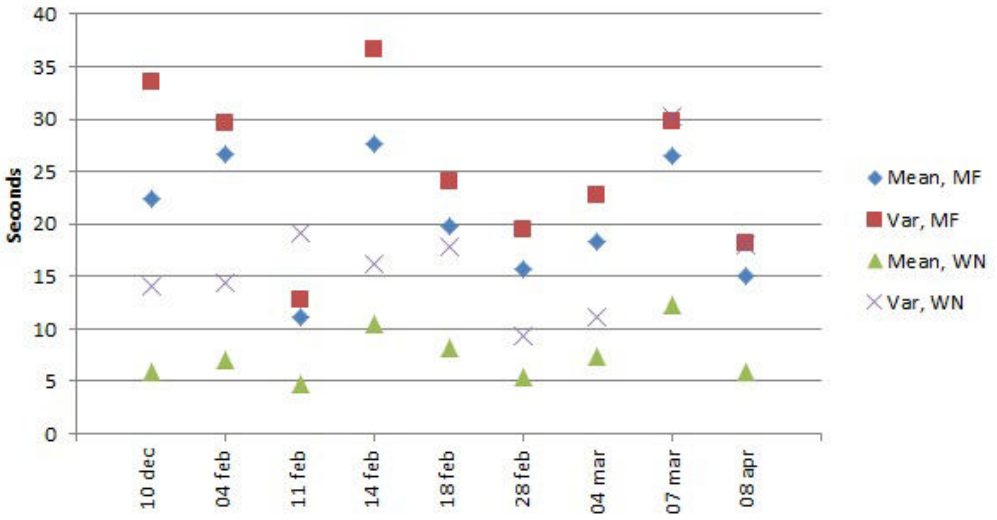

FIGURE 3.23: Statistics for time-prediction errors over 9 days for 1,000 flights

comparison of Figures 3.23 and 3.24 reveals an obvious correlation between the accuracy of time prediction and that of conflict prediction for both prediction methods.

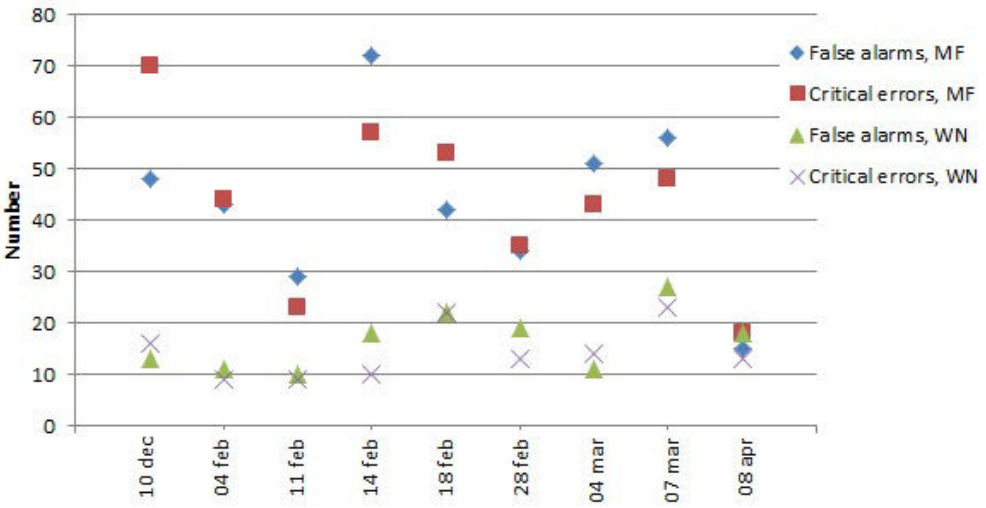

FIGURE 3.24: Number of errors in conflict prediction over 9 days for 1,000 flights

Chapter 4

Deconflicting wind-optimal aircraft trajectories

The last chapter of the presented work is devoted to the introduction of the *Free Flight Concept* (FFC) in the North Atlantic oceanic airspace (NAT). The FFC permits aircraft to follow Wind Optimal (WO) routes and to perform on-board separation, benefiting from Reduced Separation Standards (RSS).

The chapter is organized as follows. First, we present several works existing in the frame of FFC, including research on Aircraft Trajectory (AT) optimization taking into account meteorological conditions, in particular, the winds; and research on conflict resolution in a free-flight environment. Then, we specifies the track of our particular research interest, aimed at minimizing the number of potential conflicts induced by WO ATs. We propose a mathematical model of this problem, and we specifies the optimization algorithm implemented for AT-deconflicting. We conclude the chapter with the results of conflict resolution of real NAT traffic for one month.

4.1 Problem statement and literature review

In this section, the research works related to *Free Flight Concept* (FFC) are discussed. First, we highlight several studies aimed at validating the free-flight operations from the point of view of Air Traffic Control (ATC) and providing the support to such operations. After that, we present independently the studies that address the two main tasks involved

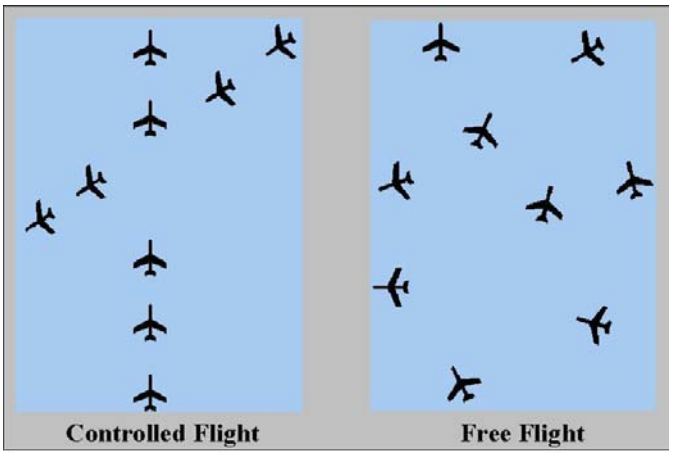

FIGURE 4.1: Controlled flights vs. free flights [1]

in the FFC, *i.e.* generating optimal ATs to be free-flown by aircraft, and deconflicting such ATs. Finally, we discuss how these two tasks can be resolved simultaneously.

4.1.1 Free Flight Concept Support

An advanced FFC in Air Traffic Management (ATM) is a decentralized control system that permits aircraft to fly user-preferred routes by removing most of airspace restrictions (such as sector workloads and predefined airways, see Figure 4.1) and delegating partly the collision-avoidance responsibility from ATC controllers to Air Navigation System (ANS) users (pilots). It is claimed in [86] that FFC will improve the ANS users flexibility thanks to:

- collaborative decision making (sharing information and responsibilities between controllers and pilots);
- flexible scheduling (flight planning based on user-preferred departure/arrival times);
- flexible routing (flight planning based on user-preferred optimal ATs).

It would be fair to mention that despite the evident advantages in the flight flexibility, on one hand, the FFC leads to the increase of workload of ANS users, on the other hand. Investigation of human factors in the ATC system and of their impact on the complexity of multi-aircraft conflict resolution is therefore an important subject in FFC validation.

[1] From http://freeflight.nlr.nl/idxconc.htm

For example, in [87], Lupu *et al.* address the influence of varied optimization strategies (heading- and speed-change maneuvers) of individual aircraft on the global performance of decentralized control within two intersecting flows. The authors conclude that added maneuvering freedom may generate larger aircraft deviations, especially in high aircraft density. However, research works that address this field of study are rare.

In contrast, many studies are devoted to the investigation of ATC efficiency. In the frame of FFC, the efficiency of ATC is also supposed to be improved, thanks to the following enhancements:

- collaborative decision making (reducing the controller workload associated with tactical requests);
- shifting the ATC focus from tactical situation reactions to strategic planning;
- improving the supporting capabilities.

FFC is developed in the frame of the new generation ATM (see Section 1.1.4). Thus, innovative technologies are supposed to be used in order to support the FFC, such as CPDLC (Controller-Pilot Data Link Communications, see Appendix B) that reduce the number of voice interactions, or ADS-B (Automatic Dependent Surveillance-Broadcast, see Appendix L). In addition to this, new support tools and automated systems relying on enhanced numerical algorithms are being developed in order to provide the basis for conflict resolution in a decentralized FFC. In [86], several experiments involving different FFC facilities are described, with the objective to evaluate the impact of these facilities on the ATC efficiency.

For example, one such facility is the User Request Evaluation Tool (URET), that intends to provide the en-route sector radar controller with automatic problem (conflict) detection and trial planning capabilities [88]. It uses the filed Flight Plans (FPLs), key aircraft performance data and meteorological information to build 4-dimensional ATs, and adapts these ATs to the observed aircraft behavior. Further, these ATs are used to detect potential conflicts up to 20 minutes in the future.

The set of incremental enhancements to URET is termed Problem Analyses, Resolution and Ranking (PARR) [88]. It focuses primarily on the development of strategic resolutions for aircraft-to-aircraft and aircraft-to-airspace problems. In addition to the URET

functionality, PARR also provides the controllers with a set of candidate problem resolution advisories, based on speed-, altitude-, latitude- or longitude-maneuvers. Kirk *et al.* claim that PARR will provide safe, orderly, expeditious air traffic flow and increased controller productivity.

Another system for analysis of FFC is described in [89] and referred to as Air Traffic Operations and Management Simulator (ATOMS). It models en-route airspace over contiguous regions, taking into account flight schedules, aircraft performance, airspace structure and meteorological forecast. Three different *Conflict Detection and Resolution* (CDR) strategies are implemented and tested in ATOMS. As a result, ATOMS provides a high flexibility in rapid prototyping of advanced ATM concepts.

There exist large number of other ATM systems and system simulators, that we will not discuss in detail in this study. Note, that most of such systems are aimed to deal with *tactical* conflict resolution. An exhaustive summary of existing works, papers and research projects related to the FFC concept can be found in [90]. In the following sections, we discuss several such approaches and algorithms, that we roughly divide into three categories:

- algorithms aimed at generating optimal (often, wind-optimal) trajectories (Section 4.1.2);
- algorithms aimed at eliminating conflicts in a given set of trajectories (Section 4.1.3);
- algorithms performing the two above-mentioned tasks simultaneously (Section 4.1.4).

4.1.2 Generating optimal aircraft trajectories

Generating optimal ATs may be performed under different criteria of optimality, among which:

- minimizing the total cruising time;
- minimizing the fuel consumption;
- minimizing aircraft emissions;

- minimizing various climate impacts.

In most cases, the AT optimization problem involves not only a particular aircraft performance characteristics, but also environmental (meteorological) conditions (winds, temperature, etc.). A full assessment of the feasible climate-optimal route planning is a complex task [91], that demands in first turn, to choose the climate metrics to adopt. Thus, one of the first necessary steps in the process of climate-optimal AT evaluation is determining the particular weather characteristics.

A comprehensive study analyzing the weather patterns in NAT, the region of our interest, is presented in [91]. The authors analyze the climate impact from flights over NAT in terms of CO_2 and O_3 emissions, water vapors and contrails for several days under different meteorological conditions (in summer and winter). Since they conclude that this impact is greater for long flights, generating climate-optimal ATs is particularly important for NAT.

In [92], Sridhar *et al.* present a practical optimization method to generate WO 2D-ATs (in the horizontal section, on a spherical surface) for NAT flights. Here we describe this method in more detail, as we will use the results of its application further in our simulations. WO ATs are generated by applying Pontryagin's Minimum Principle [93]. A 2D-AT is optimized by determining the heading angle that minimizes travel time in the presence of winds, using the aircraft equations of motion at a constant altitude above the Earth surface approximated with a sphere, subject to the conditions that stipulate that thrust equals drag and flight path angle is zero:

$$\dot{\lambda} = \frac{V\cos\psi + u(\lambda,\phi,a)}{R\cos\phi}, \tag{4.1}$$

$$\dot{\phi} = \frac{V\sin\psi + v(\lambda,\phi,a)}{R}, \tag{4.2}$$

where λ and ϕ are the longitude and latitude at a point on the spherical Earth respectively, ψ is the aircraft heading angle at this point, V is aircraft True Air Speed (TAS), u and v are west-east south-north wind speed components respectively at point (λ, ϕ) at altitude a, and R is the mean Earth radius. To simplify the model, the aircraft altitude above the Earth surface is neglected by supposing $a << R$. The function of aircraft

heading dynamics in response to wind, $F_{wind}(\psi, \lambda, \phi, u, v, V)$, is defined and integrated into the wind-optimal dynamical equation:

$$\dot{\psi} = \frac{-F_{wind}(\psi, \lambda, \phi, u, v, V)}{R \cos \phi}, \tag{4.3}$$

Derivating of equation (4.3) reduces AT optimization problem to an initial-value problem that can be determined using collocation methods or interpolation techniques. The described optimization method is applied independently for each AT over NAT. As a result, a set of individually time-optimal ATs is produced. Note that a time-optimal AT for an aircraft cruising at a constant altitude is fuel-optimal as well. In the remaining of the paper [92], the authors compare the generated trajectory with baseline trajectories (filed in FPLs) and estimate encountered time savings, that turn to be remarkable.

The described AT optimization method was first proposed by Jardin *et al.* in [94], where its mathematical justification is given. It is further developed by Ng *et al.* in [95]. The extended model, in addition to winds, also takes into account the impact on the climate produced by cruising aircraft, including emissions in terms of Global Warming Potential (GWP), and persistent contrail formations related to critical relative humidity. The cost of GWP is formulated explicitly as a function of aircraft parameters, while the cost related to contrails is accounted by penalizing the contrail-favorable regions. The result of the optimization is therefore a set of climate-optimal trajectories. The proposed method is applied in [95] to optimize the Cross-Polar ATs.

The same approach is used in [96] to optimize ATs between Chicago (O'Hare International Airport) and Washington (Dulles International Airport). The paper presents more mathematical formulas and results of Pontryagin's Minimum Principle application.

In [97], the AT optimization method from [92, 95, 96] is extended to 3D. Ng *et al.* develop an aircraft vertical profile based on the fuel consumption model from BADA[2]. Optimal cruise altitudes depend on atmospheric parameters, aircraft-dependent aerodynamic drag coefficients, aircraft mass and airspeed. In [97], the optimization is performed in the wind field only. The proposed method is applied to commercial cargo flight operation at Anchorage (Alaska).

[2]Eurocontrol Base of Aircraft Data

Finally, the study [98] combines the optimization approaches from [95] (minimization of climate impact) and [97] (3D-optimization), and relies on dynamic programming to produce climate-optimal 3D-ATs for NAT flights.

Dynamic programming is also applied in an earlier study [99] for generating WO ATs for Central East Pacific flights. These ATs are iteratively calculated on a grid composed of latitude/longitude values that is primarily constructed for each pair of involved airports via a multi-stage process. The major contribution of this study with respect to the previously presented ones is that it does not demand solving an optimization problem.

A specific grid that predefines the variability of possible solutions for the AT optimization problem is also used in [100]. Andresson uses the method described in [95] to construct such a grid, and applies Dijkstra's algorithm to find a minimal-time path through the grid. The optimization is performed for flights in Reykjavik Oceanic Control Area (OCA), which experience strong NAT Jet Streams (JSs).

In [101], Wickramasinghe *et al.* also develop an approach based on a grid scheme and dynamic programming. The authors propose to use the 3D translation motion model and to minimize fuel consumption expressed in terms of performance index, via step-by-step progress within the grid of possible transitions. The method is then applied to flights between Haneda (Tokyo International Airport) and Fukuoka (Fukuoka Airport, Japan).

Finally, Girardet *et al.* propose in [102] a new model for the AT planning problem in the presence of winds. The model is based on the resolution of the Hamilton-Jacobi equation that defines the correspondence between the optimal-trajectory problem and wave propagation. The Ordered Upwind algorithm is implemented for step-by-step generation of wave fronts in the discretized 2D space. An optimal AT then follows such minimal-time fronts. The zones that an aircraft is supposed to avoid (*e.g.,* severe meteorological conditions, or highly congested areas) are modeled by penalizing aircraft passing through such zones. This penalization is simply implemented by decreasing the speed of the propagation.

All the discussed works reveal evident benefits in time- and fuel-savings when flying WO routes (and in case of climate-optimal ATs, also the benefits in decreasing the aircraft

impact on the climate) in comparison to nominal (currently used) routes. Some more related works are presented below in Section 4.1.4).

4.1.3 Deconflicting aircraft trajectories

The problem of trajectory (or route) *deconflicting*, that consists in searching for a conflict-free trajectory configuration for a set of moving objects with given dynamical characteristics, takes its origins in robotics [103]. When applied to conflict resolution for a set of aircraft, the problem becomes more complicated, because of operational restrictions imposed on possible variations of aircraft speeds (aircraft do not stop) and AT shape smoothness (aircraft do not turn abruptly). In [103] such a general problem is shown to be NP-hard. A large amount of works are devoted to developing AT CDR methods. An exhaustive overview of early studies can be found in [104]. Below, we present a brief summary of several (more recent) studies.

In [105], the problem of conflict resolution within two intersecting flight flows is considered in the frame of FFC, *i.e.* under decentralized conflict-avoidance rules. The aircraft flying at a constant speed are organized into two flows at a constant altitude, and two types of maneuvers can be applied to avoid conflicts: heading change and lateral position change (offset). The paper presents a theoretical proof of existence of such bounded maneuvers for conflict resolution for two intersecting flows.

In [106], also performed in the frame of FCC, a *cooperative* approach is developed, *i.e.* when all aircraft involved in a conflict collaborate to its resolution. Here again, a 2-dimensional problem for a set of aircraft flying with a constant speed at a constant Flight Level (FL) is considered, and two independent strategies of conflict avoidance are investigated separately: speed change and heading change. For both cases, the problem is formulated as a Mixed-Integer Programming (MIP) problem and resolved for several test flight configurations by a classical MIP solver (CPLEX). The authors note that when considering both heading and speed changes, the problem in the proposed formulation becomes non-linear.

In [107], Peng *et al.* study the practical implementation of such collision-avoidance strategy based on speed- and heading-changing maneuvers in the aircraft on-board Traffic

Alert and Collision-Avoidance System (TCAS). They do not perform simultaneous conflict resolution for a set of multiple aircraft, but for each pair of aircraft involved in a conflict, independently. In [108], Christodoulou *et al.* extend the method from [106] to the 3D case. The authors allow the speed-changing maneuvers only, and formulate the problem as non-linear MIP. The approach is verified on several test cases. In [109], Bicchi *et al.* formulate a problem similar to that presented in [106], as an optimal control problem. The important contribution of the paper is the decentralized cooperative implementation of the method.

In [110] a different approach is proposed. Dougui *et al.* introduce and implement the light-ray propagation method while avoiding obstacles, inspired from geometric optics and based on Fermat's principle of least action, to model a flight progress between two airports. The surrounding traffic is modeled as dynamic obstacles to be avoided by a given flight. The method is applied to 2D ATs that are successively constructed from discretized light-propagation fronts using a Branch & Bound algorithm. The method is devoted to tactical AT planning, *i.e.* to conflict resolution within 20-minute time windows. The advantage of this approach is that it relies on a deterministic optimization method. However, the quality of the resulting solution depends on the order in which the flights are considered.

Another approach, based on a stochastic method of optimization, is described in [111]. Here, a B-Spline is used to model a 2D AT between two airports in a horizontal section (nominally considered to be a straight line), whose shape is defined by specifying two control points. The control point positions for a set of ATs are stochastically varied by Genetic Algorithm (GA) in order to obtain conflict-free AT configurations. The resulting solution does not depend on any flight order consideration, but the algorithm convergence to a conflict-free solution is not guaranteed.

Another stochastic method of optimization, Simulated Annealing (SA), is applied in [112] to resolve conflicts on the strategic level and at a continental scale (for full European traffic, involving up to 39,000 flights). An initial AT between two airports is considered to be a straight line in horizontal section, and to satisfy the optimal flight altitude profile in the vertical dimension. Chaimatanan *et al.* propose to vary the aircraft departure times and 2D AT shapes in order to avoid potential conflicts. The 2D AT offset maneuver is defined by specification of two control points that are stochastically generated by SA.

The conflicts are detected in 3D space. In addition to this, the uncertainty in the time at which an aircraft is expected to arrive at a given point of its AT, is taken into account. In our work, we will use this approach as a basis and adapt it to our particular case of NAT traffic. Thus, it will be explained in more detail in Section 4.3.

All the algorithms presented above resolve the problem of free-flight progress while avoiding conflicts, not taking into account the winds. Once accounting for winds, the problem becomes more complicated, as an AT deformed in order to avoid conflicts, might strongly loose in terms of wind-optimality. Thus, it is sometimes more efficient to join the tasks of wind- (climate-) optimal AT construction and the task of deconflicting. Such methods are presented in the next section.

4.1.4 Generating and deconflicting of wind-optimal trajectories

Below we present several works that apply different conflict resolution strategies to wind-optimal ATs and that take into account the winds in the simulations.

In [113], Jardin proposes an approximate solution approach to generate conflict-free WO ATs in real time. The approach consists of iteratively computing a WO AT for each aircraft, using the aircraft dynamic motion model from [94], while holding previously-planned trajectories fixed. Each new AT is iteratively modified in order to avoid all the conflicts encountered with ATs computed in the previous steps. In this study, only the heading change maneuvers are considered. Conflict detection is performed based on so-called *Conflict Grid*, defining an airspace discretization, where each cell can be occupied by only one aircraft. A WO AT is stochastically perturbed until it passes through empty cells only. The main advantage of the method is that it produces a conflict-free solution in real time (computations are very fast). On the other hand, the result depends on the order in which the flights are treated, and the algorithm is likely to yield sub-optimal solutions.

A related conflict-detection approach, also based on the Conflict Grid, is described in [114]. Here, a Conflict-Grid cell to be occupied by not more than one aircraft at any time is represented as a machine intended to process not more than one operation at any time. An AT is then represented as a job, consisting of a sequence of single operations, and the problem of conflict resolution is formulated as a job-shop problem. The approach

is applied to deconflicting WO ATs for Central East Pacific flights that are generated using the method from [99]. The only optimization variables considered in this study are the flight departure times. Thus, the AT-optimization problem is reduced to a flight scheduling problem, which is further formulated with a Binary Integer Programming model. Numerical solving of such a problem yields a set of conflict-free 4D-ATs. The advantage of the method is that the resulting ATs remain wind-optimal as their shape is not changed (in the case of static wind fields, as it is supposed in all the studies described above). On the other hand, the resulting solution may account for very large flight delays, a severe disadvantage from the operational point of view. More detail on this study can be found in [115].

In [116], the work from [102] is extended from one AT to the case of multiple trajectories, and an SA algorithm is applied to reduce the airspace congestion induced by the generated WO trajectories. The congestion here is related to the density of aircraft present in a given area. Such highly-congested areas are to be avoided by aircraft. Thus, another set of ATs, avoiding the previously-defined congested areas, is generated in addition to WO ATs. On each iteration of the implemented SA, an AT encountering high congestion is perturbed and a new AT is generated as a compromise between the WO AT and a congestion-avoiding AT. Then, this new AT is reevaluated. The described approach is applied to the European traffic for a 2-hour time period. The advantage of the method is that it produces a globally optimal solution that does not depend on the flight order. Moreover, with this approach ATs inducing more congestion are more likely to be modified. The drawback is its prohibitive computational time.

In the next section, we specifies the conflict-resolution method for wind-optimal trajectories, implemented in the current study.

4.1.5 Perspectives of wind-optimal trajectory deconflicting examined in the present thesis framework

The research track that we present in the current chapter, is situated in the context of CDR strategies for FFC. Its objectives are similar to the systems mentioned above (Section 4.1.1):

- to simulate the flight progress under the FFC,

- to detect potential conflicts,
- and to propose alternative ATs to avoid these conflicts.

This study differs from the study presented in Chapter 2, having the same objectives, as we do not assume any fixed route structure (such as Organized Track System, OTS) that can be exploited during conflict resolution. In this research, we combine several existing approaches:

- the method from [92], for obtaining WO ATs,
- the method from [112], for deconflicting a given set of ATs.

We bring several important modifications to the algorithm proposed in [112], in order to adapt it to model the traffic in NAT. The advantages of the proposed approach, originating from [112], are that:

- ATs are treated in a *full-day scale* on a *strategic level*,
- it attempts at optimizing *globally* (relying on a stochastic method, SA).

The advantages of our algorithm, related to the proposed modifications are, that:

- we treat ATs on a *spherical Earth surface*; thus, the method is applicable to *long-distance flights* (and in particular, to NAT flights);
- we recalculate the new ATs taking into account *wind fields* while deconflicting;
- we *accelerate the computations*, which are particular long for the NAT region, because of large separation norms resulting in a large number of conflicts.

The next section explains the particular features of our mathematical model in detail.

4.2 Mathematical model of the free flight concept

In this section, we present a mathematical model that is used to formulate our optimization problem, aimed at searching a conflict-free configuration of flights for a set of

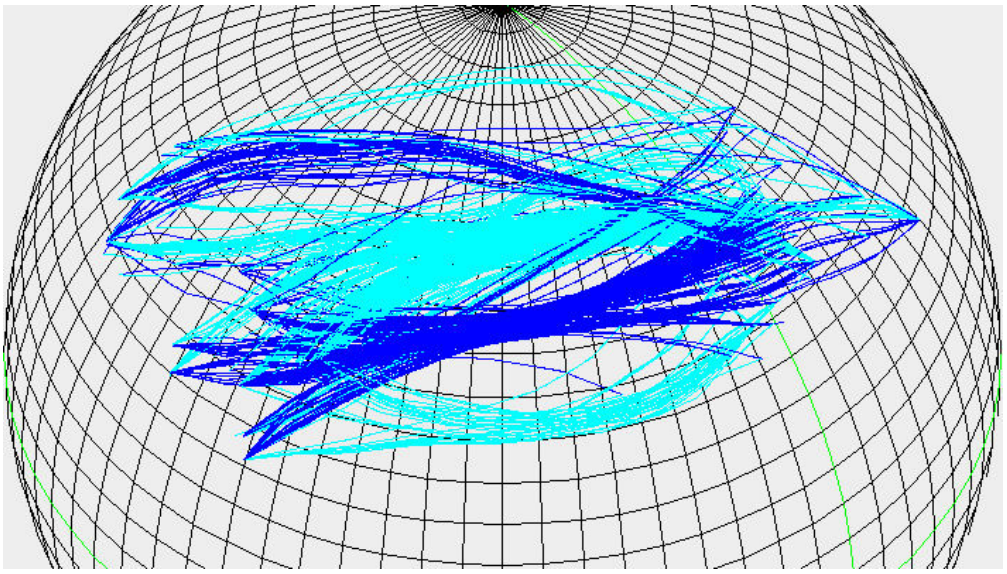

FIGURE 4.2: Wind optimal aircraft trajectories on July 1st, 2012

wind-optimal ATs in NAT. First we describe how we model NAT flights and the wind-optimal trajectories. Next, we introduce the AT-modification maneuvers that we accept in our simulations, and we define the procedure to recalculate an AT in the wind field, based on these maneuvers. After that, we explain the procedure of conflict detection. Finally, we propose a mathematical formulation of our optimization problem based on the introduced features.

4.2.1 Wind-optimal aircraft trajectory model

In the computational experiments performed in the frame of the present study, we use the data on 2D WO trajectories generated using the optimization approach from [92], that was provided to us by the research team from NASA Ames Research Center (Mountain View, CA, USA). This data is available for 31 days in July 2012. Figure 4.2 displays a set of such WO ATs for July 1st. The eastbound trajectories are shown with blue, while westbound trajectories are shown with cyan.

Each given AT corresponds to a flight performed with a constant TAS and at a constant FL, and in horizontal section, it is constructed so as to be optimal in terms of cruising time. As stated in [92], such an AT is also optimal in terms of fuel consumption. Although a theoretical optimal AT is a continuous 2D-curve on a sphere, the numerical optimization algorithm used for WO AT computation produces a discrete approximation

of a curve. Thus, each AT is represented as a sequence of 2D-geographical points at a fixed altitude, together with times at which the concerned aircraft passes these points.

We consider N flights, and for each flight f ($f = 1, ..., N$) we denote its WO AT as $\bar{\tau}^f$. We use the upper bar in the notations in order to distinguish the initial WO AT from the modified ATs that will be generated as the deconflicting algorithm runs. A modified AT for aircraft f will further be referred to as τ^f, and its construction is defined in the next section. An initial WO AT, $\bar{\tau}^f$, is characterized by the following **initial input parameters**:

- FL^f - aircraft FL;
- v^f - aircraft TAS;
- $\bar{q}_i^f(\bar{\lambda}_i^f, \bar{\phi}_i^f)$, $i = 1, ..., M^f$ - a sequence of 2D points of the AT, where:
- M^f is the number of points encountered by the AT of flight f,
- $\bar{\lambda}_i^f$ is the point longitude on the spherical Earth, and
- $\bar{\phi}_i^f$ is the point latitude;
- $\bar{t}_i^f$, $i = 1, ..., M^f$ - the times at which aircraft f passes points $\bar{q}_i^f$ ($i = 1, ..., M^f$).

The points $\bar{q}_i^f$ ($i = 1, ..., M^f$, $f = 1, ..., N$) in the provided data are stored with a time step of 1 minute ($\bar{t}_i^f - \bar{t}_{i-1}^f = 1$ min), and are recorded from aircraft departure airport to arrival airport. As our research interest concerns the particular NAT region, we choose, at this stage of our study, to extract for each AT, only its segment situated within NAT. To simplify the model, we replace the real NAT-region borders (defined in Section 1.2.1) with rectangular borders in geographical coordinates. Thus, in the following of this section, when speaking of an initial AT, $\bar{\tau}^f$, of aircraft f, we suppose that its 2D points $\bar{q}_i^f$, $i = i_{start}^f, ..., i_{end}^f$ ($i_{start}^f \geq 1$, $i_{end}^f \leq M^f$) lie between -70°W and 0°W degrees of longitude in Northern Hemisphere. To simplify the notations, in the sequel of this section, we assume that $i_{start}^f = 1$ and $i_{end}^f = M^f$. Figure 4.3 displays in color such reduced ATs, and in black their omitted parts.

Note that, when it is convenient, this sequence of 2D points at constant altitude with recorded times can be also viewed as a sequence of 4D points. We introduce the following corresponding notations:

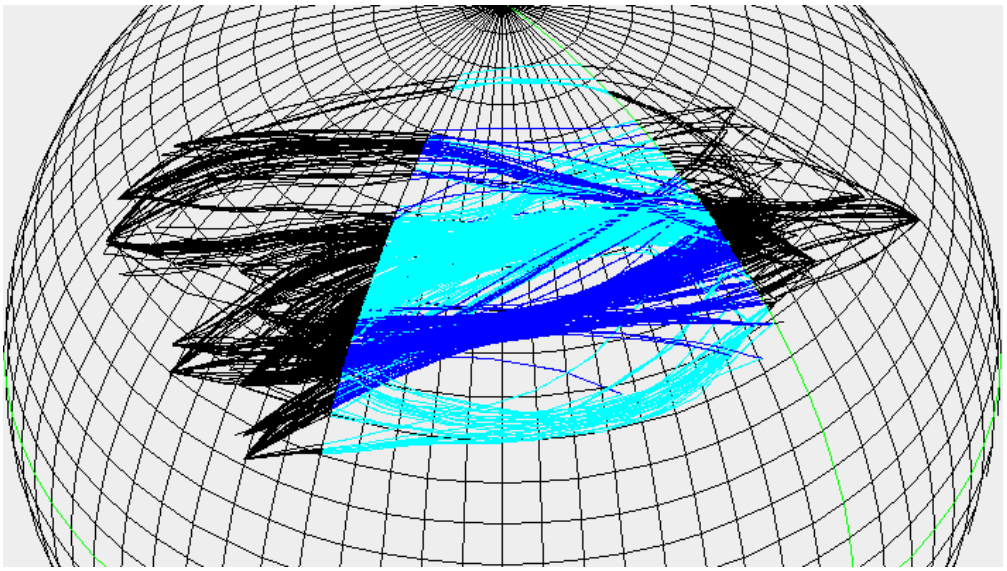

FIGURE 4.3: Wind optimal aircraft trajectories on July 1st, 2012, reduced to NAT region

- $\bar{Q}_i^f(\bar{q}_i^f, FL^f, \bar{t}_i^f)$, $i = 1, ..., M^f$ - a sequence of 4D points of the AT.

To summarize, in this section, we have introduced two equivalent ways to define an initial WO AT of aircraft f:

- $\bar{\tau}^f(v^f, FL^f, \{\bar{q}_i^f\}_{i=1}^{M^f}, \{\bar{t}_i^f\}_{i=1}^{M^f})$; and
- $\bar{\tau}^f(v^f, \{\bar{Q}_i^f\}_{i=1}^{M^f})$.

In the next section, we discuss how we propose to modify any given WO ATs in order to avoid potential conflicts.

4.2.2 Aircraft trajectory modification model

In this study, we choose to modify two parameters of an AT:

- the departure time, and
- the geometrical shape (operationally performed by modifying the aircraft heading at each AT point).

The procedure of departure time modification is very simple: it suffices to delay an aircraft f at each point $\bar{q}_i^f$ of its trajectory by a fixed time delay, d^f. More precisely, we obtain an AT $\tau_{d^f}^f$ from an AT $\bar{\tau}^f$ as follows:

$$\bar{\tau}^f(FL^f, v^f, \{\bar{q}_i^f\}_{i=1}^{M^f}, \{\bar{t}_i^f\}_{i=1}^{M^f}) \xrightarrow{d^f} \tau_{d^f}^f(FL^f, v^f, \{\bar{q}_i^f\}_{i=1}^{M^f}, \{\bar{t}_i^f + d^f\}_{i=1}^{M^f}). \tag{4.4}$$

For our simulations, we only allow departure time modification among a finite number of discrete time delays, d^f, using a time step equal to 1 minute, *i.e.* $d^f \in \{0, 1, 2, ..., N_d\}$ (in minutes).

The procedure of AT-shape modification is less obvious. It consists of two steps:

- modification of the given AT geometrical shape, *i.e.* changing the geographical position of points $\bar{q}_i^f \to q_i^f$, for $i = 1, ..., M^f$;
- recalculation of the times at which aircraft f passes these new points q_i^f, *i.e.* $\bar{t}_i^f \to t_i^f$, for $i = 1, ..., M^f$.

To modify the geometrical shape of an AT, we exploit a bijective transformation between an arbitrary curve on a sphere and a curve on the xy-plane. More precisely, we proceed by the following steps.

- First, we construct a bijection between the given initial WO AT on a spherical Earth (to simplify the notations, we will omit the index of the flight f here) and a straight segment $[0, 1]$ on the x-axis of the xy-plane, *i.e.* $\bar{q}_i \leftrightarrow x_i$ $(i = 1, ..., M^f)$ as follows:

$$x_i = \frac{length(\bar{q}_1, \bar{q}_i)}{L}, \tag{4.5}$$

  where $length(\bar{q}_1, \bar{q}_i)$ is the length of the AT segment from the initial AT point, $\bar{q}_1$, to the current point, $\bar{q}_i$, and L is the total AT length: $L = length(\bar{q}_1, \bar{q}_M)$. The length of an AT segment is computed by summing up the distances between all the trajectory points $\bar{q}_j$ encountered by this segment:

$$length(\bar{q}_1, \bar{q}_i) = \sum_{j=1}^{i-1} dist(\bar{q}_j, \bar{q}_{j+1}), \tag{4.6}$$

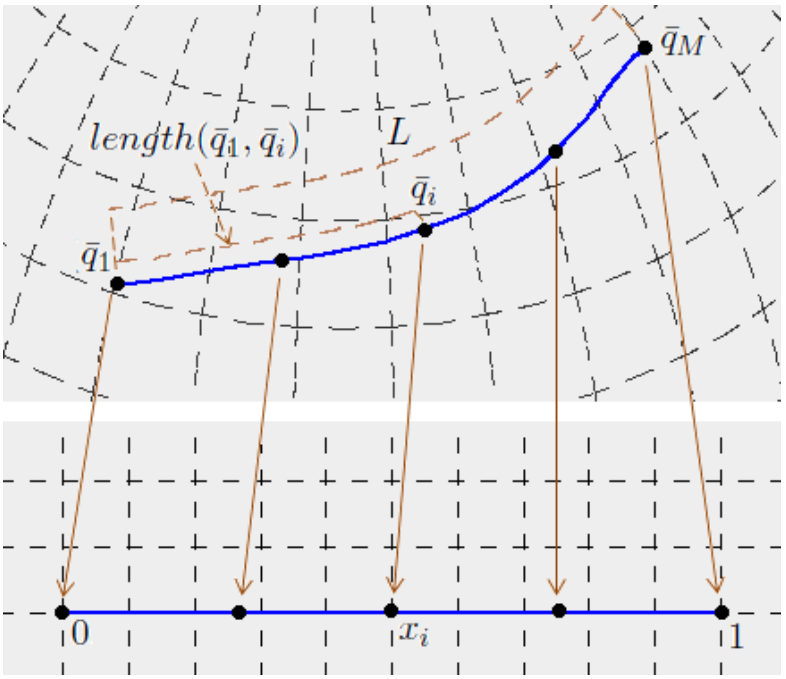

FIGURE 4.4: Topological transformation of a trajectory on a sphere to a straight segment on a plane

where $dist(\bar{q}_j, \bar{q}_{j+1})$ is the distance between consecutive geographical points $\bar{q}_j$ and $\bar{q}_{j+1}$ along the arc of the Great Circle (GC). This operation is shown in Figure 4.4.

- Then, we modify the straight-line segment, joining (0,0) and (1,0), in xy-plane by

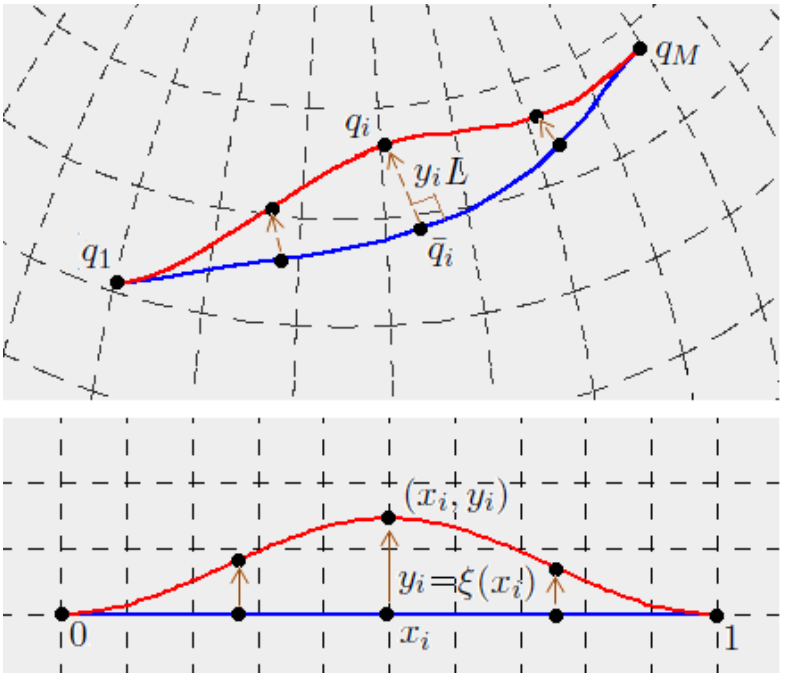

FIGURE 4.5: Smooth modification of a trajectory on a sphere corresponding to the segment-modification

using some given smooth curve defined by a function $y = \xi(x)$. More precisely, this modification maps each straight-line segment point, $(x_i, 0)$ on the point $(x_i, \xi(x_i))$: $(x_i, 0) \rightarrow (x_i, y_i) = (x_i, \xi(x_i))$ $(i = 1, ..., M^f)$ (see Figure 4.5, bottom).

- Finally, we apply again the bijection to construct the new AT on a sphere from the modified smooth curve on a plane (see Figure 4.5, top), $(x_i, y_i) \leftrightarrow q_i$ $(i = 1, ..., M^f)$, so that the i-th point q_i lies on the GCs perpendicular to the initial AT at the point $\bar{q}_i$, and such that :

$$dist(\bar{q}_i, q_i) = y_i \cdot L. \tag{4.7}$$

Roughly speaking, the value of function ξ stipulates by how far a point of the AT is to be displaced to the left-hand side of the AT (to the rough-hand side when ξ takes negative value).

The actual formulas used to compute the distances between geographical points, the perpendicular GCs, and other operations on a sphere, are detailed in Appendix Y. Once the choice of the function $\xi(x)$ is made, then the smooth deformation of the AT directly follows.

In [111], B-splines are used for modeling trajectory deformations, as approximation by B-splines is very efficient in terms of both quality and computational time. Moreover, B-splines features C2-continuity, robustness and flexibility. This could be a good choice for our model as well. Nevertheless, for this preliminary study, we choose to rely on simpler curves, and to approximate our trajectory deformations with a symmetric cosine-like function, *i.e.* $\xi(x) = a \cdot \cos(bx) + c$. We would like to choose this function, $\xi(x)$, (to choose the values for a, b, and c) so as to satisfy the following conditions:

- $\xi(0) = \xi(1) = 0$ (boundary conditions, guaranteeing that the first and last AT points are not to be changed);
- $\xi'(0) = \xi'(1) = 0$ (boundary conditions, guaranteeing smoothness at the extreme points, so that the aircraft leaves its AT tangentially to the AT);
- $\xi(x) = \xi(1 - x)$ (symmetry about line $x = 0.5$, for simplification);
- $\xi(0.5) = y_{max}$, where y_{max} is the parameter that will control the new AT curvature.

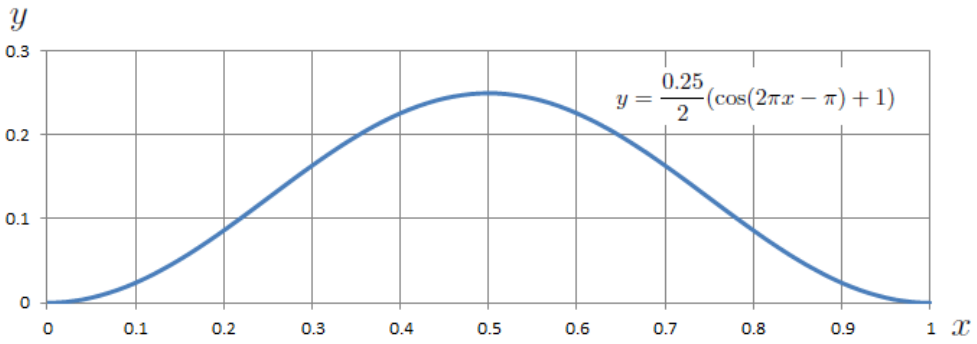

FIGURE 4.6: A cosine-like function used for trajectory transformation

Simple calculations applying these conditions, give us the following function, that is therefore selected for our simulations:

$$\xi(x) = \frac{y_{max}}{2}(\cos(2\pi x - \pi) + 1). \tag{4.8}$$

Figure 4.6 displays the function $\xi(x)$ for $y_{max} = 0.25$. Function (4.8) is C^{∞}-continuous on the segment [0,1] (when prolongated to the constant-value function zero for $x \leq 0$ and $x \geq 1$). As a sequence, the trajectory obtained by the proposed transformation, will not loose any smoothness and the boundary conditions on the derivative yield AT smoothness even at boundary points upon leaving the initial AT if the modified part of AT is concatenated with non-modified parts (defined by points $\bar{q}_i$ for $i < i_{start}$ and $i > i_{end}$). Figure 4.7 demonstrates several examples of such transformation with different values of y_{max}, applied to NAT parts of initial WO ATs. The initial ATs are shown with blue, while the resulting modified ATs are shown with red and green, for two different y_{max}.

To define the parameter y^f_{max} to randomly modify a particular AT, $\bar{\tau}^f$, we introduce a *continuous variable* $b^f \in [-1, 1]$, and we consider, for any given value of b^f in the range from -1 to 1:

$$y^f_{max} = b^f \cdot Y_{max}, \tag{4.9}$$

where Y_{max} is a global user-defined parameter whose value impacts the modified curve deviation. In our computational experiments, the value of Y_{max} is empirically set so that the length of initial ATs does not increase by more than 10%:

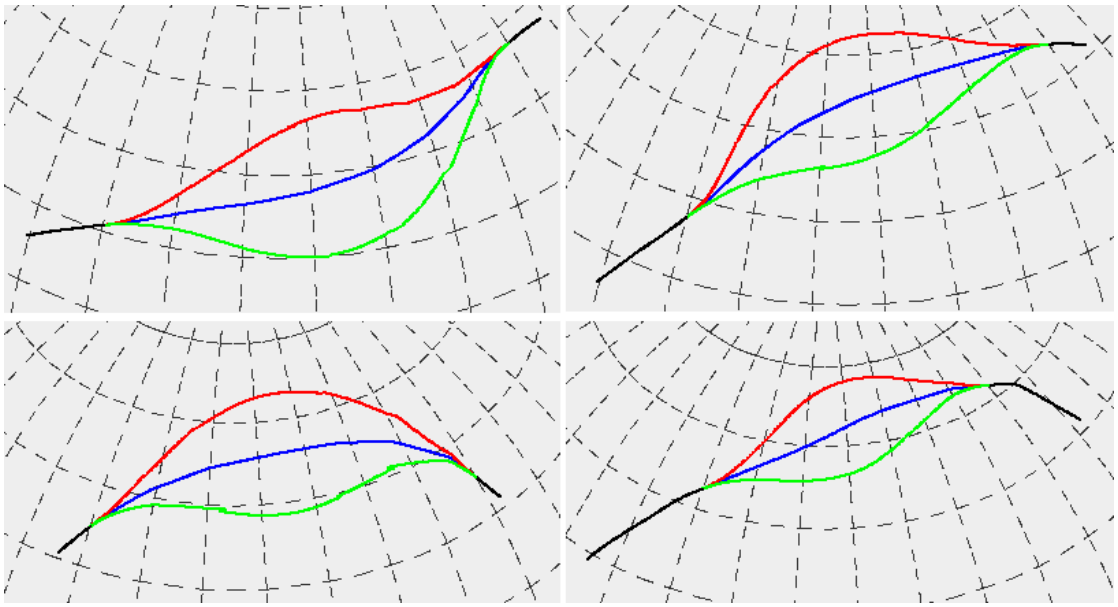

FIGURE 4.7: Several aircraft trajectories modified by topological transformation

$$length(\tau^f) - length(\bar{\tau}^f) \leq 0.1 \cdot length(\bar{\tau}^f), \;\; f = 1, ..., N. \tag{4.10}$$

Thus, for each flight f, a single continuous variable $b^f \in [-1, 1]$ completely defines the sequence of points $\{q_i^f\}_{i=1}^{M^f}$ that are obtained from the initial points $\{\bar{q}_i^f\}_{i=1}^{M^f}$ by the topological transformation described above, and therefore it defines the geometrical shape of the new AT, $\tau_{b^f}^f$.

Nevertheless, to define completely the AT $\tau_{b^f}^f$, we also need to recalculate the times, $\{t_i^f\}_{i=1}^{M^f}$, at which aircraft f passes the new AT points $\{q_i^f\}_{i=1}^{M^f}$. To do so, we simulate the flight progress in the wind field through calculations explained in the next section.

4.2.3 Wind model and flight progress model

To simulate the progress of flight f in the wind field, we need to know the aircraft Ground Speed (GS), $\vec{V}^f$. It is naturally obtained as the vector sum of the aircraft TAS, $\vec{v}^f$, and the Wind Speed (WS), $\vec{W}$, using speed triangle rule (F.1) (see Figure 1.5 and Appendix F).

The wind field at a particular time is modeled by a 3D grid of geographical points, for which the west-east (u) and south-north (v) wind components are defined at each grid point. The wind data for such a grid is obtained from GRIB files in the same manner

as explained in Section 3.2.3. Here, we use only the forecast winds for our simulations, as we are placed in the concept of strategic trajectory planning. The longitudinal and vertical grid resolution is 0.5° degrees; the vertical grid resolution is 1,000 feet (1 FL). The wind data for each FL is obtained by linear interpolation of GRIB data available for 200 hPa and 300 hPa.

For each day, four forecast wind fields are produced, every six hours. Thus, four different GRIB files are available daily. The wind is supposed to be constant in time during the time period between the two forecast. To obtain the values of the wind encountered by an aircraft flying in a period between two forecasts, the values from the latest available forecast GRIB file are taken as reference. Thus, we consider, that each flight f may be assigned a single 3D wind grid (available all along this flight). We will not modify this assignment in our simulations (although a flight may be delayed as a result of our deconflicting procedure). Moreover, as each flight f is performed at a constant FL, we can extract a 2D wind grid (in longitude/latitude only) to be assigned to such a flight.

In Chapter 3, we used a bilinear interpolation to obtain the value of the wind at a given geographical point from the values of the 4 closest nodes of the 2D wind grid. However, in [92], no bilinear interpolation is performed, and for a given geographical point, the wind value from the closest 2D wind grid node is assigned. Thus, in this study, we also use the closest-node wind value, in order to obtain results consistent with the initial data.

Now, once the wind vector $\vec{W}$ is defined for each point $q_i^f = (\lambda_i^f, \phi_i^f, t_i^f)$ $(i = 1, ..., M^f)$ of the AT of aircraft f, the flight progress of aircraft f can be simulated using formulas similar to (3.1)-(3.3) (Section 3.2.1). A brief summary of the formulas used to perform the geometrical computations on the spherical Earth in geographical coordinates (distance between the points, vector projection, etc.) can be found in Appendix Y.

Thus, for a particular AT τ^f whose geometrical shape is defined by a sequence of points $\{q_i^f\}_{i=1}^{M^f}$, we can calculate the times $\{t_i^f\}_{i=1}^{M^f}$, at which aircraft f passes these points. Furthermore, using this data for a set of N aircraft, we can calculate the number of conflicts encountered by these aircraft. The procedure to do so is explained in the next section.

Algorithm 4.1 formally describes the procedure of modification of an initial AT, $\bar{\tau}^f$, explained above, given values of decision variables d^f and b^f. To simplify the notation, the flight index f is omitted in the algorithm description. Note, that in practical realization, in most cases, perturbations of the variables d^f and b^f are made successively. Thus, it is more efficient from the computational point of view to use the procedures of AT recalculation when d^f is changed, or when b^f is changed, separately.

Algorithm 4.1 Recalculating aircraft trajectory based on time-delay and shape-modification

Input: $\bar{\tau}(FL, v, \{\bar{q}_i\}_{i=1}^{Q}, \{\bar{t}_i\}_{i=1}^{Q})$ - initial AT;
d - time delay for flight departure;
b - parameter, specifying the curvature of the modified AT;
W_{FL} - wind-field grid at FL

Output: $\tau(FL, v, \{q_i\}_{i=1}^{Q}, \{t_i\}_{i=1}^{Q})$ - modified AT

1: $q_1 := \bar{q}_1$ // the first AT point is not modified
2: $t_1 := \bar{t}_1 + d$ // delaying the flight at the first point
3: $len := 0$ // length of AT segment from $\bar{q}_1$ to $\bar{q}_i$
4: $L :=$ LENGTH$(\bar{\tau})$ // length of initial AT $\bar{\tau}$
5: **for** $i := 2$ to Q **do**
// Recalculating position of point q_i
6: $li :=$ DIST$(\bar{q}_{i-1}, \bar{q}_i)$
7: $len := len + li$
8: $x := len/L$
9: $y := \xi_b(x)$
10: $Y := y \cdot L$
11: $q_i :=$ SHIFT$(\bar{q}_i, \bar{q}_{i-1}, Y)$ // move $\bar{q}_i$ by $Y \perp$ to arc $(\bar{q}_{i-1}, \bar{q}_i)$
// Recalculating time for point q_i
12: $l :=$ DIST(q_{i-1}, q_i)
13: $\vec{W} :=$ WINDSPEED(q_{i-1}, W_{FL}) // wind vector at previous point q_{i-1}
14: $V :=$ GROUNDSPEED$(v, \vec{W}, q_{i-1}, q_i)$ // aircraft GS between q_{i-1} and q_i
15: $\Delta t := l/V$ // cruising time between q_{i-1} and q_i
16: $t_i := t_{i-1} + \Delta t$

4.2.4 Conflict model

By a classical definition, a *conflict* is a violation of the established *Minimum Separation Standards* (MSS) (see Section 1.1.3 for more detail). In the frame of FCC, we define the following MMS (that further are referred as *Reduced Separation Standards*, RSS):

- vertical MSS, Δ_v, which is typically equal to 1000 feet (1 FL);

- horizontal MSS, Δ_h, which is supposed in this study to be reduced to 30 NM in the NAT airspace thanks to new generation surveillance and broadcast technologies; and
- temporal MMS, Δ_{temp}, that we consider to be equal to 3 minutes in the frame of the current study.

For our case study, the aircraft are prescribed to cruise at a constant predefined FL. Thus, for aircraft on different FLs, the vertical separation norm is automatically verified. As a consequence, the procedure of conflict detection for a set of flights can be performed separately for each FL, and consists of verifying if horizontal and temporal MSS are maintained for a given set of ATs on a single FL. Note, that 3-minute MSS is approximately equal to the time required by the fastest commercial aircraft ($v_{max} \approx 600kts = 10$ NM/min) to overfly 30 NM. Thus, in this sense, the horizontal and vertical MSS coincide. In the frame of this study, we will distinguish:

- point-to-point conflicts, and
- AT-to-AT conflicts (or, flight-to-flight conflicts).

A *point-to-point conflict* involving aircraft f and g is detected between two points, $Q_i^f(q_i^f, FL^f, t_i^f)$ and $Q_j^g(q_j^g, FL^g, t_j^g)$ when:

- point q_i^f is passed by aircraft f at time t_i^f when flying along AT τ^f at constant altitude FL^f $(i \in \{1, ..., M^f\})$, and
- point q_j^g is passed by aircraft g at time t_j^g when flying along AT τ^g at constant altitude FL^g $(i \in \{1, ..., M^g\})$, and
- the three separation standards are violated simultaneously, *i.e.*:

$$FL^f = FL^g, \tag{4.11}$$

$$dist(q_i^f, q_j^g) < \Delta_h, \text{ and} \tag{4.12}$$

$$|t_i^f - t_j^g| < \Delta_{temp}. \tag{4.13}$$

Let us introduce the following binary parameters:

$$\delta(Q_i^f, Q_j^g) = \begin{cases} 1 & \text{if } FL^f = FL^g, \\ & \& \ dist(q_i^f, q_j^g) < \Delta_h, \\ & \& \ |t_i^f - t_j^g| < \Delta_{temp} \\ 0 & \text{otherwise.} \end{cases} \tag{4.14}$$

Parameter $\delta(Q_i^f, Q_j^g)$ indicates if Q_i^f and Q_j^g are in conflict ($\delta(Q_i^f, Q_j^g) = 1$) or not ($\delta(Q_i^f, Q_j^g) = 0$). Then, the number of point-to-point conflicts induced by two ATs, τ^f and τ^g, noted $C(\tau^f, \tau^g)$, is equal to:

$$C(\tau^f, \tau^g) = \sum_{i=1}^{M^f} \sum_{j=1}^{M^g} \delta(Q_i^f, Q_j^g) \tag{4.15}$$

The *total number of point-to-point conflicts*, C_t, induced by a set of N flights can be calculated as:

$$C_t = \frac{1}{2} \sum_{f,g=1}^{N} C(\tau^f, \tau^g). \tag{4.16}$$

We will use this number of point-to-point conflicts, C_t, in our numerical calculations. Nevertheless, when displaying results, it is more understandable to operate with the numbers of AT-to-AT conflicts.

An *AT-to-AT conflict* is detected between two ATs, τ^f and τ^g if at least one point-to-point conflict is detected between any pair of points belonging to these ATs, *i.e.* if $C(\tau^f, \tau^g) > 0$. Let us define a binary parameter, $\delta(\tau^f, \tau^g)$, as follows:

$$\delta(\tau^f, \tau^g) = \begin{cases} 1 & \text{if } C(\tau^f, \tau^g) > 0 \\ 0 & \text{if } C(\tau^f, \tau^g) = 0. \end{cases} \tag{4.17}$$

Then, the total number of AT-to-AT conflicts, $\tilde{C}_t$, induced by a set of N flights can be calculated as:

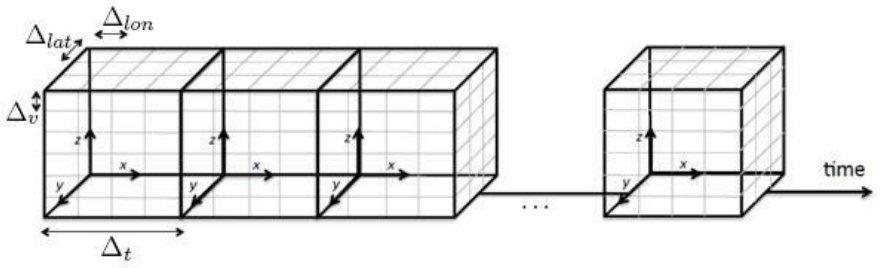

FIGURE 4.8: Four-dimensional grid for conflict detection [3]

$$\tilde{C}_t = \frac{1}{2} \sum_{f,g=1}^{N} \delta(\tau^f, \tau^g) \tag{4.18}$$

Note that $C_t = 0 \Leftrightarrow \tilde{C}_t = 0$. To calculate the number of point-to-point conflicts (further referred simply to as the number of conflicts), we use the grid-based conflict-detection scheme described in [112], implemented in a hash table. According to this scheme, the airspace is discretized using a 4-dimensional grid (3D-space + time), as illustrated in Figure 4.8. The size of each cell in the 4D grid, $(\Delta_{lon}, \Delta_{lat}, \Delta_v, \Delta_t)$, is defined by the minimal separation requirement and the discretization time step, appropriately chosen:

- In contrast to [112], in our case the discretization in the horizontal section is made in longitude/latitude (and not in xy). The choice of Δ_{lon} and Δ_{lat}, expressed in degrees, depends on the horizontal separation norm, Δ_h, expressed in NM and must be such that the size of the cell is at least as large as Δ_h (30 NM).
- Further, the vertical cell size is set to be equal to the vertical separation norm, Δ_v (1,000 feet). As mentioned above, for our case, conflict detection may be performed separately for different FLs. This assumption simplifies the general procedure described in [112].
- Finally, we set the discretization time step, Δ_t, to be equal to 15 seconds. This value is sufficiently small to assume that all the important conflicts can be detected (in the scale of the temporal MSS, $\Delta_{temp} = 3$ min), but large enough to avoid prohibitive computation times (see Appendix Z for detail).

Further, for each flight f and for each 4D point, Q_i^f, of its AT, τ^f, we compute the 4D index of the cell corresponding to this point: $(I_\lambda, I_\phi, I_{FL}, I_t)$; and for each such cell we

[3] From [112]

record all the AT points of all other flights that belong to this cell. Thus, we establish the unique correspondence between AT points and grid cells. Now, to detect the number of conflicts induced by a set of flights and related to a given 4D point, Q_i^f, it suffices to check the distances (in space and time) between this given point, and the points of other ATs belonging to the same cell and to a sufficiently large number of neighboring cells.

By construction of the grid, one can easily verify that in order to detect all the conflicts with a point belonging to cell $(I_\lambda, I_\phi, I_{FL}, I_t)$, we only need to check the cells $(I'_\lambda, I'_\phi, I_{FL}, I'_t)$, where $(I'_\lambda \in \{I_\lambda - 1, I_\lambda, I_\lambda + 1\}$; $I'_\phi \in \{I_\phi - 1, I_\phi, I_\phi + 1\}$ and $I'_t \in \{I_t - 3, I_t - 2, ..., I_t + 2, I_t + 3\}$. Note that we do not look for neighbor cells in the vertical direction, as aircraft are *a priori* separated vertically, when belonging to different FL. The described procedure is formalized in Algorithms 4.2 and 4.3.

Algorithm 4.2 Calculating the number of point-to-point conflicts related to a given point

Input: $Q(\lambda, \phi, FL, t)$ - a 4D points of a given AT;
$HashMap$ - conflict-detection grid, where
each cell $(I_\lambda, I_\phi, I_{FL}, I_t)$ contains a list of points Q_i belonging to this cell

Output: C_Q - number of point-to-point conflicts induced by point Q

```
1: function NumberOfConflictsAtPoint(Q, HashMap)
2:     C_Q := 0
3:     (I_λ, I_φ, I_FL, I_t) := HashKey(HashMap, Q)   // get 4D-grid index for point Q
4:     for I'_λ := I_λ − 1 to I_λ + 1 do              // neighbor cells in longitude
5:         for I'_φ := I_φ − 1 to I_φ + 1 do          // neighbor cells in latitude
6:             for I'_t := I_t − 3 to I_t + 3 do      // neighbor cells in time
7:                 for each Q_i ∈ HashMap(I'_λ, I'_φ, I_FL, I'_t) do
8:                     C_Q := C_Q + δ(Q, Q_i)         // increased if Q and Q_i are in conflict
       return C_Q
```

4.2.5 Optimization problem formulation

In this section, we propose an optimization formulation of our problem expressed in terms of the notations, decision variables and input data presented in the previous section. Our objective here will be to minimize the number of conflicts (not necessarily to eliminate all the conflicts), as a conflict-free solution might not exist in the frame of FFC, with the number of decision variables introduced in the present formulation, and the range of values of these variables. Thus, similarly to the formulation (2.13) from Section

Algorithm 4.3 Calculating the number of point-to-point conflicts for a set of aircraft trajectories

Input: $\{\tau^f\}_{f=1}^{N}$ - set of ATs, where N is the number of flights in the set; and
$\tau^f(\{Q_i^f\}_{i=1}^{M^f})$ is an AT represented by a set of 4D points at constant FL
$HashMap$ - conflict-detection grid, where
each cell $(I_\lambda, I_\phi, I_{FL}, I_t)$ contains a list of points Q_i^f belonging to this cell

Output: C_t - total number of point-to-point conflicts

1: **function** NumberOfConflictsTotal($\{\tau^f\}_{f=1}^{N}$, $HashMap$)
2: $C_t := 0$
3: **for** $f := 1$ to N **do**
4: **for** $i := 1$ to M^f **do**
5: $C_t := C_t +$ NumberOfConflictsAtPoint(Q_i^f, $HashMap$)
return C_t

2.2.5, here we also penalize the number of conflicts into the objective function instead of considering a hard constraint. Moreover, for this preliminary study, we consider the number of conflicts to be the only criterion to be minimized

For each flight f ($f = 1, ..., N$), the following **input data** are given:

- FL^f - aircraft FL;
- v^f - aircraft TAS;
- $\bar{Q}_i^f = (\bar{\lambda}_i^f, \bar{\phi}_i^f, FL^f, \bar{t}_i^f)$, $i = 1, ..., M^f$ - a sequence of 4D points of the AT in NAT (as defined in Section 4.2.1).

Furthermore, for each flight f, the following **decision variables** are introduced:

- $d^f \in \{0, 1, 2, ..., 30\}$ - discrete aircraft departure delay (in minutes);
- $b^f \in [-1, 1]$ - continuous variable controlling the displacement of the modified AT with respect to the initial AT.

To simplify the notation, we accumulate the decision variables for all the flights in a single vector, z:

- $z = (d^1, b^1, d^2, b^2, ..., d^N, b^N)$.

The only **constraints** of the problem are the lower- and upper-bound constraints for the decision variables. The objective function is given by the total number of point-to-point conflicts, C_t. Thus, our optimization problem is stated as follows:

$$\begin{aligned} &\min_{z} C_t(z), \\ &\text{s.t.} \quad d^f \in \{0, 1, 2, ..., 30\}, \quad f = 1, ..., N; \\ &b^f \in [-1, 1] \; f = 1, ..., N. \end{aligned} \tag{4.19}$$

Problem formulation (4.19) involves $2N$ decision variables, among which:

- N discrete decision variables, each of which can take $N_d + 1$ discrete values, and
- N continuous decision variables.

The objective function, $C_t(z)$ cannot be explicitly represented in terms of decision variables, z. The value of this function for each instantiation of the decision variables, z, is to be evaluated in the simulations, via Algorithms 4.1, 4.2 and 4.3. This problem is therefore a difficult mixed-integer black box (derivative-free) optimization problem as its dimension is relatively high. This explains our choice to tackle this problem with a stochastic algorithm, which is presented in the next section.

4.3 Optimization algorithm

In this section, we describe an existing optimization algorithm, that we use as a basis to solve our optimization problem. We identify several new features, implemented in this study in order to adapt this algorithm to our particular NAT traffic situation.

4.3.1 Hybrid metaheuristic algorithm

As mentioned above, in the current track of our study, we choose to use a stochastic metaheuristic approach developed in [112]. In this work, Chaimatanan *et al.* combine a classical *Simulated Annealing* (SA) algorithm with a *Local Search* (LS), in order to

accelerate the convergence of SA. The detailed description of this approach can be found in [117]. Below, we present a brief summary of the proposed method and we specify the exact values chosen (empirically) for a number of algorithm parameters used in our implementation.

The basic scheme of a classical SA was already presented in Section 2.3.2. For the current study, we define the main features of SA as follows:

- the representation of a state of the system is given by an instantiation of the decision variables, $s = z$;
- the system energy is given by the objective function, $E(s) = C_t(z)$;
- the initial temperature T_0 is deduced from the relation:

$$\tilde{\mu} = \exp \frac{\Delta E_{ave}}{T_0}, \tag{4.20}$$

  where $\tilde{\mu}$ is the user-defined probability of acceptance of degrading solutions, and ΔE_{ave} is the average energy variation, computed empirically by evaluating N_h randomly-generated states s;
- the cooling is performed via the exponential law, $T_i = \gamma \cdot T_{i-1}$;
- the minimal temperature (stopping criterion) is set to $T_f = 0.01 \cdot T_0$.

In order to generate a *neighborhood solution* (τ^f) for a *given flight*, f, from its initial AT ($\bar{\tau}^f$), our algorithm first determines whether to modify the AT shape (b^f), or to modify the departure time (d^f) in the next move. The choice is made randomly according to a user-defined probability, P_m, to select one of the two ways. In order to generate a neighborhood solution for a *set of flights*, we implement the combination of the two search strategies introduced in [117] and referred to as PTIT: modifying one Particular Trajectory (PT), and modifying all Trajectories Interacting with the given one (IT).

Thus, our implementation performs the following steps at each iteration:

- randomly choose one flight, f;
- randomly modify its AT, τ^f (shape or departure time);

- randomly modify all ATs inducing conflicts with the τ^f, *i.e.,* all τ^g, such that $\delta(\tau^f, \tau^g) = 1$;
- reevaluate the new trajectory set (new solution);
- accept or reject this solution, according to the SA scheme.

The following user-defined parameters are set to values as a result of empirical algorithm adjustment:

- $\tilde{\mu} = 0.3$;
- $M = 100$;
- $\gamma = 0.99$;
- $N_t = 100$;
- $P_m = 0.5$.

LS is an algorithm that starts from a given initial solution, and then iteratively replaces the current solution with a better solution (a solution that yields an improvement of the objective function) value in a pre-defined neighborhood. We generate a neighbor state for LS in the same way as for SA, using the PTIT strategy.

At each iteration, the hybrid-metaheuristic algorithm randomly selects whether to use SA or LS, or both methods consecutively. Again, the choice is made according to user-defined probabilities. These probabilities depend on the current temperature (or the number of iterations performed), in such a way that at high temperatures SA is applied more often, in order to widely explore the state space, while at low temperatures LS is preferably executed, in order to favor convergence.

In order to adapt further the algorithm developed in [117] to our case-study of NAT traffic, we slightly modify it and supply it with several new features. These features are specified in the next section.

4.3.2 Algorithm adaptation

The hybrid metaheuristic algorithm described in [117], has two main characteristics, given below, that prevent it to be applied directly for deconflicting our NAT-traffic ATs.

- The algorithm is based on the plane geometry, and accepts the ATs defined by a sequence of points in xy-coordinates as input data. The approximation of a spherical Earth by the xy-plane is acceptable for short-distance flights (European scale), but starts to yield significant errors for long-distance flights such as NAT oceanic flights.

- In the algorithm from [117], a different approach of AT-shape modification is implemented: the initial straight segment is replaced by three straight-line segment joining the initial segment borders and two randomly-chosen offset waypoints. As a result, this method yields piecewise ATs. In our study, in the context of FFC, we would like to preserve the smoothness of the initial WO ATs, and to avoid sharp heading changes.

- In [117], the flight progress is performed without taking into account the winds (with zero winds).

Thus, in order to use the proposed method for our problem, we implement the following modifications to the initial algorithm.

- We replace the operations of plane geometry in xy-coordinates by operations on the spherical Earth in geographical (λ, ϕ) coordinates (the mathematical basis for such operations is given in Appendix Y). Note that such operations are less efficient in terms of computational time, as they demand evaluation of time-consuming trigonometrical functions.

- We replace the procedure of AT-shape modification from the initial algorithm by our procedure (Algorithm 4.1). Again, this procedure is slower than the procedure of [117], because of the computations on a sphere.

- At the same time, we have added the wind-structure to the algorithm, as well as the functionality responsible to take winds into account when recalculating trajectories (also defined in Algorithm 4.1). This modification also slows down further the computations.

As it can be seen, the proposed necessary modifications are more expensive in terms of computational time. Moreover, the initial algorithm of [117] is already computing-time

intensive. However, the most expensive operation of both algorithms (initial and modified) is the objective function evaluation, *i.e.,* recalculating the total number of conflicts once several ATs are modified. The complexity of AT reevaluation depends actually on the number of neighbor hash-table cells, and on the number of points encountered at each cell concerned. In order to accelerate the computations, we simplify the initial algorithm, exploiting the fact that our flights maintain constant FLs. Indeed, the neighbor cells in the vertical section do not need to be considered, and the procedure complexity is reduced by a factor of three. This simplified procedure is described by Algorithm 4.2, and its complexity can be simply obtained from the number of algorithm loops: $3 \times 3 \times 7 \times \overline{|HashMap(I_\lambda, I_\phi, I_{FL}, I_t)|}$, where the last terms stands for the average number of points in a hash-table cell.

However, the algorithm computational time remains very high when applied to the NAT ATs. This is due to large horizontal MSS in NAT on one hand (30 NM in contrast to 5 NM established in the radar-covered airspace), and to the presence of JSs on the other hand. Large MSS result in large hash-table cells volumes, which, in turns, results in a large number of AT points encountered for a single cell. Moreover, because of the strong winds present in the core of JSs (see Appendix M), and the wind-optimality of the ATs, exploiting (for west-east ATs) or avoiding (for east-west ATs) these winds, the trajectories of different flights happen to be very close to each other by construction. This fact also augments the density of AT points in certain cells. As a result, the algorithm complexity may rise significantly (in comparison to the complexity of the same algorithm applied to continental flights, as in [117]).

Thus, we also bring a technical modification to the initial algorithm of [117], aimed at accelerating the algorithm. This acceleration is achieved by storing data that is expected to be reused in further computations, instead of recalculating it in real time. In particular, we save the current trajectory prior to modify it and to reevaluate the objective function. Thus, if this modified AT is rejected by SA, the come-back process simply replace it with the previously-stored AT.

4.3.3 Computational environment

The hybrid metaheuristic algorithm is implemented in Java and run under Windows-64 operational system, on Intel Core i7-3610QM CPU with 2.30 GHz.

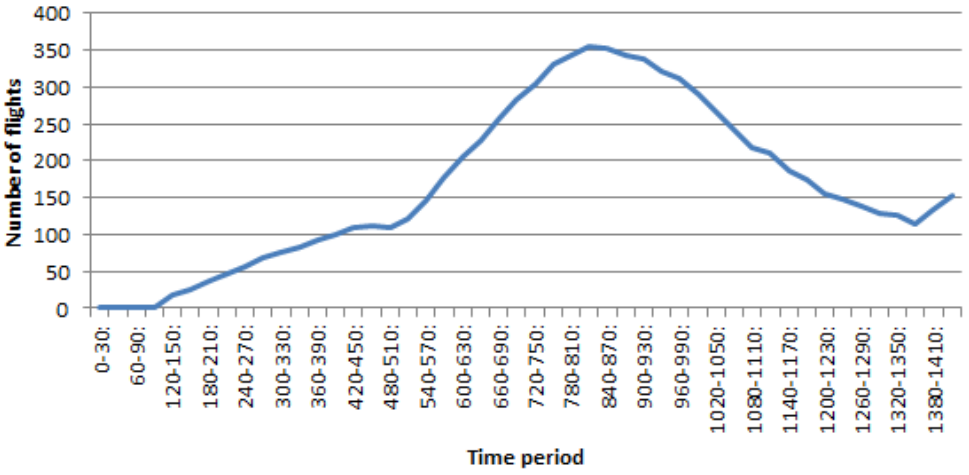

FIGURE 4.9: The distribution of flights in time for July 1st, 2012

4.4 Results of simulations

In this section, we present preliminary results of our simulations. First, we describe these results precisely for one day, July 1st. Next, we display general results for 31 days of July 2012.

4.4.1 Results for July 1st, 2012

The set of initial WO ATs for July 1st, 2012, is represented in Figure 4.3, where the AT segments corresponding to NAT region are shown with color, while the continental AT segments are displayed in black. This set contains $N = 839$ ATs. Figure 4.9 displays the distribution of these flights in time, for 24 hours of July 1st, with a discretization step of 30 minutes. This diagram evidently distinguishes one peak of traffic around 1300 UTC (at 780 minutes), and the tendency of traffic increase by midnight. Unfortunately, the real quantity of aircraft at this period (from midnight until early morning) is underestimated in Figure 4.9, because of the lack of data at the beginning of the time period. Indeed, the provided data sample contains only the flights departing on July 1st, while actually the NAT airspace at these periods accommodates as well the flights departing on June 30th, but not yet landed by midnight.

In this study, we perform conflict detection with RSS (30 NM for horizontal separation, and 3 minutes for temporal separation, as defined in Section 4.2.4). For the initial flight set, we detect 524 AT-to-AT conflicts (524 pairs of aircraft in conflict). In the sequel

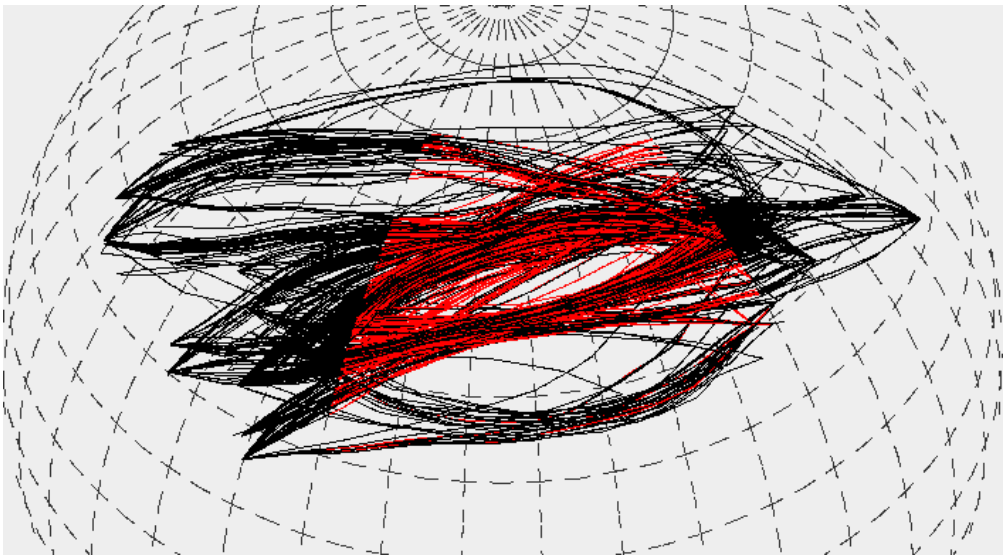

FIGURE 4.10: Conflict induced by initial wind optimal aircraft trajectories

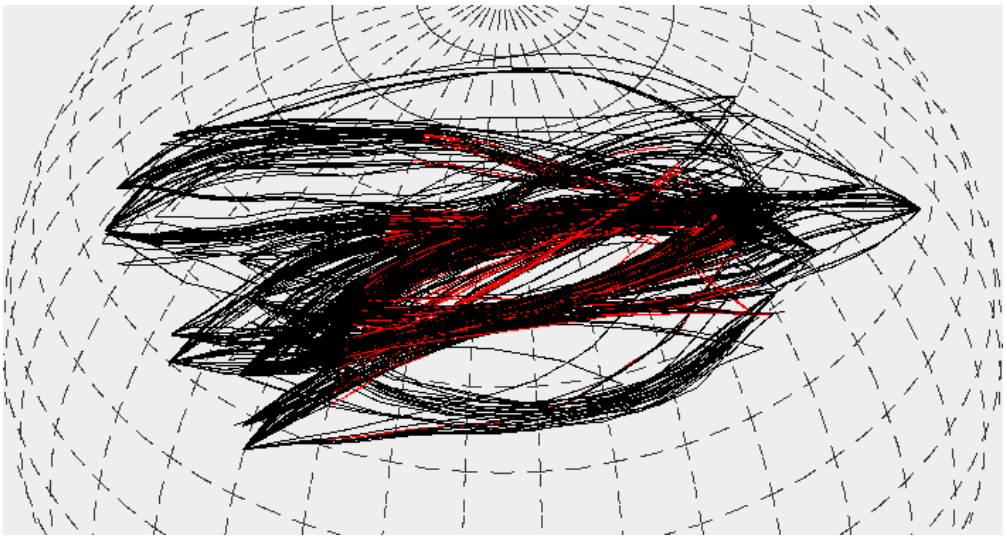

FIGURE 4.11: Remaining conflict after applying conflict-resolution algorithm with departure time modifications

of this section, we will refer to "AT-to-AT" conflicts simply as "conflicts". Figure 4.10 displays the aircraft being in conflict with red color.

We examine two versions of the conflict resolution algorithm. In the first case, we allow applying only departure delays, without any AT-shape modifications. The advantage of such an approach is that all the trajectories remain wind optimal. The maximal acceptable delay is set to $N_d = 30$ minutes. As a result of deconflicting with time-delays, the number of conflicts for the given flight set is reduced by 65%. The remaining 183 pairs of ATs in conflict are displayed in Figure 4.11. To obtain these results, 57% of aircraft are delayed, and the average value of assigned delays is 9.1 minutes.

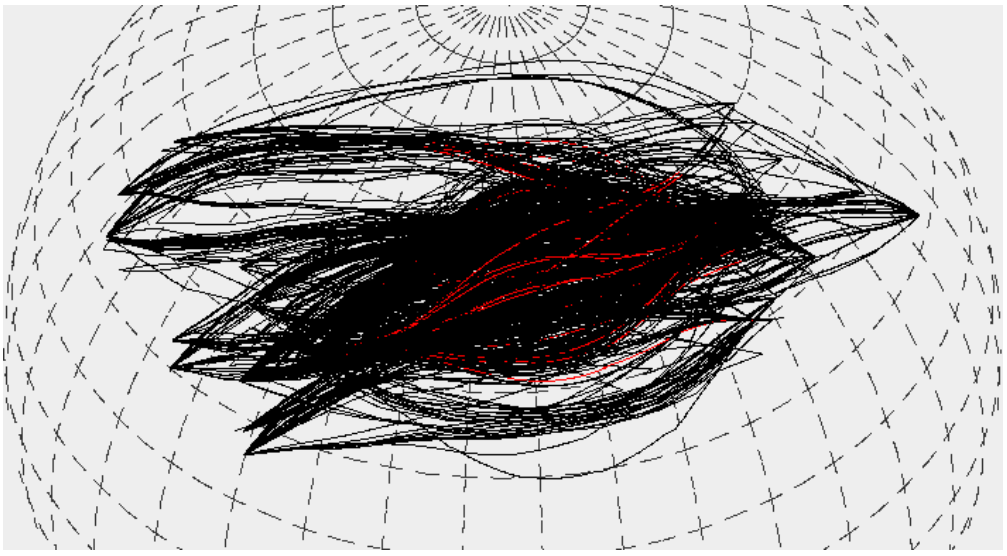

FIGURE 4.12: Remaining conflict after applying conflict-resolution algorithm with departure-time and trajectory-shape modifications

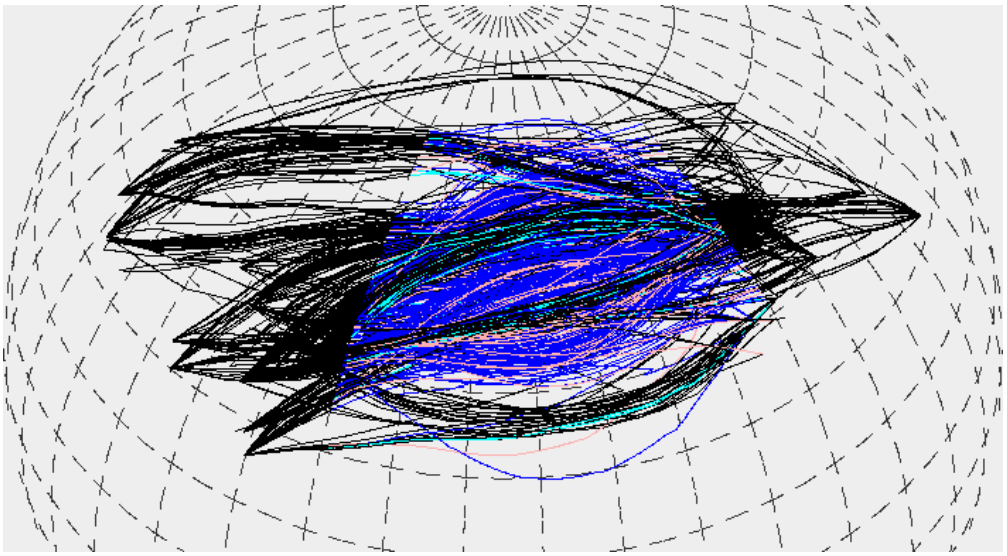

FIGURE 4.13: Flights after deconflicting with different trajectory modifications applied

In the second case, we allow applying both departure delays and AT-shape modifications. Doing so, on the one hand, we loose the trajectory wind-optimality, but on the other hand, we increase the search space, permitting the optimization algorithm to resolve more conflicts. Indeed, in this test, only 18 conflicts, shown in Figure 4.12, remain after algorithm execution. To obtain these results, 53% of aircraft are delayed, and 56% are deviated. Figure 4.13 displays the delayed flights in cyan color, the deviated flights in pink, and the flights that experience both delays and deviations, in blue.

The average value of assigned delays is 8.3 minutes. The average value of AT-length increase is 2.6% for deviated flights, and the average value of flight cuising time increase

ATs	Initial	Modified	
Allowed modifications	-	Delay	Delay & Shape
Number of point-to-point conflicts	225220	10990	484
Number of AT-to-AT conflicts	524	183	18
Percentage of resolved conflicts	-	65.1%	96.6%
Percentage of delayed flights	-	57.4%	52.6%
Mean delay, min.	-	9.1	8.3
Delay standard deviation, min.	-	10.6	10.5
Percentage of AT-shapes modified	-	-	56.5%
Mean AT-length increase, deviated flights, %	-	-	2.6%
Mean cruis. time increase, deviated flights, %	-	-	4.4%
Mean AT-length increase, all flights, %	-	-	1.5%
Mean cruis. time increase, all flights, %	-	-	2.5%

TABLE 4.1: Comparison of the result of conflict resolution with different allowed modifications

is 4.4%, also for deviated flights. The relative increase of cruising time overcomes that of AT-length, which is not surprising, as the deviated ATs becomes non-optimal with regards to winds. Note that increase in cruising time is, in our case (constant TASs and FLs), directly related to the increase in fuel consumption. Thus, flying such ATs will demand on average 4.4% more kerosene for the concerned flights.

Table 4.1 presents the summary of different parameter values obtained as a result of conflict resolution, for both cases. Figure 4.14 displays the number of AT-to-AT conflicts as a function of time, for 24 hours of July 1st, with a time discretization step of 30 minutes. It is easily seen, that the peak of conflicts at this diagram reflects the peak of flights from Figure 4.9. Moreover, we observe a great decrease in the number of conflicts after applying the resolution procedure, especially when the AT-shape is modified.

Figure 4.15 displays the progress value of the best solution encountered so far of the conflict resolution algorithm with the number of iterations. As one can see, the great amelioration of a solution is achieved during several first iterations, while the further convergence to the optimal solution is quite slow. Remark that when allowing the AT-shape modification, already on the 5-th iteration the algorithm yields a solution that is better than the resulting solution with only delay-modifications.

The obtained results lead us to the following conclusion.

- The number of conflicts induced by a set of WO ATs in NAT is excessively large. This arises from the values of MSS, that, even being reduced, exceeds significantly

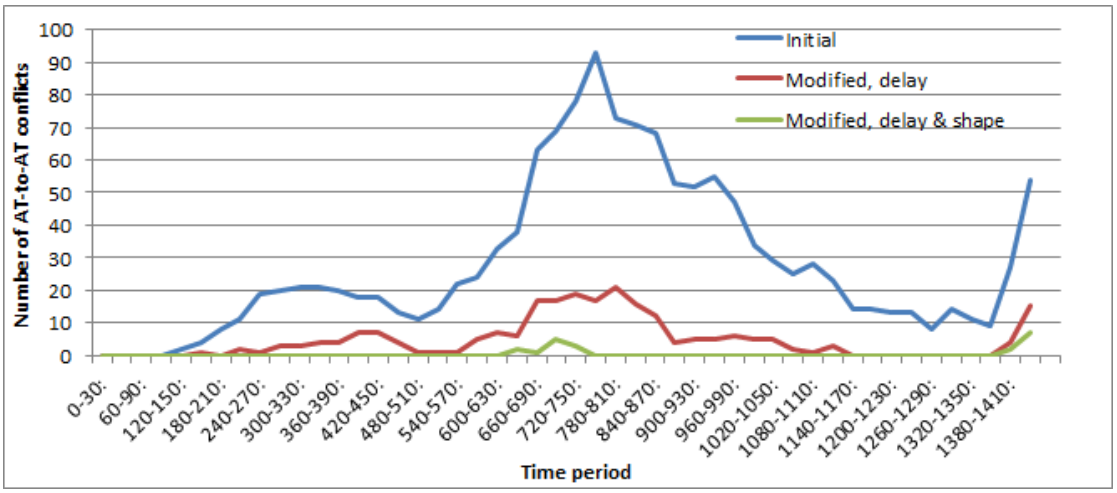

FIGURE 4.14: Number of AT-to-AT conflicts as a function of time for initial and deconflicted flight sets

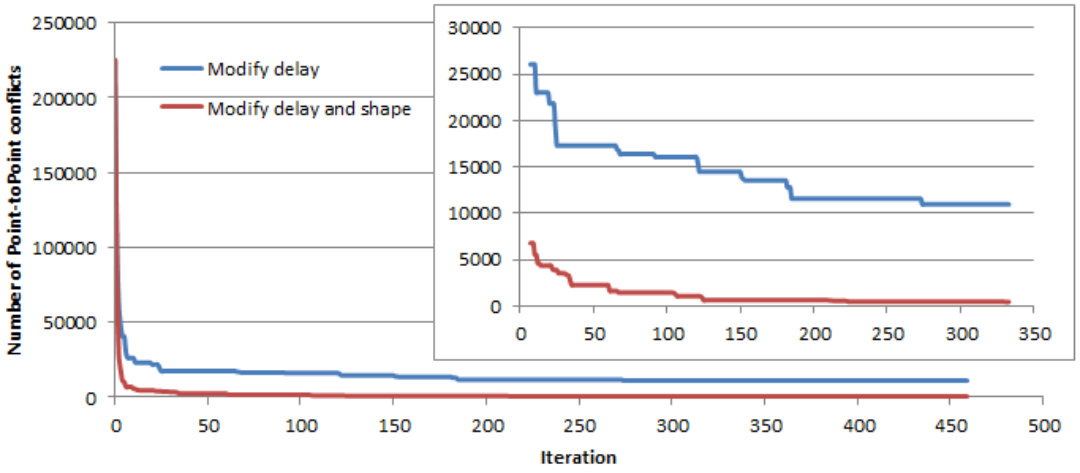

FIGURE 4.15: Number of point-to-point conflicts as a function of number of iterations during the deconflicting algorithm execution for two modification strategies (right-hand side: a zoom on a smaller range of values

the continental MSS.

- Our deconflicting algorithm permits to reduce significantly the number of conflicts, by applying reasonable delays, or delays and AT deviations.
- The approach of AT modification that combines time delays with AT-shape deviations is much more efficient than that considering only delays.
- The conflicts, being reduced significantly, nevertheless, are not completely eliminated. This is not critical for the current study, as:

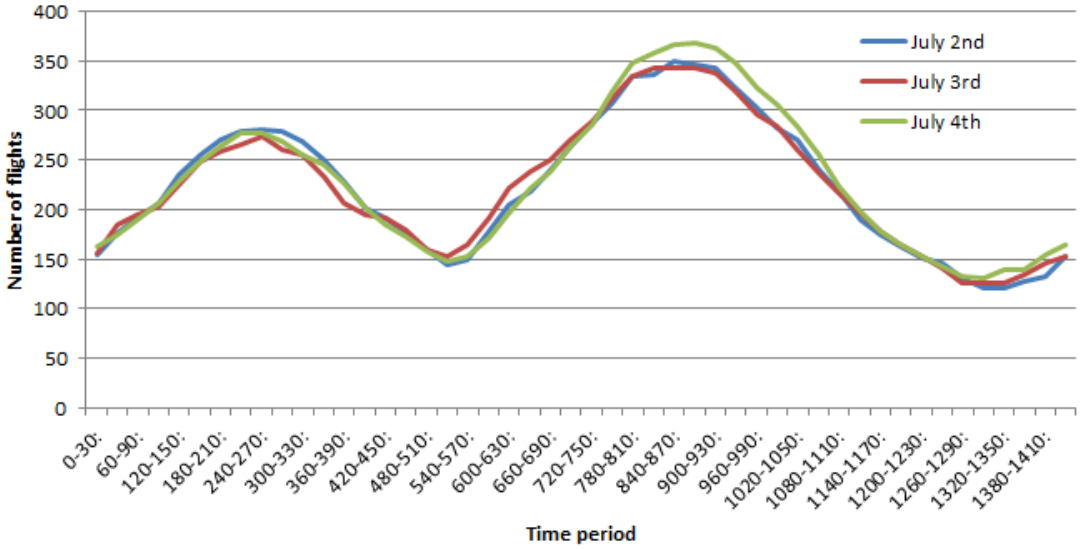

FIGURE 4.16: The distribution of flights in time for July 2nd, 3rd and 4th, 2012

- first, these results are obtained in the frame of a preliminary study, that should be extended by applying more sophisticated (probably data-oriented) approaches of conflict resolution;
- second, this study is performed in the frame of strategic trajectory planning, and the remaining conflicts would be resolved at the tactical stage (once uncertainty is greatly reduced), by applying tactical maneuvers.

The next section presents similar results, but for the whole month of July 2012.

4.4.2 Results for 30 days of July 2012

In this section, we examine the remaining 30 days of July 2012. As an example, Figure 4.16 presents the distribution of flights in time for three of these 30 days, *i.e.,* July 2nd, 3rd and 4th. The data for each day is completed with the flights that departed on the previous day, but have not landed before midnight. Thus, in this figure, the two nominal (night-time and day-time) traffic peaks are clearly distinguished (as opposed to Figure 4.9). Moreover, we remark that the traffic distribution is quite homogeneous over the month.

We perform simulations for the 30 flight sets, similar to that described in the previous section for July 1st, using two trajectory modification approaches, that are referred further as “delay” and “delay&shape”. The results of these simulations are presented

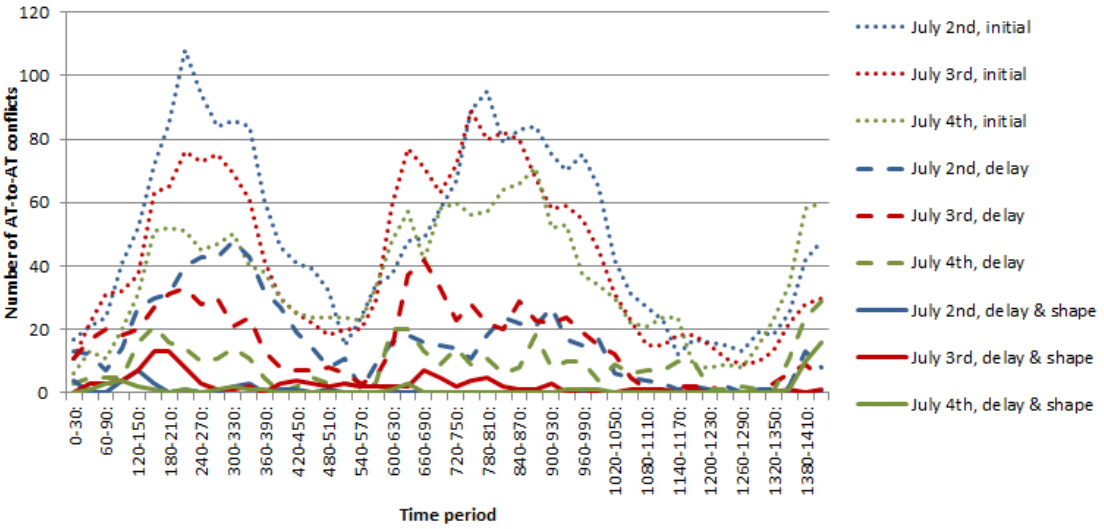

FIGURE 4.17: Number of AT-to-AT conflicts as a function of time for initial and deconflicted flight sets on July 2nd, 3rd and 4th

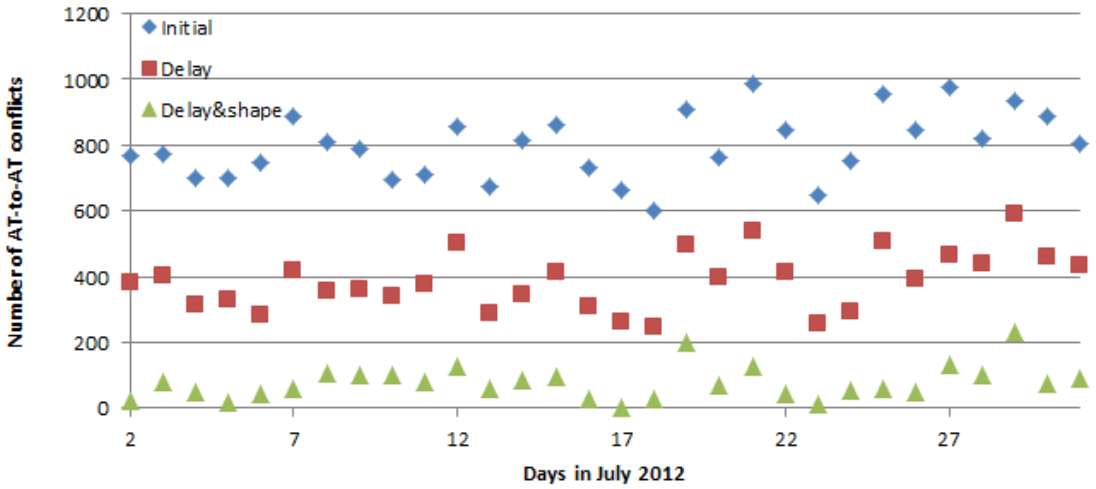

FIGURE 4.18: Number of AT-to-AT conflicts as a function of day in July 2012

below. Figure 4.17 displays the distribution of AT-to-AT conflicts in time, for the same three days, for initial flight sets, and for those modified with "delay"- or "delay&shape"-approaches. While the initial number of conflicts may be quite different for different days, the peaks of conflicts corresponding to the peaks of traffic can be easily distinguished here as well. Moreover, again, one can notice a great decrease in the number of conflicts when the "delay&shape"-approach is applied.

Figure 4.18 presents the distribution of initial and optimized number of conflicts over the 30 days. It highlights once more the evident conflict reduction achieved by the algorithm application. Figure 4.19, in its turn, displays the percentage of reduced conflicts for both

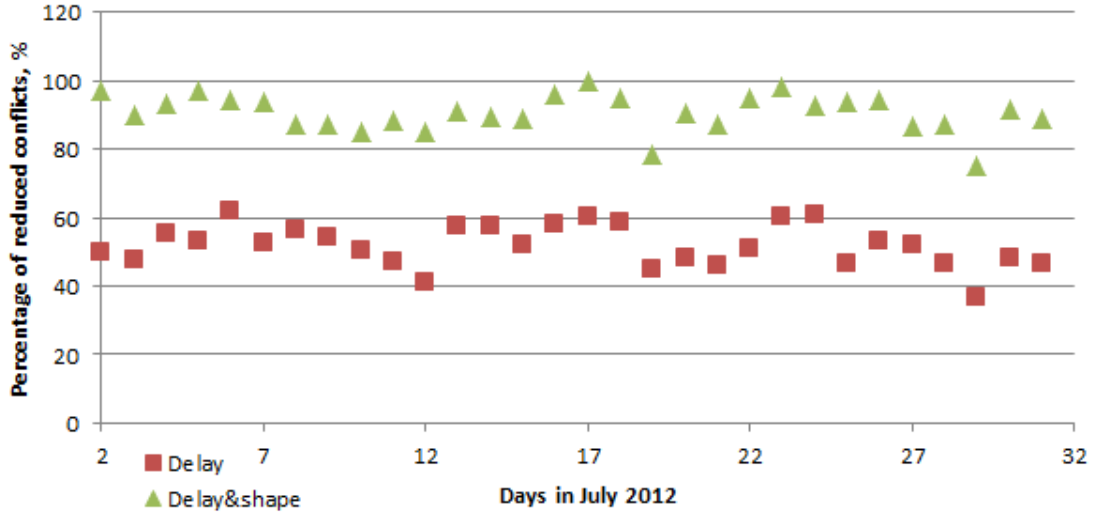

FIGURE 4.19: Percentage of reduced AT-to-AT conflicts as a function of day in July 2012

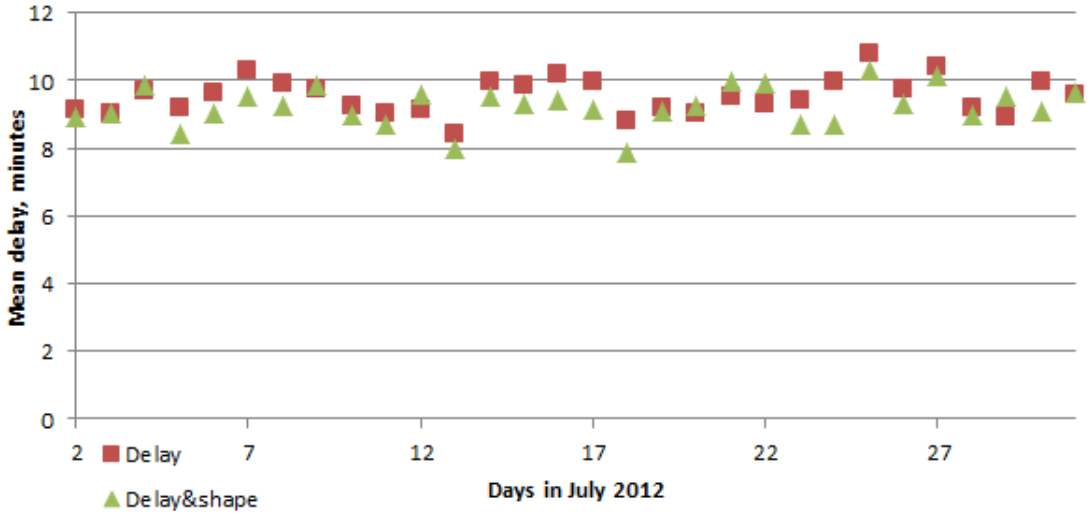

FIGURE 4.20: Average assigned delay, for 30 days in July 2012, in minutes

of the AT-modification approaches. The average value of conflict-reduction rate for the "delay" approach is 51.9%, while for the "delay&shape"-approache it is equal to 90.6%. Moreover, for this last approach for most of the days more than 80% of initial conflicts are resolved.

Furthermore, Figure 4.20 displays the distribution of the average value of assigned delays for both of the AT-modification approaches. As it can be seen, the distribution of these values is quite homogeneous over the month: the average delays are generally confined between 8 and 10 minutes. Moreover, these values are quite close for both approaches, and no one of the approaches could be considered being better in terms of

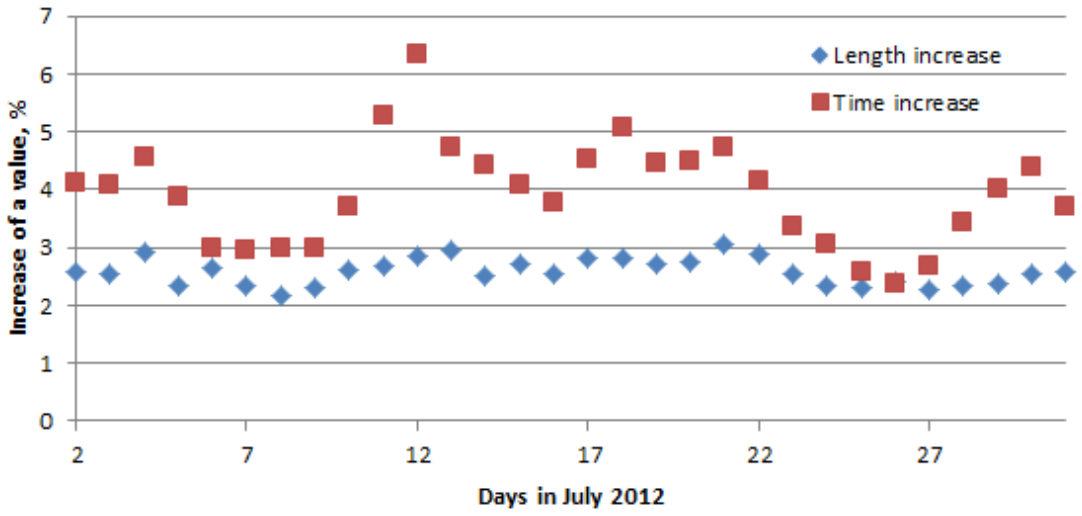

FIGURE 4.21: Average resulting AT-length increase and cruising-time increase, when trajectory shape modification is applied, for 30 days in July 2012, in %

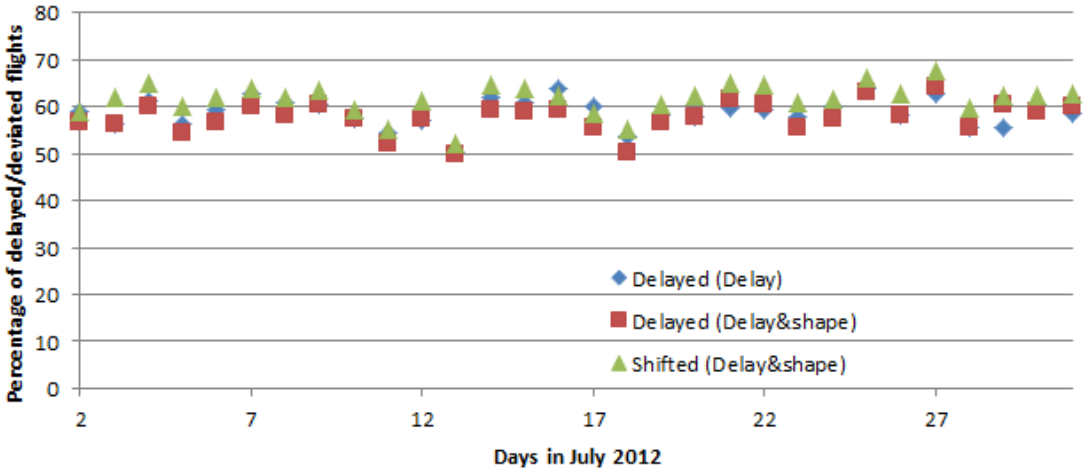

FIGURE 4.22: Percentage of flights with assigned AT-modifications, for 30 days in July 2012, in %

delay attributing.

Figure 4.21 shows the distribution of the average values of AT-length increase, and of cruising-time increase for "delay&shape"-modification. It is evidently seen that the percentage of time increase is much higher than that of the length increase. Moreover, while the length increase is quite homogeneous over the 30 days of July, being between 2 and 3 percent, the time increase vary significantly depending on the days. It could be as small as the length increase (for example, for July 26th), or could overcome 6% (for example, for July 12th). This fact should be related to particular wind field structure, different for different days.

Finally, Figure 4.22 presents the percentage of flights being delayed or deviated. These values vary only slightly from one day to another, being confined between 50 and 65 percent for most cases. At the same time, we notice that the percentages of affected flights (whether being delayed in both approaches or shifted) are highly correlated.

To sum up, as can be seen from the presented diagrams, the results for 30 days are similar and demonstrate similar tendencies. These results confirm the observations stated in Section 4.4.1. The developed algorithm, in its preliminary version, succeeds to eliminate about 90% of the initial conflicts. Thus, it represents a promising approach for conflict resolution in the frame of FFC.

Conclusion

The research work presented in the current thesis, had for objective to study several different tracks of possible improvements of air traffic conditions in the North Atlantic oceanic airspace (NAT). It is situated in the frame of new generation Air Traffic Management (ATM) concept and evokes such innovated features as Reduced Separation Standards (RSS), Wind Networking (WN) approach and Free Flight Concept (FFC). To conclude this thesis, we present below a brief summary of the main contributions of the current research, followed by perspectives inspired by the study.

Contributions

The first track of our research considered the current air traffic regulations in NAT, prescribing aircraft to follow a predefined track from the Organized Track System (OTS). We proposed to give more flexibility to the aircraft crossing NAT, and allowed them to change tracks within OTS. We developed several optimization formulations of this problem and we introduced solving methodologies. Applying the obtained re-routing maneuvers yields several important benefits that were observed in our study:

- aircraft can follow trajectories involving OTS tracks that are closer to their departure/arrival airports;
- thanks to that, the congestion level in the pre-oceanic continental airspace is reduced;
- aircraft have also the possibility to choose better trajectories in terms of fuel consumption, exploiting benefits from tail wind, or avoiding head winds.

We examined the air traffic behavior under the Current Separation Standards (CSS), and under the RSS. As a result, we concluded, that the CSS do not permit aircraft to exploit fully re-routing, due to strong separation constraints. On the other hand, the RSS guarantees the existence of conflict-free flight configurations for flights over NAT performing re-routings within OTS. This conclusion should motivate the Air Navigation System (ANS) users (and in particular, airlines) to equip their fleet with new-generation surveillance and broadcast technologies that would permit Minimal Separation Standards (MSS) reduction.

The second track of our work introduced a WN approach. WN permits the aircraft being close to each other en-route, to exchange mutually the information available on board, and in particular the data from accurate wind measurements, and to adjust their trajectory predictions (time prediction and conflict prediction). Our results revealed that WN can bring a significant improvement in Aircraft Trajectory (AT) prediction. Moreover, we remarked that it is especially efficient in a dense traffic environment, where aircraft are close to one another and thereby can benefit from more recent information for their AT-prediction adjustments. In order to apply the WN, the aircraft should also be appropriately equipped.

Finally, the last track of our work was devoted to conflict resolution for flight sets with Wind Optimal (WO) ATs. We presented a mixed-integer black-box optimization formulation of the problem. Then we developed a methodology adapting features of an existing algorithm taking into account the specificities of the NAT traffic. The algorithm permitted to decrease significantly the number of conflicts induced by WO flight sets, by delaying flight departure times and/or by modifying smoothly the AT shapes. Advantages of the proposed method include:

- resulting smooth trajectories, crucial for commercial airlines (passenger-comfort criterion);
- conflict-free near WO solutions, that do not depend on any flight order consideration (typical for some previous approaches).

The above research tracks can be viewed as a preliminary study, with numerous perspectives for future research. Some of them have already been mentioned along the thesis. The next section summarizes some of research track directions.

Perspectives

For the conflict resolution within OTS, a simplified model (presented in Section 2.2) was considered. Below, we give some remarks on how this model can be extended to include more options and criteria to approach the real air-traffic situation in NAT.

- Different criteria reflecting the traffic performance (*e.g.,* total flight duration, total fuel consumption, airline cost index) can be added to the "total number of conflicts" criterion into the objective function with corresponding weighting coefficients.
- The weighting coefficients for different criteria in the objective function can be adjusted independently for each flight, in order to permit the airlines to define the optimization priorities for each particular flight.
- Instead of using a single objective function with weighting coefficients, a multiobjective approach can be applied, yielding the results in terms of Pareto curves.
- Aircraft True Air Speeds (TASs) and/or Flight Levels (FLs) at waypoints (WPs) can be considered as further decision variables, while taking into account a fuel consumption criterion. This would give more flexibility to find feasible solutions.
- Aircraft TASs and Flight Altitude Profiles (FAPs) could vary depending on the OTS tracks attributed to the flight. The input data of the model can be modified so as to accept track-dependent TASs and FLs for each flight.

The Integer Program presented in Chapter 2 inspires implementing deterministic methods for integer programming. While the problem size for real-case flight sets remains relatively large, the specific problem involving a specific underlying graph (the OTS) could be exploited in order to tackle real-size instances.

Another interesting track in this direction, is to determine the complexity status of the presented problem. Even if it looks very similar to some classes of classical NP-hard problems established, its complexity status remains an open question.

The problem of finding a conflict-free flight configuration in the frame of FFC yields, in its turn, some interesting possible perspectives.

- The algorithm of trajectory shape modification can be refined in order to perform smaller local deviations whenever possible. Indeed, a weak point of the current method is that is deviates the whole AT, while the conflict may well be very local. In this case, it is more desirable to deviate the AT only in the concerned region.

- Besides the delay and shape modification, we can investigate the possibility of FL and speed modifications in the deconflicting process. Currently, the algorithm was adapted for the data sets in which each flight maintained constant FL and constant TAS. The proposed extension will enrich the problem search space, giving more flexibility for conflict avoidance.

- Further, we can extend the algorithm of conflict detection from 2D to 3D trajectories, leaving aside the constant-FL assumption of this thesis. Currently aircraft perform *step* climbs to approach their optimal FAPs. In the FFC conditions, flights could be authorized to follow their real continuous optimal FAPs. Thus, a challenge here is to deal with continuous 3-dimensional trajectories. In this case, a conflict may occur not only in the horizontal plane (considering flight levels to be separated *a priori*) but also in the vertical plane.

- The algorithm of trajectory modification can also be extended to 3D ATs. When deconflicting 3D ATs, we can try to modify not only trajectory shapes in the horizontal plane but also the FAPs. In the case of continuous FAPs, such altitude modifications could be rather small. Thus, we expect to lose less in terms of trajectory optimality than when jumping between discrete FLs.

- We can combine WO AT construction and deconflicting into a single global problem. Currently, these problems are addressed sequentially.

Finally, from the practical point of view, the proposed algorithms could be implemented as a support in the Airline Planning Process (APP). This would permit the airlines elaborating better trajectories for their flights in a collaborative manner, *i.e.* avoiding potential conflicts with other flights. As a consequence, the controllers workload could be decreased.

Appendix A

Air Traffic Control operations for different flight phases

In this appendix, the particular ATC operations established for each of the flight phases are described. Typical *flight phases* are presented in Figure 1.2. Each of them is delegated to a separate controller.

- The *ground controller* (*Preflight* phase) is responsible for governing safely the aircraft to the departure end of the appropriate runway, as well as for controlling other vehicles in the airport movement area.
- The *local controller* (*Takeoff* phase) is in charge of safely sequencing departing aircraft into the local traffic flow.
- The *departure controller* separates departing aircraft from all other aircraft while complying with appropriate facility procedures. The departure controller also yields the approval for local controller. Depending on the complexity of the controlled area, departure control may be performed by the approach controller (see below), by an independent position, or may be subdivided into several subsections.
- The *en-route controller* is responsible for separating aircraft en route within one control sector. While an aircraft cruise towards its destination, it passes from one sector to another (within the same ARTCC, or between adjacent ARTCCs), being handed off to different controllers when crossing sector boundaries (see below).

At low altitudes, aircraft are separated by *low-sector controllers*. Once climbed to higher altitudes, they are redirected to *high-sector controllers*. As an aircraft approaches the destination airport, each successive controller starts assigning progressively lower altitudes (*Descent* phase).

- The *approach controller* may be introduced as a separate facility, depending on the occupancy of the arrival airport, in order to match the inbound traffic flow with airport acceptance rate, by assigning necessary delays to a number of aircraft. Sometimes this facility is merged with departure control.

- The *final approach controller* is in charge of merging the incoming traffic flows into runway direction. Once an aircraft has landed on the runway, it is redirected to be controlled again by the ground controller.

When an aircraft changes its flight phase, or when it crosses a sector boundary while enroute, the responsibility for separating this aircraft passes from one controller to another. This action is known as *transfer of control*, and the process of control transferring from one controller to the next is called a *handoff*. The initial controller is referred as the *transferring controller*, and the next one is called the *receiving controller*. The detail of handoff regulations rests out of the scope of the present work.

Appendix B

Air Traffic Control generic systems

In this appendix, principle elements of ATC systems are introduced. All ATC systems must accomplish fundamental tasks such as traffic surveillance, communication, navigation, separation assurance, and information gathering. The *generic systems* of ATC are shown in Figure 1.3 and listed below (from [16, Chapter 13]):

- Communication Systems;
- Navigation Systems;
- Surveillance Systems.

Communication Systems provide the possibility for pilots and controllers to interact with each other: via these systems controllers issue *Clearances* (CLRs[1]) to aircraft (see Appendix I), and pilots send *Position Reports* (POSs) to ATC while cruising along the defined routes (see in the following). Below, several currently used communication systems are mentioned, characterized by their advantages and drawbacks.

- Voice radio channels in *Very High Frequency* (VHF[2]) band:
  - most-used way of communication;

[1] Authorization, or permission given to an aircraft crew by an ATC facility to operate over a predefined flight route.

[2] Usually, from 108 to 117.95 MHz

  - very reliable;
  - only one transmission can be conducted at a time;
  - confirmation by *readback* is required;
  - the number of aircraft managed on a single frequency is limited;
  - range is limited (only transmit along a *line of sight*);
  - a network of ground stations is required.

- *High Frequency* (HF[3]) shortwave radios:
  - used where the VHF communications are impossible (e.g., over oceanic airspace);
  - capable to communicate *over the horizon* (by reflecting off the ionosphere);
  - the quality is poor (due to interference by atmospheric disturbances, ionospheric propagation conditions, electrical storms);
- *Satellite-based voice Communications* (SATCOM).
- *Controller-Pilot Data Link Communications* (CPDLC):
  - high performance *Voice Data Links* (VDLs);
  - Satellite-based CPDLC.

The worldwide implementation of the last two systems, although being efficient in terms of communication quality, is limited by equipment and message costs, and blocked by lack of agreements and technical standards.

Navigation Systems permit the aircraft to fly exactly the cleared routes, or *Aircraft Trajectories* (ATs), by defining an underlying structure of *airways* and *waypoints* (WPs) (see Appendix H). According to their designation, Navigation Systems are subdivided into two types:

- En-route Navigation Systems, that must be capable of longer-range coverage, and
- Approach Navigation Systems, demanding a higher precision to avoid obstacles at low altitude.

[3] Up to 30 MHz

FIGURE B.1: VHF Omnidirectional Range ground station[4]

From a technical point of view, the following systems are currently in use by ATC:

- *VHF Omnidirectional Range* (VOR), the standard navigational system in the world, that enables appropriately-equipped aircraft to determine their position and stay on course by receiving radio signals transmitted by a network of fixed ground radio beacons (Fig. B.1) in the VHF band, but is limited to the line of sight;
- *Global Positioning System* (GPS), that provides satellite-based navigation;
- *Inertial Navigation System* (INS), that uses motion sensors (accelerometers) and rotation sensors (gyroscopes);
- *Non-Directional Beacon* (NDB), a radio transmitter at a known location (Fig. B.2), whose signals do not include inherent directional information and follow the curvature of the Earth, used mainly in non-precision approaches[5];
- *Instrument Landing System* (ILS), used worldwide for precision approaches.

Surveillance Systems are the mean by which controllers monitor the traffic situation. Below, a list of existing methods applied for surveillance is presented.

- *Position reports* (POSs), by which pilots communicate aircraft position, altitude and other complementary information to ATC. POSs are the primary means of

[4]From http://www.panoramio.com/photo/27950105

[5]The NDB signals can be received at much greater distances at lower altitudes than VOR. However, they are also affected more by atmospheric conditions, mountainous terrains, coastal refraction and electrical storms, particularly at long range.

FIGURE B.2: Non-Directional Beacon[6]

FIGURE B.3: Secondary radar[7]

surveillance in regions where other methods are not available (e.g. over the oceans, see Section 1.2).

- *Radars*, used for most domestic ATC. There are two types of radars:
  - *primary* radars, that measure distance by the round-trip time of a sent signal reflected off the surface;
  - *secondary* radars (Fig. B.3), that require aircraft to be equipped with a transponder receiving and retransmitting the signal with the aircraft identifier and other data.

[6] From http://www.approachnavigation.com/Products/NavigationSystems/

[7] From http://www.airport-technology.com/contractors/traffic/geci-espanola/geci-espanola3.html

- *Automatic Dependent Surveillance* (ADS), that emerges the technologies by which aircraft automatically transmit POSs. A number of different ADS exist:
  - *ADS-A* (Addressed), that transmits POSs to the ground when requested by ATC;
  - *ADS-C* (Contract), that transmits POSs to ATC at predefined time intervals and on special events;
  - *ADS-B* (Broadcast), that transmits aircraft position and other information in signals that can be received by ATC as well as other properly-equipped surrounding aircraft (see more detail in Appendix L).

Appendix C

Airline Planning Process

Airline Planning Process (APP) includes the following strategic decision steps (from [16]):

- fleet planning;
- route planning;
- schedule development.

An airline *fleet* is described by the total number of aircraft being operated at any given time, and specific aircraft types (see an example in Figure C.1). The most important aircraft selection criteria for an airline are:

- technical and performance characteristics, including:
  - aerodynamic design,
  - engine technology,
  - fuel capacity and consumption,
  - passenger/cargo configuration,
  - maximum takeoff and landing weights,
  - minimum runway requirements,
  - necessary ground equipment;
- financial and economic issues;

FIGURE C.1: Delta airline fleet[1]

- environmental concerns and regulations, such as:
  - noise performance,
  - type and quantity of aircraft emissions;
- marketing issues, for example
  - passenger preference;
- political influence and international trade issues.

A fleet planning evaluation process is ideally an ongoing effort that requires input from many sources within the airline. Because of the lack of detailed optimization models

[1]From http://worldairlinenews.com/2014/04/14/delta-paints-a-boeing-757-in-the-1966-livery-for-its-upcoming-85th-anniversary/

FIGURE C.2: BA CityFlyer route network at London City Airport[2]

describing this process, most airlines rely primarily on relatively sophisticated financial models to make fleet planning decisions.

Given a fleet plan that defines the availability of aircraft with different capacity and *range*[3] characteristics, the next step of APP is to determine the appropriate routes to be used (see an example in Figure C.2). *Route planning* is driven mainly by economic considerations and expected profitability which depends on the route-require demands and revenue forecasts. The route selection decision is both strategic and tactical, and is made on the basis of "route profitability models" that require knowing (for a certain period in the future):

- fleet and capacity constraints;
- forecasts of potential passenger and cargo demands;
- traffic flow support from connecting flights;

[2]From http://www.bacityflyerjobs.com/templates/BACity/about.aspx?raparam=6B4C5648425533566E7059514A4C3762414B4B624A6767734341644D584F726B

[3]The maximum distance an aircraft can fly without stopping for additional fuel while carrying reasonable payload of passengers/cargo

- forecast of expected revenues;
- physical infrastructure, ground resources, airport facilities, staff relocation;
- aircraft operating cost (crew, fuel, maintenance, passenger service).

Given a set of routes to be operated in an airline network and a fleet of aircraft, the next major step in the APP is *schedule development* that involves four sequential but interrelated tasks performed with different time horizons (prior to departure date):

- *frequency planning* (2-5 years), defining how often to operate flights on selected routes based on:
  - demand forecasts, including:
    - local demand between origin and destination,
    - connecting passengers demand;
  - expected market share;
  - aircraft availability;
  - elements of competitive strategy;
- *timetable development* (1-2 years), defining the flight departure times that requires a trade-off between:
  - passenger convenience:
    - providing departures at peak hours (09:00 and 17:00);
    - taking into account time zone differences (for long-haul flights);
  - maximal aircraft utilization, that can be achieved by:
    - minimization of *ground times*[4] (most often are kept to the aircraft *minimum turnaround times*[5]), or
    - keeping the aircraft on the ground until the next peak period;
- *fleet assignment* (tactical decision, 2-6 months), defining the type of aircraft to be used for each departure time by minimizing simultaneously:

[4]The times aircraft spend on the ground between arrival and next departure

[5]The times required at each airport to deplane and enplane passengers, refuel and clean aircraft that depend on aircraft types and flight characteristics

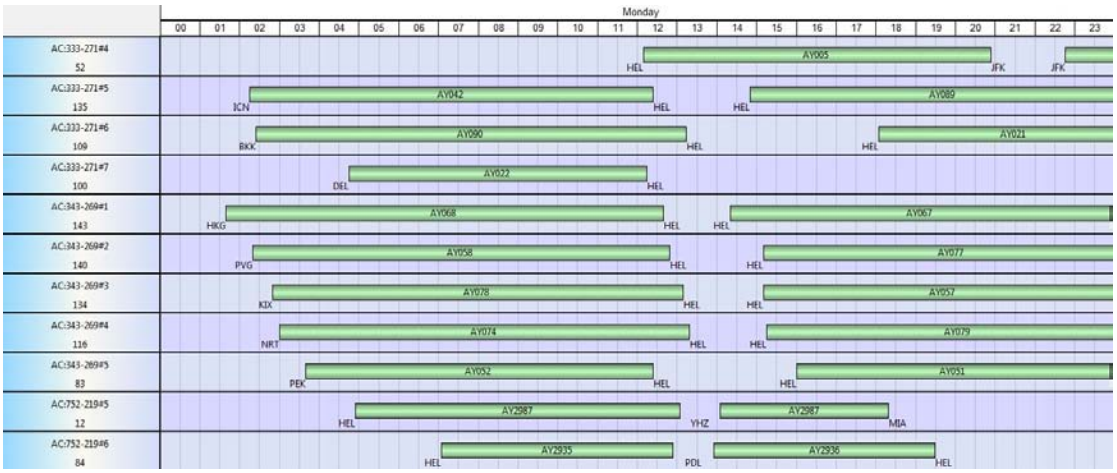

FIGURE C.3: An example of an airline schedule assigning the aircraft to the rotations[6]

  - the cost of *spills*[7], and
  - aircraft operating cost;

  subject to constraints such as:

  - minimum turnaround times;
  - maintenance requirements;
  - aircraft type availability in the fleet.

- *aircraft rotation planning*, ensuring an overall balance of each aircraft type arrivals and departures at each airport, made in parallel with fleet assignment (see Fig. C.3 as example).

Even if the airline schedule is developed much in advance, final revisions (up to cancellation) can be made up to the departure, because of unexpected operational constraints (e.g. maintenance, weather) and *irregular* operations. Flight cancellations and deviations from planned timetable are rather wasteful for airlines as they can completely disrupt aircraft rotations, crew schedules, maintenance plans and passenger trips. In such conditions, the primary airline objective is to return to *normal* operations as quickly as possible.

[6] From http://www.openairlines.com/optifleet.html

[7] Rejected demand, the loss of bookings (and thus, of potential revenues) due to the fact that the flight has been fully booked to capacity, that occurs when an aircraft assigned to a flight departure is too small

Appendix D

Flight Plan main contents

The *flight planning process* consists of selecting the *best path* (in terms of time, fuel burn, ride conditions, etc.) given the available information. It accounts for:

- aircraft type;
- forecast weather conditions;
- aircraft performance;
- load and operating weights;
- aircraft mechanical conditions;
- marketing constraints;
- airport limitations;
- company priorities, e.g. *cost index*[1] parameter.

The output of this activity is the generated *Flight Plan* (FPL) (see an example in Figure D.1). Its main contents are:

- FPL summary
  - flight type;

[1]The ratio of time-related costs to fuel-related costs, which is the major drive of FPL optimization, as minimum-time and minimum-fuel trajectories can be quite different

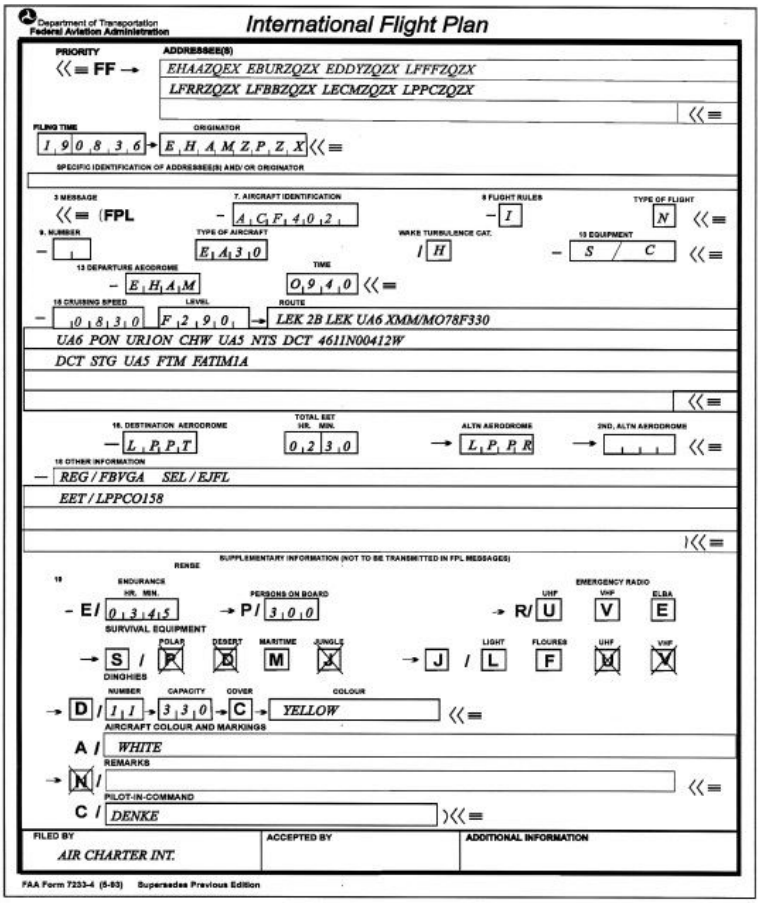

FIGURE D.1: An example of a filed flight plan[2]

  - registration;
  - departure airport;
  - arrival airport;
- fuel summary:
  - minimum required;
  - release amount;
  - planned fuel burn;
  - reserves;
- alternative destination routing;
- aircraft type and aircraft equipage;
- departure details (airport and time);

[2]From http://webapp1.dlib.indiana.edu/virtual_disk_library/index.cgi/4300833/FID2415/ATPUBS/fss/fssapdb.htm

- flight route, including (described below in more detail):
  - cruising speed (*Mach*);
  - cruising altitude (*flight level*, FL);
  - routing *waypoints* (WPs);
- destination detail:
  - main and alternative arrival airports;
  - estimated en route flight time;
- estimated flight times to ATC sector boundary crossings;
- flight detail at each WP:
  - WP identification;
  - FL;
  - forecast wind;
  - WP geographical coordinates (latitude/longitude);
  - magnetic course and heading;
  - aircraft speeds (see below);
  - forecast temperature and turbulence;
  - distance from previous WP and total remaining distance;
  - segment time from previous WP and total time from departure;
  - segment fuel burn and total fuel used from departure.

Appendix E

Flight Altitude Profile

Aircraft altitude is measured in feet with an *altimeter* through barometric pressure (lower pressures correspond to higher altitude). In order to provide accurate measurements, an aircraft altimeter must be referenced to the local surface pressure, which changes with weather. The *altimeter setting* is measured at weather reporting stations or airports and is transmitted to the aircraft by ATC. Above *transition altitude* and *transition level*, all altimeters are set to the *standard atmospheric surface pressure*[1] in order to minimize the chance of aircraft being on different altimeter settings in the same area[2]. Altitudes referenced in this way are termed *flight levels* (FLs). "Switching" from feet to FLs is made at *transition altitude* during climb; and "switching" from FLs to feet - at *transition level* during descent. Transition altitudes and levels are determined by local governing authorities[3] and are often identical.

FLs are measured in hundred of feet (1 FL = 100 feet), but they are defined for each thousand of feet and regularly written in the form FLxx0. For example, FL270 corresponds to the altitude 27,000 feet. The next available FL then is FL280, corresponding to 28,000 feet. If the number before the final zero in FL definition is even, then the FL is referred as *even flight level* (e.g. FL180, FL240). If this number is odd, the corresponding FL is called *odd fight level* (e.g. FL150, FL330). The maximum controlled FL

[1] 1,013.25 hPa, or 29.92 inHg, or 760 mmHg

[2] At high altitudes aircraft usually fly at fairly high speeds. As a consequence, the pilots would be required to adjust their altimeter setting every few minutes when passing from one area to another. This increases the possibility of incorrect setting, and therefore increases the potential collision probability. Setting the altimeter to standard pressure ensures that all aircraft are measuring altitude from a common datum

[3] For example, in the USA the transition altitude is established to be 18,000 feet. In Europe, the transition altitude varies and can be as low as 3,000 feet

is usually FL660. The cruise FLs used during *En route* phase of flight depend on the aircraft type (its optimal FAP) and the environmental conditions and are typically in the range from FL310 to FL410.

The FAP is determined by both ATC/airspace requirements and aircraft specific performance characteristics. Here, the following performance problems are typically stated:

- define the best cruise altitudes and speeds from the point of view of minimum fuel per unit time elapsed or per distance traveled for specified aircraft-engine combination;
- estimate the (minimum) amount of fuel and time required for a specific aircraft mission, including:
  - cruise fuel and time;
  - fuel quantities required for climb;
  - fuel required for descent;
  - reserve fuel estimation;
- find the best operational FAP of an aircraft (with or without constraints on range or cruising time), resulting in minimization of:
  - fuel consumed, or
  - time traveled, or
  - *Direct Operating Costs* (DOC[4]).

The first problem is the most basic and is usually treated as an instantaneous performance problem, assuming equilibrium of forces in horizontal flight. Extensive mathematical description of the problem can be found in [17, Section 2.6]. More mathematical models of optimum cruise performance for high-speed commercial aircraft are presented in [18], where the second problem (prediction of the fuel load) is treated as well. The third problem is the most complicated from the mathematical and numerical points of view, requiring calculus of variations or optimal control theory. Applications are mostly

[4] Also referred as *flight operating costs*, or *aircraft operating costs*; all expenses associated with operating aircraft, including *flying operations* (expenses incurred directly in the in-flight operation of aircraft, e.g. all costs associated with flight crew and fuel costs), *maintenance expenses* (expenses, both direct and indirect, specifically identifiable with the repair and upkeep of aircraft and equipment), depreciation and amortization (spreading the capital cost of aircraft over their expected lifetime)

found in the operational use, with the objective of achieving fuel reductions or devising optimum ATC procedures. We will not go deeper in the details as that is not the subject of the present study.

Based on the models of aircraft dynamics, the optimal FAP can be derived from maximization of aircraft cruising range. It depends on aircraft dynamic characteristics (aircraft wing area, aircraft mass, W, and speed) and environmental characteristics (air density, ρ). Without going into details, we give here a brief summary of such mathematical calculations: in an optimal FAP (given by optimal fuel consumption model) of an aircraft cruising at *constant speed* the altitude should increase as fuel is burned, keeping W/ρ constant. As a result, the optimal FAP (at constant speed) is a continuous function of aircraft mass, and thus, of a distance flown (green line in Figure 1.4).

Flying at non-optimum altitudes cause significant fuel penalties, thus, the ideal scenario would be to follow the continuous optimum FAP up to descent. However, in practice, this scenario is applicable only in the climbing cruise (in the *Takeoff* phase, Fig. 1.2) at low altitudes. After passing the transition altitude, the aircraft are prescribed to maintain constant cruising FLs en route, due to ATC constraints, performance and buffet limits. Such ATC regulations are applied in order to perform safe flight progress (see more details in Section 1.1.3). At the same time, it is desirable to keep the aircraft as close to its optimal FAP as possible while it gets lighter. To do so, the procedure of changing the cruising FL with *step climbs* is applied. We can mention three possible step climb profiles (from [19]):

- *Low profile*, that initiates the step climb at the weight where the next available FL is the optimum FL at that weight (magenta line in Fig. 1.4);
- *High profile*, that initiates the step climb at the weight where the next available FL is the maximum FL at that weight (red line in Fig. 1.4);
- *Mid profile*, that initiates the step climb at the weight where the specific range at the next available FL is better than that at the current FL (blue line in Fig. 1.4), and thus, enables the FAP remain as close to the optimal one as it is practically possible (recommended technique).

Thus, to summarize, the optimum cruising FLs filed in the FPL are calculated by airlines on the base of optimal (in terms of best fuel economy) FAP and depend on aircraft

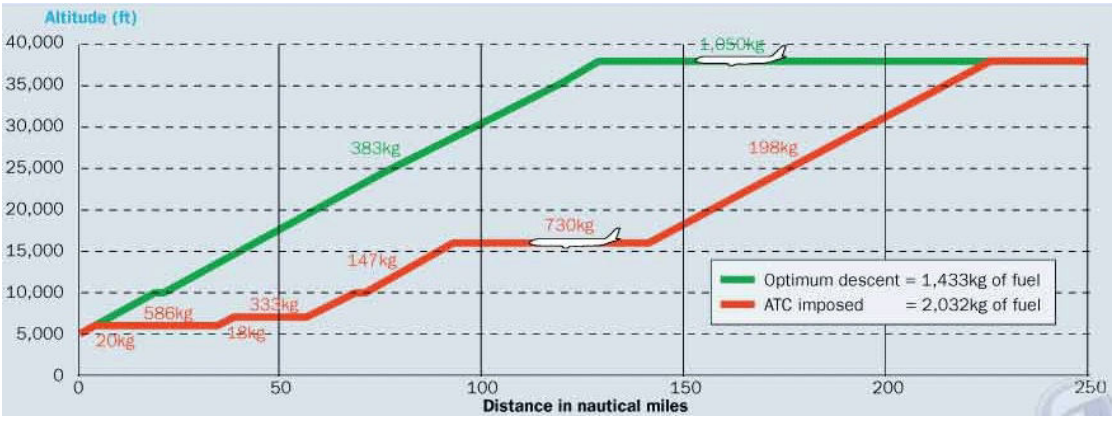

FIGURE E.1: Optimal vs. ATC imposed descent profiles for SAS fights into Newark using A330[5]

specific characteristics as well as on the optimal aircraft cruising speed (see more details in the next Section). In addition to this, a number of other factors, such as company priorities, ride comfort, traffic and airspace limitations, should be taken into account.

For the *Descent* phase, similar particularities can be mentioned: the optimal fuel-saving FAP is given by continuous descent, which is not applicable in practice because of ATC restrictions, and thus, is replaced by step descent with sections of constant-altitude cruise (see Fig. E.1 as an example).

[5]From http://www.flightglobal.com/news/articles/environment-special-scandinavian-airlines-takes-a-greener-221277/

Appendix F

Aircraft speeds

In air navigation, three terms describing *aircraft speed* are commonly used:

- *True Air Speed* (TAS),
- *Ground Speed* (GS) and
- *Mach number* (Mach).

TAS is the speed of the aircraft relative to the airmass in which it is flying. It is the true measure of aircraft performance in cruise, before considering the effects of wind. Thus it is the speed listed in aircraft specifications, manuals, performance comparisons, pilot reports, FPLs and every situation when actual performance needs to be measured. TAS is traditionally measured in knots.

GS, $\vec{V}$, is the horizontal speed of an aircraft relative to the ground, thus it is the speed defining the actual aircraft position en route. It can be determined by the vector sum of the aircraft TAS, $\vec{v}$, and the current *Wind Speed* (WS), $\vec{W}$, and direction, often referred as *speed triangle* (Fig. 1.5):

$$\vec{V} = \vec{v} + \vec{W}. \tag{F.1}$$

For example, a *headwind* subtracts from the GS, while a *tailwind* adds to it[1]. Depending on the wind, GS can be quite different from TAS. It is measured in knots, mph or m/s according to the applications.

As an aircraft moves through the air, the air molecules near the aircraft are disturbed and move around the aircraft. If for low speeds (less than 250 mph), the density of the air remains constant, for higher speeds, some of the energy of the aircraft goes into compressing the air and locally changing the density of the air. This *compressibility effect* alters the amount of resulting force on the aircraft and becomes more significant with speed increasing. One of the most important characteristics, determining the the magnitude of compressibility effects, is the ratio of the speed of the aircraft to the speed of sound in the gas. This ratio is designated it with a special parameter called the *Mach number* (Mach[2]). By definition, a Mach is a dimensionless quantity:

$$M = \frac{v}{c}, \tag{F.2}$$

where c is the speed of the sound in the surrounding air that depends on the air conditions, in particular the temperature and pressure. More practical formulas relating Mach, TAS and altitude can be found in Appendix G.

According to the value of Mach, NASA has defined several *flight regimes* in which compressibility effects vary:

- Subsonic ($M < 0.8$)
- Transonic ($0.8 < M < 1.2$)
- Supersonic ($1.2 < M < 5$)
- Hypersonic ($M > 5$).

Civil aviation, being the subject of the current study, deals mainly with *subsonic* aircraft ($M < 1$). Here, the term *Mach Number Technique* (MNT) is used to describe a technique whereby subsonic turbojet aircraft operating successively along suitable routes are

[1] A *tailwind* is a wind that blows in the direction of aircraft travel, while a *headwind* blows against the direction of travel. Thus, a tailwind increases the aircraft speed and reduces the time required to reach its destination, while a headwind has the opposite effect.

[2] In honor of Ernst Mach, a late 19th century physicist who studied gas dynamics

prescribed to maintain appropriate Machs for a relevant portion of the en-route phase of their flight. The principal objective of the use of MNT is to achieve improved utilization of the airspace. Practical experience has shown that when two aircraft, operating along the same route at the same altitude, maintain the same Mach, they are more likely to maintain a constant time interval between each other than when using other methods, as they are subjected to approximately the same wind and air temperature conditions, and minor variations in GS tend to be neutralized over long periods of flight.

In the same manner than the optimal FAP depends on the particular aircraft characteristics, the optimal flight speed profile also depends on aircraft dynamic parameters (in particular, aircraft weight) and is established by airlines within the APP and FPL elaboration. Typical takeoff TASs for jetliners are in the 130-155 knot range. For a given aircraft, the takeoff speed is usually directly proportional to the aircraft weight; the heavier the weight, the greater the speed needed. By the end of the *Takeoff* phase (Fig. 1.2) the aircraft is accelerated to maximum low-altitude climb speed which is nominally 250 knots (below 10000 feet in the USA) unless restricted by the ATC. When the *Departure* phase is reached, the aircraft is accelerated from 250 knots to the optimal climb speed, that can range from 270 to 350 knots.

Depending on the outside air temperature and indicated TAS, the aircraft typically changes over from TAS to Mach reference[3] between FL270 and FL330 (from [16, Section 8.3]). Once cruise altitude reached, the Mach target is established, which usually remains constant during the *En route* phase of flight. Anyway, sometimes the cruise Mach can be changed to more desirable one if accepted by ATC. Commercial or passenger aircraft are designed for optimum performance at their cruise speed, that is typically 475-500 knots. Thus, most common cruise Machs are ranged between 0.75 and 0.85.

[3]The TAS/Mach transition occurs to account for the difference in the nature of the critical limits at low and high altitudes. Most cruise performance data is specified in terms of Mach because the critical limits during this phase are associated with transonic flows over portions of the wings. At lower altitudes, the critical limits are associated with pressure loads on the airframe governed by the TAS.

Appendix G

Relations between True Air Speed, Mach Number and Altitude

In this Appendix we present short mathematical calculations permitting to obtain aircraft TAS, V_{TAS} (measured in m/s) from given Mach, M, and flight altitude, a (km).

From the definition of Mach and formulas (F.2) we immediately derive:

$$V_{TAS} = M \cdot c. \tag{G.1}$$

The speed of the sound, c (m/s), is related to the absolute atmosphere temperature, T (K) by:

$$c = \sqrt{\gamma RT}, \tag{G.2}$$

where γ is the ratio of the specific heats of air at constant pressure and volume, equal to 1.4, and R is the gas constant of air, equal to 287.05 $m^2/K{\cdot}s^2$ (see [17, Section 2.1]).

In practice, the absolute atmosphere temperature can be measured directly on board of the aircraft during flight (see Section ... for more details), and thus, its TAS can be precisely calculated. During flight planning process (as well as in the simulations presented

in the current work) the exact temperature value is unknown, thus, we should rely on mathematical models for its approximation. Here, we will refer to *International Standard Atmosphere* (ISA) model (see [118] for more details), which basic idea is dividing the atmosphere into layers with linear temperature distributions.

At see level ($a = 0$) the ISA gives a pressure, P_0, of 1013.25 hPa and a temperature, T_0, of 15°C equal to 289.15 K. Furthermore, in the troposphere, where the commercial subsonic aircraft cruising take place, the initial *lapse rate*[1], Γ, is set to be -6.5 K/km, meaning that the temperature decreases linearly by 6.5 K for each 1000 m. Thus, T can be obtained by:

$$T = T_0 + \Gamma \cdot a. \tag{G.3}$$

That gives the following relation for TAS, Mach and altitude:

$$V_{TAS} = M \cdot \sqrt{\gamma R(T_0 + \Gamma \cdot a)}, \tag{G.4}$$

or, numerically:

$$V_{TAS} \approx 20.05 \cdot M \cdot \sqrt{289.15 - 6.5 \cdot a}. \tag{G.5}$$

In (G.5) the units are ommited to avoid formula overloading, but one should keep in mind that the altitude a here is measured in km, and the resulting speed V_{TAS} is in m/s. If one needs to provide the TAS in knots, the conversion is simple:

$$V_{TAS}^{knots} = V_{TAS}^{m/s} \cdot 3600/1.852. \tag{G.6}$$

Finally, if the altitude is given in terms of flight level (FL), again a simple conversion to km is needed:

$$a = FL * 100 * 0.3048/1000. \tag{G.7}$$

[1]The rate at which atmospheric temperature decreases with increase in altitude

Appendix H

Lateral Flight Profile

Theoretically, an optimal *Lateral Flight Profile* (LFP) is to be elaborated by airlines according to the preferred strategies, minimizing:

- total travel distance (actually, resulting in straight routes from origin to destination), or
- total cruising time, or
- fuel consumption,

under several additional constraints arising from:

- special airspace restrictions, e.g. reserved military areas;
- air traffic restrictions, i.e. highly congested areas (see Section 1.1.3);
- meteorological (weather) conditions (see Appendix J).

That is a complex non-linear optimal control problem, that has been treated in a number of studies, some of which are discussed in Chapter 4. LFPs of *Aircraft Trajectories* (ATs) constructed in this way are often referred as *Wind Optimal Routes* (WORs), or *climate optimal routes*, or *free flight routes*, and the ANS allowing aircraft to follow their WORs is known under the term of *Free Flight Concept* (FFC). However, application of FFC in reality till recently was practically impossible because of technical ATC limitations (see

Section 1.1.3). Thus, currently the ATs are defined according to rigid constraints, that are appropriately established by ATM for each flight phase.

The en-route portion of ATs is constrained by the *En-Route Airspace Structure* (ERAS) specific for the region the flight is operating. The ERAS consists of a set of established *airways* (also called *air routes*, or *tracks*, or *corridors*). Airways can be thought of as three-dimensional highways for aircraft. They are defined with segments within a specific altitude block, corridor width, and between fixed geographic coordinates for satellite navigation systems, or between ground-based radio transmitter *Navigational Aids* (Navaids[1]) (such as VORs or NDBs, see Appendix B) or the intersection of specific radials of two navaids.

For continental airspace, the ERAS usually consists of two layers (strata), defining different airway systems for low and high altitudes. Altitude separating the low and high airway structure varies from county to country. For example, in Switzerland it is 19500 feet and 25000 feet in Egypt. For European airspace, these airway systems are called (from [20, Chapter 1]):

- airways (see en example in Fig. H.1) - low altitude airways, usually covering altitudes from FL070 to FL100, extending to FL195 (link major airports giving protection to flights during the climb and descent phases, and often for non-jet aircraft, cruise phase of flight);
- *Upper Air Routes* - high altitudes airways, typically above FL195.

In the ERAS of National US airspace, such systems are referred as (from [21, Chapter 2]):

- *Victor Airways* - low altitude airways, covering altitudes from 1200 feet up to 18000 feet;
- *Jet Routes* (see en example in Fig. H.2) - high altitudes airways, running from 18000 feet to 45000 feet.

Besides these commonly used ERAS continental airways, there exist a number of other airway systems, e.g., oceanic airways (described in details for NAT in Section

[1] Any device external to an aircraft specifically intended to assist navigators in determining their position and safe course, or to warn them of dangers or obstructions to navigation.

FIGURE H.1: European low altitude airways depicted on an aeronautical chart[2]

1.2.2), *Standard Instrument Departure routes* (SIDs), *Standard Terminal Arrival Routes* (STARs), etc., that are not considered here in details.

Unless authorized by ATC, the aircraft must either fly along the centerline of corresponding ERAS airways, or, on routes other than airways, along the direct course between navaids or fixes defining the route. Such navaids and fixes, including those defining the airways, are usually called *Waypoints* (WPs). The WPs can be defined in several different ways (from [22, Chapter 15]):

- Named WPs - explicitly given by the existing in the ERAS named navaids (VORs, NDBs) and named fixed (defined by their geographical coordinates);
- PBD WPs - specified as bearing/distance off existing named fixes, navaids, or airports;
- PB/PB WPs - specified as the intersections of bearings from two defined WPs;

[2]From http://www.peter2000.co.uk/aviation/ifr-flying/

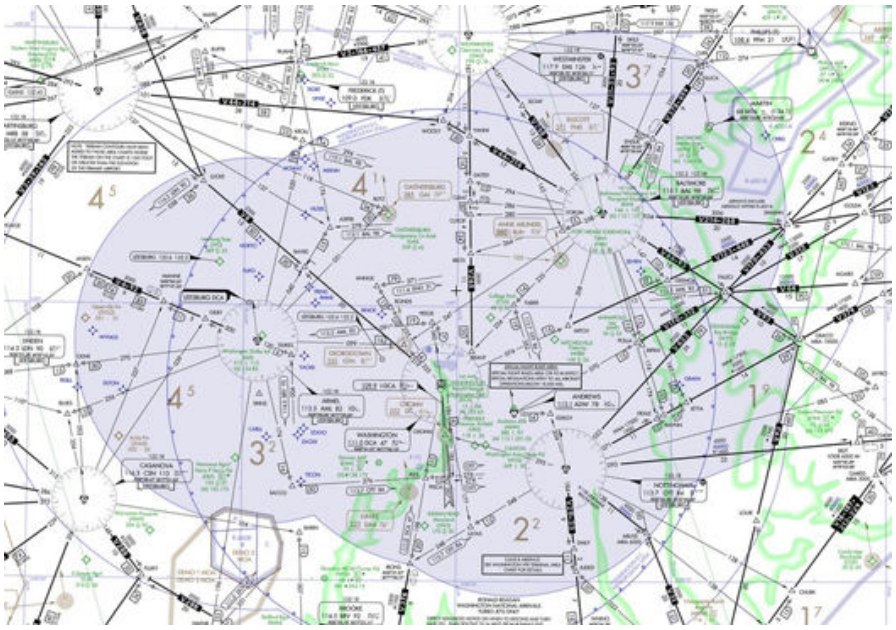

FIGURE H.2: Jet routes around Washington, DC, depicted on an aeronautical chart[3]

- ATO WPs - specified by an *Along-Track Offset* (ATO[4]) from an existing FPL WP;
- Lat/Lon WPs - specified by the latitude/longitude coordinates of the desired WP;
- Lat/Lon Crossing WPs - created by specifying a latitude or longitude, placed where the active FPL crosses that latitude or longitude;
- Intersection of Airways - created by specifying two airways, placed where the airways cross for the first time;
- FIR/SUA Intersection WPs - created and placed where the current FPL crosses FIRs boundaries and SUAs[5].

Thus, an AT in horizontal section is defined in the FPL as a sequence WPs to be followed by aircraft (see an example in Fig. 1.6). As a first approximation, an LFP can be treated as a sequence of straight segments, called *legs*, connecting fix WPs. These legs are actually the arcs of GC joining these WPs. This definition has particular sense

[3]From http://m.ammoth.us/blog/page/10/

[4]The created WP is located at the distance (*offset*) entered and along the current FPL path from the WP used as the fix. A positive distance results in a WP after the FPL fix, while a negative distance results in a WP before the fix point.

[5]*Special Use Areas*, designated for operations of a nature such that limitations may be imposed on aircraft not participating in those operations (often being of a military nature). SUAs include: restricted airspace, prohibited airspace, military operations areas, warning areas, alert areas, temporary flight restriction, national security areas, and controlled firing areas. They are defined and stored in the navigation data base.

for *En route* phase of long-distance flights, while for short distances the GCs can be approximated by straight lines in Cartesian coordinates. In the reality, an LFP contains much more data, i.e. in addition to legs, it also includes the turn segments beginning and ending at fixed or floating geographical points. Computing these segments can be difficult because the turn transition distance and certain leg termination points depend on TAS, WS and altitude. We neglect these segments in the present work.

Appendix I

Clearance

The Clearance (CLR) is issued to the aircraft by the ATM prior to take-off, as a result of its initial FPL elaboration. It finalizes the definition of ATs to be flown by aircraft and must include the following information (from [15, Chapter 3]):

- flight identification;
- CLR limitations - the farthest location to which the aircraft is authorized to fly (typically, the destination airport, if not, than an additional CLR should be received before reaching the limit);
- departure procedures;
- route of flight, that may include any airway and WPs (same as in FPL definition);
- altitude assignment (should never be lower the minimum en-route altitude);
- holding instructions - if an aircraft is to be hold over a particular fix;
- the departure control frequency and transponder code assignment.

Usually, the ATM controllers attempt to clear the aircraft so that it could execute its desired FPL, but that is not always possible because of meteorological conditions, airspace capacity restrictions, traffic density and congestion. Thus, in some cases the issued CLR differs from the filed FPL; then the pilots should modify the flight setting

entered in the FMS[1] in accordance to the CLR received. If the FPL modifications are inevitable, the ATM attempts to perform them on the FPL components in the following order:

- time (usually, by delaying the aircraft on the ground);
- LFP (by assigning different airways and WPs for a part of/total route);
- FL (by assigning FLs below or above the optimal one);
- TAS/Mach (by assigning the speed higher/lower the optimal one).

Altitude and speed modifications were shown to induce significant losses in efficiency of fuel consumption, leading to increase of DOC. Thus, the ATM controllers attempt to keep them as close to filed optimal values as possible, and prefer flight rescheduling or rerouting in horizontal plane. If necessary, additional CLRs are to be issued in the course of the flight, that can bring complementary modifications of ATs. For example, demanding and receiving corresponding CLRs is obligatory when crossing some particular FIR bounds (see Section 1.2.3 for more details).

[1] *Flight Management System*, a specialized computer system that automates the in-flight tasks, reducing the workload on the flight crew, which primary function is in-flight management of the flight plan.

Appendix J

Difficult meteorological conditions

In this Appendix, several most important particular meteorological conditions that can affect aircraft FPL (see Fig. 1.7) are listed (from [23]).

- Changing wind fields, which are the most prevalent and complex natural disturbance to aircraft FPL. They can originate from:
  - gust fronts,
  - sea-breeze fronts,
  - air-mass fronts,
  - gravity or solitary waves,
  - terrain-induced wind shear,
  - mountain waves,
  - low- and high-altitude *Jet Streams* (JSs) (see Appendix M for more details),
  - tornadoes, microbursts.
- Non-convective turbulence, which is a major aviation hazard, as it can be present at any altitude and in a wide range of weather conditions, often occurring in relatively clear skies as *clear-air turbulence*. Any aircraft entering turbulent conditions is vulnerable to damage.
- Thunderstorms, and other convective weather, that provoke:
  - severe turbulence (convective),

  - intense up- and downdrafts,
  - lightning,
  - hail,
  - heavy precipitation,
  - icing,
  - mountain waves,
  - wind shear, microbursts, strong low-level winds, tornadoes.
- In-flight icing:
  - structural icing on wings and control surfaces, that increases aircraft weight and generates false instrument readings,
  - mechanical icing in engine (carburetors, fuel cells), that leads to reduction of power.
- Low ceiling and reduced visibility.
- Volcanic ash, which is composed of:
  - pulverized rock materials (with melting temperature below the operating temperature of a jet engine at cruise altitude), and
  - acidic gaseous solutions (sulphur dioxide, chlorine).

Most bad weather conditions are to be strictly avoid (by delaying aircraft on the ground, or deviating it from desired AT and/or optimal cruise FL), others can be traversed, but than their affect on aircraft performance efficiency should be taken into account (in terms of fuel consumption and cruising time modifications). The main meteorological component the aircraft and ATC are always to deal with is the *wind*. The forecast winds should be taken into account during FPL elaboration, as they effect the GSs and thus, the estimated times of passing the WPs recorded in FPLs. The wind forecast is based on the meteorological numerical forecast models (e.g. MOGREPS[1], ECMWF[2], WRF[3]), that may have different levels of precision. Evidently, such models always contain prediction uncertainties (difference between forecast and really observed winds),

[1] The UK *Met Office Global and Regional Ensemble Prediction System* models
[2] *European Center for Medium range Weather Forecasting* forecast model
[3] A next-generation *Weather Research and Forecasting* model

that in turns result in flight time (as well as fuel consumption) estimation errors. More details on wind prediction errors and the methods aimed to overcome these uncertainties are given in Chapter 3.

Appendix K

Congestion

Airspace *Congestion* is the crucial notion for ATM. It is primarily related with *airspace capacity*, that can be mainly identified with the two following interrelated notions:

- airways network capacity, and;
- ATC sectors capacity.

The *capacity of a single airway* is defined as the number of aircraft that can be accommodated by this airway being safely separated. It is determined by several factors, among which:

- MSS between consecutive aircraft within this airway;
- aircraft performance characteristics (speed, weight);
- airway geometrical characteristics;
- types of maneuvers (climbing/descending, rerouting);
- intersections with other airways in the network.

Thus, the airways capacity is primarily limited by MSS, and the congestion induced by such capacity overloads corresponds to the rate of potential conflicts (MSS violations). On the other hand, the *capacity of an ATC sector* is mainly limited by the *controller*

[1]From http://www.avsim.com/pages/0702/asrc/asrc_preview.html

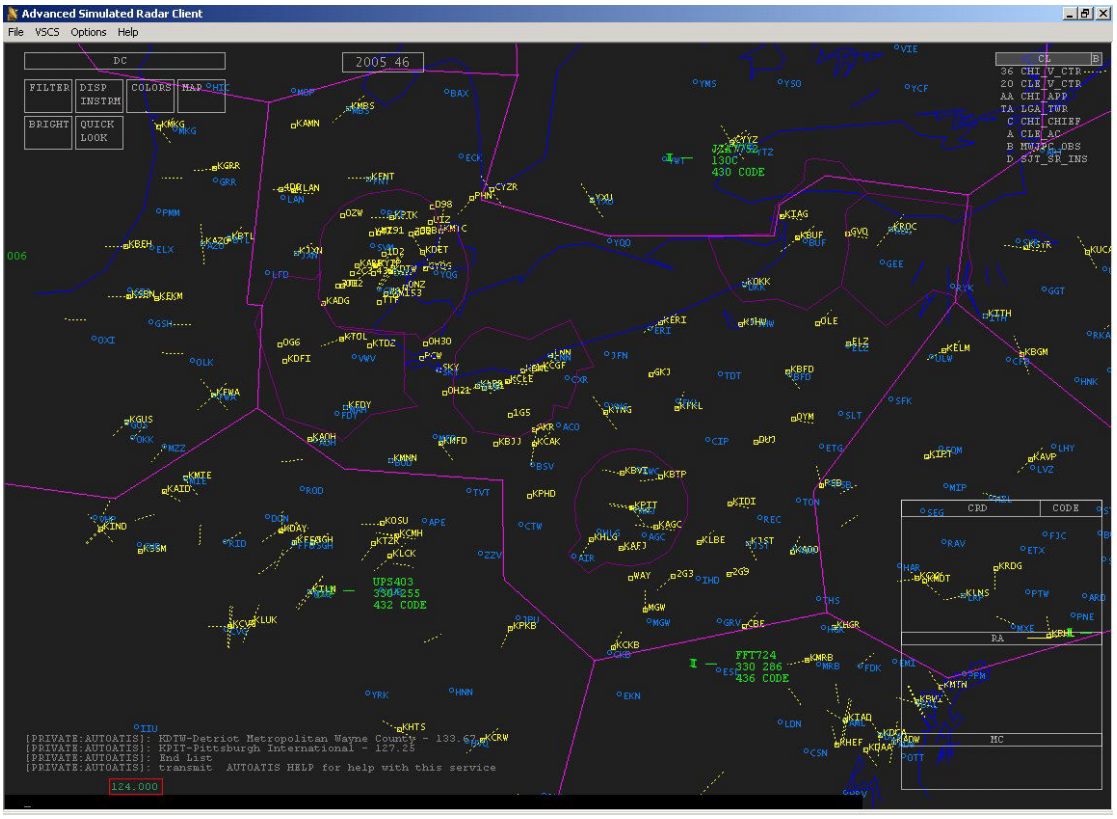

FIGURE K.1: Display of air traffic within a control sector[1]

workload, which is defined through *complexity of traffic patterns*. In the first approximation, the sector capacity is measured as a maximal number of aircraft flying across the sector during a given period of time, that a controller is capable to deal with[2] (Fig. K.1). But in reality, simple measure of traffic rate does not fully describe the controller's workload. [24] presents an exhaustive overview of different factors, influencing the controller's workload, among which:

- air traffic complexity;
- cognitive information display and processing strategies;
- equipment quality;
- individual characteristics (e.g. age, amount of experience).

Further, we will focus on *air traffic complexity*, as it can be also considered as a measure of airspace congestion. As revealed in the previous studies, air traffic complexity is related to numerous factors, among which:

[2]Typically, one controller can safely manage 10-20 aircraft simultaneously presented in the sector he is responsible of in radar-supported environment

- sector size and geometry;
- number of airport terminals within a sector;
- restricted areas (e.g. military areas);
- traffic volume and density;
- traffic distribution;
- traffic mixture (aircraft arriving in/departing from/overflying an ATC sector);
- mixture of aircraft types;
- number of communications with aircraft;
- coordination with other controllers;
- climbing/descending ATs;
- number of intersecting ATs;
- number of AT changes;
- number of en-route aircraft requiring/not-requiring control functions;
- preventing of crossing conflicts;
- preventing of overtaking conflicts;
- weather conditions.

Thus, sophisticated *Air Traffic Complexity Metrics* (ATCMs) are needed to capture the effects of different traffic configuration and reflect more precisely congestion situations. Roughly speaking, an ATCM is a measure of the difficulty that a particular traffic situation presents to ATC. A great amount of studies are devoted to elaboration of appropriate ATCMs. There overview can be found in [25, 26]. However, we will not go deeper into details in the current work.

The management of airspace capacity, potential conflicts, congestion and induced delays is one of the most important ATM functions. Here, the three levels of management are distinguished:

- strategic level, responsible for system capacity evaluation on a time horizon of several hours to several days;
- pre-tactical level, responsible for flow planning at timescales from 30 minutes to 2 hours;
- tactical level, responsible for traffic planning at the 5- to 20-minute time scale.

Strategic management is performed by ATFM before the aircraft takes off. ATFM calculate traffic loads based on filed FPLs and compares the resulting demand with expected system capacity, taking into account weather forecast and other related factors. Once potentially congested areas are identified, strategies to manage the traffic are generated. On strategic level, mainly two types of intervention are provided (discussed in Appendix I):

- *ground holding*, i.e. delaying flight departure time by a specified time slot;
- *rerouting*, i.e. changing or restructuring some flight routes (FLs, WPs, airways).

Tactical management is destinated to prevent the aircraft being already en route to enter into restricted (due to high congestion level, bad weather conditions, etc.) areas as well as to resolve potential conflicts between flying aircraft. It is the ATC responsibility. Here, again the two types of intervention can be stated:

- *delaying* techniques, and;
- *rerouting* techniques.

Rerouting may result in:

- step climbs/descends;
- changing of airways/WPs sequence;
- vectoring.

Vectoring is a technique by which a pilot is permitted to make a turn that takes an aircraft off course by a defined distance and then to return to course (Fig. K.2). This

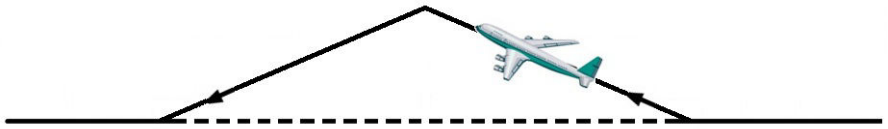

FIGURE K.2: Aircraft trajectory modification by vectoring

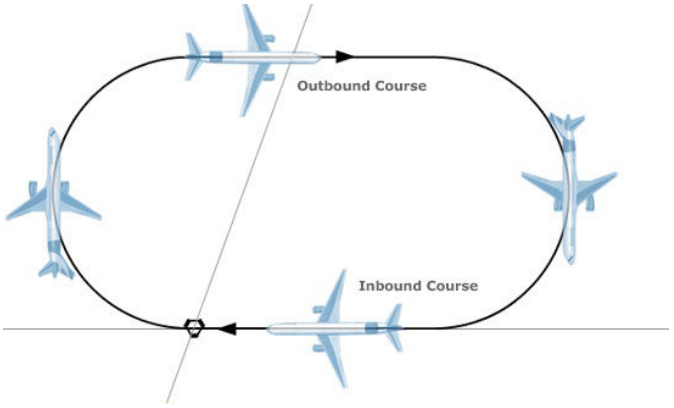

FIGURE K.3: A holding pattern[3]

technique is preferable as it causes minor local AT modifications and thus, is the most efficient in terms of supplementary fuel costs. On the other hand, as vectoring demands an aircraft to stay off an airway during a short time period, it can be used only if there is sufficient space to accomplish the maneuver, and is applied mainly in radar-supported environment.

Delaying techniques on tactical level are more complicated than those of the strategic one, as an aircraft cannot be stopped en route. The following strategies can be applied:

- *speed control*, i.e. issuing speed restrictions (not very preferable, as affects not only the performance of the restricted aircraft, but also of those, following it within the same airway);
- *vectoring* (same as described above, also used as delaying technique, as additional distance results in additional time);
- *holding*, i.e. providing an aircraft with a *holding pattern* (a fairly small area of airspace, safely separated with surrounding traffic and other holding patterns) where it is prescribed to turn around until permitted to continue towards its destination (Fig. K.3).

[3]From http://fleet.freeworld-airways.com/training/holds.html

Appendix L

Automatic Dependent Surveillance-Broadcast technology

ADS-B is a key component of ATM modernization program, intended to move the ATC from a radar-based system to a satellite-derived aircraft location system.

ADS-B uses GPS satellite signals to provide controllers and pilots with much more accurate information that is used to keep aircraft safely separated in the airspace. Aircraft transponders receive GPS signals and use them to determine precisely the aircraft position. These and other data are then broadcasted within data link technologies and can be received by ground ATM facilities as well as by other aircraft within a specified area (Fig. 1.14). Data link permits the broadcast reports to be sent with a rather high update rate, thus possible flight deviations from cleared FPL can be detected very quickly, and corrective procedures can be implemented more faster as well. Controller and pilots are to be provided with computer monitors displaying the aircraft location in real time. Thus, for the first time both pilots and controllers will see the same air traffic situation, that will substantially improve safety and permit reducing of MSS.

In first turn, implementing of ADS-B is supposed to bring a significant improvement of the ATM in airspaces where radar surveillance is unavailable, e.g. in oceanic airspaces, as described in [119]. From a user's perspective, the initial benefit will be reduced fuel costs, while global airline industry will gain on ANS acceptance of increased traffic

volume. The paper [27] presents a sophisticated analysis of benefits and costs related with integrating of ADS-B technologies into ANS over Atlantic and Pacific oceanic airspaces, and the estimated budget savings are revealed as a result of such an analysis.

In addition to this, even in radar-covered airspace the efficiency of modern ADS-B tends to overcome that of traditional radars. Indeed, an ADS-B update rate can be as fast as 0.5 sec while that of radar is at least 4 sec; and position accuracy of ADS-B is about 33 m in contrast to that of conventional radar being 200 m [120]. Nevertheless, the reliability of ADS-B informations is defined by GPS, and thus, include GPS errors. There are several sources of GPS errors:

- ionosphere and troposphere disturbances (actually, the main error source), that slow down the satellite signal;
- signal reflection (from high objects, like mountains), that causes signal delays;
- ephimeric (or, orbital) errors, i.e. the errors in satellite position;
- clock errors, meaning that the GPS receiver built clock is not as accurate as satellite atomic clocks;
- satellite visibility, related to the number of satellites GPS receiver can see at one time;
- satellite shading, resulting from poor geometry (e.g. tight grouping) and leading to signal interference.

In order to increase the GPS (and ADS-B) accuracy, the GPS system incorporates built-in models that are destinated to take into account the majority of possible errors, in particular, atmosphere disturbances. Some of them exist already, others are being elaborated. For example, [121] proposes to use Unscented Kalman Filter to improve aircraft position information. However, these models stay out of the scope of the current study.

ADS-B communication function includes two services:

- *ADS-B Out* periodically broadcasts information about each aircraft, such as identification, current position, altitude, and velocity, through an on-board transmitter

[122]. Its broadcast rate is not only automatic, but also depends on aircraft onboard equipment, where the cooperative and dependent nature of ADS-B comes from.

- *ADS-B In* provides appropriately equipped aircraft with the ability to receive and display the information broadcasted by ADS-B Out of other aircraft as well as by special ADS-B services of ground systems (see below). The necessary aircraft equipment is known as Universal Access Transceivers (UATs) operating at frequency 978 MHz.

Three types of ground broadcast services provide benefits to ADS-B In equipped aircraft (more information can be found in [123]):

- *Automatic Dependent Surveillance-Rebroadcast* (ADS-R) collects traffic information from each ADS-B Out equipped aircraft and rebroadcast it to ADS-B In-equipped operators via another broadcast link. Traffic delivery is performed within 15 NM radius and 5000 feet above/below relative to the receiving aircraft position.

- *Traffic Information Service-Broadcast* (TIS-B) uses radars or any other navigation systems (including ADS-B Out), to provide proximate aircraft altitude, track, speed, distance and traffic situational awareness. This data may not provide as much information as could be received directly via an aircraft ADS-B Out broadcast, but it permit ADS-B In equipped aircraft to see all the aircraft flying nearby, even if those are not equipped with ADS-B Out. One should note that TIS-B is an advisory service that is not destinated for aircraft surveillance or separation, and cannot be used for either purpose.

- *Flight Information Service-Broadcast* (FIS-B) broadcasts weather information, notices to airmen, temporary flight restrictions, and other relevant flight information, at no additional cost.

All these services are aimed at ameliorating pilots' situation awareness of in-flight hazard and facilitating accidents preventing. ADS-B is currently being implemented all around the world, starting with regions with lack of radar surveillance, and it has already yields remarkable benefits, that can be expressed in savings in distance, time, fuel and flight cost [9].

Appendix M

Jet Streams

Jet Streams (JSs) are fast narrow predominantly west-east air currents mainly located in the upper troposphere that are caused by a combination of the earth rotation and atmospheric heating (Fig. 1.16). There are mainly two physical processes, that the JSs are originated from, and thus, the two two types of JSs are distinguished in NAT correspondingly.

- *Subtropical Jet Streams* (STJSs) are baroclinic flows, associated with the strong temperature gradients. They are risen by the westerly acceleration of poleward moving air in the upper tropical circulation, that are associated with the local vorticity balance. The STJSs form a spiral spanning the entire globe. They are usually relatively low-powered and restricted to the upper troposphere. The details, identifying and characterizing such JSs can be found, for example, in [124].
- *Eddy-driven Jet Streams* (EDJSs) are provoked by the momentum and heat forcing from transient mid-latitude eddies, that tend to accelerate more the winds at low levels, in particular. EDJSs extend throughout the depth of the troposphere down to the surface and has equivalent barotropic structure. The upper-level wind is much stronger than that at the surface, as the wind speed tends to increase with altitude. The detailed diagnostics of such JSs can be found in [125].

According to the study from [125], there are three preferred latitude locations of the NAT JS currents[1]: *northern*, *central* and *southern*. In both northern and central JSs

[1] *Trimodal* distribution of JSs latitude seems to be unique for NAT, as in other areas of the globe the *bimodal* distribution is revealed.

EDJSs are distinctly separated from STJSs, while in southern JS, the separation is not clear. During the year, all the JS currents shift north and south, with a period of several days. The meridional shifts of the EDJSs are provoked by the variations in the eddy forcing, which main effect however is to keep the JS at its basic location.

Another climate phenomenon that impacts JSs locations is *blocking*. Blocking events in NAT occurs when a large mass of subtropical air is moved north across the JSs, diverting the JS to the south. It is related with the passage of cyclones (low pressure) anticyclones (high pressure). Blocking provokes a large-scale *wave-breaking event*. For example, the southern JS seems to be associated with high blocking occurrence over NAT[2].

Roughly speaking, the JSs are the result of atmospheric circulation variability, including the anomalies in pressure, temperature and geopotential height field. These anomalies are discovered to be spatially correlated and are organized into *teleconnection patterns*. As these patterns reflect the periodic oscillations of atmospheric variables (shortly speaking, the waves), it is common to distinguish *positive* and *negative phases* of the patterns. Teleconnection patterns are related with preferred planetary wave configurations, which relatively small changes may lead to important impact on regional weather. They may be initiated by *external forcing* of the atmosphere or by disturbances due to barotropic instability [124].

Recurrent regional external forcing of the atmosphere can arise from the temperature land-sea contrast and is called *thermal forcing* in this case. For example, on the eastern coast of North America, there is a sharp change between the region of cooling (the continent) and the region of warming (the ocean). The cooling at high latitudes increases the temperature gradient to the south, inducing a local baroclinic zone, while the heating reduces the gradient, making this zone weaker. This contrast is the strongest at the surface and disappears with altitude [126].

Another source of external forcing is the ground *topography*, or *orography*, i.e. the shape and height of the mountains. The air mass flow can be diverted vertically (over the mountain) or horizontally (around the mountain). This deviation may cause potential perturbations in temperature. In addition to this, there is a critical height, which exceeding provokes *blocking*. In general, the orography tends to localize and intensify

[2]That is one possible explanation of the existence of the third JS location, in contrast to the two typically observed.

the JSs on the downstream side of the mountain and to weaken them elsewhere. As shown in the previous studies, the Rocky Mountains in particular seem to play an important role in the north JSs formation [127].

In NAT, the periodical changing of surface pressure is mainly meridionally oriented between the high latitudes and mid-latitudes. This pattern is referred as *North Atlantic Oscillation* (NAO) and is considered to be the dominant component of JSs. It was discovered that negative phase of NAO is associated with cyclonic wave breaking, while positive phase is related to anticyclonic one. NAO also can be seen as the interaction of STJSs and EDJSs. A positive phase of NAO then corresponds to splitting of the JSs, while the negative phase - to their merging. NAO structure is explicitly described in [126].

Nevertheless, NAO solely does not define all the variations of JSs: the *East Atlantic pattern* (EA) is found to be also important [128]. Actually, JS latitude ans speed variations can be defined by the combination of the NAO and the EA. The anomalies associated with southern JS location correspond well to the negative phase of the NAO, while the central and northern JS locations closely resemble the positive and negative phases of the EA [125].

There are some other meteorological phenomenon, tightly related with the JSs, i.e.

- *North Atlantic Storm Tracks* (NASTs), closely linked to extreme winds and precipitation events, formed in regions of strong baroclinicity and mid-latitude sea surface temperature front. The mechanisms of NASTs are explicitly analyzed in [127].
- *Strong and Persistent Ridge Events* (SPREs), characterized by:
  - strengthening of the North Atlantic ridge,
  - northward shifting of the NAST,
  - extended spreading of the western STJSs and EDJSs over the NAT,
  - upper-tropospheric wave breaking;

  and distinguished mostly by their persistence (at least 10 strong ridge days) rather than amplitude. More details on SPRE can be found in [128].

Thus, as it can be concluded from the numerous studies, JSs, NASTs, SPREs and other phenomena, that determine the meteorological conditions over NAT, have very complex driving physical mechanisms. Their understanding is important for weather prediction, which in turns, play a crucial role for air traffic planning in NAT. In this study, however, we interpret JSs simply as a wind field over NAT, defined by the amplitude and direction of WS vector at a given geographical point (as in Figure 1.16).

Appendix N

NAT Track Messages

The *NAT Track Message* gives full information on the coordinates of the OTS tracks (their WPs) as well as the FLs that are expected to be in use for each track. In most cases, it also includes the details of domestic entry and exit routings associated with individual tracks. One more important element of this message is the remark section that provides essential information that Shanwick and Gander OACCs need to bring to the attention of operators. Below, an example of a NAT Track Message published for eastbound OTS on August 3d 2006 is given followed by the explanation of each section.

(NAT-1/2 TRACKS FLS 320/400 INCLUSIVE

AUG 03/0100Z TO AUG 03/0800Z

PART ONE OF TWO PARTS-

U YAY HECKK 53/50 55/40 56/30 56/20 PIKIL MIMKU MORAG

EAST LVLS 320 330 340 350 360 370 380 390 400

WEST LVLS NIL

EUR RTS EAST NIL

NAR N125A N129B-

V DOTTY CRONO 52/50 54/40 55/30 55/20 RESNO NIBOG NURSI

EAST LVLS 320 330 340 350 360 370 380 390 400

WEST LVLS NIL

EUR RTS EAST NIL

NAR N109B N113B N115B-

W CYMON DENDU 51/50 53/40 54/30 54/20 DOGAL BABAN

EAST LVLS 320 330 340 350 360 370 380 390 400

WEST LVLS NIL

EUR RTS EAST NIL

NAR N93B N97B N99A-

X YQX KOBEV 50/50 52/40 53/30 53/20 MALOT BURAK

EAST LVLS 320 330 340 350 360 370 380 390 400

WEST LVLS NIL

EUR RTS EAST NIL

NAR N77B N83B N85A-

Y VIXUN LOGSU 49/50 51/40 52/30 52/20 LIMRI DOLIP

EAST LVLS 320 330 340 350 360 370 380 390 400

WEST LVLS NIL

EUR RTS EAST NIL

NAR N61B N67B-

END OF PART ONE OF TWO PARTS)

(NAT-2/2 TRACKS FLS 320/400 INCLUSIVE

AUG 03/0100Z TO AUG 03/0800Z

PART TWO OF TWO PARTS-

Z YYT NOVEP 48/50 50/40 51/30 51/20 DINIM GIPER

EAST LVLS 320 330 340 350 360 370 380 390 400

WEST LVLS NIL

EUR RTS EAST NIL

NAR N51B N59A-

REMARKS:

1.TRACK MESSAGE IDENTIFICATION NUMBER IS 215 AND OPERATORS ARE REMINDED TO INCLUDE THE TMI NUMBER AS PART OF THE OCEANIC CLEARANCE READ BACK.

2.PILOTS ARE ADVISED NOTAM NUMBER A2843/06 OCEANIC CLEARANCE PROCESSOR 3 ?OCP3? IS IN EFFECT. PILOTS ARE REQUIRED TO SEND AN RCL THAT INCLUDES AN ESTIMATE FOR THE OCEANIC ENTRY POINT.

3.CLEARANCE DELIVERY FREQUENCY ASSIGNMENTS FOR AIRCRAFT OPERATING FROM MOATT TO BOBTU INCLUSIVE:

MOATT TO SCROD 128.7

OYSTR TO DOTTY 135.45

CYMON TO YQX 135.05

VIXUN TO YYT 128.45

COLOR TO BOBTU 119.42

4.80 PERCENT OF GROSS NAVIGATIONAL ERRORS RESULT FROM POOR COCKPIT PROCEDURES. ALWAYS CARRY OUT PROPER WAYPOINT CHECKS.

5.ALL OPERATORS ARE REMINDED OF THE NECESSITY TO PROVIDE VOICE REPORTS OF ANY OBSERVED NON ROUTINE WEATHER PHENOMENA.

6.NERS ARE APPLICABLE FROM 0100 TO 0600 UTC AT 30W. EGTT NOTAM B0862/06 REFERS.

7.CREWS ARE REMINDED THAT THE STRATEGIC LATERAL OFFSET PROCEDURE ?SLOP? SHOULD BE USED AS A STANDARD OPERATING PROCEDURE AND NOT SOLELY FOR TURBULENCE/WEATHER AVOIDANCE.-

END OF PART TWO OF TWO PARTS)

In this example the eastbound OTS tracks are defined via two NAT messages. Each message is bounded with the brackets "(" and ")" and starts with the key abbreviation "NAT". The total number of messages published for the OTS as well as the consecutive number of the current message are presented in the 1st and 3d lines and in the end of the message:

(NAT-**1/2** TRACKS FLS 320/400 INCLUSIVE

...

PART ONE OF TWO PARTS-

...

END OF PART ONE OF TWO PARTS)

Further the first of the two messages is considered. The hyphen "**-**" is used to separate the consecutive fields of the message.

The 1st line defines the FLs available for the current OTS:

(NAT-1/2 TRACKS **FLS 320/400 INCLUSIVE**

The 2nd line defines the date and time, when the current OTS is available (date/-time_in_UTC):

AUG 03/0100Z TO AUG 03/0800Z

The lines starting with the 4th define the OTS tracks. They are grouped by five lines, where the last line in the group ends with "**-**". Each of the groups corresponds to a particular track. Further the definition of the first track is examined:

U YAY HECKK 53/50 55/40 56/30 56/20 PIKIL MIMKU MORAG

EAST LVLS 320 330 340 350 360 370 380 390 400

WEST LVLS NIL

EUR RTS EAST NIL

NAR N125A N129B-

The 1st line starts with the track letter ("**U**") and is followed by enumeration with space separation of the track WPs starting with the most western. The WPs enumeration includes named WPs ("**YAY**", "**HECKK**", "**PIKIL**", "**MIMKU**", "**MORAG**") and WPs defined by their coordinates ("**53/50**", "**55/40**", "**56/30**", "**56/20**") where the first number corresponds to WP latitude and the second - to WP longitude.

The 2nd line starts with the key abbreviation "**EAST LVLS**" and is followed by enumeration with space separation of the eastbound FLs available for this track starting from the least ("**320**", ... , "**400**").

The 3d line starts with the key abbreviation "**WEST LVLS**" and should be followed by enumeration of the westbound FLs available for this track. The keyword "**NIL**" used in this case means that this track is not intended to be used for westbound flights.

The rest lines of the first NAT message are to be treated in the similar way. In this example this message contains five OTS tracks ("**U**", "**V**", "**W**", "**X**" and "**Y**"). The last 6th OTS track ("**Z**") is defined in the second NAT message. This message is concluded with the section "**REMARKS:**" that contains some extra information used by OACCs.

Appendix O

FPL Messages in NAT

An *FPL message* defines the aircraft flight plan. The part of the flight route over NAT is recorded in such a message in a special format. We will describe this part in details and omit the FPL message sections that are not related to the flight progress within NAT. Below, an example of an FPL message is presented. The message is bounded with brackets "(" and ")", the hyphen "-" is used to separate the consecutive fields of the message.

(FPL-AAL100-IS

-B772/H-SXWDHIRGY/SD

-KJFK2215

-N0496F350 BETTE3 ACK DCT TUSKY N77B YQX/M084F370 NATX MALOT/M084F370 NATX BURAK/N0484F370 UL9 STU UP2 NUMPO Y3 NIGIT

-EGLL0617 EGCC

-EET/CZQM0057 YQX0206 KOBEV0220 050W0226 040W0310 EGGX0352 020W0434 EISN0455 BURAK0507 EGTT0534

SEL/KPRS REG/N775AN

)

The 1st line provides the following information: message identification (**FPL**) **-** flight identification, or callsign (**AAL100**) **-** flight rules and type of flight (**IS**). The flight flight callsign is to be used to identify the flights.

The 2nd line represents the following information: number and type of aircraft (**B772**) / wake turbulence category (**H**) **-** flight equipment (**SXWDHIRGY/SD**).

The 3d line identifies the departure airport coded in ICAO[1] (**KJFK**) and estimated departure time in UTC (**2215**).

The following several lines (here, 4th and 5th) define the flight route. They contain the sequence of WPs, including the control points in continental airspace and OTS WPs, and route segments (such as OTS tracks). Different ways of OTS track definition in the FPL are discussed below.

The next line (6th) defines the arrival airport coded in ICAO (**EGLL**), the total *Estimated Elapsed Time* (EET) from departure to arrival (**0617**), and optionally one or more alternative airports used in case if the arrival airport cannot accept the aircraft (**EGCC**).

The last several lines (7th and 8th) represent the EETs needed for cruising up to significant WPs. The EET format is described below.

There are two ways to define the flight route via OTS in FPL. The most common way is to include in the route field of FPL message the keyword **NAT** and the identification of the OTS track to be used (the track letter). In this case the NAT route description contains several OTS WPs - obligatory track entry and exit WPs and may be some more WPs - that are separated with **NAT** keywords (as in the given example):

-N0496F350 BETTE3 ACK DCT TUSKY N77B **YQX/M084F370 NATX MALOT/M084F370 NATX BURAK/N0484F370** UL9 STU UP2 NUMPO Y3 NIGIT

In this case the aircraft is intended to use the track X (NAT**X**), which has **YQX** as entry WP, **BURAK** as exit WP, and WP **MALOT** preceding the exit.

The WPs included in the FPL are usually followed by the definition of Mach and FL prescribed for the aircraft at this WP, e.g. YQX/**M084F370**. This definition has the following format: **M0xxFyyy**, where **xx** stands for the Mach (the hundredths of the

[1]The *ICAO airport code* is a four-character alphanumeric code designating each airport around the world, defined by the ICAO and published in its documents. ICAO codes are used by ATC and airlines for flight operations, e.g. flight planning. They differ from IATA (*International Air Transport Association*) codes, which are three-letter codes, generally used for airline timetables, reservations, and baggage tags. In general, IATA codes are usually derived from the name of the airport or the city it serves, while ICAO codes are distributed by region and country. For example, the IATA code for London's Heathrow Airport is LHR and its ICAO code is EGLL.

Mach number which is less than 1) and **yyy** defines the FL. Thus, in the example above, the aircraft is planned to pass the YQX WP at FL370 with Mach equal to 0.84. For the exit WP, the speed is usually defined in knots, and the corresponding record in the FPL has the following format: **N0zzzFyyy**, where **zzz** is the speed in knots and **yyy** is the FL, e.g. BURAK/**N0484F370**.

Entry and exit FLs and/or speeds can differ. Each WP, where the FL/Mach number changing is to be done, should be included in the FPL. For example, according to the FPL presented below, the aircraft is planning to perform a climb from FL390 to FL400 at WP **56N030W** defined by its coordinates .

(FPL-ETD502-IS

-A332/H-SXDHIRWY/S

-CYYZ0340

-N0482F370 J586 YCF J588 YMX J553 **YAY/M082F390 NATU 56N030W/M082F400 NATU MIMKU/M082F400 NATU MORAG/N0471F400** UL10 HON UL186 BIG UL9 KONAN UL607 KOK

-EBBR0632 LFPG EGLL

-EET/CZUL0023 CZQX0154 CZQX0214 50W0229 40W0313 EGGX0353 20W0433 PIKIL0452 EGPX0511 EISN0520 EGPX0524 EGTT0532 EBUR0613

REG/A6EYE SEL/JKDP OPR/ETIHAD AIRWAYS RMK/TCAS EQUIPPED RVR/75 E/0828 P/TBN R/VE S/MD J/LF D/08 470 C YLW

A/PEARL/GOLD/RED

C/KUG JIANNWEN

)

Another way to define the NAT route is to include in the FPL all the WPs of an OTS track (tracks) in their sequential order from entry to exit point. In this case, the **NAT** keyword is not used. This method is applied usually if the flight is planned to perform the re-routing from one track to another at any WP, as for such a flight a single track cannot be attributed. But nothing imposes to include all WPs in the FPL even if they all belong to one track. As in the previous case, the entry WP is followed by Mach/FL definition, as well as any other WPs where Mach/FL changing is required. An example of such route definition is given below. In this case the WPs **YQX**, **KOBEV** and **50N050W**

belong to track X, and the WPs **51N040W**, **52N030W**, **52N020W**, **LIMRI** and **DOLIP** belong to track Y.

(FPL-AFR031-IS

-A332/H-SPRIJWYX/SD

-KIAH0300

-N0478F370 **YQX/M082F390 DCT KOBEV DCT 50N050W 51N040W 52N030W 52N020W DCT LIMRI DOLIP**

-LFPG0900 LFPO

-EET/CZYZ0215 CZUL0245 KZBW0248 CZUL0256 KZBW0316 CZQM0333 CZQX0401 50N050W0451 51N040W0535 EGGX0618 52N020W0702 EISN0724 EGTT0756 LFRR0817 LFFF0835

REG/FGZCO SEL/EJBF DAT/SV RMK/A330 AGCS EQUIPPED DOF/060803

)

The EET field of FPL message starts with keyword **EET** and is followed with the sequence of significant WPs at which the EETs are defined. This definition includes the WP identification (name or coordinates) and the EET of cruising from departure to this point in UTC. The EET fields from the FPLs for the examples given above demonstrate the different types of WP identifications that can be used in the NAT part of flight route.

-EET/CZQM0057 **YQX0206 KOBEV0220 050W0226 040W0310 EGGX0352 020W0434 EISN0455 BURAK0507** EGTT0534

-EET/CZUL0023 CZQX0154 CZQX0214 **50W0229 40W0313 EGGX0353 20W0433 PIKIL0452 EGPX0511** EISN0520 EGPX0524 EGTT0532 EBUR0613

-EET/CZYZ0215 CZUL0245 KZBW0248 CZUL0256 KZBW0316 CZQM0333 CZQX0401 **50N050W0451 51N040W0535 EGGX0618 52N020W0702 EISN0724** EGTT0756 LFRR0817 LFFF0835

There are the following types of such identifications:

- the OTS named WPs, e.g. **YQX0206**),
- the OTS WPs defined by their coordinates in latitude/longitude, e.g. **50N050W0451**,
- the ten degrees of longitude via NAT, i.e. **050W0226**, and
- the special airspace identifications, that include:
  - the enter to the Shanwick OCA denoted as **EGGX** and corresponding for eastbound flights to the longitude **030W**, e.g. **EGGX0352**,
  - the enter to the Ireland control area denoted as **EISN** and corresponding to the longitude **015W** between the latitudes from **49N** to **54N**, e.g. **EISN0455**,
  - the enter to the England control area denoted as **EGPX** and corresponding to the longitude **010W** between the latitudes from **55N** to **61N**, e.g. **EGPX0511**.

The EET information is used by ATC to estimate future aircraft positions and discover potential conflicts.

Appendix P

ATM performance metrics

Below we present a brief summary on the *performance metrics* used in ATM, in particular, in oceanic airspaces, to measure the quality of the provided air navigation services, i.e. their predictability, flexibility and capability to handle the users priority requests. The presentation relies on the study provided in [30].

Traditionally, the *safety* and *delays* were used as the most common metrics of air traffic system effectiveness and performance. Nevertheless, they solely do not provide a complete information on the quality of services provided to airspace users. To measure this quality correctly, we need to know, in first turn, what the users priorities are. Below, the most significant of them are stated in the order of decreasing priority:

- safety, *i.e.,* avoiding:
  - conflicts with surrounding traffic,
  - highly congested areas,
  - dangerous areas, *e.g.,* turbulence, SUAs;
- on-time performance, including:
  - on-time arrival, and
  - on-time departure;
- fuel consumption, that in many respects guide the next priority;
- flying the filed FPL (supposed to be the optimal one), *i.e.,* getting the requested:

  - speeds,
  - altitudes,
  - routes,
  - times;
- flexibility, *i.e.,* the ability to change their routes and altitudes in order to:
  - assure safety,
  - maintain passenger comfort,
  - minimize flight time,
  - minimize fuel.

In [30], two types of oceanic metrics are distinguished:

- environmental metrics, and
- performance metrics.

The *environmental metrics* are defined as follows:

- the number of aircraft in the system for a specific time period,
- the distribution of aircraft types,
- the distribution of aircraft avionic equipment,
- the primary means of communications (HF voice POSs vs. CPDLC),
- the flight types (civil, commercial, international, domestic, etc.)

Among the *performance metrics* the following can be highlighted:

- the number of OACC operational errors,
- the percentage of cleared FPLs, *i.e.,* the percentage of flights that are attributed the demanded:
  - speed,

  - FL,
  - track;
- altitude change demands, where the next quantities can be measured:
  - the number of requests in order to fly more optimal FAP,
  - the number of requests due to weather restrictions,
  - the number of accepted/denied requests,
  - the response time;
- deviation demands, *i.e.,* the number of requested/accepted changes of LFP, measured with the same quantities as stated above;
- fuel burn, *i.e.,* the variance of necessary fuel in different flight scenarios;
- departure and arrival delays, that in both cases include:
  - the number of delayed flights,
  - the amount of time they were delayed;
- oceanic transit time[1].

Evidently, it is not always possible to achieve the improvements in all the metrics simultaneously[2], thus, ideally, all the metrics should be analyzed in complex, and the optimization of the system performance requires elaborating the trade-offs between some of them.

In addition to these user-related metrics, we can remind the existence of *ATC-related* metrics, *i.e.,* those, measuring *airspace capacity and congestion*, discussed in Appendix K. In the studies presented in this thesis, different performance metrics or a complex of metrics are used. For example, [30] quantifies the benefits induced by the communications via CPDLC instead of HF radio basing on the number of altitude changing demands handling by controllers per day and the average response time to such requests.

[1] A better metric to evaluate in particular oceanic system performance, than departure/arrival delays, as these last depend on a great amount of factors and not necessarily reflect the oceanic service quality

[2] For example, the greater the number of aircraft in the system is, the lower is the percentage of altitude changing demands acceptance. At the same time, the absolute number of accepted demands could be increased.

Appendix Q

Genetic Algorithm specifications

In this Appendix we discuss how the genetic operators, i.e. selection, crossover and mutation, were adapted for the GA used to resolve the conflicts between the aircraft within the OTS.

First, the **selection operator** was adjusted for the algorithm. Below we present several selection strategies that were tested for the GA:

- *Tournament selection* begins with randomly selecting β_1 individuals from the current population and then keeps the β_2 bests of them ($\beta_1 > \beta_2$). These two steps are repeated until the new (intermediate) population is completed. We have tested several combinations of (β_1, β_2), namely $(5, 2)$, $(6, 2)$, $(7, 3)$.

- *Rank selection* requires sorting of the individuals according to their fitness and then associating to each individual the probability of its selection p_i according to its rank i ($i = 1, ..., S_P$, where S_P is the population size). The typical probability distribution is defined as following:

$$p_i = A \cdot \exp(-B \cdot i + C). \tag{Q.1}$$

  If the parameter B is fixed ($B > 1$), then the values of A and C can be calculated from the following conditions: $p_1 = 1$, $p_{S_P} = 0$. We have performed the tests with several values of B, more precisely, $B = 0.1, 0.3, 0.5$.

- *Roulette wheel selection* consists of associating to each individual i of a segment of length l_i proportional to its fitness and normalized between 0 and 1:

$$l_i = \frac{fitness_i}{\sum_{j=1}^{S_P} fitness_j}. \tag{Q.2}$$

  These segments are then concatenated on the axis, and the random value is generated in the range from 0 to 1, that defines the appropriate segment and the corresponding individual to be selected for the next generation.

- *Stochastic reminder without replacement selection* starts with the calculation for each individual i of the ratio r_i of its fitness to the average fitness:

$$l_i = S_P \frac{fitness_i}{\sum_{j=1}^{S_P} fitness_j}. \tag{Q.3}$$

  Then each individual is represented in the new population exactly $\lfloor r_i \rfloor$ times, where $\lfloor r_i \rfloor$ is the integer part of the ratio r_i. To complete the new population the Roulette wheel selection is applied to all individuals with the modified fitness $fitness'_i = r_i - \lfloor r_i \rfloor$.

- *Truncation selection* consists of choosing the $\lfloor \beta \cdot S_P \rfloor$ best individuals from the current population ($0 < \beta < 1$) and performing the random uniform selection on their set to complete the new population. Several values of β were tested, i.e. $\beta = 0.3, 0.5, 0.7$.

Several test were performed with different input data in order to find the selection method guaranteeing the best GA convergence. Figures Q.1 and Q.2 demonstrate a typical result of comparison of selection methods. From these preliminary tests, we remarked that Roulette selection and Stochastic reminder selection seem to give the results much worth than other methods, so they were not considered further. In the majority of cases the Rank selection gave the best convergence, but for several flight sets, the conflict-free configuration was not found with Rank selection implemented. That is more likely explained by the fact, that converging too fast, the GA falls into a local minima. The Tournament selection showed to most stable performance. Being much slower than Rank selection on one hand, it is capable of producing the solution every time on the other hand.

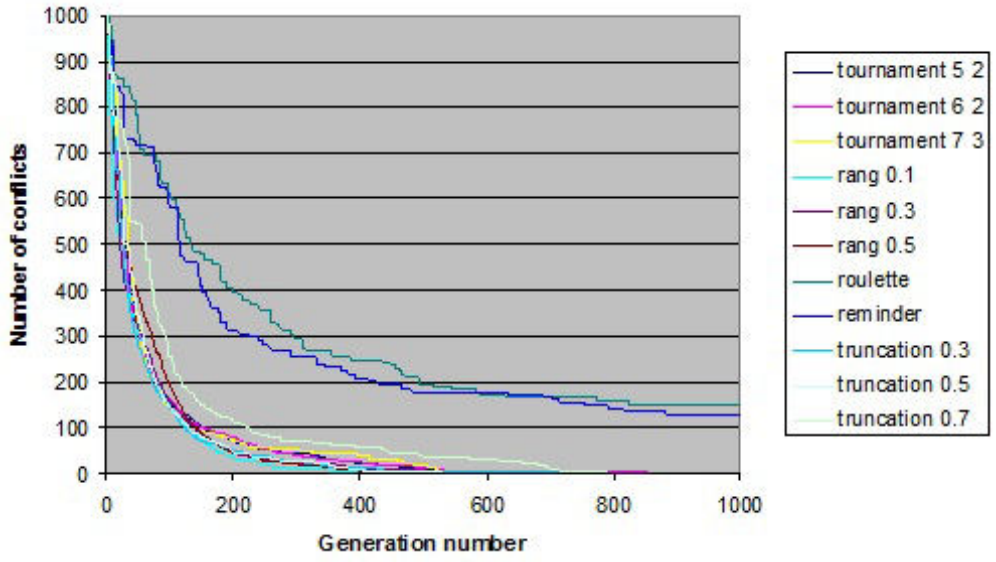

FIGURE Q.1: Convergence of GA with different selection methods

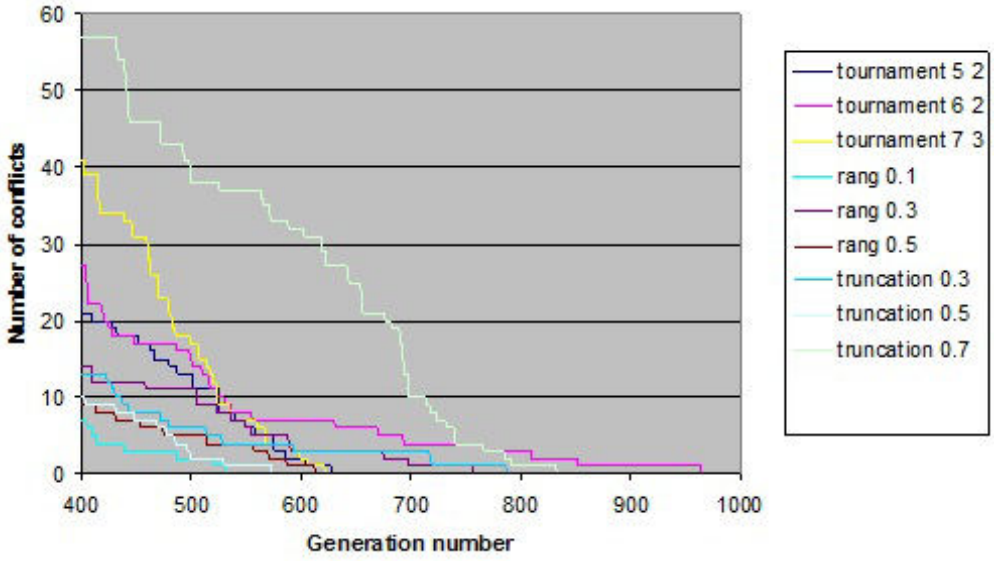

FIGURE Q.2: Convergence of GA with different selection methods in logarithmic scale

Thus, in the result of all the performed experiments, we chose to use the *consecutive combination of Rank and Tournament selection*: first, for the early generations, we eliminate as much conflicts as possible with Rank selection, after that, for older generations, we switch to the Tournament selection, to avoid to fast convergence to a local minimum. The following parameters were adjusted for these selection method:

- $\beta_1 = 5$;
- $\beta_2 = 2$;

- $B = 0.5$;

At the next step, the **crossover operator** was adjusted for the GA. Several possible methods, presented below, were tested.

- *Slicing crossover* consists of choosing randomly a flight index in the individual and exchanging all the flights with indices more than the given one between the two parent individuals.
- *Mixed crossover* defines independently for each flight index if the corresponding flights from the two parent individuals are to be exchanged. The choice of exchanging is made randomly and uniformly.
- *Oriented crossover* defines for each flight f_1 of one parent individual if it is replaced by the corresponding flight f_2 of another parent individual. The probability of replacement $p_{f_1 \to f_2}$ depends on the cost F^{f_1} and F^{f_2} produced by the corresponding flights (the cost depends on the choice of the objective function, F):

$$p_{f_1 \to f_2} = \frac{1 + F^{f_1}}{2 + F^{f_1} + F^{f^2}}. \tag{Q.4}$$

  Thus the best flights (with the cheapest cost, if the problem is formulated in terms of minimization problem) are higher probability to be represented in the next generation individuals.
- *Uniform combination* applies by turns Oriented crossover method and one of the other methods, where the method to use is defined randomly and uniformly.
- *Generation dependent combination* also applies by turns Oriented crossover method and one of the other methods, but the choice of the method to use depends on the current generation index i_G: the Oriented crossover is applied with the probability:

$$p_{i_G} = \frac{i_G}{N_G}, \tag{Q.5}$$

  where N_G is the total number of generations to be produced.

Several test were performed with different input data in order to identify the crossover method inducing the best GA convergence. A typical result of comparison of crossover

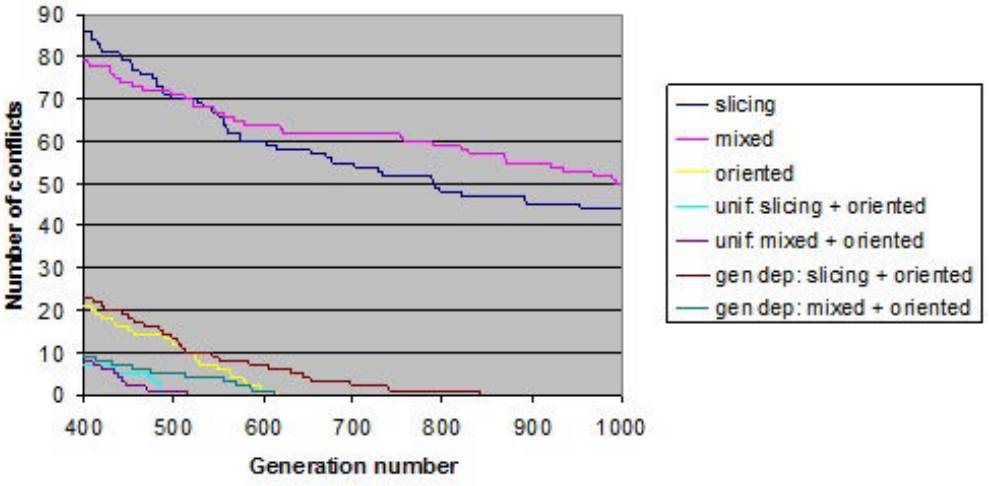

FIGURE Q.3: Convergence of GA with different crossover methods in logarithmic scale

methods can be found in Figure Q.3. From these preliminary tests, we noticed that the methods of Slicing and Mixed crossover using separately give the results much worth than Oriented crossover and its combinations, so they were not considered in further tests. Furthermore, we concluded that the best convergence is obtained using Uniform combination of Slicing and Oriented crossover methods and Generation dependent combination of Mixed and Oriented crossover methods.

We decided to implement the *Generation dependent combination of Mixed and Oriented crossover* for further simulations, as it gives in general better results, than any other method.

Finally, at the next step the **mutation operator** was adjusted for the algorithm. Several possible methods, that were tested within this study, are presented below. They are prefollowed by a definition of a *Unique mutation*, being the base of all the mutations in use.

- *Unique mutation* performs the mutation of one of the flight variables with predefined probabilities: p_r for re-routing decision variables x_i^f, p_d for track entry delay δ^f, p_t for entry track TA_{in}^f and exit track TA_{out}^f. We recall that a particular AT of a flight f $(f = 1, ..., N)$ is encoded with a vector of decision variables which is denoted as $y^f = (\delta^f, e^f, x^f, o^f)$. Let us denote further $M(y^f)$ a set of ATs that can be obtained from the AT y^f as a result of unique mutation. Below we give a formal description of this set. To simplify the explanation, first we consider each type of

unique mutation (re-routing, delaying, deviation) separately, and we denote the corresponding resulting AT sets: $M^x(y^f)$, $M^\delta(y^f)$, $M^e(y^f)$ and $M^o(y^f)$. Then:

$$\begin{aligned}
M^x(y^f) = \{\bar{y}^f = (\delta^f, e^f, \bar{x}^f, o^f) : \bar{x}^f = (\bar{x}^f_1, ..., \bar{x}^f_{Nx-1}) \ \& \\
\exists i, j = 1, ..., Nx-1,\ i \neq j \text{ s.t. } x^f_i \neq x^f_j \ \& \ \bar{x}^f_i = x^f_j \ \& \ \bar{x}^f_j = x^f_i \ \& \\
\bar{x}^f_k = x^f_k, k = 1, ..., Nx-1, k \neq i, k \neq j\}; \\
M^\delta(y^f) = \{\bar{y}^f = (\bar{\delta}^f, e^f, x^f, o^f) : \bar{\delta}^f \neq \delta^f\}; \\
M^e(y^f) = \{\bar{y}^f = (\delta^f, \bar{e}^f, \bar{x}^f, o^f) : (\bar{e}^f = e^f - 1 \ || \ \bar{e}^f = e^f + 1) \ \& \\
\exists i = 1, ..., Nx-1 \text{ s.t. } \bar{x}^f_i - x^f_i = |o^f - \bar{e}^f| - |o^f - e^f| \ \& \\
\bar{x}^f_k = x^f_k, k = 1, ..., Nx-1, k \neq i\}; \\
M^o(y^f) = \{\bar{y}^f = (\delta^f, e^f, \bar{x}^f, \bar{o}^f) : (\bar{o}^f = o^f - 1 \ || \ \bar{o}^f = o^f + 1) \ \& \\
\exists i = 1, ..., Nx-1 \text{ s.t. } \bar{x}^f_i - x^f_i = |\bar{o}^f - e^f| - |o^f - e^f| \ \& \\
\bar{x}^f_k = x^f_k, k = 1, ..., Nx-1, k \neq i\}; \\
M(y^f) = M^x(y^f) \cup M^\delta(y^f) \cup M^e(y^f) \cup M^o(y^f).
\end{aligned}$$

- *Simple mutation* consists in choosing randomly the flight index and in applying the operator of unique mutation to this flight. More formally, a simple mutation replaces a current solution, $y = (y^1, ..., y^N)$ by one of its neighbor solutions $\bar{y}$, where the neighborhood $U(y)$ is defined as:

$$\begin{aligned}
U(y) = \{\bar{y} = (\bar{y}^1, ..., \bar{y}^N \ : \ \exists!\ f = 1, ..., N, \text{ s.t. } \bar{y}^f \in M(y^f) \ \& \\
\bar{y}^g = y^g,\ g = 1, ..., N,\ g \neq f\}
\end{aligned} \tag{Q.6}$$

- *Simple x% mutation* is the simple mutation applied not to one flight but to $x\%$ of all flights of the individual.

- *Simple generation dependent mutation* is the simple mutation applied not to one but to k flights of the individual, where k depends on the generation number i_G:

$$k = k_{i_G} = N(0.5\frac{N_G - i_G}{N_G} + 0.01). \tag{Q.7}$$

- *Random oriented mutation* starts with assigning to each flight f its quality, q^f, depending on its cost (which, in turn, depends on the chosen objective function, F):

$$q^f = \frac{F^f}{\sum_{g=1}^{N} F^g}. \tag{Q.8}$$

Then the current flight index, f_c, is randomly chosen and the qualities of all consecutive flights starting with the current one are summarized until the sum exceeds some value γ in the range from 0 to 1 chosen randomly:

$$\sum_{f=f_s}^{f_e} q_f > \gamma, \text{ where } 0 < \gamma < 1. \tag{Q.9}$$

The last flight, f_e, which quality was added to the sum (that led to overflow of this sum) is subjected to the unique mutation.

- *Random oriented x% mutation* is the random oriented mutation applied not to one flight but to x% of all flights of the individual.

- *Random oriented generation dependent mutation* is the Random oriented mutation applied not to one but to k flights of the individual, where k depends on the generation number the same way as for Simple generation dependent mutation (Q.7).

- *Determined oriented mutation* starts with calculation of the average cost for all flights:

$$F_{ave} = \frac{\sum_{f=1}^{N} F^f}{N}. \tag{Q.10}$$

Then to each flight f which number of conflicts exceeds the average value ($F^f > F_{ave}$) the unique mutation is applied with the probability defined by this number of conflicts:

$$p_{mut}^f = \frac{F^f - F_{ave}}{F_{ave}}. \tag{Q.11}$$

Several test were performed with different input data in order to identify the best mutation operator. As a result, the following mutation parameters were set:

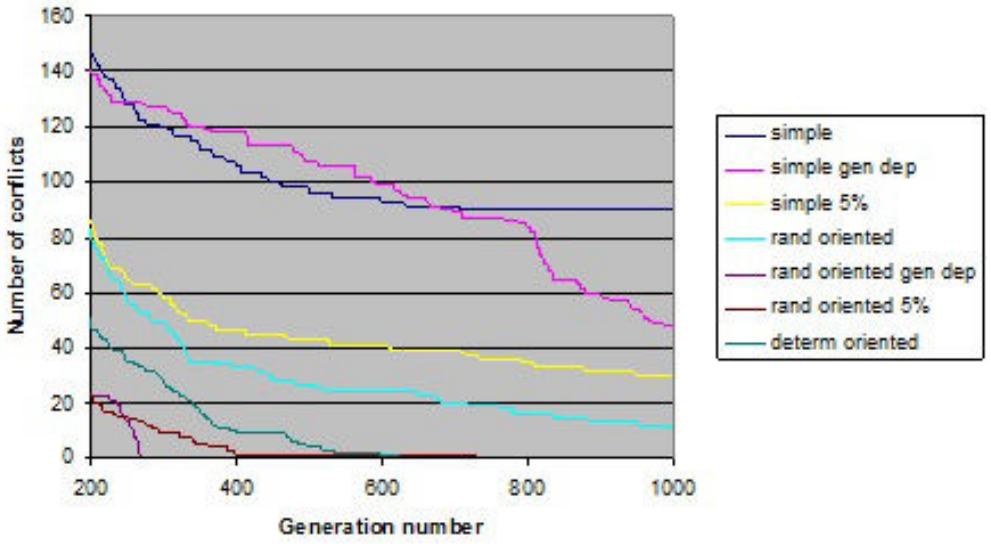

FIGURE Q.4: Convergence of GA with different mutation methods in logarithmic scale

- $p_r = 0.75$;
- $p_d = 0.125$;
- $p_t = 0.0625$;
- $x = 5\%$.

A typical result of comparison of mutation methods is presented in Figure Q.4. From these preliminary tests, we concluded that all Simple mutation methods and the Random oriented mutation performed much worthier than the last three methods, so they were not considered in further tests.

We continued with testing different combinations of described mutation methods, that are mentioned below.

- *Uniform combination* of Random oriented $x\%$ mutation and Determined oriented mutation.
- *Uniform combination* of Random oriented generation dependent mutation and Determined oriented mutations.
- *Generation-dependent combination* of simple $x\%$ mutation, Random oriented $x\%$ mutation and Determined oriented mutation. Here, the choice of the method to

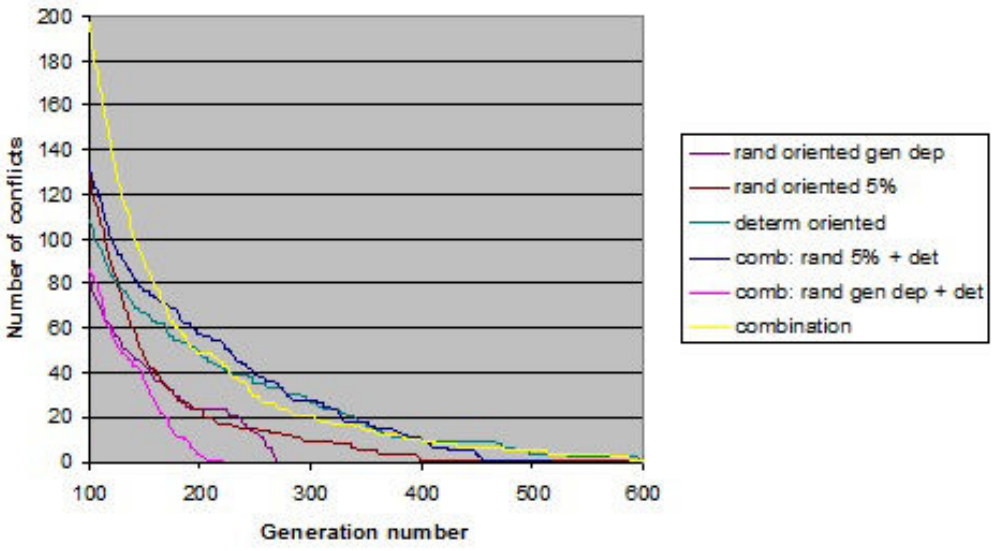

FIGURE Q.5: Convergence of GA with different mutation methods and their combinations

use depends on the current generation index: the Simple mutation is applied with the probability:

$$p_{i_G} = \frac{N_G - i_G}{N_G}. \tag{Q.12}$$

the Random and Determined oriented mutations are applied uniformly.

Some results of the comparison of such methods can be found in Figure Q.5.

From the obtained results, it was not evident to select one mutation method that gave the best convergence for the majority of studied tests. For example, the Random oriented generation dependent mutation and its Uniform combination provided very fast convergence for some tests while for others they were not able to find the appropriate solution. However, our goal was to select the method capable of solving the problem for any input data in reasonable time. For this reason, the *Generation dependent combination of Simple 5% mutation, Random oriented 5% mutation and Determined oriented mutation* was chosen to be used in the algorithm as the method giving the best average results for all the studied tests.

Several mutation probabilities, p_m were also tested for the GA. As a result, it was found out that the mutation with probability $p_m = 0.4$ leads to the best convergence, thus this value was used for further simulations.

Appendix R

Simulated Annealing specifications

In this Appendix we discuss how the SA algorithm was adapted, in order to be used to resolve the conflicts between the aircraft within the OTS.

To generate the neighboring state s' from the current state s, several mutation methods, analogues to those used in GA and described in Appendix Q, were implemented and tested in order to establish the one giving the best convergence. They are stated below. The formal definition of the solution neighborhood (for the simple mutation) is given by formula (Q.6).

- *Simple temperature dependent mutation* is the simple mutation (described for GA, Appendix Q) applied not to one but to k flights of the state s, where k depends on the current temperature T:

$$k = k_T = N(0.5\frac{T}{T_0} + 0.01). \tag{R.1}$$

- *Random oriented temperature dependent mutation* is the Random oriented mutation (Appendix Q) applied not to one but to k flights of the state, where k depends on the current temperature T the same way as for Simple temperature dependent mutation, defined in the equation (R.1).

- *Determined oriented mutation* is exactly the same as described for the GA (Appendix Q).
- *Temperature dependent combination* of Simple temperature dependent mutation and Random oriented temperature dependent mutation.
- *Uniform combination* of Simple temperature dependent mutation and Determined oriented mutation.
- *Temperature dependent combination* of Simple temperature dependent mutation, Random oriented temperature dependent mutation and Determined oriented mutation.

Temperature dependent combinations include the mentioned mutation methods, where the Simple mutation was applied with the probability

$$p_s(T) = \frac{T}{T_0}. \tag{R.2}$$

The probability of acceptance of the state transition in the classical SA is defined by the following formula (2.16). In addition to this, we studied the variation of the SA called *Rescaled Simulation Annealing* (RSA), where the rescaling of the system energy is used in order to achieve the faster convergence. Then the probability of acceptance is defined by the following formula:

$$p_a(s \to s', T) = \begin{cases} 1 & \text{if } E(s') < E(s) \\ e^{\frac{-\Delta\tilde{E}(s,s')}{T}} & \text{if } E(s') \geq E(s) \end{cases}, \tag{R.3}$$

where

$$\Delta\tilde{E}(s, s') = E(s') - E(s) - c \cdot T(\sqrt{E(s')} - \sqrt{E(s)}). \tag{R.4}$$

Here c is the coefficient to be adjusted proceeding from the particular problem:

$$c = \frac{2}{T_0}\sqrt{E_{ave}}, \tag{R.5}$$

where E_{ave} is the average value of energy of all states of the search space. Evidently, this value is unknown; instead its approximation based on some finite number of states is used.

To adjust the algorithm to our particular problem, first we compare the results given by the classical SA and the RSA were compared. It was found out, that the RSA for this particular optimization problem does not ameliorate the process of solution finding, thus further just the classical SA was used in the experiments.

Next, different mutation methods and their combinations were tested. The obtained results showed that the methods Simple temperature dependent mutation and Determined oriented mutation gave the convergence much worth than other methods; for some tests, they did not even provide the optimal solution with the given ratio of temperature decreasing. Thus, these methods were not taken into consideration further. Furthermore, the methods of Random oriented temperature dependent mutation and its combination with Determined oriented mutation, in general, gave better results than other methods. It seems to be logical, as these methods are intended to generate the better state from the current one (according to the definition of the Oriented methods given for the GA). But this particularity of the methods sometimes resulted in the fact that not all states of the search space had the chance to be explored. Thus, using Oriented methods leads to fast convergence, but at the same time it can lead to sticking in a local minimum. The Simple temperature dependent mutation, in its turn, avoids these inconveniences. But independent using of this method gives very slow convergence.

As a compromise, the *Temperature dependent combination of Simple mutation and Random oriented mutation* was chosen to be used for the algorithm.

Different values of the parameter of temperature decreasing γ were examined during the study. For the tests with RSS these values were $\gamma = 0.9$ and $\gamma = 0.95$. The algorithm was able to find the optimal solution for all the tests with the both values used, but its convergence with $\gamma = 0.9$ is better. The maximum number of iterations that the algorithm can perform with this value of temperature decreasing is 88. For the tests with RSS this number is sufficient, thus the value $\gamma = 0.9$ is preferred to be used. At the same time, for the test without CSS the algorithm did not produce the optimal solution via 88 iterations. Thus, greater values of γ were tested in this case in order to obtain

better solution: $\gamma = 0.95$ and $\gamma = 0.99$. The results of these simulations are represented in Section 2.4.1.

Appendix S

Extracting of the real oceanic data from report files

The oceanic traffic data was obtained from the report files from Shanwick OACC. Each such file is named according to the date when it was recorded. For example, the information about the oceanic traffic for August 3d 2006 is contained in the file 03AUG06.txt.

Each such file contains the report messages received by Shanwick OACC from different sources, including NAT messages, FPL messages (see Appendix O), OCLR messages, flight POSs etc. The legal records in report files normally run from midnight to midnight, so the entries at the beginning of the file are the earliest for that day. All the messages in the file are displayed in time recorded order, as a result the messages of different types are mixed up.

For our simulations, it was necessary to get the FPLs (the planned routes and times) for the set of eastbound flights intended to use the night-time OTS tracks during their period of validity. These FPLs are extracted from the record files with rough oceanic data in several stages. To obtain the set of FPLs for the current day (denoted further as *Date*) it is necessary to investigate the record file from the current day (*Date.txt*) and from the previous one (*Prev_date.txt*).

1. The NAT (see Appendix N) and ETAF (see Appendix T) messages are read from record file *Prev_date.txt* and processed in the appropriate way as this data would be necessary for FPL message processing.

2. All FPL (see Appendix O) messages are extracted from record file Date.txt and assembled into two files: *Date_FPL-0800.txt* and *Date_FPL+0800.txt* according to the time when the FPL message was published. The same is made for the file *Prev_date.txt*. "-0800" corresponds to FPLs published between 0000 and 1100 UTC, and "+0800" - to FPLs published after 1100 UTC. Flights from file *Date_FPL+0800.txt* cannot use the night-time OTS tracks during the period of their validity on the current day (*Date*), so they are not taken into consideration. On the other hand, the FPLs from file *Prev_date_FPL+0800.txt* could use these tracks, as they are intended to depart in the evening of the previous day. Thus, the files to be proceeded are: *Date_FPL-0800.txt* and *Prev_date_FPL+0800.txt*. Further, if any identical operation is to be made with both files, for convenience they will be referred to as *FPL_file.txt*.

3. All flights from each file *FPL_file.txt* are separated into three groups: eastbound flights are placed into file *FPL_file_eastbound.txt*, westbound flights are placed into file *FPL_file_westbound.txt* and the rest - into file *FPL_file_rest.txt*. The separation is made according to the airports of departure and arrival. The eastbound flights depart from North America and arrive in Europe. All American airports according to ICAO notation start with the letters: *B, C, K, M, P, S* or *T*; all European airports start with the letters: *E, H, L, O, R, U* or *V*. Further, only the eastbound flights (thus, files *FPL_file_eastbound.txt*) are treated.

4. All flights from each file *FPL_file_eastbound.txt* are separated into three groups: those flights that intend to utilize the OTS along its entire length (to utilize one OTS track from its entry point to the exit point, or to perform the re-routing from one track to another but with respect to the WPs sequence) are placed into file *FPL_file_onOTS.txt*; those flights that include some but not all OTS WPs in their FPLs (join and/or leave any OTS track in the middle) are placed into file *FPL_file_partOTS.txt*; and those flights that have no OTS WPs in the FPLs - into file *FPL_file_notOTS.txt*.

   The flights intended to use OTS along its entire length should include in their FPL either the track declaration (NAT keyword followed with track letter), or the total sequence of OTS WPs (may be not all from the same track) (see Appendix O for more detail). Further just these flights (from files *FPL_file_onOTS.txt*) are investigated. For these flights, the OTS WPs are extracted (either from the route

field of FPL message, or from the OTS structure, prepared on the 1st sep) and registered.

5. The FPLs of the OTS flights published on the current and previous days (from files *Date_FPL_onOTS.txt* and *Prev_date_FPL_onOTS.txt*) are combined in one file *Date_FPL_onOTS_total.txt*. The duplicated flights are merged. The duplication may have place, as FPL messages for a particular flight can be published several times (2 times in most cases). These messages can be identical or slightly different. In case of difference the latest one is considered. Also on this step the EETs are extracted and registered for the flight route WPs where they are defined (see Appendix O for more detail).

6. On this step, only the flights having all information necessary for further simulations are selected. In our simulations, we can deal only with flights that have the declaration in the FPL of Machs, FLs in the appropriate range, and EETs, at least at one of WPs. The FPLs having no FL declared are placed in file *Date_fpl_hasNoLevel.txt*, those having the FL out of the range defined for OTS tracks - in file *Date_fpl_levelsNotInRange.txt*; the flights having no Mach declaration - in file *Date_fpl_hasNoSpeed.txt*, the flights having no EET for any of the WPs - in file *Date_fpl_hasNoTime.txt*. The rest flights are combined in file *Date_fpl_hasAnyTime.txt* and are to be processed further. Also on this step, the file *Date_fpl_hasEnterTime.txt* is generated, which contains the flights having the declared track entry time (the EET in the first WP). This information is used for statistics.

7. At the last step, the track entry time t_{in}^{f} is to be set for those flights f that have at least one EET declared for any of the WPs i (not necessarily the entry WP). This is done with the help of ETAF information, as it was described in Appendix T. The resulted flight plans are placed in file *Date_fpl_withEntryTime.txt*, that is further used directly in simulations. Such resulting files with extracted data can be found at [45].

The file obtained as a result of the process of FPL message information extracting (*Date_fpl_withEntryTime.txt*) contains in the first line the total number of defined flights, and each of the following lines describes a single flight route. The flights are ordered

Date	August 3d 2006	August 4th 2006
Num of FPLs on OTS, previous day	**383**	**421**
Num of FPLs partly on OTS, previous day	80	83
Num of FPLs out of OTS, previous day	179	180
Num of FPLs on OTS, current day	**66**	**78**
Num of FPLs partly on OTS, current day	89	89
Num of FPLs out of OTS, current day	81	59
Total num of FPLs on OTS	**356**	**404**
Num of FPLs having no defined FL or speed	1	1
Num of FPLs having FLs not in OTS range	9	3
Num of FPLs having no defined EET	15	22
Num of FPLs having track entry time	96	106
Final number of applicable FPLs	**331**	**378**

TABLE S.1: Results of FPL extraction

according to their callsigns. An example of a single flight description is represented below.

AAL100 KJFK/2215 EGLL/0617

YQX/48.6N054.8W/M084/370/0021 KOBEV/49.7N051.5W/M084/370/0035

50N050W/50N050W/M084/370/0041 52N040W/52N040W/M084/370/0125

53N030W/53N030W/M084/370/0207 53N020W/53N020W/M084/370/0249

MALOT/53N015W/M084/370/0310 BURAK/53N012W/M084/370/0322

The fields of this description are separated with spaces. The 1st field defines the flight callsign (**AAL100**). The 2nd field defines the departure airport (**KJFK**) and estimated departure time (**2215**). The 3d field defines the arrival airport (**EGLL**) and the estimated elapsed time from departure to arrival (**0617**).

The next fields represent the sequence of route WPs and the data defined for these WPs: name (**YQX**), coordinates (**48.6N054.8W**), Mach number (**M084**), FL (**370**), EET from departure to this WP (**0021**).

Below we present several statistics on the procedure of extracting the FPLs described above. The two days, August 3d 2006 and August 4th 2006, were selected to perform the simulations. Table S.1 represents some values obtained via the steps of FPL extraction.

As it can be seen from Table S.1, the number of flights, utilizing the OTS tracks during their period of validity, for which the FLs and Machs are defined, is between 300 and

Date		August 3d 2006	August 4th 2006
Total num of FPLs		331	378
Num of FPLs having any WP, where the defined EET differs from ETAF-computed for more than X minutes	$X = 0$	220	266
	$X = 1$	33	98
	$X = 2$	4	7
	$X = 3$	3	0
	$X = 5$	0	0

TABLE S.2: Difference between declared and computed EETs

400 per day. At the same time, the number of flights, for which the track entry time is defined directly in the FPL, is significantly smaller (about 100). In order to use, however, the rest of the flights in our simulations, we apply on step 7 the procedure of track entry time definition, that is introduced in Appendix T. The main disadvantage of this approach is that it is based on using the EETs defined in ETAF messages, that can be rather rough. Thus, the EETs at some WPs, computed on the base of ETAFs and the given track entry time, and the EETs at these WPs, defined directly in the FPL, may differ. The additional study showed that this difference does not exceed 5 minutes. Some more results on this study are presented in table S.2.

Appendix T

ETAF messages in NAT

The ETAF (Elapsed Time And Forecast) message contains a set of EETs for three different speeds for a particular OTS track at a particular FL of this track. The ETAF messages are produced for each OTS track and for each published FL. They are published twice a day for both eastbound and westbound OTS. They are produced on the base of the information about the expected meteorological conditions for the oncoming day. ETAF messages are used in case of a control system failure, to calculate route times for aircraft on OTS.

Below an example of ETAF message is introduced. Further the main components of this massage are explained.

1304 ETAF FORECAST TIME 020000

TRACK U FLIGHT LEVEL 320 EASTBOUND

YAY HECKK 53N50W 55N40W 56N30W 56N20W 56N15W MIMKU MORAG

M080 0013 0016 0045 0038 0038 0020 0020 0003 0313

M082 0013 0015 0043 0037 0037 0019 0019 0002 0305

M084 0012 0015 0043 0037 0037 0019 0019 0002 0304

The 1st line of this message starts with a four digit number ("**1304**") representing the time when the message is being published in UTC. It is followed with the message identifier "**ETAF**".

The 2nd line defines the OTS track ("**TRACK U**"), the FL for which the EETs are defined ("**FLIGHT LEVEL 320**") and the direction in which the track is used ("**EASTBOUND**").

The 3d line represents the sequence of WPs defined for the current track starting from the most western ("**YAY**", ... , "**MORAG**").

The next three lines define the EETs between the WPs for the particular Mach. Each of these lines starts with Mach declaration. There are three standard Machs: "**M080**", "**M082**" and "**M084**". Further, the sequence of EETs needed for cruising between the consecutive WPs at this Mach is listed. The times are expressed in minutes (in 4-digit-UTC format). For example, at speed M080 the aircraft is estimated to spend 13 minutes for cruising from YAY to HECKK, 16 minutes from HECKK to 53N50W, 45 minutes from 53N50W to 55N40W, etc. The last number in this sequence of EETs represents the estimated total time of the aircraft cruising the track from its entry point to the exit point. For example, at speed M080 the duration of the flight via OTS is estimated to be 3 hours 13 minutes, and at speed M084 - 3 hours 4 minutes.

The EETs are used in our simulations for two reasons. First, we base on these values to estimate the track entry time for those flights for which this time is not defined in their FPLs. For example, if for any flight f the track entry time, t^f_{in}, is not defined, but the time of its arrival at WP i (denoted as t^f_i) is known, then t^f_{in} can be estimated using the EETs up to this WP i (the EET between WPs j and $j+1$ is denoted as e^f_j):

$$t^f_{in} \equiv t^f_0 = t^f_i - \sum_{j=0}^{i-1} e^f_j. \tag{T.1}$$

In addition to this, the EETs are used to estimate the WSs along the OTS tracks. If we designate the distance between WPs i and $i+1$ as l_i, and recall, that the TAS between these WPs, v^f_i, can be obtained from the declared Mach, then the WS between these WPs, W_ijj, can be calculated using the formula:

$$WS_{ijj} = \frac{l_i}{e^f_i} - v^f_i. \tag{T.2}$$

Evidently, in such formulation, the WS depends on the TAS. To obtain more general results, the WS can be averaged over the three defined Machs. Further in the flight

simulations, the obtained wind speed W_{ijj} is to be added to the given TAS when cruising between WPs i and $i + 1$.

Appendix U

Air navigation errors

Flight safety is the leading priority for air carriers and the ATM, and all the effords are made to assure the safe flight progress. Nevertheless, the navigation errors do occur, having different levels of gravity: from simple arriving delays to aviacatastrophes with fatal outcomes. There are numerous factors that contribute to such erroneous events in navigation [55], including:

- human factor, that is the major source of critical navigation errors, and can be related to
  - mistakes made by the aircrew while operating an aircraft,
  - violation of rules and regulations by the aircrew,
  - improper actions taken by the aircrew due to mental or psycological problems,
  - improper command/supervision and its negative effect on the aircrew;
- technological factor, including possible falures in
  - the engine,
  - display equipement,
  - navigation equipement,
  - communication, etc.;
- environmental factor, including
  - changing weather conditions being the most essential component,

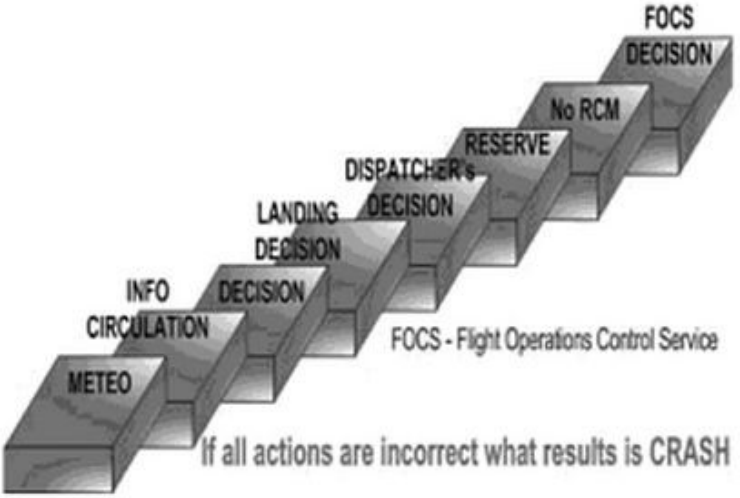

FIGURE U.1: An example of chain of errors during the flight[1]

– Bird Aircraft Strick Hazard (BASH),

– terrain configuration, urbain areas, etc.

In the majority of cases of erroneous events it is more reasonable to speak not of one cause, but of a *chain of errors*, that lead to such an event. In [55], an example of such a chain is given (Fig. U.1). Several chain links are mentioned below:

- the erroneous weather forecast was provided,
- the information on weather conditions getting worse did not reach the flight operation control centre due to communication falure,
- the fact of non-delivered information was ignored on the management level,
- the aircraft was issued not a suitable FPL,
- the aircrew decided to land despite the actual weather condition,
- the approach controller did not deviate the aircraft to an alternative airfield,
- the aircrew members did not cooperate during landing,
- all this resulted in an excessive descent rate,
- the landing controller did not abort the landing,
- and that finally lead to a ground collision.

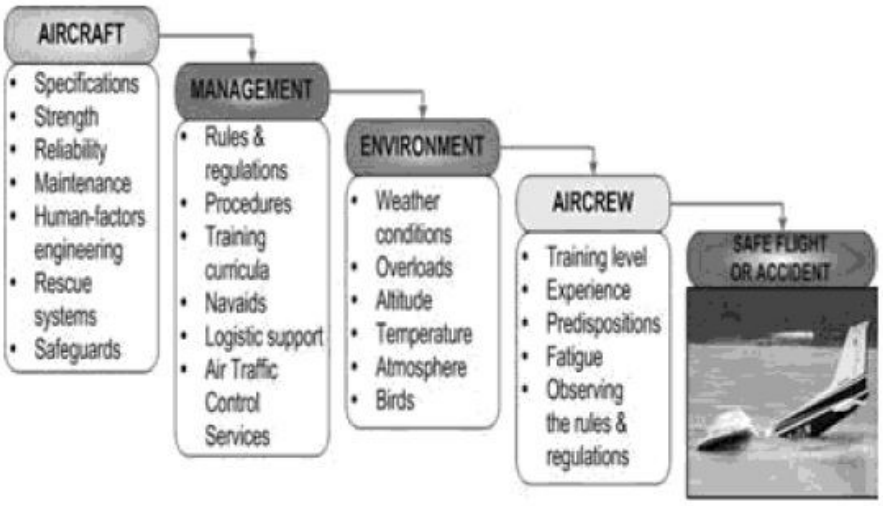

FIGURE U.2: A chain of safaty for a flight[2]

In addition to the chain of errors, Zurek et all. introduce also a *chain of safety* (Fig. U.2), which objective is to link all the factors having impact on the aircraft accidenatal errors rate in order to perform a sophisticated analyses of the overwhole system and propose the solutions to the system improvement. One of the most imporatant measures taken in this direction, is establishing of safety rules and regulations that are to be followed by crew memebers in first turn in case of erroneus event.

For example, in [129], such rules for air navigation in the NAT are discribed. ICAO North Atlantic Working Groups have noted repetitive oceanic errors, that are subdivided into three major groups:

- large height deviations (300 feet or more), that are mainly the result of *Conditional CLRs*[3], inproperly treated ,
- Gross Navigation Errors (GNES) (25 NM or more), which prime cause is the reclearence scenario[4]
- errosion of longitudinal separation, that may arise from:
  - on-board clock inaccuracy,

[1]From [55]
[2]From [55]
[3]An ATC CLR given to an aircraft with certain conditions or restrictions, e.g. FL changing based on a UTC time or specific geographical position
[4]When a CLR, different from the initial FPL or initial CRL, is issued to a flight, the aircraft crew must reprogram the FMS (or other on-board equipement) update the computed FPL, update the plotting chart, etc.

- mistakes in Mach assigning/executing,
- chaning meteorological conditions being the most often factor.

To summarize, the recommendations from [129] inciter the pilots to pay extreem attention to follow the issured CLRs (and not the FPL), especially in cases of reclearance or conditional CLR, to verify the functionality of the equipement, to compare continiously the actual aircraft position with the planned one, and the ATAs with ETAs.

Flight delays, that is another flight performance criterion crucially important for airlines, have the same origins as the violations of longitudinal separation. Flight delays are also calculated as the difference between the ATAs and ETAs. In [56], several categories of aircraft delays are distinguished. They are listed below in the order of decrease of their impact on the aircraft on-time arrival performance:

- Late Arriving Aircraft Delay, caused by the late arrival of the previous flight with the same aircraft;
- National Aviation System (NAS) Delay, referred to a broad set of conditions (e.g. non-extreme weather conditions, airport operations, heavy traffic volume, air traffic control, etc.);
- Air Carrier Delay, induced by the circumstances within the airline control (e.g. maintenance or crew problems, etc.);
- Extreme Weather Delay, related to significant meteorological conditions (actual or forecasted) that, delay or prevent the operation of a flight;
- Security Delay, caused by evacuation of terminal or concourse, re-boarding of aircraft because of security breech, inoperative screening equipment and long lines in excess of 29 minutes at screening areas.

The contribution of each delay category into the percentage of delayed flights can be seen in Figure 3.1.

Appendix V

Wind forecast facilities

Nowadays, the wind forecast is made by the means of the *Numerical Weather Prediction* (NWP) models [58]. These models, being constantly improved, nevertheless are confronted to the difficulties related to the wind nature. Winds, being the atmospheric air motions, are created by two main sources:

- the differences in atmospheric pressure on a constant altitude, pushing the air parcels from the areas of high pressure to the areas of low pressure;
- and the earth rotation, pulling the air parcels toward the right in the Northern Hemisphere and toward the left in the Southern Hemisphere.

Thus, to produce an accurate wind forecast one need to know:

- the strength of the wind at the beginning of the forecast,
- its direction, and
- the gradient of the slope of the constant pressure surfaces along which the air parcels are moving,
- which is directly related to the temperature changes not only at the current pressure level, but also at all points below,
- that, in turns, are caused by advection[1].

[1]The process by which warmer and colder masses are moved from one location to another

As a result, wind forecasting turns to be a complicated problem, which requires numerous precise meteorological information. Modern NWP analysis systems are designed to use the combination of all available data sets, which are given by:

- radiosondes, that
  - provide good observations of winds, temperature and moisture,
  - but are confined to land masses (primarily, to the more affluent areas of the Northern Hemisphere),
  - and are available only several times (often, once or twice) per day;
- satellite systems, that
  - provide more global coverage (especially, for oceans),
  - but are restricted to temperature and moisture,
  - and do not depict sudden changes in temperature in the vertical (e.g. below the JS);
- automated aircraft reports, which are
  - the major source of direct observations of the atmosphere,
  - and the only source of weather information in the upper atmosphere,
  - available at non-synoptic times,
  - exceptionally accurate and having high resolution (wind data is even considered to be one of the most accurate data from any atmospheric measurement system) [58],
  - but highly sensitive to the extreme weather conditions in comparison to other data sources,
  - and often unavailable in such conditions (aircraft do not fly in the regions of strong storms) [63].

Appendix W

On-board meteorological measurements

Each modern commercial aircraft is capable of performing instant measurements of meteorological conditions, such as:

- temperature,
- air pressure,
- wind magnitude and direction.

These measurements are made directly during the flight using the special on-board equipment. The overview of such capabilities can be found, for example, in [59, Chapter 2]. The study of meteorology was performed in parallel with the aircraft development, since these last were provided with the first flight recorders.

In 1940th the TAS was measured using pitot-static[1] principle, vertical acceleration, and altitude, and its magnitude was estimated due to the aircraft response to a gust. The WS, thus, was deduced from this TAS and the GS. This method had several serious drawbacks, one of which was its dependence on the aircraft weight.

[1] A pitot-static system is a system of pressure-sensitive instruments, generally consisting of a pitot tube, a static port, and the pitot-static instruments. This equipment is used to measure the forces acting on a vehicle as a function of the temperature, density, pressure and viscosity of the fluid in which it is operating.

In 1950th a much more comprehensive platform was developed, that measured the three components of the WS relative to the ground using three orthogonally-mounted accelerometers, and those relative to the aircraft using fixed wind vanes and pitot-static system.

In 1960th a vertically stabilized platform for measuring vertical acceleration was implemented, which is now the major component of the INS. The pressure probes were also improved with the time in comparison to the temperamental wind vanes sensitive to icing effects.

Using the moving platform, the true WS can be calculated as a simple vector sum of the air speed relative to the moving platform, and the platform speed relative to a coordinate system fixed with respect to the earth. It must be noted, that the magnitudes of the last two speeds is much greater than the resulting WS, thus, they must be known with a high degree of accuracy.

The air speed of the moving platform is defined by combination of the TAS with the airflow incidence angles. The TAS is obtained using pitot-static system, from the differential pressure, the absolute static pressure and the air temperature. There are several techniques to measure the airflow angles:

- using freely rotating vanes that align themselves with the airstream;
- using fixed vanes upon which the air force is measured;
- using inviscid flow theory, applied to the pressure difference measured between two points on a probe mounted ahead of the aircraft.

The platform speed relative to the Earth is obtained by measuring the aircraft GS, which is performed by combining the inertial data and navigational reference data. The main difficulty is that the GS cannot be measured directly, but should be derived from aircraft position and acceleration, that in turn can be measured directly. The following systems are used for GS measurements:

- INS, providing accurate short-term values of aircraft acceleration, based on the three orthogonal accelerometers;

- DME-VOR, providing the distance and angle to one of a range transmitters, from which the aircraft position is dedicated by triangulation;
- GPS, providing the aircraft position based on the satellite position known with a high precision.

Once the auxiliary data obtained, the GS magnitude and direction are to be determined from these data. From the practical point of view it is more instructive to deal with vertical and horizontal GS components separately:

- the vertical GS is computed as a combination of the accelerometer data with a static pressure-derived altitude in a third-order baro-inertial feedback loop;
- the horizontal GS is derived from the external navigation systems measurements, by applying any appropriate kind of filtering, e.g. Fourier transform filter, Kalman filter, etc.

These basic techniques and corresponding mathematical formulations are briefly discussed in [59]. More detailed mathematical models for TAS and wind measurements and sophisticated formulas used can be found in [60]. Furthermore, more modern methods were proposed and implemented in order to provide more accurate wind measurements on-board of the aircraft.

For example, in [61], the new mathematical approaches are developed to be applied for wind measurements of a research aircraft, the most significant of which are listed below.

- For the horizontal GS component calculation, Khelif et all. chose to use the difference between the GPS and INS data, appropriately processed by the low-pass filtering and then added to the raw INS data. On doing so, they reduced the high-frequency INS errors and eliminated the higher-frequency fluctuations of the GPS data.
- Moreover, they found out the necessity to use the moist-air thermodynamic properties in the compressible flow equations in the prevailing conditions of high humidity and low winds (e.g. tropical conditions) instead of the dry-air properties.

- Furthermore, the calibration of the random and fuselage sideslip differential pressure was performed on data from reverse heading maneuvers, in order to obtain the sideslip angle.

- For vertical GS measurements, a new technique was used to calculate the slow-rate in order to overcome the differences in the values, calculated in the baro-inertial feedback loop with different frequencies. The method takes the two sources of speed - one at high frequency, obtained from the INS vertical acceleration output, another at low frequency, calculated by taking the time-derivative of barometric pressure altitude - filter their inaccurate portions digitally and combine them together.

- The angle of attack was obtained based on the measurements from the two independent sensors, and a new technique of its calibration was proposed.

The results of the experiments performed on the two appropriately equipped research aircraft demonstrate a good correspondence for the measured winds.

Another example of a possibility to improve wind measurements is described in [62], where it is shown how the wind information can be extracted from radar observations. Several situations are considered:

- Mode S radar[2], when the Kalman filter was used to extract the wind by removing the noise;

- Standard radar and one aircraft, for which executing of the *two assymetric turns*[3] is required;

- Standard radar and two aircraft, when executing of only one turn for both aircraft is needed.

Delahaye et all. describe the principle of the Kalman filter and its known improvements: the Extended Kalman filter and the Unscented Kalman filter. Further, they define the mathematical models used in each of the cases in terms of state vectors and matrices, relating these states with each other and with measurements. The simulations, performed

[2]Mode S is the radar system, that establishes a data link between the radar and the aircraft, which gives the radar the access to the on-board aircraft parameters, in particular, the TAS.

[3]Three straight line separated by two turns

on the realistic data, seemed to produce accurate wind estimates under appropriate assumptions:

- when TAS are available, linear models can be used with regular Kalman filter,
- when only position measures are available, closed form of the wind is to be used.

In addition to this, the authors proposed a method of reconstruction of the continuous wind field from the point wind measurements. The method uses the differential operator of the shallow-water model, kernel functions and interpolating vector splines. The authors draw the attention to the fact that this method can be used only for the en-route flight portion because of the limitations of the shallow-water model.

We will not go deeper in the details of the physical processes being the background for airborne wind measurements.

Appendix X

Different extrapolation methods to adjust winds

In our computational experiments, we have tested several extrapolation approaches of how an aircraft f following aircraft $f_1, ..., f_M$ on *the same track* j at the same FL k can obtain the adjusted value of wind $\vec{\hat{W}}^f_{adj}(\hat{t}^f_{i,s}, \lambda_{i,s}, \phi_{i,s}, a_k)$ from the wind values measured by these M preceding aircraft $\vec{\hat{W}}^{f_m}(t^{f_m}_{i,s}, \lambda_{i,s}, \phi_{i,s}, a_k)$, $m = 1, ..., M$ (equation (3.6)). For these tests we consider all the aircraft to report over common points $s = 1, ..., N^f_{ijj} + 1$, $i = 1, ..., Nx$. Thus, further, in order to simplify the notations, we will omit explicit terms of s-point coordinates in the expression of the wind-vector functions, assuming, evidently, that the values of these functions are computed at these points. Moreover, we will also omit the altitude variable a_k in the wind-function dependence, as it does not change along the flights. In other words, the following notation is used throughout of this appendix, for example, for adjusted wind: $\vec{\hat{W}}^f_{adj}(\hat{t}^f_{i,s}, \lambda_{i,s}, \phi_{i,s}, a_k) = \vec{\hat{W}}^f_{adj}(\hat{t}^f_{i,s})$.

The most simple way of extrapolation (further referred as *Last Measured Extrapolation*, LME) is to use just the last measured value (from aircraft f_1) and to consider:

$$\vec{\hat{W}}^f_{adj}(\hat{t}^f_{i,s}) = \vec{\hat{W}}^{f_m}(t^{f_m}_{i,s}). \tag{X.1}$$

Another way is to use the last p ($p \geq 2$) measurements and construct the interpolating polynomial of degree $p-1$ taking the values $\vec{\hat{W}}^{f_k}_{i,s}(t^{f_k}_{i,s})$ at time moments $t^{f_k}_{i,s}$, $k = 1, ..., p$. This approach gives excellent results in case we consider the aircraft to measure winds

exactly ($\delta_i^f = 0$). But in real case, considering measurement errors, it tends to be inefficient.

The last tested approach is to construct an approximation polynomial of degree p using the values from M aircraft ($p < M$) by the method of least squares. We apply this method to polynomials of $p = 1$, $p = 2$ and $p = 3$. Also we use two types of values:

- directly the values of measured winds $\vec{\tilde{W}}_{i,s}^{f_k}(t_{i,s}^{f_k})$, $k = 1, ..., p$ (this method is further referred to as *Least Squares p-Approximation by Values*, LSVA-p):

$$\vec{\hat{W}}_{adj}^{f}(\hat{t}_{i,s}^{f}) = least\_squares(p, \vec{\tilde{W}}_{i,s}^{f_1}(t_{i,s}^{f_1}), ..., \vec{\tilde{W}}_{i,s}^{f_M}(t_{i,s}^{f_M})). \tag{X.2}$$

- the differences between the measured and estimated wind values: $\Delta\vec{\hat{W}}_{i,s}^{f_k}(t_{i,s}^{f_k}) = \vec{\hat{W}}_{i,s}^{f_k}(t_{i,s}^{f_k}) - \vec{\tilde{W}}(t_{i,s}^{f_k})$, $k = 1, ..., M$ (this approach is further referred to as *Least Squares p-Approximation by Differences*, LSDA-p):

$$\Delta\vec{\hat{W}}_{adj}^{f}(\hat{t}_{i,s}^{f}) = least\_squares(p, \Delta\vec{\tilde{W}}_{i,s}^{f_1}(t_{i,s}^{f_1}), ..., \Delta\vec{\hat{W}}_{i,s}^{f_M}(t_{i,s}^{f_M})); \tag{X.3}$$

$$\vec{\hat{W}}_{adj}^{f}(\hat{t}_{i,s}^{f}) = \vec{\tilde{W}}(\hat{t}_{i,s}^{f}) + \Delta\vec{\hat{W}}_{adj}^{f}(\hat{t}_{i,s}^{f}). \tag{X.4}$$

Our experiments show that, for the LSVA-p and LSDA-p approaches, the best results are given when approximating by linear function ($p = 1$). That is not surprising, as the real-wind function, $W(t, \lambda, \phi, a)$, is constructed by linear interpolation. The quadratic polynomial ($p = 2$) also gives good results, while the results from higher polynomial degrees are much worst. We also note that using the LSDA-p instead of the LSVA-p slightly ameliorates the results.

Furthermore, we have also tried to use for approximation not all but just the m last from M preceding aircraft ($m < M$). The truncation of aircraft sequence was made either by the number of aircraft (fixed m), or by time period (e.g. just the aircraft having past during last 20 minutes). However, this approach provides no noticeable amelioration, so we are not going to present these results.

In order to test the proposed extrapolation methods, we performed two series of simulations with $N = 20$ aircraft following one predefined OTS track (middle track, $j = 3$).

f	Speed v^f (m/s)	Track entry time t_{in}^f (s)
1	254.65	20.33
2	257.22	332.79
3	241.79	1209.80
4	252.08	1320.33
5	231.50	1534.68
6	241.79	1692.07
7	254.65	1751.93
8	234.07	2532.54
9	257.22	2562.23
10	246.93	2890.66
11	231.50	4499.87
12	252.08	4948.49
13	231.50	6200.60
14	241.79	6504.59
15	252.08	6721.59
16	249.51	8475.58
17	234.07	8948.42
18	236.64	10065.67
19	246.93	10144.18
20	239.22	10592.99

TABLE X.1: Generated aircraft speeds and track entry times

For the first series, the aircraft track entry times are randomly distributed in the 2-hours time period ($t_{in}^f \in [0,2]h$), and for the first series - in the 3-hours time period ($t_{in}^f \in [0,3]h$). On during so, we assure that all these aircraft exit the OTS track within the period of OTS validity. We suppose that the aircraft are sorted according to their track entry time: $t_{in}^f \leq t_{in}^{f+1}$ for $f = 1, ..., N-1$. An example of the flight data for 3-hours entry-time distribution is presented in Table X.1. Note that for this preliminary study, we do not care whether the generated configuration of flights produces any conflicts, *i.e.* we do not verify the separation between the aircraft.

Table X.2 presents the results of simulations for the flight set from Table X.1 using the wind forecast for April 26, 2013 (several corresponding wind fields are presented in Figure 3.7). In this table, $\tilde{\epsilon}^f$ is the absolute error of the AT prediction at track exit using MF, *i.e.* $\tilde{\epsilon}^f = \tilde{t}_{out}^f - t_{out}^f$, where $\tilde{t}_{out}^f$ and t_{out}^f are forecast and real track exit time of aircraft f correspondingly. Further, $\tilde{\varepsilon}^f$ is the relative value of the AT prediction at track exit using MF, *i.e.* $\tilde{\varepsilon}^f = \frac{|\epsilon^f|}{p^f} \cdot 100\%$, where $p^f = (t_{out}^f - t_{in}^f)$ being the *total cruising time* of aircraft f along the track. $\hat{\epsilon}^f$ and $\hat{\varepsilon}^f$ being absolute and relative AT prediction errors using WN, are defined in the same manner.

	MF prediction		WN prediction using extrapolation method:				
			LME		LSDA-2	LSVA-1	LSDA-1
	$\lvert\tilde{\epsilon}^f\rvert$, s	$\tilde{\varepsilon}^f$, %	$\lvert\hat{\epsilon}^f\rvert$, s	$\hat{\varepsilon}^f$, %	$\hat{\varepsilon}^f$, %	$\hat{\varepsilon}^f$, %	$\hat{\varepsilon}^f$, %
2	50.50	0.499	2.06	0.020	0.005	0.020	0.005
3	59.65	0.557	17.39	0.162	0.360	0.355	0.360
4	54.92	0.533	9.81	0.095	0.064	0.104	0.103
5	66.06	0.593	0.36	0.003	0.264	0.040	0.048
6	60.68	0.567	4.37	0.041	0.018	0.043	0.044
7	54.61	0.535	5.84	0.057	0.013	0.014	0.013
8	66.93	0.608	0.22	0.002	0.207	0.042	0.036
9	55.04	0.545	5.60	0.055	0.021	0.024	0.022
10	60.66	0.578	3.53	0.034	0.042	0.034	0.032
11	70.84	0.637	28.23	0.254	0.223	0.008	0.009
12	60.48	0.588	5.30	0.052	0.041	0.033	0.034
13	71.86	0.647	15.13	0.136	0.026	0.054	0.024
14	66.10	0.619	2.16	0.020	0.020	0.044	0.027
15	61.08	0.595	1.47	0.014	0.023	0.036	0.025
16	60.42	0.583	3.25	0.031	0.058	0.146	0.076
17	68.25	0.621	1.34	0.012	0.022	0.149	0.072
18	68.78	0.632	5.69	0.052	0.044	0.129	0.038
19	63.64	0.608	2.58	0.025	0.029	0.079	0.018
20	68.44	0.77	0.007	0.024	0.040	0.082	0.012
Ave	**62.57**	**0.589**	**6.06**	**0.057**	**0.080**	**0.076**	**0.052**

TABLE X.2: Comparison of AT exit time prediction errors for aircraft on a single OTS track when using MF and WN

Note that Table X.2 does not include the first flight, as for this flight there are no preceding aircraft, thus, the adjusted track exit time cannot be calculated. For the 19 rest of flights, the table presents the values for the adjusted track exit time obtained by approximation methods giving the best results, i.e. LME, LSDA-2, LSVA-1 and LSDA-1. The last row (**Ave**) contains the corresponding average values for 19 flights.

On examining the results presented in Table X.2, that reflect the common tendency, we obtain the following conclusions concerning the extrapolation methods:

- the best extrapolation methods to adjust wind function from the preceding aircraft wind measurements are found to be LME and LSDA-1;
- using the information from all (or several) preceding aircraft on the same track does not give noticeably better results than using the information from the latest aircraft only.

Thus, we choose to implement the simple LME approach for further simulations.

In addition to this, we can provide several observations concerning the qualities of the presented prediction methods (MF and WN) for this artificial flight set:

- the aircraft MF track-exit time, $\tilde{t}^f_{out}$, differs from the real track-exit time, t^f_{out}, by about 1 minute in average, which involves 0.6% from the total cruising time;
- the track-exit time adjusted by WN, $\hat{t}^f_{out}$, obtained by the best approximation method (LME) differs from the real track-exit time, t^f_{out}, by about 5 second, which constitute 0.05% from the total cruising time;
- thus, using the information (wind measurements) from preceding aircraft on the same track ameliorates the flight prediction (track exit time) for the following aircraft by about 10 times.

Such results clearly demonstrate that using WN would be beneficent for AT prediction. At the same time, the quantitative values of benefits obtained in this preliminary study might differ from the reality, as these values are partly related to the particular artificial data-set structure.

Appendix Y

Geometrical operations on a sphere in geographical coordinates

In this appendix, we summarize the mathematical formulas used to perform different operations and transformations applied to geographical points on a sphere (in practice, on the Earth). Let us first introduce the following notations:

- $q(\lambda, \phi)$ - a geographical point on a sphere, where
- λ is the point longitude in radians, and
- ϕ is the point latitude in radians;
- R - the radius of the sphere;
- $q(x, y, z)$ - a 3D-point in Cartesian coordinates;
- $\vec{q}$ - a 3D-vector with the origine in the center of the sphere (in the origine of the coordinate system) and the end at point q;
- $\arctan 2(y, x)$ - a function returning the angle θ from the convertion of rectangular coordinates (x, y) to polar coordinates (ρ, θ) in the range from $-\pi$ to π;
- $\vec{W}(u, v)$ - a wind vector at a point defined by its west-east (u) and south-north (v) components.

Transformation between Cartesian and spherical coordinate systems

For a given point $q(\lambda, \phi)$ on a sphere of radius R, the 3D-coordinates, (x, y, z), of this point in the left-hand Cartesian system with the origine in the center of the sphere, are defined by the formulas:

$$x = R\cos\phi \cdot \cos\lambda; \tag{Y.1}$$

$$y = R\cos\phi \cdot \sin\lambda; \tag{Y.2}$$

$$z = R\sin\phi. \tag{Y.3}$$

For a given 3D point, $q(x, y, z)$, in the left-hand Cartesian system, its geographical coordinates on a sphere with the center at the system origine, are defined by the formulas:

$$\lambda = \arctan 2(y, x); \tag{Y.4}$$

$$\phi = \arctan 2(z, \sqrt{x^2 + y^2}). \tag{Y.5}$$

Distance between points

The distance from point q_1 to point q_2 along an arc of the Great Circle (GC) of the sphere of radius R is defined by:

$$dist(q_1, q_2) = R\arccos(\sin\phi_1 \sin\phi_2 + \cos\phi_1 \cos\phi_2 \cos(\lambda_2 - \lambda_1)). \tag{Y.6}$$

We appoximate the Earth with a sphere with average radius $R_{Earth} = 6,371.21$ km.

Intermediate points on GC

The coordinates (λ, ϕ) of a point q situated on the GC between points q_1 and q_2, at a ratio r from the first point p_1 ($r = dist(q_1, q)/dist(q_1, q_2)$) are given by the following formulas:

$$\phi = \arcsin(\cos\alpha_0 \cdot \sin\sigma); \tag{Y.7}$$

$$\lambda = \lambda_0 + \arctan 2(\sin\alpha_0 \cdot \sin\sigma, \cos\sigma); \tag{Y.8}$$

where

$$\alpha_0 = \arcsin(\sin\alpha_1 \cos\phi_1); \tag{Y.9}$$

$$\sigma = \sigma_{01} + r(\sigma_{02} - \sigma_{01}); \tag{Y.10}$$

$$\sigma_{0i} = \arctan 2(\tan\phi_i, \cos\alpha_i),\ i = 1, 2; \tag{Y.11}$$

$$\alpha_1 = \arctan 2(\sin(\lambda_2 - \lambda_1), \cos\phi_1 \cdot \tan\phi_2 - \sin\phi_1 \cdot \cos(\lambda_2 - \lambda_1)); \tag{Y.12}$$

$$\alpha_2 = \arctan 2(\sin(\lambda_2 - \lambda_1), -\cos\phi_2 \cdot \tan\phi_1 + \sin\phi_2 \cdot \cos(\lambda_2 - \lambda_1)); \tag{Y.13}$$

$$\lambda_0 = \lambda_1 - \arctan 2(\sin\alpha_0 \cdot \sin\sigma_{01}, \cos\sigma_{01}). \tag{Y.14}$$

Perpendicular to the GC

For two given points q_1 and q_2 on a sphere of radius R, we would like to find a point q_0 such, that the arc of GC (q_2, q_0) is perpendicular to the arc of GC (q_1, q_2). To simplify the notations, we consider that the points are given in Cartesian coordinates;

transformation to/from spherical coordinates is simply made through equations (Y.1)-(Y.5). Furthermore, for simplification, we consider $R = 1$; the generalization for an arbitrary R is simple. Finally, with each point q_i $(i = 0, 1, 2)$ we associate a vector $\vec{q_i}$ with the origine in the center of the sphere and the end at point q_i. Then, the coordinates of the vector $\vec{q_i}$ and the coordinates of the point q_i are equal. Vector $\vec{q_0}$ is obtained by a cross product:

$$\vec{q_0} = \frac{\vec{q_1} \times \vec{q_2}}{|\vec{q_1} \times \vec{q_2}|}. \tag{Y.15}$$

Thus, the Cartesian coordinates of point q_0 are obtained by:

$$q_0(x_0, y_0, z_0) = (\frac{\tilde{x}_0}{\tilde{R}_0}, \frac{\tilde{y}_0}{\tilde{R}_0}, \frac{\tilde{z}_0}{\tilde{R}_0}), \tag{Y.16}$$

where

$$\tilde{x}_0 = z_1 y_2 - y_1 z_2, \tag{Y.17}$$

$$\tilde{y}_0 = x_1 z_2 - z_1 x_2, \tag{Y.18}$$

$$\tilde{z}_0 = y_1 x_2 - x_1 y_2, \tag{Y.19}$$

$$\tilde{R}_0 = \sqrt{\tilde{x}_0^2 + \tilde{y}_0^2 + \tilde{z}_0^2}. \tag{Y.20}$$

Offset point on the perpendicular to the GC

For two given points q_1 and q_2 on a sphere of radius R, we would like to find a point q such, that the arc of GC (q_2, q) is perpendicular to the arc of GC (q_1, q_2) and the distance from point q_2 to point q is equal to r. Here again, without loss of generality, we can consider $R = 1$. To find the needed point q, we proceed in two steps. First, we find a point p_0, such as defined by equations (Y.16)-(Y.20). Thus, we obtain a GC

arc (q_2, q_0) perpendicular to the arc (q_1, q_2). Second, we need to find a point q on this arc (q_2, q_0) lying at the distance r from point q_2. To do so, we can apply equations (Y.7)-(Y.14) to points q_2 and q_0. Nevertheless, for this particular case, when vector $\vec{q}_0$ is perpendicular (by construction) to vector $\vec{q}_2$, there is a more simple way to find point q, using operations on vectors:

$$\vec{q} = \frac{\vec{q}_2 + \tan(r)\vec{q}_0}{|\vec{q}_2 + \tan(r)\vec{q}_0|}. \tag{Y.21}$$

The Cartesian coordinates of point q can be simply deduced from equation Y.21.

Initial bearing along the GC

For two given points q_1 and q_2 on a sphere of radius R, we would like to find an initial *bearing*, or *course*, *i.e.* an angle θ between the initial direction to follow when moving from point q_1 to point q_2 and the direction to the North. The initial bearing is defined by the equation:

$$\theta = \arctan 2(\sin(\lambda_2 - \lambda_1) \cdot \cos\phi_2, X), \tag{Y.22}$$

where

$$X = \cos\phi_1 \cdot \sin\phi_2 - \sin\phi_1 \cdot \cos\phi_2 \cos(\lambda_2 - \lambda_1). \tag{Y.23}$$

Projection of the wind vector on the GC

For two given points q_1 and q_2 and for a wind vector $\vec{W}(u, v)$ defined at point q_1 we would like to find the magnitude of the wind in the direction of cruise between points q_1 and q_2, or, in other words, we would like to compute the projection of the wind vector on the GC arc (q_1, q_2). The cruising direction (the bearing), or direction of the projection, is constantly changing along this GC arc. To simplify the computations, we thus perform the projection on the initial direction (initial bearing). We proceed in three steps. First, we compute the bearing θ using equations (Y.22)-(Y.23). Next, we compute the direction of the wind vector by equation:

$$\theta_w = \arctan 2(\frac{u}{|\vec{W}|}, \frac{v}{|\vec{W}|}), \tag{Y.24}$$

where

$$|\vec{W}| = \sqrt{u^2 + v^2}. \tag{Y.25}$$

Finally, we obtain the projection simply by formular:

$$W_{(q_1,q_2)} = |\vec{W}| \cos(\theta - \theta_w). \tag{Y.26}$$

Appendix Z

Choice of the discretization time step

The choice of the discretization time step for the algorithm of conflict detection should be justified. Ideally, the time step should be sufficiently small in order to detect all possible conflicts between two aircraft en-route. In other words, this choice should guarantee that the definition of the AT-to-AT conflict (4.17) is correct, *i.e.* the ATs of two flights are conflict-free if and only if no one pair of points of AT-discretization is in conflict.

Let us consider the worst scenario for conflict detection as it is made in [130]. It is quite easy to see that it is the case, when two aircraft are following parallel routes, separated by a distance D which is less than but very close to the horizontal separation norm Δ_h ($D \leq \Delta_h$), in opposite directions at the highest TAS, v_{max} (see Figure Z.1). Then the relative aircraft speed is $2v_{max}$.

Let us denote as S the length of the intersection segment of the AT of aircraft g and the protection circle of aircraft f (the circle with a center at current position of aircraft f and radius Δ_h, forbidden for penetration for other aircraft). Thus, S defines the part of AT of aircraft g being in conflict with aircraft f. S can be easily calculated from the simple geometry:

$$S = 2 \cdot \sqrt{\Delta_h^2 - D^2} \tag{Z.1}$$

On the other hand, S is equal to:

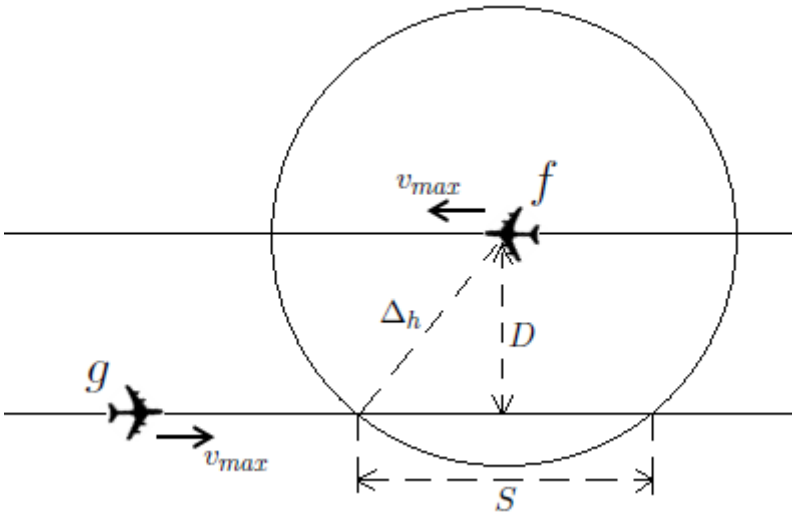

FIGURE Z.1: Worst scenario for conflict detection between two aircraft

$$S = 2v_{max}t_c, \tag{Z.2}$$

where t_c is the time that the aircraft g spends in the protection circle of the aircraft f. Thus, from the above formulas, this time is defined by:

$$t_c = \frac{\sqrt{\Delta_h^2 - D^2}}{v_{max}}. \tag{Z.3}$$

Thus, in order to detect this conflict of duration t_c using the discretization technique, the discretization time step, Δ_t, should be less than t_c ($\Delta_t < t_c$) for any possible t_c. As the distance between the ATs, D, can be as close to the separation norm Δ_h as desired, than t_c can be as close to 0 as desired. This makes it impossible to choose one fixed time step Δ_t that would guarantee that no conflicts, even too short, are missed.

However, by fixing time step Δ_t sufficiently small, we can control the maximal duration of the conflict that could be missed by our algorithm. Indeed, that would be the conflict with duration $t_c \leq \Delta_h$. This actually mean that the conflicts could be missed for parallel trajectories separated by the distance D less than Δ_h but more than D_{max} ($D_{max} \leq D \leq \Delta_h$), where:

$$D_{max} = \sqrt{\Delta_h^2 - v_{max}^2\Delta_h^2}. \tag{Z.4}$$

In other words, in this case we assure that the aircraft keep being separated with the norm D_{max} and not Δ_h. One of the solutions to avoid this drawback is to rise slightly the real separation norm, Δ_h, by replacing it with $\tilde{\Delta}_h = \Delta_h + \epsilon$, and then to fix D_{max} equal to current separation norm $D_{max} = \Delta_h$. Then we can guarantee total conflict avoidance with time step:

$$\Delta_t \leq \frac{\sqrt{2\Delta_h\epsilon + \epsilon^2}}{v_{max}}. \tag{Z.5}$$

With such an approach the number of conflicts is never underestimated, but can be overestimated (as the separation norm is increased). Thus, for this preliminary study we decided to keep the current separation norm and to neglect the probability to miss some conflicts, as:

- the presented deconflicting is made on the strategic level of AT planning, and the resulting ATs would be surely modified further at the tactical level;
- second, the number of missed conflicts should be relatively small, as the probability to obtain the "worst" AT configuration described in Figure Z.1 is very small for free flights;
- and third, these conflicts, if occur, are of a very short period and on the very border of the protection circle, and thus, would not affect the flight progress in the reality.

Recall that v_{max} for transatlantic flights is about 600 kts (600 NM per hour), Δ_h in our study was set to 30NM, and Δ_t was chosen to be 15 seconds. Then, in our case, we obtain from (Z.4):

$$D_{max} = \sqrt{30^2 - \frac{600^2}{3600^2} \cdot 15^2} \approx 29.9\ NM. \tag{Z.6}$$

Thus, in our study we guarantee conflict resolution with separation norm 29.9 NM, and the possible conflict neglect does not exceed the distance of 0.1 NM at the border of the protection volume, which is found to be acceptable from the practical point of view considering the particularities of the study.

Bibliography

[1] International Civil Aviation Organisation (ICAO). 2013-2028: Global Air Navigation Capacity & Efficiency Plan, 2014. Doc 9750.

[2] Air Transport Action Group (ATAG). Aviation Benefits Beyond Borders, April 2014.

[3] Federal Aviation Administration. National Airspace and Procedures Plan, 2010.

[4] Federal Aviation Administration. FAA's NextGen Implementation Plan, March 2011.

[5] NextGen. URL https://www.faa.gov/nextgen/.

[6] European Commission. Commission staff working paper on preparing a deployment strategy for the Single European Sky technological pillar. Technical report, December 2010.

[7] European Commission. SESAR: The futur of flying, 2010.

[8] SESAR. URL http://www.sesarju.eu/.

[9] Federal Aviation Administration. NextGen Implementation Plan, August 2014.

[10] SESAR Joint Undertaking. SESAR: Annual report 2013, 2014.

[11] O. Rodionova, M. Sbihi, D. Delahaye, and M. Mongeau. Optimization of aicraft trajectories in North Atlantic oceanic airspace. In *ICRAT 2012, 5th International Conference on Research in Air Transportation, University of California, Berkeley (USA)*, May 2012.

[12] O. Rodionova, M. Sbihi, D. Delahaye, and M. Mongeau. North Atlantic Aircraft Trajectory Optimization. *IEEE Transactions on Intelligent Transportation Systems*, 15(5):2202–2212, October 2014.

[13] O. Rodionova, D. Delahaye, M. Sbihi, and M. Mongeau. Trajectory Prediction in North Atlantic Oceanic Airspace by Wind Networking. In *33rd Digital Avionics Systems Conference (DASC)*, October 2014.

[14] B. Sridhar, N.Y. Chen, H.K. Ng, O. Rodionova, D. Delahaye, and F. Linke. Strategic Planning of Efficient Oceanic Flights. In *Eleventh USA/Europe Air Traffic Management Research and Development Seminar (ATM2015)*, 2015. accepted.

[15] M.S. Nolan. *Fundamentals of Air Traffic Control*. Cengage Learning, 5th edition, 2010.

[16] P. Belobaba, A. Odoni, and C. Barnhart, editors. *The Global Airline Industry*. John Wiley & Sons, 2009.

[17] R.F. Stengel. *Flight Dynamics*. Princeton University Press, 2004.

[18] E. Torenbeek. Optimum Cruise Performance of Subsonic Transport Aircraft. Technical report, Delft University Press, 1998.

[19] *Getting to grips with fuel economy*. AIRBUS Flight Operations Support & Line Assistance, 4th edition, October 2004.

[20] A. Cook, editor. *European Air Traffic Management: Principles, Practice and Research*. MPG Books Ltd, Bodmin, Cornwall, 2007.

[21] *Instrument Procedures Handbook*. U.S. Department of Transportation, Federal Aviation Administration, Flight Standards Service, 2014. FAA-H-8083-16.

[22] C.R. Spitzer, editor. *Digital Avionics Handbook*. CRC Press Ltd, 2nd edition, 2000.

[23] G. Kulesa. Weather and Aviation: How Does Weather Affect the Safety and Operations of Airports and Aviation, and How Does FAA Work to Manage Weather-related Effects? In *The Potential Impacts of Climate Change on Transportation*, 2003.

[24] R.H Morgford, J.A. Guttman, S.L. Morrow, and P. Kopardekar. The Complexity Construct in Air Traffic Control: A Review ans Synthesis of the Literature. Technical report, U.S. Department of Transportation, Federal Aviation Administration, 1995. DOT/FAA/CT-TN95/22.

[25] D. Delahaye, S. Puechmorel, J. Hansman, and J. Histon. Air Traffic Complexity Map Based on Non Linear Dynamical Systems. *Air Traffic Control Quarterly*, 12 (4):367–388, October 2004.

[26] M. Prandini, L. Piroddi, S. Puechmorel, and S.L. Brazdilova. Towards Air Traffic Complexity Assessment in New Generation Air Traffic Management Systems. *IEEE Transactions on Intelligent Transportation Systems*, 12(3):809–818, September 2011.

[27] G.J. Couluris. Automatic dependent surveillance benefit and cost analysis. Technical report, U.S. Department of Transportation, Federal Aviation Administration, November 1990. DOT/FAA/RD-90/34.

[28] *NAT Doc 007, Guidance concerning air navigation in and above the North Atlantic MNPS airspace*. International Civil Aviation Organisation (ICAO), 2012th edition, 2012. Published on behalf of the North Atlantic Systems Planning Group (NAT SPG) by the European and North Atlantic Office of ICAO.

[29] *Doc4444, Air Traffic Management*. International Civil Aviation Organisation, 15th edition, 2007.

[30] Y.S. Wu, L. Hamrick, T. Karakis, and M. Merkle. Performance Metrics for Oceanic Air Traffic Management. *Air Traffic Control Quarterly*, 12(4):315–338, 2004.

[31] S.C. Mohleji and J. Hoffman. Performance Analysis of North Pacific Operations Using an Automated Air Traffic Control System Simulation. *IEEE Transactions on Control Systems Technology*, 1(3):179–185, 1993.

[32] C.M. Gerhardt-Falk, E.A. Elsayed, D. Livingston, and B. Colamosca. Simulation of the North Atlantic Air Traffic and Separation Scenarios. Technical report, U.S. Department of Transportation, Federal Aviation Administration, 2000. DOT/FAA/CT-TN00/04.

[33] A. Williams, S. Mondoloni, R. Western, T. Karakis, and K. Jones. Beneficial Applications of Airborne Separation Assurance Systems (ASAS) in the Southern Pacific Airspace. In *AIAA 5th Aviation, Technology, Integration, and Operations Conference (ATIO)*, September 2005.

[34] A. Williams, S. Mondoloni, R. Western, T. Karakis, and K. Jones. Application of Airborne Systems for Improving North Atlantic Organized Track System Operations. In *AIAA 5th Aviation, Technology, Integration, and Operations Conference (ATIO)*, September 2005.

[35] R.C. Chartrand, F.J.L. Bussink, T.J. Graff, J.L. Murdoch, and K.M. Jones. Operational Improvements from the In-Trail Procedure in the North Atlantic Organized Track System. In *The 26th Congress of International Council of the Aeronautical Science (ICAS)*, September 2008.

[36] A. Williams and I. Greenfeld. Benefits Assessment of Reduced Separations in North Atlantic Organized Track System. In *6th AIAA Aviation, Technology, Integration, and Operations Conference (ATIO)*, September 2006.

[37] A.R. Williams. Benefits Assessment of Reduced Separations in North Atlantic Organized Track System. Technical report, CSSI Inc., Advanced Programs, 2005.

[38] Draft Implementation Plan for the Trial Application of RLatSM in the NAT Region. Technical report, European and North Atlantic (EUR/NAT) Office, 2013.

[39] P. Louyot. ASEP-ITM simulations from traffic data. Technical report, Advanced Safe Separation Technologies and Algorithms (ASSTAR) Project, October 2007. Version 1.0.

[40] M.R. Garey and D.S. Johnson. *Computers and Intractability: A Guide to the Theory of NP-Completeness*. A Series of Books in the Mathematical Sciences, 1979.

[41] D. Goldberg. *Genetic Algorithms in Search Optimization and Machine Learning*. Addision Wesley, 1989.

[42] J. Koza. *Genetic Programming*. MIT press, 1992.

[43] S. Kirkpatrick, C.D. Gelatt, and M.P.G. Vecchi. Optimization by Simulated Annealing. *Science*, 220:671–680, 1983.

[44] E. Aarts and J. Korst. *Simulated Annealing and Boltzmann Machine*. John Wiley and Sons, 1989.

[45] O. Rodionova. http://www.recherche.enac.fr/~mongeau/NATdata.zip, 2013.

[46] M.E. Lubbecke and J. Desrosiers. Selected topics in column generation. *Operations Research*, 53(6):1007–1023, November 2005.

[47] I. Muter, I. Birnil, and Bulbul K. Simultaneous column-and-row generation for large-scale linear programs with column-dependent-rows. *Mathematical Programming*, 142:47–82, December 2013.

[48] G. Diepen, J.M. van den Akker, J.A. Hoogeveen, and J.W. Smeltink. Using column generation for gate planning at Amsterdam Airport Schiphol. Technical report, Department of Information and Computing Sciences, Utrecht University, 2007.

[49] Z. Lianf. *Column generation and network modeling in large-scale logistics networks.* PhD thesis, New Brunswick Rutgers, The State University of New Jersey, May 2011.

[50] S. Gabteni and M. Gronkvist. A Hybrid Column Generation and Constraint Programming Optimizer for the Tail Assignment Problem. *Integration of AI and OR Techniques in Constraint Programming for Combinatorial Optimization Problems Lecture Notes in Computer Science*, 3990:89–103, 2006.

[51] M.S. Rasmussen, R.M. Lusby, D.M. Ryan, and J. Larsen. A Subsequence Generation Approach for the Airline Crew Pairing Problem. Technical report, DTU Management Engineering, 2011.

[52] I. Muter, S. Birbil, K. Bulbul, G. Sahin, and H. Yenigun. Solving a robust airline crew pairing problem with column generation. *Computers & Operations Research*, 40:815–830, 2013.

[53] A. Mercier and F. Soumis. An integrated aircraft routing, crew scheduling and flight retiming model. *Computers & Operations Research*, 34:2251–2265, 2007.

[54] S. Maher. Solving the integrated airline recovery problem using column-and-row generation. *Operations Research*, 2014. accepted.

[55] J. Zurek, Z. Smalko, and M. Zieja. Methods applied to identify causes of air events. *Reliability, Risk and Safety: Theory and Applications*, 3:1817–1822, 2010.

[56] Office of Aviation Enforcement and Aviation Consumer Protection Division Proceedings. Air Travel Consumer Report. Technical report, U.S. Department of Transportation, February 2015.

[57] Understanding the Reporting of Causes of Flight Delays and Cancellations. URL http://www.rita.dot.gov/bts/help/aviation/html/understanding.html.

[58] R.A. Petersen. Do automated meteorological data reports from commercial aircraft improve forecast? In *ICAO Magazine*, 2004.

[59] R. Wood. *Aircraft Observations of Boundary Layer Structure*. PhD thesis, The University of Manchester Institute of Science and Technology, 1997.

[60] Leise J.A. and Masters J.M. Wind Measurement from Aircraft. Technical report, U.S. Department of Commerce, National Oceanic and Atmospheric Administration, Aircraft Operations Center, 1993.

[61] D. Khelif, S.P. Burns, and C.A. Friehe. Improved Wind Measurements on Research Aircraft. *Journal of Atmospheric and Oceanic Technology*, 16:860–875, July 1999.

[62] D. Delahaye and S. Puechmorel. TAS and wind estimation from radar data. In *28th Digital Avionics Systems Conference (DASC '09)*, October 2009.

[63] W.R. Moninger, Mamrosh R.D., and P.M. Pauley. Automated Meteorological Reports from Commercial Aircraft. *Bulletin, American Meteorological Society*, 84:203–216, February 2003.

[64] R.E. Cole, C. Richard, S. Kim, and D. Bailey. An Assessment of the 60 km Rapid Update Cycle (RUC) with Near Real-Time Aircraft Reports. Technical report, Lincoln Laboratory, Massachusetts Institute of Technology, July 1998.

[65] R.E. Cole, S.M. Green, and M.R. Jardin. Improving RUC-1 Wind Estimates by Incorporating Near-Real-Time Aircraft Reports. *Weather and Forecasting*, 15: 447–460, August 2000.

[66] B.E. Schwartz, S.G. Benjamin, S.M. Green, and M.R. Jardin. Accuracy of RUC-1 and RUC-2 Wind and Aircraft Trajectory Forecast by Comparison with ACARS observations. *Weather and Forecasting*, 15:313–326, June 2000.

[67] S.G. Benjamin, Jamison B.D., Moninger W.R., S.R. Sahm, B.E. Schwartz, and T.W. Schlatter. Relative Short-Range Forecast Impact from Aircraft, Profiler, Radiosonde, VAD, GPS-PW, METAR, and Mesonet Observations via the RUC Hourly Assimilation Cycle. *Mounthly Weather Review*, 138:1319–1343, April 2010.

[68] Moninger W.R., S.G. Benjamin, Jamison B.D., T.W. Schlatter, Smith T.L., and E.J. Szoke. Evaluation of regional aircraft observations using tamdar. *Weather and Forecasting*, 25:627–645, April 2010.

[69] Moninger W.R., S.G. Benjamin, Jamison B.D., Smith T.L., and T.W. Schlatter. TAMDAR and MDCRS impact on RUC foresact. Technical report, Federal Aviation Administration, March 2010.

[70] C. Cardinali, L. Rukhovets, and J. Tenenbaum. Jet Stream Analysis and Forecast Errors Using GADS Aircraft Observations in the DAO, ECMWF, and NCEP Models. *Mounthly Weather Review*, 132:764–779, March 2004.

[71] S.G. Benjamin, B.E. Schwartz, and R.E. Cole. Accuracy of ACARS Wind and Temperature Observation Determined by Collocation. *Weather and Forecasting*, 14:1032–1038, 1999.

[72] Moninger W.R., S.G. Benjamin, Jamison B.D., T.W. Schlatter, Smith T.L., and E.J. Szoke. Evaluation of Regional Aircraft Observations Using TAMDAR. *Weather and Forecasting*, 25:627–645, April 2010.

[73] C. Drue, W. Frey, A. Hoff, and T. Hauf. Aircraft type-specific errors in AMDAR weather reports from commercial aircraft. *Quarterly Journal of the Royal Meteorological Society*, 134:229–239, 2008.

[74] zyGrib - GRIB File Viewer. Weather data visualization, . URL http://www.zygrib.org/.

[75] C. Dey. The WMO format for the storage of weather product information and the exchange of weather product messages in gridded binary form as used by NCEP central operations. Technical report, U.S. Department of Commerce, National Oceanic and Atmospheric Administration, National Weather Service, National Centers for Environmental Prediction, 1998. office Note 388.

[76] JGRIB, . URL http://jgrib.sourceforge.net/.

[77] A. Hollingsworth and P. Lonnberg. The statistical structure of shortrange forecast errors as determined from radiosonde data. Part I: The wind field. *Tellus*, 38A(2): 111–136, 1986.

[78] S. Mondoloni. Aircraft trajectory prediction errors: Including a summary of error sources and data. Technical report, FAA/Eurocontrol Action Plan 16, 1998. Version 0.2.

[79] W. Glover and J. Lygeros. A Multi-Aircraft Model for Conflict Detection and Resolution Algorithm Evaluation. Technical report, Distributed Control and Stochastic Analysis of Hybrid Systems Supporting Safety Critical Real-Time Systems Design (HYBRIDGE), February 2004.

[80] I. Lymperopoulos, G. Chaloulos, and J. Lygeros. An advanced particle filtering algorithm for improving conflict detection in Air Traffic Control. In *International Conference on Research in Air Transportation (ICRAT)*, 2010.

[81] I. Lymperopoulos and J. Lygeros. Sequential Monte Carlo methods for multi-aircraft trajectory prediction in air traffic management. *International Journal of Adaptive Control and Signal Processing*, 24:830–849, 2010.

[82] I.R. Oliveira, R. Quachio, and P.S. Cugnasca. Improving Computation of Simulated Wind-Prediction Error for Air Traffic Applications. *Journal of Aerospace Information Systems*, 11(7):423–432, 2014.

[83] A.G. Lee, S.S. Weygandt, and J.R. Schwartz, B. Murphy. Performance of Trajectory Models with Wind Uncertainty. In *AIAA Modeling and Simulation Technologies Conference*, 2009.

[84] Current NAT tracks, . URL http://aviation.allanville.com/nattracks/.

[85] North Atlantic tracker (NAT). Enroute Flightplanning Resource & Archive., . URL http://blackswan.ch/nat/.

[86] K.J. Viets and C.G. Ball. Validating of Future Operational Concept for En Route Air Traffic Control. *IEEE Transactions on Intelligent Transportation Systems*, 2 (2):63–71, June 2001.

[87] M.F. Lupu, E. Feron, and Z.-H. Mao. Influence of aircrfaft maneuver preference variability on airspace usage. *IEEE Transactions on Intelligent Transportation Systems*, 12(4):1446–1461, December 2011.

[88] D.B. Kirk, S.H. Heagy, and M.J. Yablonski. Problem Resolution Support for Free Flight Operations. *IEEE Transactions on Intelligent Transportation Systems*, 2 (2):72–80, June 2001.

[89] S. Alam and H.A. Abbass. ATOMS: Air Traffic Operations and Management Simulator. *IEEE Transactions on Intelligent Transportation Systems*, 9(2):209–225, June 2008.

[90] J. Krozel. Free Flight Research Issues and Literature Search. Technical report, NASA Ames Research Center, September 2000.

[91] E.A. Irvine, B.J. Hoskins, K.P. Shine, R.W. Lunnon, and C. Froemming. Characterizing North Atlantic weather patterns for climate-optimal aircraft routing. *Meteorological Applications*, 20:80–93, 2013.

[92] B. Sridhar, H.K. Ng, F. Linke, and N.Y. Chen. Benefits Analysis of Wind-Optimal Operations For Trans-Atlantic Flights. In *14th AIAA Aviation Technology, Integration, and Operations Conference*, June 2014.

[93] A.E. Bryson and Y.C. Ho. *Applied Optimal Control*. Taylor and Fransic, 1975.

[94] M. Jardin and A.E. Bryson. Neighboring Optimal Aircraft Guidance in Winds. *Journal of Guidance, Control and Dynamics*, 24(4):710–715, 2001.

[95] H.K. Ng, B. Sridhar, S. Grabbe, and N.Y. Chen. Cross-Polar Aircrfat Trajectory Optimization and the Potential Climate Impact. In *IEEE/AIAA 30th Digital Avionics System Conference*, October 2011.

[96] B. Sridhar, N.Y. Chen, H.K. Ng, and F. Linke. Design of Aircraft Trajectories based on Trade-offs between Emission Sources. In *9th USA/Europe Air Traffic Management Research and Development Seminar (ATM11)*, 2011.

[97] H.K. Ng and B. Sridhar. A Practical Approach for Optimizing Aircraft Trajectories in Winds. In *IEEE/AIAA 31th Digital Avionics System Conference*, October 2012.

[98] H.K. Ng, B. Sridhar, N.Y. Chen, and J. Li. Three-Dimensional Trajectory Design for Reducing Climate Impact of Trans-Atlantic Flights. In *14th AIAA Aviation Technology, Integration, and Operations Conference*, June 2014.

[99] S. Grabbe and B. Sridhar. Central East Pacific Flight Routing. In *AIAA Guidance, Navigation, and Control Conference and Exhibition*, August 2006.

[100] E.I. Andresson. *Lateral Optimization of Aircraft Tracks in Reykjavik Air Traffic Control Area*. PhD thesis, School of Science and Engineering, Reykjavík University, 2012.

[101] N.K. Wickramasinghe, A. Harada, and Miyazawa Y. Flight Trajectory Optimization for an Efficient Air Transportation System. In *28th International Congress of the Aeronautical Science (ICAS 2012)*, 2012.

[102] B. Girardet, L. Lapasset, D. Delahaye, and C. Rabut. Wind-optimal path planning: Application to aircraft trajectories. In *13th International Conference on Control, Automation, Robotics and Vision*, December 2014.

[103] J. Reif and M. Sharir. Motion Planning in the Presence of Moving Obstacles. *Journal of the Association for Computing Machinery*, 41(4):764–790, July 1994.

[104] J.K. Kuchar and L.C. Yang. A Review of Conflict Detection and Resolution Modeling Methods. *IEEE Transactions on Intelligent Transportation Systems*, 1 (4):179–189, December 2000.

[105] Z.H. Mao, E. Feron, and K. Bilimoria. Stability and Performance of Intersecting Aircraft Flows Under Decentralized Conflict Avoidance Rules. *IEEE Transactions on Intelligent Transportation Systems*, 2(2):101–109, June 2001.

[106] L. Pallottino, E. Feron, and A. Bucchi. Conflict Resolution Problem for Air Traffic Management Systems Solved with Mixed Integer Programming. *IEEE Transactions on Intelligent Transportation Systems*, 3(1):3–11, March 2002.

[107] L. Peng and Y. Lin. Study on the Model for Horizontal Escape Maneuvers in TCAS. *IEEE Transactions on Intelligent Transportation Systems*, 11(2):392–398, June 2010.

[108] M.A. Christodoulou and S.G. Kodaxakis. Automatic Commercial Aircraft-Collision Avoidance in Free Flight: The Three-Dimentional Problem. *IEEE Transactions on Intelligent Transportation Systems*, 7(2):242–249, June 2006.

[109] A. Bicchi and L. Pallottino. On Optimal Cooperative Conflict Resolution for Air Traffic Management Systems. *IEEE Transactions on Intelligent Transportation Systems*, 1(4):221–232, December 2000.

[110] N. Dougui, D. Delahaye, S. Peuchmorel, and M. Mongeau. A light propagation model for aircraft trajectory planning. *Journal of Global Optimization*, 56(3): 873–895, July 2013.

[111] D. Delahaye, C. Peyronne, M. Mongeau, and S. Peuchmorel. Aircraft conflict resolution by genetic algorithm and b-spline approximation. In *2nd ENRI International Workshop on ATM/CNS*, pages 71–78, November 2011.

[112] S. Chaimatanan, D. Delahaye, and M. Mongeau. A Hybrid Metaheuristic Optimization Algorithm for Strategic Planning of 4D Aircraft Trajectories at the Continental Scale. *IEEE Computational Intelligence Magazine*, 9(4):46–61, November 2014.

[113] M.R. Jardin. Real-time conflict-free trajectory optimization. In *5th USA/Europe Air Traffic Management Research and Development Seminar (ATM 2003 R&D)*, June 2003.

[114] S. Grabbe, B. Sridhar, and A. Mukherjee. Central East Pacific Flight Scheduling. In *AIAA Guidance, Navigation and Control Conference and Exhibition*, August 2007.

[115] S. Grabbe, B. Sridhar, and A. Mukherjee. Scheduling Wind-Optimal Central East Pacific Flights. *Air Traffic Control Quaterly*, 16(3):187–210, 2008.

[116] B. Girardet. *Trafic aerien: determination optimale et globale des trajectoires d'avion en presence de vent.* PhD thesis, General Mathematics, Toulouse INSA, 2014.

[117] S. Chaimatanan. *Strategic aircraft trajectory planning.* PhD thesis, Toulouse University lll Paul Sabatier, 2014.

[118] G. Gyatt. *The Standard Atmosphere.* Atmosculator, 2011. A mathematical model of the 1976 U.S. Standard Atmosphere.

[119] P.L. Massoglia, M.T. Pozesky, and G.T. Germana. The Use of Satellite Technology for Oceanic Air Traffic Control. *Proceedings of the IEEE*, 77(11):1695–1708, November 1989.

[120] J. Zhang, W. Liu, and Y. Zhu. Study of ADS-B Data Evaluation. *Chinese Journal of Aeronautics*, 24:461–466, 2011.

[121] T. Cho, I. Song, E. Jang, W. Yoon, and S. Choi. The Improvement of Aircraft Position Information with Unscented Kalman Filter. *International Journal of Database Theory and Application*, 5(2):75–82, June 2012.

[122] *Automatic Dependent Surveillance–Broadcast (ADS–B) Out Performance Requirements to Support Air Traffic Control (ATC) Service*. Department of Transportation, Federal Aviation Administration, 2010. Final Rule.

[123] T. Gilbert and R. Bruno. Surveillance and Broadcast Services – An Effective Nationwide Solution. In *The Integrated Communications Navigation and Surveillance (ICNS) Conference*, May 2009.

[124] C. Strong and R.E. Davis. Variability in the Position and Strength of Winter Jet Stream Cores Related to Northern Hemisphere Teleconnections. *Journal of Climate*, 21:584–592, 2008.

[125] T. Woollings, A. Hannachi, and B. Hoskins. Variability of the North Atlantic eddy-driven jet stream. *Quarterly Journal of the Royal Meteorological Society*, 136:856–868, April 2010.

[126] E.P. Gerber and G.K. Vallis. On the Zonal Structure of the North Atlantic Oscillation and Annular Models. *Journal of the Atmospheric Science*, 66:332–352, February 2009.

[127] D.J. Brayshaw, B. Hoskins, and M. Blackburn. The Basic Ingredients of the North Atlantic Storm Track. Part I: Land-Sea Contrast and Orography. *Journal of the Atmospheric Science*, 66:2539–2558, September 2009.

[128] T. Woollings, Pinto J.G., and Santos J.A. Dynamic Evolution of North Atlantic Ridges and Poleward Jet Stream Displacements. *Journal of the Atmospheric Science*, 68:954–963, May 2011.

[129] The International Federation of Air Line Pilots' Associations (IFALPA). Safety Bulletin: Navigation errors in the North Atlantic, 2011.

[130] C. Allignol. *Planification de trajectoires pour l'optimisation du trafic aérien*. PhD thesis, Institut de Recherche en Informatique de Toulouse (IRIT), 2011.

Résumé

Cette thèse explore des pistes d'amélioration du système de trafic aérien dans l'espace océanique de l'Atlantique Nord (NAT). D'abord, on considère le système actuel, où les avions suivent les rails prédefinis. On favorise les re-routages entre rails, diminuant la congestion dans l'espace continental. On applique des méthodes stochastiques d'optimisation pour trouver une configuration de vols sans conflits avec la séparation reduite entre aéronefs. Ensuite, on simule la planification des trajectoires avec le Wind Networking (WN). La source prinicipale des erreurs dans la prédiction de trajectoires étant l'incertitude dans la prévision du vent, le WN permet aux avions d'échanger leurs vents mesurés afin d'ajuster leurs prédictions. Enfin, on introduit le concept de free-flight dans NAT. Etant donné des trajectoires vent-optimales, on applique une méthode stochastique d'optimisation pour réduire le nombre de conflits au niveau stratégique, tout en conservant les trajectoires proches de leur optimum. Nos résultats numériques mettent en évidence plusieurs pistes pour améliorer le système de trafic aérien dans NAT, en considérant de nouvelles technologies et de nouveaux concepts.

Abstract

This thesis investigates the ways to improve the air traffic system in the highly congested North Atlantic oceanic airspace (NAT). First, we consider the current system, where aircraft follow predefined NAT tracks. We favor the re-routings between tracks, decreasing congestion in pre-oceanic airspace, and apply stochastic methods of optimization to find a conflict-free flight configuration with reduced separation between aircraft. Second, we simulate trajectory prediction by Wind Networking (WN). While the main source of time prediction errors is the uncertainty in wind forecast, WN permits aircraft to exchange measured winds and adjust their predictions using this recent and accurate information. Third, we study the impact of introducing the free flight concept in NAT. We apply a stochastic method of optimization on data provided by NASA consisting of NAT flights with wind optimal trajectories. The aim is to reduce the number of conflicts on the strategic level, while keeping the trajectories close to the optimal routes. Our computational experiments show that the air traffic situation in NAT can be improved in several different ways, considering new technologies and new trajectory planning concepts.